

Genetic Aberrations in High-Grade Astrocytic Gliomas

Paul James Mulholland

Human Cytogenetics Laboratory
Cancer Research UK
London Research Institute

Thesis submitted for the degree of
Doctor of Philosophy

University College London
2005

UMI Number: U593033

All rights reserved

INFORMATION TO ALL USERS

The quality of this reproduction is dependent upon the quality of the copy submitted.

In the unlikely event that the author did not send a complete manuscript and there are missing pages, these will be noted. Also, if material had to be removed, a note will indicate the deletion.



UMI U593033

Published by ProQuest LLC 2013. Copyright in the Dissertation held by the Author.
Microform Edition © ProQuest LLC.

All rights reserved. This work is protected against
unauthorized copying under Title 17, United States Code.



ProQuest LLC
789 East Eisenhower Parkway
P.O. Box 1346
Ann Arbor, MI 48106-1346

*This thesis is dedicated to
my mother and brother*

Abstract

Astrocytic gliomas are the most common tumours arising in the central nervous system. This thesis focuses on examining genetic changes in high-grade astrocytic gliomas. It describes the development of an analytical tool to facilitate systematic analysis of array comparative genomic hybridisation (CGH) results and catalogues copy number changes in high-grade astrocytic glioma cell lines and patient samples. Molecular cytogenetic analysis of chromosome 6 was used to explore the relationship between copy number changes and positional aberrations. Three regions of copy number associated with translocation breakpoints are described. The first translocation associated with a copy number change was in the cell line U87, loss of 6pter to 6p21 arises from an unbalanced translocation between chromosomes 6 and 7, with the breakpoint at 6p21 being close to the *POLH* and *GTPBP2* genes. The second is a discrete deletion in 6q23-24 in U87 is associated with a translocation between chromosomes 6 and 12, and involves several genes including *MAP3K5* and *MAP7*. The third is a discrete deletion of 6q26-27 in cell lines CRL2020 and CRL1620 involving *IGF2R*, *PARK2*, *PACRG* and *QKI* is associated chromosome translocations. Inactivation of a tumour suppressor gene near the breakpoint may be a primary consequence of certain translocations in solid tumours, in contrast to the oncogenic gene fusions present in haematological and mesenchymal malignancies.

Acknowledgements

My thanks go to Cancer Research UK and their supporters for giving me the opportunity to study at the London Research Institute. I am especially grateful to Denise Sheer for her supervision, rigor and continuous support. I am also grateful to my Second Supervisor Antony Michalski for his helpful advice, to Peter Sasieni for being patient and generous with his time with the statistical analysis, and Alistair Newall for his guidance. Many thanks to all the members of the Human Cytogenetics Laboratory, Tania Jones, Jane Babbage, Radost Vatcheva, Srinjan Basu, Rossen Donev, Andreas Bolzer, Pei Jun Wu, Chiara Mazzanti, Chrysanthos Poullikas, Diego Ottaviani and Petros Takousis. Also to Pat Gorman, Christina Thirlwell and Ian Tomlinson in the Molecular and Population Genetics Laboratory, Phil East in Computational Genome Analysis, and also the Mutation Detection Laboratory, Cell Services and Equipment Park. I would like to thank Heike Fiegler and Nigel Carter for teaching me how to perform array CGH and Peter Collins and Paul Lewis for patient material. I would also like to thank Edward Newlands and Ian Jusdon for giving me the opportunity to see patients with high-grade astrocytic glioma and gaining additional experience with molecularly targeted agents. Finally, I would like to thank Jane Greig, Sandra Cockburn, Peter McLoughlin, Ruth Tatevossian and Kate Mulholland for their support and advice.

Table of Contents

Abstract.....	3
Acknowledgements.....	4
Table of Contents.....	5
Abbreviations.....	9
List of Tables	11
List of Figures.....	13

Chapter 1 Introduction

1.1 Overview.....	18
1.2 Cancer Genetics.....	19
1.2.1 Cell cycle control and apoptosis.....	21
1.2.2 Oncogenes.....	23
1.2.2.1 Tumour viruses and oncogenes.....	23
1.2.2.2 Point mutation and oncogene activation.....	24
1.2.2.3 DNA amplification and oncogenes.....	24
1.2.2.4 Translocations and oncogene activation.....	27
1.2.3 Tumour suppressor genes.....	31
1.2.3.1 Family cancer syndromes.....	32
1.2.3.2 Deletions and tumour suppressor gene inactivation.....	33
1.2.4 Aneuploidy theory of tumorigenesis.....	35
1.2.5 Mechanisms of genetic change.....	36
1.2.6 DNA repair.....	37
1.2.7 Genome-wide methods of analysis of genetic change.....	40
1.3 Astrocytic gliomas.....	43
1.3.1 Description of astrocytic gliomas.....	43
1.3.2 Genetics of astrocytic gliomas.....	48
1.3.2.1 Family syndromes.....	48
1.3.2.2 Studies examining genetic changes in astrocytic gliomas....	49
1.3.2.2.1 Regions of LOH or copy number loss.....	50
1.3.2.2.2 Regions of genetic gain.....	51

1.3.2.2.3	Translocations.....	52
1.3.2.3	Molecular pathways.....	52
1.3.2.4	Genetic aberrations in different grades of astrocytic glioma.....	57
1.3.2.5	Genetic changes and prognosis.....	59
1.4	Aims of this research.....	60

Chapter 2 Materials and Methods

2.1	Cell lines and patient samples.....	62
2.2	DNA extraction.....	64
2.3	Metaphase CGH.....	65
2.4	Array CGH.....	71
2.5	FISH.....	76
2.6	M-FISH.....	81

Chapter 3 Development of analysis parameters for array CGH

3.1	Introduction.....	83
3.1.1	Thresholds and experimental variation.....	85
3.1.2	Analysis parameters used in other array CGH studies.....	88
3.1.3	Aims.....	90
3.2	Materials and methods.....	91
3.2.1	Additional pre-processing.....	91
3.2.2	Sensitivity and specificity.....	92
3.3	Results.....	93
3.3.1	Discarded clones.....	94
3.3.2	Chromosome scaling factors.....	94
3.3.3	Identification of thresholds from the ROC	
3.3.3.1	Dual thresholds.....	95
3.3.3.2	Single threshold based on multiple parameters.....	97

3.4	Discussion.....	99
3.4.1	Errors.....	99
3.4.1.1	Statistical issues.....	99
3.4.1.2	Clone characteristics.....	100
3.4.1.3	Genetic heterogeneity.....	100

Chapter 4 DNA Copy Number Changes in High-Grade Astrocytic gliomas

4.1	Introduction.....	102
4.2	Results.....	103
4.2.1	Copy number changes presented in numerical chromosome order...	104
4.3	Discussion.....	165

Chapter 5 Cytogenetic and Molecular Analysis of high-grade astrocytic glioma cell lines

5.1	Introduction.....	170
5.2	Results.....	172
5.2.1	M-FISH karyotypes of the cell lines.....	172
5.2.2	Confirmation of copy number change at specific genomic regions..	181
5.2.2.1	Amplification.....	181
5.2.2.2	Homozygous deletion.....	181
5.2.2.3	Reduced copy number.....	185
5.2.3	Translocations associated with deletions involving chromosome 6..	187
5.2.3.1	Cell line U87.....	187
5.2.3.1.1	Characterisation of der(6)t(6;7)(p21;q31).....	188
5.2.3.1.2	Characterisation of the der(6)t(6;12) and the der(12)t(6;12).....	194
5.2.3.2	Cell line CRL2020.....	199
5.2.3.3	Cell line CRL2610.....	205
5.3	Discussion.....	209
5.3.1	Further work.....	215
5.3.2	Conclusion.....	217

Chapter 6 Final Discussion

6.1	Review of the aims.....	219
6.2	Project methodology and results	
6.2.1	Overview.....	219
6.2.2	Evolution of array technology.....	220
6.2.3	Advantages and disadvantages of using cell lines and patient samples.....	221
6.3	Significance of thesis.....	224
6.3.1	Copy number change and underlying mutation.....	224
6.3.2	Temporal relationship between development of copy number change and underlying mutation.....	226
6.3.3	Patterns of genetic change.....	227
6.3.4	Fragile sites.....	231
6.4	Clinical perspective of this thesis.....	232
6.5	Conclusions.....	234

References.....	235
------------------------	------------

Appendices

Appendix A	Reagents.....	257
Appendix B	Cytogenetic Nomenclature.....	258
Appendix C	Array CGH profiles of Tumour samples and cell lines.....	259

Abbreviations

2-ME	2-mercaptoethanol
5-FU	5-fluorouracil
AA	Anaplastic astrocytoma
ALL	Acute lymphocytic leukaemia
CML	Chronic myeloid leukaemia
BAC	Bacterial artificial chromosome
BFB	Breakage-fusion-bridge cycle
CCD	charge-coupled device
cDNA	complementary DNA
CGH	Comparative genomic hybridisation
DAPI	4,6-diaminidino-2-phenylindole
dmin	double minutes
DN	<i>de novo</i>
EST	Expressed sequence tag
FISH	Fluorescence <i>in situ</i> hybridisation
FITC	fluorescein isothiocyanate
GBM	Glioblastoma multiforme
HNPCC	Hereditary non-polyposis colorectal cancer
HPV	Human papilloma viruses
HSRs	Homogeneously staining regions
LB	Liquid broth
LCV	Large-scale copy number variation
LOH	loss of heterozygosity
Mb	Mega base pairs
M-FISH	Multiplex-Fluorescence <i>in situ</i> hybridisation
MSI	Microsatellite instability
MSM	Microsatellite markers
MVA	Mosaic variegated aneuploidy
NA	Not applicable
NHEJ	Non-homologous end joining

PAC	P1 artificial chromosome
PBS	Phosphate-buffered saline
PCR	polymerase chain reaction
PNETs	Primitive neuro-ectodermal tumours
RFLP	Restriction Fragment Length Polymorphism
RSV	Rous sarcoma virus
ROC	Receiver operating characteristic
SNPs	Single nucleotide polymorphisms
tel	telomere
TLS	Trans-lesion synthesis
TR	Texas Red

Tables

Table 1.1	Oncogenic viruses.....	23
Table 1.2	Examples of oncogenes amplified in human cancers.....	26
Table 1.3	Examples of recurrent chromosome aberrations in myeloid and lymphoid malignancies.....	28
Table 1.4	Examples of recurrent chromosome aberrations in sarcomas.....	29
Table 1.5	Examples of prognostic associations in myeloid and lymphoid malignancies.....	29
Table 1.6	Oncogenes activated by translocation in epithelial tumours.....	30
Table 1.7	Tumour suppressor genes involved in familial cancer syndromes and associated sporadic tumours.....	33
Table 1.8	Human syndromes with defects in DNA repair.....	38
Table 1.9	Possible rearrangements following double strand chromosome breaks.....	39
Table 1.10	Modified WHO classification of gliomas showing the suggested cell of origin.....	44
Table 1.11	Conventional chemotherapeutic agents used in high-grade gliomas.....	48
Table 1.12	Summary of genetic predisposition syndromes associated with astrocytic gliomas.....	49
Table 1.13	Regions of LOH on chromosome 6 in astrocytic gliomas.....	50
Table 1.14	Tumour suppressor genes identified in astrocytic gliomas.....	51
Table 1.15	Oncogenes identified in astrocytic gliomas.....	51
Table 2.1	Cell lines used in the study.....	63
Table 2.2	Demographics of patients whose astrocytic grade IV samples were used in the study.....	64
Table 2.3	Probes obtained from Wellcome Trust Sanger Institute for FISH....	76
Table 2.4	Growth conditions for clones from the Sanger Clone Library.....	78
Table 3.1	Ideal fluorescence ratios with corresponding log ₂ values.....	85
Table 3.2	Table of results from a hypothetical experiment.....	93
Table 3.3	List of discarded clones.....	94
Table 3.4	Chromosome-specific scaling factors used in the statistical	

	analysis.....	95
Table 4.1	Chromosome size and position of the centromere (Mb).....	104
Table 4.2	Array CGH results of chromosome 1 in cell line U87.....	107
Table 4.3	Log ₂ ratios of clones in tumour samples and cell lines showing gain or amplification at 4q12.....	111
Table 4.4	Log ₂ ratios of clone RP5-1091E12 representing <i>EGFR</i> in all the tumour samples and cell lines.....	123
Table 4.5	Log ₂ values of surrounding clones where there is amplification of <i>EGFR</i>	126
Table 4.6	Log ₂ ratios of clones in tumours and cell lines showing homozygous deletion involving 9p21.....	128
Table 4.7	Comparison of copy number change, LOH and mutation status of <i>CDKN2A</i>	131
Table 4.8	Comparison of copy number change, LOH and mutation of <i>PTEN</i>	137
Table 4.9	Detection of <i>p53</i> mutations in astrocytic gliomas.....	151
Table 4.10	Regions of copy number change, which are LCVs.....	168
Table 5.1	Chromosome range and modal number of chromosomes in cell lines.....	172
Table 5.2	Deletions of chromosome 6 in U87.....	188
Table 5.3	Probes used to test the 6p21.1 breakpoint in U87.....	188
Table 5.4	Probes used to test the chromosome 6 breakpoints in t(6;12) in U87.....	194
Table 5.5	Probes used to test the 6q26-q27 breakpoint in CRL2020.....	199
Table 5.6	Tiling path probes which can be used to investigate chromosome 7 breakpoint of der(6)t(6;7) in cell line U87.....	215
Table 5.7	Tiling path probes which can be used to investigate der(6)t(6;12) and der(12)t(6;12) in cell line U87.....	216
Table 5.8	Selected genes from translocations.....	218
Table 6.1	Genomic regions associated with fragile sites in high-grade astrocytic gliomas.....	231

Figures

Figure 1.1	Diagram showing the relationship between mitogenic signalling, Ras, p53 and RB in controlling the cell cycle.....	22
Figure 1.2	Genetic changes accompanying tumour suppressor gene inactivation.....	34
Figure 1.3a	Haematoxylin & Eosin (H&E) section of an astrocytic glioma grade II.....	45
Figure 1.3b	H&E section of astrocytic glioma grade IV.....	45
Figure 1.4	MRI scan of a patient with astrocytic glioma.....	47
Figure 1.5	Functional domains of EGFR protein.....	54
Figure 1.6	EGFR signalling pathway through PI3K.....	55
Figure 1.7	Proposed paths to the development of astrocytic glioma grade IV...	58
Figure 1.8	Strategy of the study.....	61
Figure 2.1	Composite images showing the same metaphase in a male versus female control experiment.....	69
Figure 2.2	CGH of a male versus female control experiment.....	70
Figure 2.3	Cy 5 fluorescence from an array.....	75
Figure 2.4	Whole genome array profile of a male versus female DNA control experiment.....	77
Figure 3.1	Array CGH profile of chromosome 19 in a female versus male experiment.....	87
Figure 3.2	Array CGH profile of the X chromosome in a female versus male experiment.....	87
Figure 3.3	Array profile from Snidjers <i>et al.</i>	90
Figure 3.4	ROC curve.....	96
Figure 4.1	Composite array CGH profile of chromosome 1.....	106
Figure 4.2	Array CGH profile of chromosome 1 in U87.....	108
Figure 4.3	Composite array CGH profile of chromosome 2.....	109
Figure 4.4	Array CGH profile of chromosome 2 in tumour T5.....	110
Figure 4.5	Composite array CGH profile of chromosome 3.....	112
Figure 4.6	Array CGH profile of chromosome 3 in cell line CRL1620.....	113

Figure 4.7	Composite array CGH profile of chromosome 4.....	114
Figure 4.8	Array CGH profile of chromosome 4 in tumour T3.....	115
Figure 4.9	Composite array CGH profile of chromosome 5.....	117
Figure 4.10	Composite array CGH profile of chromosome 6.....	118
Figure 4.11	Metaphase CGH and array CGH profiles of chromosome 6 in cell line CRL2366.....	119
Figure 4.12	Array CGH profile of chromosome 6 in cell line U118.....	121
Figure 4.13	Metaphase CGH and array CGH profiles of chromosome 6 in cell line CRL2610.....	122
Figure 4.14	Composite array CGH profile of chromosome 7.....	124
Figure 4.15	Array CGH profile of chromosome 7 in tumour T5.....	125
Figure 4.16	Composite array CGH profile of chromosome 8.....	127
Figure 4.17	Composite array CGH profile of chromosome 9.....	129
Figure 4.18	Array CGH profile of chromosome 9 in cell line U118.....	130
Figure 4.19	Array CGH profile of chromosome 9 in cell line CRL1620.....	132
Figure 4.20	Composite array CGH profile of chromosome 10.....	134
Figure 4.21	Metaphase and array CGH profiles of chromosome 10 in cell line CRL2366.....	135
Figure 4.22	Array CGH profile of chromosome 10 in CRL1620.....	136
Figure 4.23	Composite array CGH profile of chromosome 11.....	138
Figure 4.24	Array CGH profile of chromosome 11 in tumour T3.....	139
Figure 4.25	Composite array CGH profile of chromosome 12.....	141
Figure 4.26	Composite array CGH profile of chromosome 13.....	142
Figure 4.27	Array CGH profile of chromosome 13 in cell line U87.....	143
Figure 4.28	Array CGH profile of chromosome 13 in cell line U251.....	144
Figure 4.29	Composite array CGH profile of chromosome 14.....	146
Figure 4.30	Composite array CGH profile of chromosome 15.....	147
Figure 4.31	Composite array CGH profile of chromosome 16.....	149
Figure 4.32	Composite array CGH profile of chromosome 17.....	150
Figure 4.33	Array CGH profile of chromosome 17 in cell line Htb138.....	152
Figure 4.34	Composite array CGH profile of chromosome 18.....	154

Figure 4.35	Array CGH profile of chromosome 18 in cell line CRL1620.....	155
Figure 4.36	Composite array CGH profile of chromosome 19.....	156
Figure 4.37	Array CGH profile of chromosome 19 in cell line U87.....	157
Figure 4.38	Composite array CGH profile of chromosome 20.....	158
Figure 4.39	Metaphase and array CGH profiles of chromosome 20 in cell line CRL2020.....	159
Figure 4.40	Metaphase and array CGH profiles of chromosome 20 in cell line U87.....	161
Figure 4.41	Composite array CGH profile of chromosome 21.....	162
Figure 4.42	Composite array CGH profile of chromosome 22.....	163
Figure 4.43	Array CGH profile of chromosome 22 in cell line CRL2610.....	164
Figure 5.1	M-FISH karyotype of CRL1620.....	173
Figure 5.2	M-FISH karyotype of CRL2020.....	174
Figure 5.3	M-FISH karyotype of CRL2365.....	175
Figure 5.4	M-FISH karyotype of CRL2366.....	176
Figure 5.5	M-FISH karyotype of CRL2610.....	177
Figure 5.6	M-FISH karyotype of CRL2611.....	178
Figure 5.7	M-FISH karyotype of U87.....	179
Figure 5.8	M-FISH karyotype of U251.....	180
Figure 5.9a	Array CGH profile of chromosome 7 in cell line CRL1620.....	182
Figure 5.9b	FISH analysis of CRL1620 with a dual probe for <i>EGFR</i> and the centromere of chromosome 7.....	182
Figure 5.10	Array CGH profile of chromosome 9 in cell line CRL2610.....	183
Figure 5.11	FISH analysis of CRL2610 with probes RP11-513M16 and RP11-149I2.....	184
Figure 5.12	FISH analysis of CRL2610 with probes RP11-513M16 and RP11-495L19.....	184
Figure 5.13a	Array CGH profile of chromosome arm 6q in cell line CRL2365...	186
Figure 5.13b	FISH analysis of the chromosome 6 deletion between 89 and 94 Mb in CRL2365.....	186
Figure 5.14	Characterisation of der(6)t(6;7) in cell line U87.....	189

Figure 5.15	FISH analysis of U87 with probes RP11-227E22 & RP11-344J7...	190
Figure 5.16	FISH analysis of U87 with probes RP11-227E22 and RP1-261G23148.....	190
Figure 5.17	FISH analysis of U87 with probes RP11-227E22 and RP11-22I24..	191
Figure 5.18	FISH analysis of U87 with probes RP11-227E22 & RP3-337H4....	192
Figure 5.19	FISH analysis of U87 with a paint for chromosome arm 7q.....	193
Figure 5.20	Characterisation of der(6)t(6;12) and der(12)t(6;12) in cell line U87.....	195
Figure 5.21	FISH analysis of U87 with probes RP11-557H15 and RP11-448D5.....	196
Figure 5.22	FISH analysis of U87 with probe RP11-368P1.....	196
Figure 5.23	FISH analysis of U87 with probes RP11-448D5 and RP11-86O4...	197
Figure 5.24	Summary of FISH analysis of chromosome 6 aberrations in U87...	198
Figure 5.25	Deletion associated with a translocation, involving chromosome 6 in cell line CRL2020.....	200
Figure 5.26	FISH analysis of CRL2020 with probes RP11-13P5 and RP3-495O10.....	201
Figure 5.27	FISH analysis of CRL2020 with probes RP11-13P5 and RP1-51J12.....	201
Figure 5.28	FISH analysis of CRL2020 with probe RP1-51J12 and 6q paint.....	202
Figure 5.29	FISH analysis of CRL2020 with probe RP11-471L1.....	203
Figure 5.30	Summary of FISH analysis of the chromosome 6 deletion in CRL2020.....	204
Figure 5.31	Array CGH profile of chromosome 6 in cell line CRL2610.....	206
Figure 5.32	FISH analysis of the distal chromosome 6 deletion in CRL2610, using probe RP1-51J12 and a 6q paint.....	207
Figure 5.33	FISH analysis of CRL2610 with probe RP11-471L1.....	207
Figure 5.34	Summary of FISH analysis of the distal chromosome 6q deletion in CRL2610.....	208
Appendix C1	Array CGH profile of tumour T1.....	259
Appendix C2	Array CGH profile of tumour T2.....	260

Appendix C3	Array CGH profile of tumour T3.....	261
Appendix C4	Array CGH profile of tumour T4.....	262
Appendix C5	Array CGH profile of tumour T5.....	263
Appendix C6	Array CGH profile of tumour T6.....	264
Appendix C7	Array CGH profile of tumour T7.....	265
Appendix C8	Array CGH profile of tumour T8.....	266
Appendix C9	Array CGH profile of tumour T9.....	267
Appendix C10	Array CGH profile of tumour T10.....	268
Appendix C11	Array CGH profile of cell line CRL1620.....	269
Appendix C12	Array CGH profile of cell line CRL2020.....	270
Appendix C13	Array CGH profile of cell line CRL2365.....	271
Appendix C14	Array CGH profile of cell line CRL2366.....	272
Appendix C15	Array CGH profile of cell line CRL2610.....	273
Appendix C16	Array CGH profile of cell line CRL2611.....	274
Appendix C17	Array CGH profile of cell line Htb138.....	275
Appendix C18	Array CGH profile of cell line U87.....	276
Appendix C19	Array CGH profile of cell line U118.....	277
Appendix C20	Array CGH profile of cell line.....	278

Chapter One

Introduction

1.1 Overview

This thesis examines the genetics of the most common histological group of primary brain cancer, astrocytic glioma. In particular, it focuses on the high-grade tumours, astrocytic glioma grade III and grade IV. These tumours have complex genetic aberrations that are poorly understood. Although the prevalence of these tumours is relatively low, accounting for one to two percent of primary adult malignancy, conventional treatments, namely surgery, radiotherapy and chemotherapy have had only a marginal impact on survival, and the tumours are invariably fatal. Therefore, it is necessary to explore the potential of different approaches in the treatment of these tumours. One approach that has had some success for other tumour types is the use of therapies that are rationally designed to reverse the effect of specific molecular aberrations. These have been termed molecularly targeted agents. Presently, the poor understanding of the genetic aberrations in astrocytic gliomas is a limiting factor in the use of molecularly targeted agents. However, recent developments of the human genome project provide an opportunity to gain a greater understanding of these tumours.

Currently, the human genome project has yielded a draft of the entire DNA sequence (Lander *et al.*, 2001; Venter *et al.*, 2001), and complete sequences for chromosomes 5 (Schmutz *et al.*, 2004), 6 (Mungall *et al.*, 2003), 7 (Hillier *et al.*, 2003), 9 (Humphray *et al.*, 2004), 10 (Deloukas *et al.*, 2004), 13 (Dunham *et al.*, 2004), 14 (Heilig *et al.*, 2003), 19 (Grimwood *et al.*, 2004), 20 (Deloukas *et al.*, 2001), 21 (Hattori *et al.*,

2000), 22 (Dunham *et al.*, 1999) and X (Ross *et al.*, 2005). In parallel to this advance, developments in computation and microengineering have produced micro-array technology. Several applications of this technology facilitate the study of genetics, including array comparative genomic hybridisation (CGH) and expression arrays. Array CGH is an immensely powerful emerging method that facilitates the assessment of DNA copy number across the genome in one experiment (Kraus *et al.*, 1997; Pinkel *et al.*, 1998; Solinas-Toldo *et al.*, 1997). Expression arrays give a genome-wide assessment of gene expression (Schena *et al.*, 1995). The utilisation of array technology offers great potential in elucidating the relationship between genetics and disease. In respect of cancer management, a better understanding of genetics can improve diagnostic capability, identify therapeutic targets, and can help in predicting and assessing response to treatments. The aim of the research described in this thesis is to explore the utilisation of array CGH in order to identify copy number changes present in high-grade astrocytic gliomas accurately.

1.2 Cancer Genetics

Normal human cells can be grown in culture but they can only replicate a limited number of times. After a number of generations, typically forty, the cell enters a 'crisis' phase when it dies (Hayflick and Moorhead, 1961). Normal cells in culture display the characteristics of controlled growth: anchorage dependence, dependence on serum growth factors, and density-dependent inhibition. However, some cells, at a low frequency, can become transformed, so that they become independent of growth controls and develop limitless replication potential. Cancer is a term that describes a group of

diseases that are characterised by cell transformation. Cancer has a variety of aetiological factors, but a common feature of how these may cause cancer is through their influence on the genome. The genome can be altered in various ways to cause cancer, but at the most fundamental level, alterations in two broad categories of genes, tumour suppressor genes and oncogenes, are critical. A loss of function mutation in a tumour suppressor gene confers an increased susceptibility to tumour formation. An activating mutation in an oncogene has a dominant transforming effect on the cell.

Solid tumours arise from the accumulation of multiple genetic changes, and models of carcinogenesis have been described for most major forms of cancer based on this hypothesis. The earliest model of the multi-step process of carcinogenesis was proposed for colorectal cancer. Here, each stage of tumour development is associated with aberrations in particular genes (Ashley, 1969; Fearon and Vogelstein, 1990; Moolgavkar and Knudson, 1981). The multi-step theory has been developed further to give an integrated view of the cellular physiology for all tumours. It is suggested that the cancer cell requires six essential alterations in cellular physiology namely: “self-sufficiency in growth signals, insensitivity to growth inhibitory (antigrowth) signals, evasion of programmed cell death, limitless replicative potential, sustained angiogenesis, and tissue invasion and metastasis” (Hanahan and Weinberg, 2000).

Cells containing mutations of key genes that give an increased growth potential will have a selective advantage in the population. There is interplay between the generation of mutations and selection of cells that determines how a tumour develops;

however the relative importance of each is debatable (Loeb, 2001; Tomlinson *et al.*, 1996). An additional classification of genes in cancer has been proposed, which places them into two groups, gatekeeper genes and caretaker genes (Kinzler and Vogelstein, 1997). Genes that directly regulate tumour growth by inhibiting growth or by promoting cell death are classed as gatekeeper genes. The second group are caretaker genes. Caretaker genes are involved in maintaining the integrity of the genome. Inactivated caretaker genes do not directly promote tumours. Instead their inactivation results in genetic instability, which causes an increased mutation rate affecting all genes. This increase in mutation rate will affect the gatekeeper genes, which do directly regulate tumour growth. The breast cancer susceptibility gene (*BRCA1*) is an example of a caretaker gene.

1.2.1 Cell cycle control and apoptosis

The cell cycle describes the sequence of events required to replicate the cells genetic material and separate the two copies into daughter cells. The cell cycle is divided into G1 phase, S phase, G2 phase and M phase. G1 is a gap phase, DNA replication occurs during S phase. G2 is the second gap phase where the DNA content of the cell is $4n$. M phase or mitosis follows G2, when there is division of the DNA into two daughter cells. The cell cycle is a regulated process that ensures the ordered replication and division of genetic material. There are two key control points, the first in G1 when the cell becomes committed to start replication and at G2/M, just prior to cell division. Regulation of the cell cycle occurs through a series of signalling molecules, whose activity is controlled by phosphorylation and dephosphorylation (Lewin, 2004).

Apoptosis is the process of programmed cell death. It is triggered by a variety of factors including agents that damage DNA such as irradiation and chemotherapy, activation of certain receptors such as Fas receptor, cytotoxic T cells, glucocorticoids and withdrawal of growth factors (Lewin, 2004). The cell cycle and apoptosis are intimately related as they share key molecules in their control pathways, as shown in Figure 1.1.

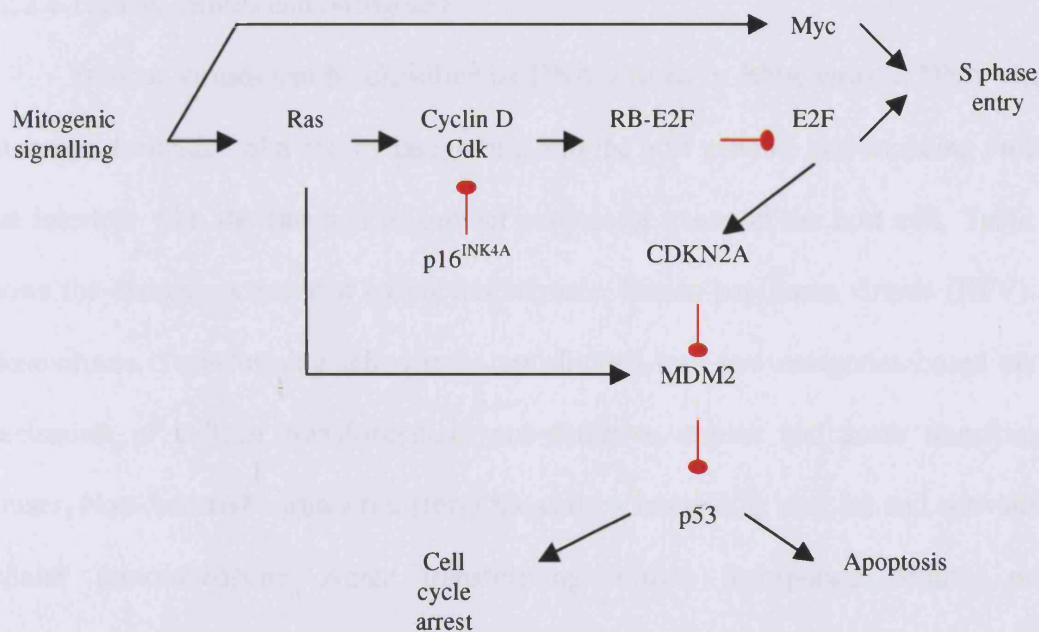


Figure 1.1 Diagram showing the relationship between mitogenic signalling, Ras, p53 and RB in controlling the cell cycle (Sherr and McCormick, 2002).

Oncogenes are typically genes that are involved in cell cycle control and apoptosis, and encode growth factors and their receptors, tyrosine kinases, serine threonine kinases, RAS proteins, transcription factors and other regulatory proteins. Key tumour suppressor genes shown in the diagram are RB, p53 and p16. The gain of function of oncogenes and loss of function of tumour suppressor genes are discussed throughout this thesis.

1.2.2 Oncogenes

Oncogenes were first identified as genes in retroviruses that can transform cells. Oncogenes can acquire gain of function through mutation, gene amplification and/ or chromosome re-arrangement.

1.2.2.1 Tumour viruses and oncogenes

Tumour viruses can be classified as DNA viruses or RNA viruses. DNA viruses cause transformation of a cell by integrating into the host genome and encoding proteins that interfere with the function of tumour suppressor genes in the host cell. Table 1.1 shows the oncogenes encoded by polyomaviruses, human papilloma viruses (HPV) and adenoviruses. Transforming retroviruses are divided into two categories based on the mechanism of cellular transformation, non-defective viruses and acute transforming viruses. Non-defective viruses transform the cell by integrating near to, and activating a cellular proto-oncogene. Acute transforming viruses incorporate cellular proto-oncogenes, into their genomes, which then become viral oncogenes by the acquisition of mutations. Following transfection, the acute transforming virus integrates into the target cell genome and transforms the cell.

Virus	Genome	Size	Oncogenes	Origin of oncogene
Polyoma	dsDNA	5-6 kb	T antigens	Early viral gene
HPV	dsDNA	8 kb	E6 and E7	Early viral gene
Adenovirus	dsDNA	37 kb	E1A and E1B	Early viral gene
Retrovirus	ssRNA	6-9 kb	Individual	Cellular

Table 1.1 Oncogenic viruses (Lewin, 2004).

Oncogenes were first identified through the transforming retrovirus, Rous sarcoma virus (RSV). Rous demonstrated that a transmissible agent was able to induce cancer in chickens (Rous, 1911). Stehelin *et al* demonstrated that the transmissible agent in Rous sarcoma virus contained novel nucleotide sequences not present in related retroviruses but related to normal nucleotide sequences in chicken DNA (Stehelin *et al.*, 1976). The transforming gene, *v-src*, is a homologue of the normal cellular gene, *SRC*, which is involved in control of cell growth.

1.2.2.2 Point mutation and oncogene activation

Ras are guanosine 5'-triphosphate (GTP)-binding proteins that are involved in transmitting signals from cell surface receptors to the nucleus. There are three different Ras proteins H-Ras, N-Ras and K-Ras. Ras proteins switch between an active state when GTP is bound and an inactive state when guanosine 5'-diphosphate (GDP) is bound (Alberts et al., 2002). Point mutations in Ras resulting in a single amino acid change have been identified which reduce hydrolysis of bound GTP and give constitutive activity to the Ras protein (Lewin, 2004). Mutant Ras is found in up to a quarter of all human cancers (Alberts et al., 2002).

1.2.2.3 DNA amplification and oncogenes

DNA amplification describes the selective increase in copy number of a region of DNA and generally there is a target gene or genes being amplified (Schwab, 1999). Gene

amplification tends to result in increased gene expression. DNA amplification is found in two situations in humans, firstly in drug resistance and secondly in cancer.

Amplification of certain genes has been found to be associated with resistance of a tumour to chemotherapy. For example, amplification of 18p11.32, containing the Thymidylate Synthase gene (*TYMS*) was found in colorectal metastases to the liver in patients being treated with 5-fluorouracil (5-FU) (Wang *et al.*, 2004). *TYMS* is a downstream target of 5-FU. Amplification of 18p11.32 was found to be associated with a shorter survival in these patients. The Multi-Drug Resistance gene *MDR1* (7q21.1) is associated with resistance to a variety of chemotherapeutic agents and amplification of the Dihydrofolate Reductase gene (*DHFR*) (5q14.1) in methotrexate resistance (Pastan and Gottesman, 1987). This has led to the hypothesis that tumours evolve to develop chemo-resistance through amplification of certain genes.

More commonly DNA amplification is found in cancer prior to treatment. In tumours, regions of amplified DNA contain oncogenes. These oncogenes become over-active by the amplification, and this contributes to the growth and survival of the tumour cell. Amplification of the Avian Myelocytomatosis Viral-Related Oncogene Neuroblastoma-Derived (*MYCN*) (2p24.1) was first found in neuroblastoma (Schwab *et al.*, 1983). It is associated with an aggressive phenotype and the patients with *MYCN* amplification have a poorer prognosis than those without *MYCN* amplification (Seeger *et al.*, 1985). Many oncogenes are amplified in cancer, and a summary is given in Table 1.2.

Gene	Cytogenetic location	Tumour
<i>AKT</i>	19q13	Ovarian cancer
<i>CYCLIN D1</i> <i>HST-1</i> <i>GST</i> <i>SEA</i>	11q13	Breast, oesophageal carcinoma and many other solid tumours
<i>CCNE</i>	19q12	Gastric cancer
<i>GLI</i> <i>SAS</i> <i>CDK-4</i> <i>MDM2</i>	12q13	Soft tissue sarcoma and Glioma
<i>EGFR</i>	7p12	Glioblastoma, Head and Neck cancer
<i>ERBB2</i>	17q11	Breast, Ovarian cancer
<i>FGFR1</i>	8p12	Breast cancer
<i>FGFR2</i>	10q25	Breast cancer
<i>HRAS</i>	11p15	Colorectal cancer, Bladder carcinoma
<i>KRAS</i>	12p13	Colorectal, Gastric cancer
<i>MDM2</i>	12q14	Sarcoma, Neuroblastoma, Glioblastoma
<i>MYB</i>	6q23	Colorectal cancer
<i>MYC</i>	8q22	Ovarian, Breast, Head and Neck, Oesophageal, Cervical, Small cell lung cancer
<i>MYCN</i>	2p24	Neuroblastoma, Retinoblastoma, Small Cell Lung Carcinoma
<i>MYCL</i>	1p32	Small cell lung carcinoma
<i>PDGFRA</i>	4q12	Glioblastoma
<i>PDGFRB</i>	5q33-35	Glioblastoma

Table 1.2 Examples of oncogenes amplified in human cancers (Sheer and Shipley, 2005; Vogelstein and Kinzler, 1998). Table shows the normal cytogenetic location of the gene.

1.2.2.4 Translocations and oncogene activation

A chromosome translocation involves a double strand break, and joining of the chromosome fragment to either a different place on the same chromosome or to a different chromosome. There are two main mechanisms of oncogene activation through chromosome translocation. The first involves translocation breakpoints between two genes and re-joining to create a tumour-specific oncogenic chimeric protein. This has been observed primarily in leukaemias, lymphomas and sarcomas (Tables 1.3 and 1.4). For example, the Philadelphia chromosome $t(9;22)(q34;q11)$ generates a fusion between two genes, Breakpoint Cluster Region (*BCR*) and Abelson (*ABL*). The normal function of *BCR* is not known; *ABL* is a tyrosine kinase-signalling molecule. The translocation generates a fusion protein giving constitutive kinase activity to the *ABL* kinase. The Philadelphia chromosome is present in the majority of cases of chronic myeloid leukaemia (CML) and in a significant minority of those with acute lymphocytic leukaemia (ALL). Translocations characteristic to specific tumours can be used in diagnosis and in some cases in predicting prognosis (Table 1.5). For example, alveolar rhabdomyosarcoma can be difficult to distinguish histologically from embryonal tumours. However, $t(2;13)(q25-37;q14)$ which occurs in the majority of alveolar rhabdomyosarcoma or $t(1;13)(p36;q14)$, a variant translocation, can be used in diagnosis.

The second mechanism described for oncogene activation occurs in B and T lymphocyte malignancies. This involves translocation of the oncogene to the regulatory elements of immunoglobulin or T cell receptor genes. Burkitt's lymphoma is an example of the mechanism. The oncogene involved in the translocation is *MYC* (8q24) and is most

commonly translocated near to the Immunoglobulin Heavy chain gene on chromosome 14 in the t(8;14)(q24;q32), or to the Immunoglobulin Light chain genes (IgL), IgLk in the t(2;8)(p12;q24) or IgLλ in the t(8;22)(q24;q11).

Malignancy	Chromosome Aberration	Affected Genes
CML	t(9;22)(q34;q11)	<i>ABL, BCR</i>
CML blast crisis	(9;22)(q34;q11), +8, +Ph, +19, or i(17q)	<i>ABL, BCR,</i> <i>p53</i>
AML-M2	t(8;21)(q22;q22)	<i>ETO, AML1</i>
APL-M3, M3V	t(15;17)(q22;q11.2)	<i>PML, RARA</i>
AMMoL-M4Eo	inv(16)(p13q22) or t(16;16)(p13;q22)	<i>MYH11, CBFB</i>
AMMoL-M4/M5	t(4;11)(q21;q23) t(11;19)(q23;p13)	<i>AF4, MLL</i> <i>ENL, MLL</i>
AML-M7 (infants)	t(1;22)(p13;q13)	<i>OTT, MAL</i>
AML	t(6;9)(p23;q34) t(3;21)(q26;q22) -5 or del(5q) 7 or del(7q) +8 t(12p) or del(12p)	<i>DEK, CAN</i> <i>EAP/EV11/MDS1,</i> <i>AML1</i>
Therapy-related AML	-5 or del(5q) -7 or del(7q) t(3;21)(q26;q22) t(9;11)(p22;q23)	<i>EAP/EV11/MDS1,</i> <i>AML1</i> <i>AF9, MLL</i>
pre-B ALL	t(1;19)(q23;p13.3)	<i>PBX1, E2A</i>
pro-B ALL	t(17;19)(q22;p13.3)	<i>HLF, E2A</i>
ALL	t(9;22)(q34;q11) t(1;11)(p32;q23) t(4;11)(q21;q23) t(11;19)(q23;p13) del(9p) del(6q), del(11q), del(12p)	<i>ABL, BCR</i> <i>eps15, MLL</i> <i>AF4, MLL</i> <i>ENL, MLL</i> <i>CDKN2A/B</i>
CLL	+12	

Table 1.3 Examples of recurrent chromosome aberrations in myeloid and lymphoid malignancies (Sheer and Shipley, 2005).

Tumour	Chromosome Aberration	Affected Genes
Ewing's sarcoma and pPNET	t(11;22)(q24;q12) t(2;22)(q33;q12) t(7;22)(p22;q12) t(17;22)(q21;q12) t(21;22)(q22;q12)	<i>FLI-1, EWS</i> <i>FEV, EWS</i> <i>ETV1, EWS</i> <i>ETV4, EWS</i> <i>ERG, EWS</i>
Ewing's sarcoma	t(1;16)(q11-25;q11-24)	
Clear cell sarcoma	t(12;22)(q13;q12)	<i>ATF1, EWS</i>
Intra-abdominal small cell sarcoma	t(11;22)(p13;q12)	<i>WT1, EWS</i>
Extraskeletal myxoid chondrosarcoma	t(9;22)(q22;q12)	<i>DDIT3, EWS</i>
Alveolar rhabdomyosarcoma	t(2;13)(q35-37;q14)	<i>PAX3, FKHR</i>
Synovial sarcoma	t(X;18)(p11.2;q11.2)	<i>SSX1/SSX2/SSX4, SYT</i>
Myxoid liposarcoma	t(12;16)(q13;p11)	<i>CHOP, TLS/FUS</i>
Dermatofibrosarcoma protruberans	t(17;22)(q22;q13)	<i>COL1A, PDGFB</i>
Congenital fibrosarcoma	t(2;15)(p13;q25)	<i>ETV6, NTRK3</i>
Alveolar soft part sarcoma	t(X;17)(p11.2;q25)	<i>ASPL, TFE3</i>

Table 1.4 Examples of recurrent chromosome aberrations in sarcomas (Sheer and Shipley, 2005).

Malignancy	PROGNOSIS		
	Good	Intermediate	Poor
CML blast crisis AML	t(8;21) t(15;17) inv(16)	del(7q) del(9q) abn 11q23 +22 Other structural & numerical abnormalities No abnormality	+Ph,+8, i(17q)or +19 abn 3q -5 or del(5q) -7 complex karyotypes +8 +11 +13 +21
ALL	>50 chromosomes t(12;21) t(10;14) +4, +10	47-50 chromosomes	<47 chromosomes ~96 chromosomes t(9;22) t(8;14) t(1;19) t(4;11), t(11;19)

Table 1.5 Examples of prognostic associations in myeloid and lymphoid malignancies (Sheer and Shipley, 2005).

While chromosome translocations are recognised as an important mechanism for oncogene activation in haematological malignancies and sarcomas, there are only a few examples where this process is described in epithelial tumours (Table 1.6). A t(15;19)(q11;p13) in association with an increased expression of *NOTCH3* gene was found in a lung carcinoma (Dang *et al.*, 2000). Tognon *et al* demonstrated a translocation, t(12;15), leading to fusion of the ETS variant 6 (*ETV6*) and Neurotrophic Tyrosine Kinase Receptor type 3 (*NTRK3*) genes in secretory breast carcinoma (Tognon *et al.*, 2002). The fusion transcript was found in 12 out of 13 secretory breast carcinomas. Barlund *et al* found over-expression of the Breast Carcinoma Amplified Sequence 3 (*BCAS3*), in 9 out of 13 breast cancer cell lines, but in cell line MCF7 they identified a fusion protein derived from *BCAS3* and *BCAS4* (Barlund *et al.*, 2002). Strictly speaking, a translocation was not described, although a rearrangement was suggested from two colour FISH, which showed colocalisation of the probes representing the two genomic regions. Adelaide *et al* studied translocations involving 8p11 in 9 pancreatic, and 34 breast cancer cell lines. Seven breakpoints involving Neuregulin 1 (*NGR1*) were identified (Adelaide *et al.*, 2003). The significance of this breakpoint cluster in these tumours has yet to be identified.

Model system	Affected genes
Secretory breast carcinoma	<i>ETV6</i> (12p13.2), <i>NTRK3</i> (15q25.3)
MCF breast cancer cell line	<i>BCAS3</i> (17q23), <i>BCAS4</i> (20q13)
Lung cancer	<i>NOTCH3</i> (19p13)

Table 1.6 Oncogenes activated by translocation in epithelial tumours (Barlund *et al.*, 2002; Dang *et al.*, 2000; Tognon *et al.*, 2002).

1.2.3 Tumour suppressor genes

Knudson first proposed the concept of a tumour suppressor gene after studying retinoblastoma (Knudson, 1971). Retinoblastoma is a tumour that arises in the retina of children. Sixty percent of cases of retinoblastoma cases are hereditary and of these, 80% arise in both eyes. The non-hereditary cases are always unilateral, that is they only arise in one eye. Knudson's 'two hit' model recognised that the transformation of a normal cell to a tumour cell requires inactivating mutations in each allele of a tumour suppressor gene. Knudson proposed that patients with hereditary retinoblastomas have one mutant allele present in the germ-line, and the addition of a second mutation in the remaining normal allele gives rise to retinoblastoma. In the non-hereditary patients both mutations are spontaneous and must occur in the same cell, hence the lower frequency of non-hereditary retinoblastoma. Subsequently, retinoblastoma has been found to be associated with mutation of both alleles of a gene termed retinoblastoma (*RB*), present on 13q14, thus supporting Knudson's hypothesis (Friend *et al.*, 1986). Knudson's 'two hit' hypothesis has been broadly supported by the identification of other tumour suppressor genes where both alleles are abrogated before tumour suppressor activity is lost.

p53 was first identified as a tumour suppressor gene in colorectal cancer. Analysis of chromosome 17p in colorectal carcinomas with microsatellite markers found a minimum region of loss from 17p12 to 17p13, containing *p53* (Baker *et al.*, 1989). It was known at this time that *p53* was involved in SV40 transformation of cells (Lane and Crawford, 1979; Linzer and Levine, 1979), and hence its coding sequence was analysed. Mutations were found in *p53* in two colorectal carcinomas with loss of heterozygosity

(LOH) at 17p13.1. Subsequently, the same group found mutations in *p53* in other common human tumours, including astrocytic glioma grade IV, breast and lung cancer (Nigro *et al.*, 1989). *p53* plays a pivotal role in integrating cell responses and influencing the balance of apoptosis and cell growth. Loss of function of *p53* leads to genomic instability, which is a common feature of cancer (Bogler *et al.*, 1995a; Bogler *et al.*, 1995b). Indeed, *p53* is mutated in half of human cancers and is the most frequently mutated tumour suppressor gene in cancer (Lane, 1992). The complexity of cancer genetics is exemplified with *p53*. Normal *p53* is a tumour suppressor gene. However, while the mutated gene loses tumour suppressor function, it also develops tumour-enhancing capabilities and hence can also be classified as an oncogene. Two independent studies reached this conclusion using mouse models (Lang *et al.*, 2004; Olive *et al.*, 2004). It was found that mice, which bear the mutant *p53* had a different tumour spectrum from *p53* null mice.

1.2.3.1 Family cancer syndromes

Certain families have a history of cancer, for example five percent of breast cancer cases have a strong family history of breast cancer. Tumour suppressor genes, including *BRCA1*, have been detected in linkage studies in family cancer syndromes (Hall *et al.*, 1990). Sporadic tumours may also have mutations of the same tumour suppressor genes but be a different tumour type to those found in familial cases (Table 1.7).

Gene	Genomic Location	Family cancer Syndrome	Sporadic cancer
<i>APC</i>	5q21	Adenomatous polyposis coli and Turcot syndrome	Colon and brain cancers
<i>BRCA1</i>	17q21	Breast/ovarian cancer	Breast, ovary and prostate
<i>BRCA2</i>	13q12-13	Breast cancer	Breast, ovarian and pancreatic
<i>NF1</i>	17q11.2	Neurofibromatosis type I	Neurofibromatosis, colon and brain
<i>NF2</i>	22q12.2	Neurofibromatosis type II	Vestibular schwannoma, meningioma and ependymoma
<i>CDKN2A</i>	9p21	Melanoma-astrocytoma	Melanoma, astrocytic glioma, pancreatic, breast and other cancers
<i>p53</i>	17p13	Li-Fraumeni syndrome	Many including brain, breast, lung, colon, bladder, ovarian and prostate
<i>RB1</i>	13q14.3	Retinoblastoma	Retinoblastoma, osteosarcoma, bladder, breast and lung cancer
<i>SMAD4</i>	18q21	Juvenile polyposis	Pancreatic, colon and lung cancer
<i>PTEN</i>	10q24-25	Cowden disease	Brain, breast and prostate cancer
<i>VHL</i>	3p25-26	Von Hippel-Lindau syndrome	Renal cell and pheochromocytoma
<i>WT1</i>	11p13-15	Wilm Tumour	Nephroblastoma

Table 1.7 Tumour suppressor genes involved in familial cancer syndromes and associated sporadic tumours (Thiagalingam *et al.*, 2002).

1.2.3.2 Deletions and tumour suppressor gene inactivation

The other method of identifying tumour suppressor genes has been the detection of regions of homozygous deletion or minimal regions of copy number loss with a mutation in a tumour suppressor gene on the remaining allele. Examples of genes identified by homozygous deletion are *CDKN2A*, *DCC* and *PTEN* (Fearon *et al.*, 1990; Hahn *et al.*, 1996; Kamb *et al.*, 1994; Steck *et al.*, 1997). In each of these examples, cases were also identified where loss of functional gene product was achieved

through LOH and mutation in the remaining allele (Fearon *et al.*, 1990; Hahn *et al.*, 1996; Kamb *et al.*, 1994; Li *et al.*, 1997; Rhei *et al.*, 1997; Steck *et al.*, 1997). Hence, tumour suppressor gene function can be lost by homozygous deletion and by loss of heterozygosity with mutation of the remaining allele, but at the chromosome level this can present as a number of different scenarios (Figure 1.2).

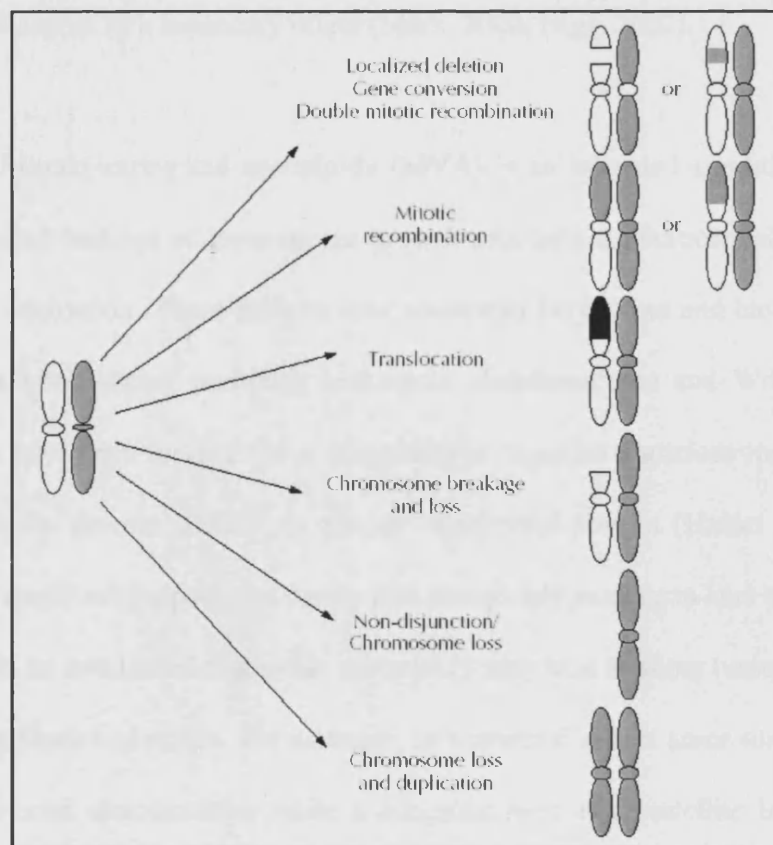


Figure 1.2 Genetic changes accompanying tumour suppressor gene inactivation (Thiagalingam *et al.*, 2002). The loss of heterozygosity by a chromosomal rearrangement accompanied by a point mutation in the remaining allele will lead to loss of tumour suppressor gene function.

1.2.4 Aneuploidy theory of tumorigenesis

Solid tumours commonly have abnormal numbers of chromosomes, termed aneuploidy. Aneuploidy is often accompanied by rearrangements of chromosomes, such as translocations. Aneuploidy can arise from a number of different proposed routes. The main proposed mechanisms start from either the diploid karyotype or the tetraploid karyotype (Storchova and Pellman, 2004). Whilst it is clear that aberrant gene function is involved in carcinogenesis, it has been debated whether aneuploidy is an underlying cause of cancer or a secondary effect (Marx, 2002; Nigg, 2002).

Mosaic variegated aneuploidy (MVA) is an inherited condition associated with the clinical findings of intra-uterine growth retardation, microcephaly (small head) and mental retardation. These patients have aneuploid karyotypes and have an increased risk of developing cancer including leukaemia, rhabdosarcoma and Wilms tumour. These patients have been found to have truncating or missense mutations in *BUB1B*. This gene encodes the protein BUBR1, a mitotic checkpoint protein (Hanks *et al.*, 2004). This genetic condition supports the theory that aneuploidy *per se* can lead to cancer. However, it should be considered that while aneuploidy may lead to some tumours, it might not be a strong feature in others. For example, in colorectal cancer some tumours have marked chromosomal abnormalities while a subgroup with microsatellite instability have few chromosome changes (Abdel-Rahman *et al.*, 2001; Douglas *et al.*, 2004; Jones *et al.*, 2005; Schlegel *et al.*, 1995).

Centrosome abnormalities are also associated with aneuploidy. The centrosome is also known as the microtubule organising centre. It is duplicated only once during the cell cycle. Abnormal number and structure of the centrosome is associated with aneuploidy arising from chromosome mis-segregation (Stearns, 2001). This occurs because during mitosis the genetic material is segregated by the two centrosomes, if there are more than two centrosomes there will be abnormal segregation of DNA. Overexpression of the gene Serine/threonine kinase 15 (*STK15*) (20q13.2) induces centrosome amplification and aneuploidy (Zhou *et al.*, 1998).

1.2.5 Mechanisms of genetic change

Amplified DNA in tumours can be found as double minutes (dmin) or incorporated in DNA as homogeneously staining regions (HSRs) (Schwab, 1999). The mechanism of amplification is not fully understood, but an impression of possible mechanisms can be made from examining the arrangement of the genes within the amplified DNA. The amplicon at 11q13 (Table 1.2) shows tandem duplication, which could have resulted from inter-chromosomal recombination and by unequal sister chromatid exchange (Roelofs *et al.*, 1993). Examination of the arrangement of *MYCN* copies in amplified DNA in neuroblastoma revealed that the gene was arranged in a tandem, head-to-tail order (Amler and Schwab, 1992; Amler *et al.*, 1992). Inverted repeats could result from a breakage-fusion-bridge (BFB) cycle. In this model, if there is a double strand break telomeric to an oncogene, this may result in fusion of sister chromatids. Following fusion of the sister chromatids the two copies of the oncogene are arranged in head-to-tail order. At anaphase the centrosomes are drawn apart, an anaphase

bridge is formed, and this results in another double strand break. If there is unequal distribution of DNA and selection for an oncogene, then on subsequent BFB cycles there is ladder amplification of the oncogene. BFB in a fragile site, FRA7G has been suggested as a mechanism of amplification of the MET oncogene in human gastric carcinoma (Hellman *et al.*, 2002).

1.2.6 DNA repair

DNA mutations can arise through internal cellular factors, such as errors during replication, and by external environmental factors, such as damage by radiation. Whilst there are mechanisms to detect and repair these genetic changes, the genes involved in these mechanisms are themselves prone to mutation and failure of function. There are two classes of DNA repair, excision and recombination. Excision repair is possible when the damage is limited to one strand of the double helix. It involves the removal (excision) of the damaged nucleotide(s) and its replacement by DNA polymerase using the complementary undamaged strand as a template. There are two types of excision repair: base excision - the replacement of a single nucleotide, and nucleotide excision, which involves the replacement of a longer stretch of nucleotides containing the DNA lesion. Recombination repair is used when both strands of a double helix are damaged. Where possible, the cell repairs these double strand breaks by homologous recombination with sequence from the sister chromatid. If a double-strand break is detected in a cell prior to S-phase (before the replication of chromosomes to give sister chromatids), the cell has no template for homologous recombination, and instead repairs the lesion by simply rejoining the broken DNA ends. This is called non-homologous end-joining (NHEJ).

Importantly, this type of repair can lead to sequence deletion. If deletion involves non-coding sequence it may be of no consequence, however at times it may interfere with gene function and be tumorigenic. Another mechanism of DNA repair that is sometimes used during replication occurs when the cell encounters a lesion that has not been repaired by other means and is called trans-lesion synthesis (TLS). This mechanism involves the synthesis of random sequence across a DNA lesion. This process is clearly error prone, however it does allow the cell to complete the process of chromosome replication (Hoeijmakers, 2001; Jackson, 2002). Table 1.8 gives examples of human syndromes where affected individuals have defects in DNA repair mechanisms. Table 1.9 shows possible chromosome rearrangements following double strand breaks and recombination.

Syndrome	Affected maintenance mechanism	Type of genome instability	Cancer predisposition
Xeroderma pigmentosum	NER	Point mutations	Skin cancer
Ataxia telangiectasia	DSB	Chromosome aberrations	Lymphomas
Nijmegen breakage syndrome	DSB	Chromosome aberrations	Lymphomas
BRCA1/BRCA2	HR	Chromosome aberrations	Breast (ovarian) cancer
Werner's syndrome	HR?/TLS	Chromosome aberrations	Various cancers
Bloom syndrome	HR?	Chromosome aberrations	Leukaemia, lymphoma and others
Rothmund-Thompson syndrome	HR?	Chromosome aberrations	Osteosarcoma
HNPCC	MMR	Point mutations	Colorectal cancer

Table 1.8 Human syndromes with defects in DNA repair (Hoeijmakers, 2001).

	One chromosome involved	Two chromosomes involved
One break	Terminal deletion	-
Two breaks	Interstitial deletion Inversion Ring chromosome Duplication/ deletion by sister chromatid exchange	Reciprocal translocation Robertsonian translocation Duplication or deletion by unequal recombination -
Three breaks	Various rearrangements	Inter-chromosomal insertion

Table 1.9 Possible rearrangements following double strand chromosome breaks (Strachan and Read, 1999).

Genetic rearrangements also arise through loss of telomeres. Telomeres are repetitive sequences that cap the ends of chromosomes. The telomeres are synthesised and maintained by a mechanism involving the enzyme telomerase. This mechanism is functional in germ line cells and stem cells. All other cells, which do not have this maintenance mechanism, lose some telomere sequence after they divide. Eventually the telomeres become very short and the cell cycle is arrested. However, in a cancer cell there is aberrant cell cycle control and the cell cycle may not be arrested by short telomeres. In this instance, the ends of the chromosomes that do not have the protective cap of the telomere are seen as double strand breaks and this leads to fusion with other chromosome ends or double strand breaks.

The mechanism of aneuploidy may lead to random copy number changes. However, if the change gives a survival advantage to the cell then the copy number change will be selected and become more prevalent in the cell population. The process of changing the selective pressures on a cell and clonal evolution of cells with genomic instability is demonstrated in two independent studies (Gorre *et al.*, 2001; Sawyers, 2001; Wang *et al.*, 2004). Gorre *et al* studied patients with chronic myeloid leukaemia in blast crisis whose cancer had become resistant to treatment with Gleevec. Gleevec is a receptor tyrosine kinase inhibitor that suppresses BCR-ABL fusion protein signal transduction. Patients with resistance to Gleevec had point mutations in the BCR-ABL and also chromosome duplications and amplifications (Gorre *et al.*, 2001). Similarly, Wang *et al* showed that aneuploid tumours resistant to the anti-cancer drug 5-fluorouracil (5-FU) had amplification of thymidylate synthase (Wang *et al.*, 2004). 5-FU inhibits Thymidylate Synthase in tumours. In both of these instances, the anti-cancer agent is believed to become ineffective by genomic instability giving rise to these cells with a growth advantage and these clones replacing the cells without the growth advantage.

1.2.7 Genome-wide methods of analysis of genetic change

Our understanding of cancer genetics is evolving and is largely dependent on the sensitivity and specificity of the method of analysis. Karyotyping was the main method used to analyse genetic changes in tumours until the 1980s, when restriction fragment length polymorphism (RFLP) was developed (Botstein *et al.*, 1980; Kan and Dozy, 1978). RFLP uses restriction enzymes to cut DNA to obtain DNA fragments, and if a polymorphism (DNA sequence change that does not alter gene function) is present at a

restriction site the enzyme may not cut the DNA. The presence of these polymorphisms generates different sized fragments that can be used to distinguish between DNA in linkage studies. The 1990s witnessed further technical advances, with the extensive use of LOH analysis to determine loss of an allele. Polymorphic alleles of the gene of interest are distinguished with polymerase chain reaction (PCR) based methods.

Fluorescence *in situ* hybridisation (FISH) is a molecular genetic technique where labelled DNA is hybridised to target DNA to obtain information about the target DNA (Pinkel *et al.*, 1986). FISH is used to give positional information as well as copy number information. FISH has been modified in Multiplex-Fluorescence *In situ* Hybridisation (M-FISH) and Comparative Genomic Hybridisation (CGH). M-FISH was first reported in 1996 (Speicher *et al.*, 1996). This technique distinguishes between different chromosomes (or regions of chromosomes) using differentially labelled DNA probes that are hybridised simultaneously. Its power lies in the breadth of information it provides. CGH was developed in the early 1990s and is a method for screening the entire genome for copy number gains and losses (Kallioniemi *et al.*, 1992). This assay is based on the competitive hybridisation of fluorescently labelled test (tumour) and reference (normal) DNA on human metaphase spreads and the subsequent measurement of the fluorescent signals along each chromosome. The relative values for normal and tumour DNA show the positions of copy number changes representing regions of genomic loss and gain. The first report of metaphase CGH demonstrated that the method could detect changes in DNA copy number using fibroblast cell lines that had one to five copies of the X chromosome. Normal female DNA labelled fluorescent red and test DNA labelled

fluorescent green were co-hybridised to metaphase spreads. The fluorescence ratio of the green and red fluorescence on the X chromosome was shown to be proportional to X chromosome copy number ($r=0.978$) (Kallioniemi *et al.*, 1992). The main limitation of conventional CGH is the resolution of detection. For amplifications it is possible to detect regions as small as 2 Mega base-pairs (Mb) but for deletions it is 5-10 Mb. Array CGH is a refinement of metaphase CGH where the target metaphase is replaced with mapped fragments of DNA sequence immobilised on a glass slide (Pinkel *et al.*, 1998; Solinas-Toldo *et al.*, 1997). This important advance will be described in more detail below, but it facilitates significantly improved resolution of detection and more accurate identification of genetic changes.

1.3 Astrocytic gliomas

1.3.1 Description of astrocytic gliomas

Two main cell types in the brain arise from the neural crest, the neural cells and the glial cells. Three types of glial cell are present: astrocytes, which supply nutritional support to neurons, oligodendrocytes, which provide the axonal myelin sheath of neurones, and ependymal cells, which form the lining of the cerebrospinal fluid ventricular system. Unlike neurones, which only have a limited potential to replicate when developed, glial cells retain their proliferative potential (Zhu and Parada, 2002). Glioma is a term used to describe a number of tumour types that appear to have followed distinct lines of differentiation, and include astrocytic gliomas, oligodendrogliomas and ependymal tumours. Although the cell of origin of gliomas is not clearly established, histological analysis suggests that they arise from glial cells, with astrocytes giving rise to astrocytic gliomas, oligodendrocytes to oligodendrogliomas and ependymal cells to ependymal tumours (Table 1.10).

Astrocytic gliomas are divided into four grades, designated I-IV, with grade IV being the most aggressive. The grade of tumour is based on the mitotic index, cellularity, nuclear pleomorphism, nuclear atypia, vascular proliferation and necrosis. This is also supported by immunocytochemistry. Grade I tumours, which are also called pilocytic astrocytomas, have a variable appearance and can be difficult to diagnose histologically. Grade II tumours are identified by a mild increase in cellularity with astrocytes having nuclei with abnormal morphology, being irregular and larger than normal (Figure 1.3 a). Grade III tumours have an increased cellularity and pleomorphism compared to grade II

astrocytic gliomas, but they lack the necrosis and vascular proliferation of the grade IV tumours. The histological hallmarks of grade IV tumours are dense cellularity, necrosis and vascular proliferation (Figure 1.3 b). There are a number of variants of astrocytic glioma grade IV, such as gliosarcoma, which is characterised by sarcomatous differentiation in the tumour vasculature. High-grade astrocytic gliomas are heterogeneous tumours, and each tumour may consist of different histological grades. Therefore a single biopsy may not give an accurate reflection of the tumour.

Suggested cell of origin	Glioma sub-type
Astrocytes	Astrocytic tumours Grade I (Pilocytic astrocytoma) Grade II (Astrocytoma) Grade III (malignant astrocytoma) (Anaplastic) Grade IV (Glioblastoma) (Glioblastoma multiforme)
Oligodendrocytes	Oligodendroglial tumours Oligodendroglioma Anaplastic malignant oligodendroglioma
Ependymal cells	Ependymal tumours Ependymoma Anaplastic (malignant) ependymoma Choroid plexus tumours Choroid plexus papilloma Choroid plexus carcinoma

Table 1.10 Modified WHO classification of gliomas showing the suggested cell of origin (Kleihues *et al.*, 2002).

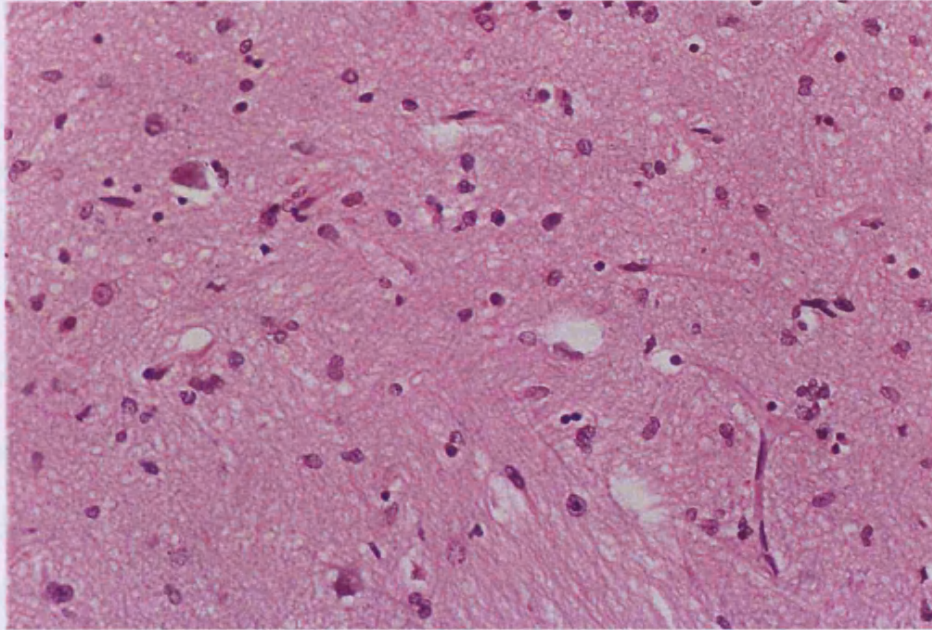


Figure 1.3 a Haematoxylin & Eosin (H&E) section of an astrocytic glioma grade II (x125). There is an increase in cellularity compared to normal brain, and the nuclei are irregular in shape and size.

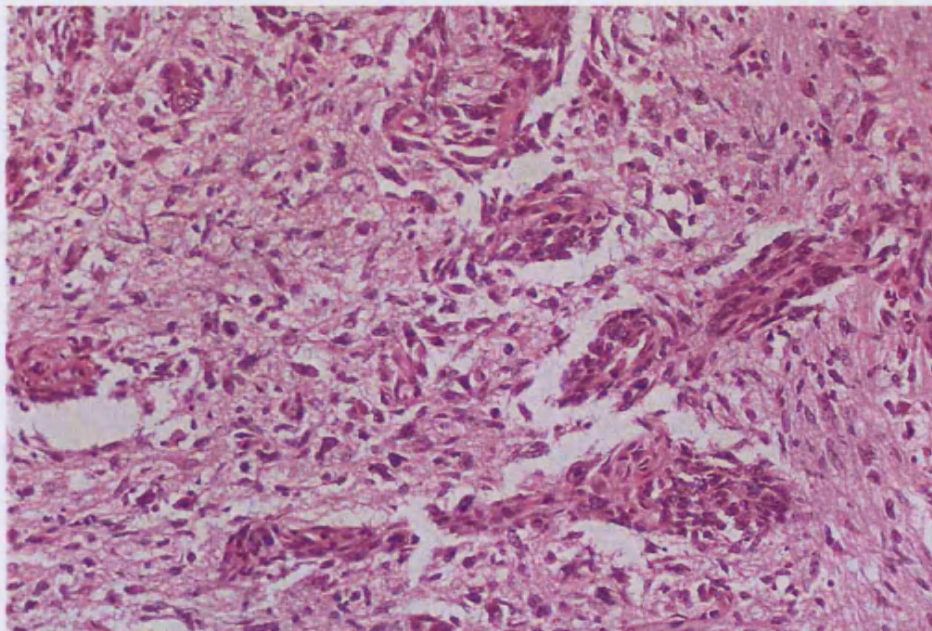


Figure 1.3 b H&E section of astrocytic glioma grade IV (x125). The hallmarks of this grade are dense cellularity and vascular proliferation.

Brain tumours are deeply destructive as, along with physical and psychological disturbance, they also cause impairment in higher cognitive function (Figure 1.4). Astrocytic gliomas are a significant cause of morbidity and mortality affecting all age groups including young adults, being the third most common cause of death from cancer in the age group 18-35 years (Steck *et al.*, 1997). Astrocytic gliomas, grade I, occur in children and the patients have a relatively good prognosis, tending not to progress to higher-grade tumours. Grade II tumours follow a relatively benign course. However, 70% progress to a grade IV tumour within 5-10 years (Kleihues *et al.*, 2002). Patients with grade III tumours can survive two to three years, but the majority of patients with astrocytic glioma grade IV die within a year, with only 10% surviving two years (Bleehen and Stenning, 1991).

Surgery, radiotherapy and chemotherapy are the main treatment modalities used in astrocytic gliomas. Astrocytic gliomas diffusely infiltrate normal brain tissue, hence complete surgical resection is not possible. Surgery may be used to reduce the size of the tumour (debulking surgery) to alleviate the patient's symptoms. To minimise neurological deficit, surgery is largely confined to patients with tumours in the frontal and temporal lobes. However, surgical biopsy remains useful for diagnostic purposes. Grade II tumours can be slow growing and clinical presentation depends on the anatomical location. If the tumour is slow growing and is having no impact on the patient, a policy of 'watch and wait' may be undertaken. If the patient becomes symptomatic, surgical intervention and radiotherapy are considered. Grade III tumours

are more aggressive and if possible, are treated with debulking surgery followed by radiotherapy. Chemotherapy can be considered either concurrently with radiotherapy or on relapse. Grade IV tumours are treated if possible, with debulking surgery followed by radiotherapy with or without concurrent chemotherapy. Palliative chemotherapy is beneficial to some patients (Table 1.11).

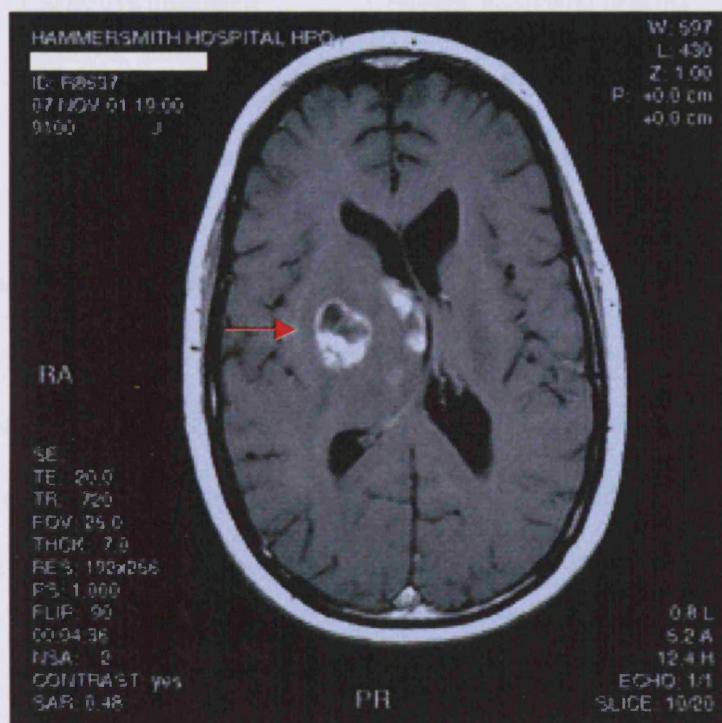


Figure 1.4 MRI scan of a patient with astrocytic glioma.

This patient had multiple astrocytic gliomas of different grades. One of the tumours is demonstrated in this MRI slice. The tumour (marked with red arrow) is enhanced by contrast and has a heterogenous appearance. This tumour is in the region of the right basal ganglia and is an astrocytic glioma grade II (shown in Figure 1.3 a).

Agent	Therapeutic action	Side-effect profile
Nitrosoureas	Alkylating agent	Myelosuppression, nausea
Temozolomide	Alkylating agent	Myelosuppression nausea
Irinotecan	Topoisomerase I inhibitor	Myelosuppression, diarrhoea, nausea
Thalidomide	TNF α inhibition, Anti-angiogenic	Peripheral sensory neuropathy, sedation
Carboplatin	DNA cross-links	Myelosuppression nausea, peripheral sensory neuropathy
Tamoxifen	Selective oestrogen receptor modulator	Nausea, peripheral oedema

Table 1.11 Conventional chemotherapeutic agents used in high-grade gliomas

1.3.2 Genetic aberrations in astrocytic gliomas

A few genes and biochemical pathways have been identified as being involved in astrocytic gliomas, and in particular p53, RB and growth factor receptor tyrosine kinases. This section reviews the genetic aberrations that have been identified from analysis of family syndromes and loss of heterozygosity studies.

1.3.2.1 Family syndromes

Identification of the genetic defect in hereditary cancer syndromes can give an insight into the genetic aetiology of sporadic tumours. Astrocytic gliomas are usually sporadic, but certain syndromes have germ-line mutations that confer an increased risk of developing these tumours (Table 1.12). However, they are not a direct parallel as the presence of a genetic defect in a family syndrome, which is associated with an astrocytic glioma, does not necessarily indicate that the same genetic defect will be present in a sporadic tumour. Patients with the Li Fraumeni syndrome have genetic defects in *p53*,

and this predisposes to many tumour types including astrocytic gliomas (Li *et al.*, 1995). Neurofibromatosis types 1 and 2 both predispose to astrocytic glioma (Listernick *et al.*, 1999). Turcot's syndrome B is associated with colorectal cancer (tumours are typical of hereditary non-polyposis colorectal cancer (HNPCC) with defects in mis-match repair machinery) and astrocytic glioma (Hamilton *et al.*, 1995).

Genetic condition	Gene	Location	Involved in sporadic tumour
Li Fraumeni	<i>p53</i>	17p13.1	Yes
Melanoma-astrocytoma syndrome	<i>CDKN2A</i>	9p21	Yes
Neurofibromatosis 1	<i>NF1</i>	17q11.2	No
Neurofibromatosis 2	<i>NF2</i>	22q12.2	No
Tuberous sclerosis	<i>TS1</i>	9q34	No
	<i>TS2</i>	16p13.3	No
Turcot's syndrome B	<i>MLH1</i>	3p21.3	No
	<i>PMS2</i>	7p22	No

Table 1.12 Summary of genetic predisposition syndromes associated with astrocytic gliomas. The aberrant genes in Li Fraumeni and melanoma-astrocytoma syndrome (*p53* and *CDKN2A* respectively) are also mutated in sporadic tumours. However, this is not the case in Neurofibromatosis, Tuberous sclerosis and Turcot's syndrome B.

1.3.2.2 Studies examining genetic changes in astrocytic gliomas

A number of studies have examined copy number changes in astrocytic gliomas using a range of analytical tools including karyotyping (Olopade *et al.*, 1992; Thiel *et al.*, 1992), RFLP (Fults *et al.*, 1990; Liang *et al.*, 1994; Ransom *et al.*, 1992), microsatellite markers (MSM) for LOH (Balesaria *et al.*, 1999; Miyakawa *et al.*, 2000; Ransom *et al.*, 1992; Saitoh *et al.*, 1998), conventional CGH (Brunner *et al.*, 2000; Mohapatra *et al.*, 1998), and low resolution array CGH (Hui *et al.*, 2001).

1.3.2.2.1 Regions of LOH or copy number loss

While a large number of genetic changes have been described in high-grade astrocytic gliomas, some consistent findings have emerged, including loss of 6q (Table 1.13) (Liang *et al.*, 1994; Miyakawa *et al.*, 2000; Mohapatra *et al.*, 1998; Saitoh *et al.*, 1998; Thiel *et al.*, 1992).

Chromosome breakpoints or allele loss have been detected in high-grade astrocytic gliomas involving 9p (Olopade *et al.*, 1992; Ransom *et al.*, 1992; Thiel *et al.*, 1992) (Mohapatra *et al.*, 1998) and chromosome 10 (Balesaria *et al.*, 1999; Brunner *et al.*, 2000; Fults *et al.*, 1990; Mohapatra *et al.*, 1998; Ransom *et al.*, 1992; Thiel *et al.*, 1992). Several tumour suppressor genes have been identified as a result of these studies, in particular *CDKN2A* and *PTEN*, on chromosomes 9 and 10 respectively (Table 1.14). No tumour suppressor gene has been identified on 6q in astrocytic gliomas.

Chromosome	MSM flanking loss	Position (Mb)
6q16.1-6q16.3	D6S275-D6S434	93.01-102.3
6q22.1-6q22.31	D6S1563-D6S407	105.5-128.47
6q24.1-6q24.2	D6S292-D6S441	135.93-153.37
6q25.2-6q25.3	D6S441-D6S437	153.37-158.2
6q26-6q27	D6S1599-D6S297	162.2-166.59

Table 1.13 Regions of LOH on chromosome 6 in astrocytic gliomas. The location refers to the nucleotide position of the gene locus in Mega base pairs (Mb), where the nucleotides are listed in order from the distal end of the short arm to the distal end of the long arm (Miyakawa *et al.*, 2000).

Gene symbol	Gene name	Cytogenetic location	Location (Mb)
<i>p53</i>	Tumour protein p53	17p13	7.5
<i>CDKN2A</i>	Cyclin dependent kinase inhibitor 2A	9p21	22
<i>RB</i>	Retinoblastoma	13q14.1-q14.2	47.8
<i>PTEN</i>	Phosphatase and tensin homologue	10q23-24	89.6
<i>DMBT1</i>	Deleted in malignant brain tumours 1	10q26.13	124.3
<i>MDM2</i>	Mouse double minute homologue 2	12q15	67.5

Table 1.14 Tumour suppressor genes identified in astrocytic gliomas.

1.3.2.2.2 Regions of genetic gain

Gains of chromosome arm 7p (Brunner *et al.*, 2000; Mohapatra *et al.*, 1998; Thiel *et al.*, 1992) and chromosome 20 (Brunner *et al.*, 2000; Mohapatra *et al.*, 1998) have been noted in astrocytic glioma grade IV. *EGFR* has been identified as an oncogene on 7p but no target gene has been identified on chromosome 20 (Table 1.15).

Gene symbol	Gene name	Cytogenetic location	Location (Mb)
<i>EGFR</i>	Epidermal growth factor receptor	7p11.2	54.9
<i>ROS1</i>	V-ROS avian UR2 sarcoma virus oncogene homologue 1	6q22.1	117.7
<i>PDGFR</i>	Platelet derived growth factor receptor	4q12	54.9
<i>VEGFR</i>	Vascular endothelial growth factor receptor	4q12	54.9
<i>CDK4</i>	Cyclin dependent kinase 4	12q14.1	56.4

Table 1.15 Oncogenes identified in astrocytic gliomas.

1.3.2.2.3 Translocations

It has been suggested that critical genes at translocation breakpoints may be involved in development of astrocytic gliomas (Chernova *et al.*, 2001; Chernova *et al.*, 1998; Krex *et al.*, 2002). In one case report, three short-term cultures were derived from three tumours isolated from a patient with multifocal astrocytic glioma grade IV (Krex *et al.*, 2002). Molecular genetic analysis revealed a consistent translocation t(1;15)(p3?6;q2?5) in all three cell cultures. Chernova *et al* described a translocation, t(10;19)(q25-26;13) in cell line CRL1620 (A172) (Chernova *et al.*, 1998). This translocation involved two genes, *WDR11* located at 10q25-26 and *ZNF320* at 19q13, and generated a transcript that encodes a truncated WDR11 (Chernova *et al.*, 2001).

1.3.2.3 Molecular pathways

The aberrations detected in astrocytic gliomas have been diverse and seemingly inconsistent. However, when genetic aberrations are placed into molecular pathways, it can be seen that key molecular pathways controlling cell growth and apoptosis are involved in these tumours but may be abrogated at different steps. Key pathways found to be involved in astrocytic gliomas include receptor tyrosine kinase signalling pathways, especially the EGFR, and the p53 or Rb pathways.

Tyrosine kinases are signalling molecules within the cell, which act by phosphorylating tyrosine residues on proteins. There are approximately ninety tyrosine kinases, of which 58 are receptor tyrosine kinases, which have 20 sub-families, and 32

are non-receptor tyrosine kinases (Robinson *et al.*, 2000). Receptor tyrosine kinase genes that have been implicated in gliomas include *EGFR*, *PDGFR*, *ROS1* and *VEGFR*.

EGFR is a transmembrane receptor tyrosine kinase that is activated by binding of ligands including transforming growth factor alpha and epidermal growth factor. *EGFR*, located at 7p11-12, is amplified in 40% of astrocytic glioma grade IV tumours and is overexpressed in 80-90 percent of gliomas (von Deimling *et al.*, 1992b). *EGFR* can acquire gain of function through DNA amplification and/or DNA mutation. Approximately half of the cases with *EGFR* amplification have a mutation. These mutations encode a truncated receptor, which has lost some of its extracellular domain (Figure 1.5). The mutated receptor is not able to bind its ligand but is constitutively active (Ekstrand *et al.*, 1994; Ekstrand *et al.*, 1992; Nishikawa *et al.*, 1994; Wong *et al.*, 1987). Ekstrand *et al* found deletions in the ligand-binding domain and within the Ca^{2+} regulatory/ internalisation domain and inhibitory domain (Ekstrand *et al.*, 1992). This group found no mutations in the *EGFR* receptors that were not amplified. Bigner *et al* found that *EGFR* amplification is associated with increased RNA expression (Bigner *et al.*, 1987).

Receptor tyrosine kinases signal through PI3K to phosphorylate PIP2 to PIP3 (Figure 1.6). The balance between PIP2 and PIP3 is maintained by PI3K and PTEN (Ramaswamy *et al.*, 1999). PIP3 signals through AKT/PKB pathway to phosphorylate Forkhead in Rhabdomyosarcoma-like 1 (FKHRL1) (6q21, 108.9Mb) at Ser256. Phosphorylated FKHRL1 promotes cell survival and dephosphorylated FKHRL1

promotes apoptosis through a Fas ligand. Loss of functional PTEN leads to increased activity of AKT/PKB. Many astrocytic glioma grade IV have no wild-type *PTEN* or they have aberrations involving other components of the AKT signal transduction pathway (Knobbe and Reifenberger, 2003). Wang *et al* found that of 15/34 (44%) astrocytic gliomas grade IV examined had a mutation in the sequence of *PTEN* (Wang *et al.*, 1997). Fan *et al* detected *PTEN* mutations in 6/22 (27%) (2 homozygous deletions and 4 point mutations) astrocytic gliomas grade IV (Fan *et al.*, 2002).

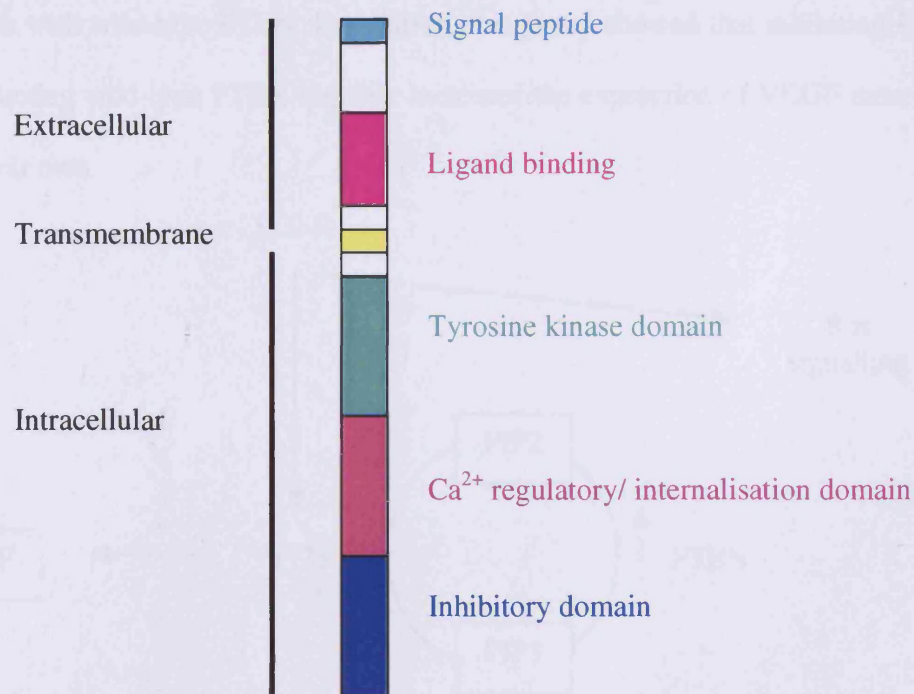


Figure 1.5 Functional domains of EGFR protein (Ekstrand *et al.*, 1992).

Other tyrosine kinases involved in astrocytic glioma include vascular endothelial growth factor (VEGF) and its receptor VEGFR and platelet derived growth factor (PDGF-B) and its receptors (Carmeliet and Jain, 2000; Ferrara, 2002). A relationship between VEGF, EGFR and PTEN has been established in high-grade astrocytic glioma

cell lines (Figure 1.6). Maity *et al* showed that inhibition of EGFR signalling by a truncated protein causes a decrease in VEGF mRNA levels (Maity *et al.*, 2000). Pore *et al* showed this was a PI3K pathway dependent effect, by transfecting wild-type PTEN into cell lines with mutant PTEN (U87 and U251), which caused a decrease in VEGF mRNA and an increase in phosphorylated AKT (Pore *et al.*, 2003). They proposed that EGFR activation and PTEN mutation co-operate through the PI3K pathway to increase VEGF mRNA levels. VEGF promoter activity was decreased by a PI3K inhibitor or by transfection with wild-type PTEN. In addition, this group showed that inhibiting EGFR and introducing wild-type PTEN together increased the expression of VEGF more than each on their own.

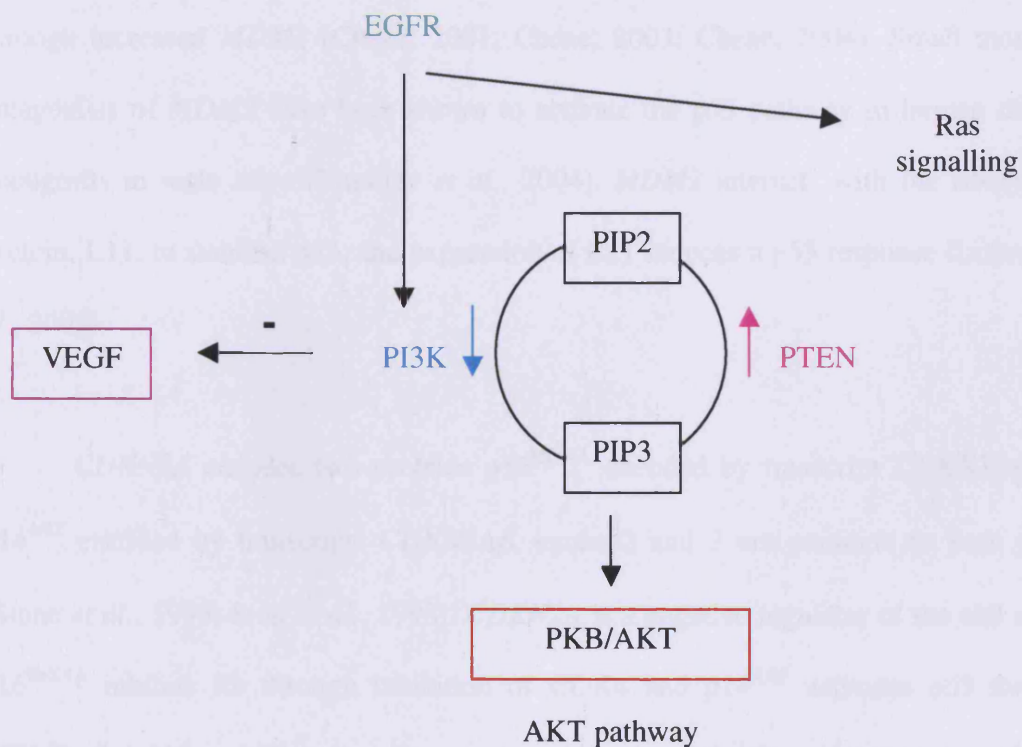


Figure 1.6 EGFR signalling pathway through PI3K. PI3K phosphorylates PIP2 to the active PIP3, while PTEN dephosphorylates PIP3. PIP3 promotes cell survival through the AKT pathway.

The majority of astrocytic glioma grade IV tumours show disruption of the p53 and retinoblastoma (RB) pathways arising from aberrations of genes such as *p53*, mouse double minute homologue 2 (*MDM2*), *RB*, cyclin dependent kinase 4 (*CDK4*), or cyclin dependent kinase inhibitor 2A (*CDKN2A/INK4A*) (Ichimura *et al.*, 1996). Each tumour generally has only one aberration from within each of the p53 or RB pathways (Ichimura *et al.*, 2000) (Collins, 2002). Loss of chromosome arm 17p was found in 40% of astrocytic gliomas grade II and III (von Deimling *et al.*, 1992a). This is associated with mutation in the remaining allele of *p53*. Loss of functional p53 within tumours can occur through p53 mutation, or the cell may have a molecular defect that limit activation of p53 or reduce response to p53 (Vousden, 2000). p53 can be down-regulated in tumours through increased *MDM2* (Chene, 2001; Chene, 2003; Chene, 2004). Small molecule antagonists of *MDM2* have been shown to activate the p53 pathway in human tumour xenografts in nude mice (Vassilev *et al.*, 2004). *MDM2* interacts with the ribosomal protein, L11, to stabilise p53, and expression of L11 induces a p53 response (Lohrum *et al.*, 2003).

CDKN2A encodes two proteins p16^{INK4A} encoded by transcript *CDKN2Aα* and p14^{ARF} encoded by transcripts *CDKN2Aβ*, exons 2 and 3 are common to both genes (Stone *et al.*, 1995; Stott *et al.*, 1998). *CDKN2A* is a negative regulator of the cell cycle, p16^{INK4A} inhibits Rb through inhibition of CDK4 and p14^{ARF} activates p53 through *MDM2* inhibition. Changes can occur in any of the components of the p14^{ARF}/*MDM2*/p53 pathway (Ichimura *et al.*, 2000). *CDKN2B* encodes p15 and this does not appear to be mutated in glioma (Schmidt *et al.*, 1997).

1.3.2.4 Genetic aberrations in different grades of astrocytic glioma

It is not possible to distinguish between astrocytic glioma grade IV tumours by histopathology. However, it is emerging that these tumours may be sub-classified using certain clinical features and genetic aberrations present in the tumour (Maher *et al.*, 2001) (Figure 1.7). Some astrocytic gliomas grade IV appear to arise *de novo*, while others appear to arise by progression from lower grade astrocytic gliomas (Kleihues and Ohgaki, 1999). Patients with *de novo* astrocytic glioma grade IV have a mean age of 55 years while secondary astrocytic glioma grade IV tends to occur in patients less than forty-five years old (Kleihues and Cavenee, 2000). However, while both forms have aberrations of both the p53 and the RB pathways, they differ in the targeted genes that code for the components of these pathways (Biernat *et al.*, 1995; Watanabe *et al.*, 1996). Primary astrocytic glioma grade IV tumours arise *de novo* and tend to have EGFR amplification and no *p53* mutation (Maher *et al.*, 2001; Watanabe *et al.*, 1997). Astrocytic glioma grade IV tumours arising through progression from lower grades also have a lower incidence of *PTEN* mutation and amplification of *EGFR* (Tohma *et al.*, 1998), and have higher expression of *PDGFRA* (Hermanson *et al.*, 1992).

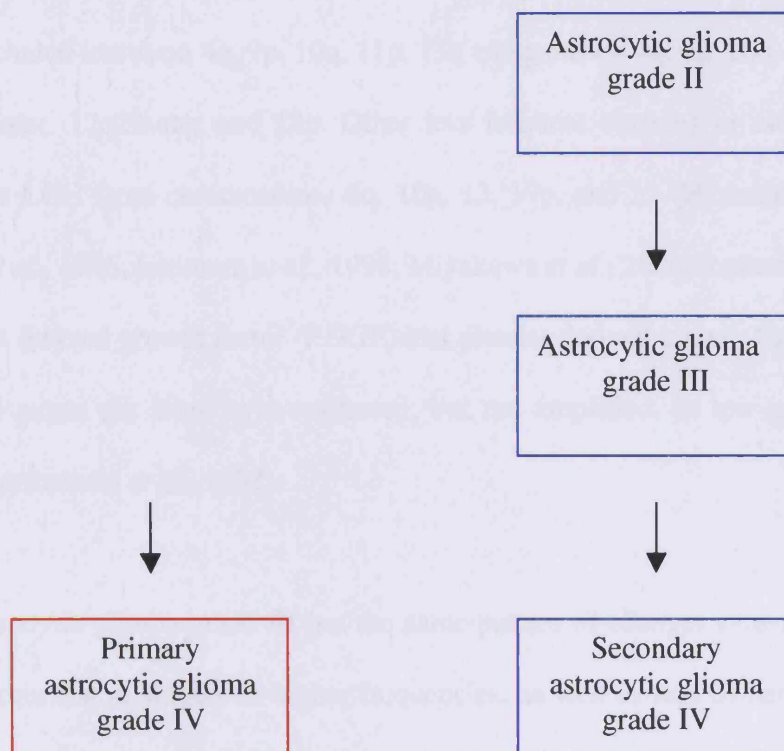


Figure 1.7 Proposed paths to the development of astrocytic glioma grade IV. Astrocytic glioma grade IV has been sub-classified into two groups, primary and secondary astrocytic glioma grade IV.

Distinctive genetic aberrations have been described in the different grades of adult astrocytic gliomas (Collins, 1999). Grade I tumours have had no consistent genetic abnormality identified (Bigner *et al.*, 1997; James *et al.*, 1990). One study examined grade II tumours and the corresponding higher-grade tumour on tumour recurrence in 15 patients (Weber *et al.*, 1996). Five of the patients had an oligodendroglioma, 10 of them were astrocytic glioma grade II, 5 developed into astrocytic glioma grade III and 5 developed into astrocytic glioma grade IV. Changes found in the astrocytic glioma grade

II included loss of Xp and 5p and gain of 8q, 19p and 12p. Progression associated changes included losses on 4q, 9p, 10q, 11p, 13q and gains on 1q, 6p, 20q, 12p13, 13q32-q34, 7q31-qter, 12q22-qter and 18p. Other less frequent changes in astrocytic glioma grade II are LOH from chromosomes 6q, 10p, 13, 17p, and 22 (Hartmann *et al.*, 2004; Ichimura *et al.*, 1996; Ichimura *et al.*, 1998; Miyakawa *et al.*, 2000; Rasheed *et al.*, 2002). The platelet derived growth factor (*PDGF*) and platelet derived growth factor receptor A (*PDGFRA*) genes are often over-expressed, but not amplified, in low-grade astrocytic gliomas (Hermanson *et al.*, 1992).

Astrocytic glioma grade III has the same pattern of changes as astrocytic glioma grade II, occurring at similar or higher frequencies, as well as loss of heterozygosity on 19q, and 10q, or mutation of the *PTEN* gene (Ichimura *et al.*, 1998; Rasheed *et al.*, 2002; von Deimling *et al.*, 1994). More than 90% of astrocytic gliomas grade IV have LOH of chromosome 10, including *PTEN* (Ichimura *et al.*, 1998; Schmidt *et al.*, 1999).

1.3.2.5 Genetic changes and prognosis

Several reports have suggested that particular genetic changes in high-grade astocytic gliomas are associated with a poorer prognosis (loss of 6q, 10q, and gain of 19q) or with better survival (loss of 19q) (Balesaria *et al.*, 1999; Burton *et al.*, 2002). Abnormalities of the genes coding for proteins in the retinoblastoma pathway (*CDKN2A*, *CDKN2B*, *CDK4* and *RB*) in combination with loss of both wild-type *PTEN* alleles are associated with shorter patient survival (Backlund *et al.*, 2003).

1.4 Aims of this research

The aim of this research is to define the key genetic changes that are pertinent to the development and survival of astrocytic gliomas. The approach taken is to utilise array CGH to identify copy number changes in high-grade astrocytic gliomas. However, as array CGH is a new analytical tool, further consideration of its advantages and limitations is necessary. Hence, three key aims are studied in this thesis:

- I The development of a comprehensive assessment tool for high-resolution array CGH (Chapter 3).
- II The analysis of high-grade astrocytic glioma cell lines and patient samples in order to identify DNA copy number changes (Chapter 4).
- III The use of FISH to explore the relationship between copy number changes identified by array CGH and translocations identified by M-FISH (Chapter 5).

The study strategy (Figure 1.8) views cell lines and patient samples as separate model systems. Similar analytical techniques will be applied to both sets of samples and the findings compared.

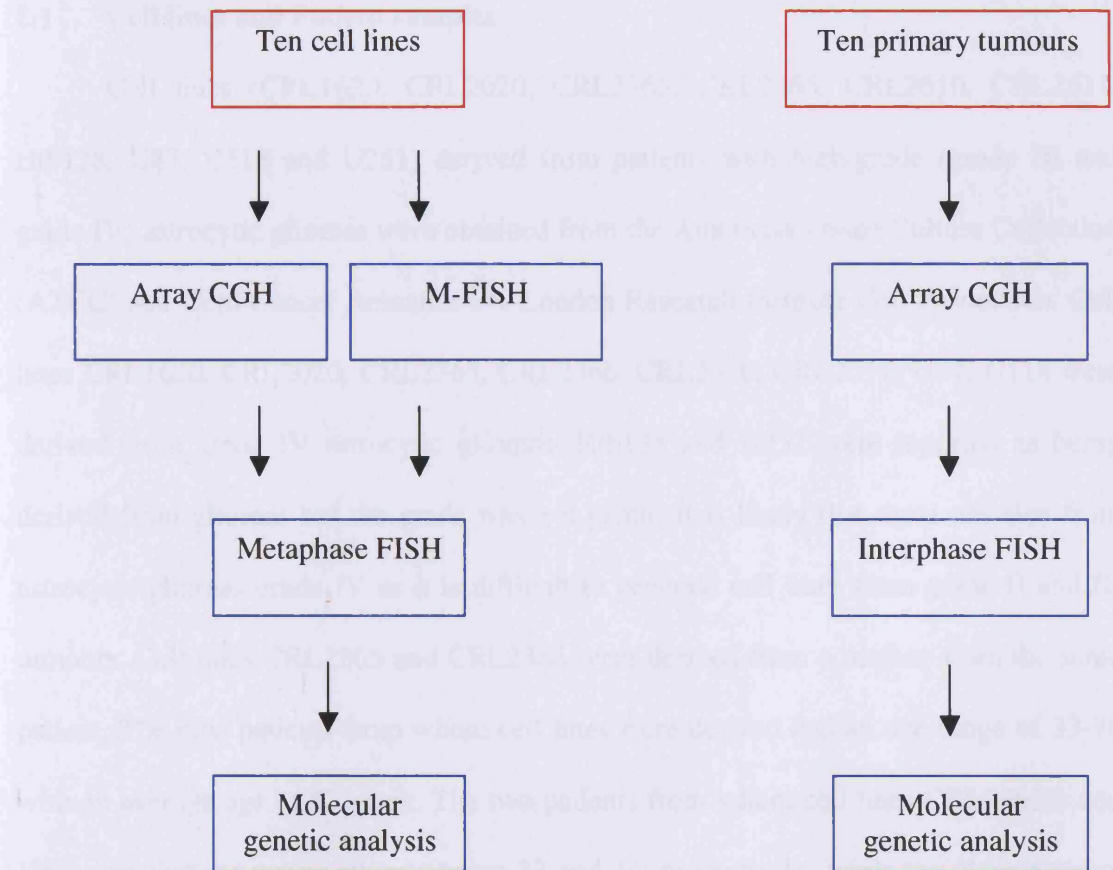


Figure 1.8 Strategy of the study

Chapter Two

Materials and Methods

2.1 Cell lines and Patient samples

Cell lines (CRL1620, CRL2020, CRL2365, CRL2366, CRL2610, CRL2611, Htb138, U87, U118 and U251) derived from patients with high-grade (grade III and grade IV) astrocytic gliomas were obtained from the American Tissue Culture Collection (ATCC) and from Cancer Research UK London Research Institute Cell Production. Cell lines CRL1620, CRL2020, CRL2365, CRL2366, CRL2610, CRL2611, U87, U118 were derived from grade IV astrocytic gliomas. Htb138 and U251 were reported as being derived from gliomas but the grade was not given. It is likely that these are also from astrocytic gliomas grade IV as it is difficult to generate cell lines from grade II and III tumours. Cell lines CRL2365 and CRL2366 were derived from a tumour from the same patient. The nine patients from whom cell lines were derived had an age range of 33-76 with an average age of 57 years. The two patients from whom cell lines CRL2365/6 and U87 were derived were younger, being 33 and 44, respectively, while the older patients were 50-76 (Table 2.1).

Cell line	Sex	Age	Prior treatment
CRL1620	M	53	NA
CRL2020	F	59	Treated chemotherapy and radiotherapy
CRL2365	M	33	Untreated
CRL2366	M	33	Untreated
CRL2610	M	65	NA
CRL2611	F	60	NA
Htb138	M	76	NA
U87	F	44	NA
U118	M	50	NA
U251	M	75	NA

Table 2.1 Cell lines used in the study

The patient samples were selected from a tissue bank in the Department of Pathology, University of Cambridge. The samples, T1-T10 were obtained from patients treated in Karolinska Hospital, Stockholm, Sweden. The samples were taken from the patients prior to treatment with radiotherapy or chemotherapy. DNA was obtained from Professor V.P. Collins, Department of Pathology, University of Cambridge. Professor Collins had previously worked in Sweden where the patients were treated. Ethics approval for use of the patient samples in this study were obtained from the Ethics Committee of Karolinska Hospital, Stockholm, Sweden (No. 91:16) and Cambridge Local Research Ethics Committee, Cambridge, UK (Ref. LREC 03/115). There were six males and four female patient samples. The age range was 55-78 with a mean age of 62.4 years (Table 2.2).

Patient ID	Sex	Age
T1	F	59
T2	F	78
T3	F	55
T4	M	71
T5	M	59
T6	M	60
T7	M	68
T8	F	56
T9	M	62
T10	M	56

Table 2.2 Demographics of patients whose astrocytic glioma grade IV samples were used in the study

Control DNA was extracted from blood samples volunteered from co-workers at Cancer Research UK London Research Institute.

2.2 DNA extraction

DNA extraction from blood and cells was performed using the QIAGEN QIAmp DNA blood maxi kit, with the protocol modified to extract DNA from cell lines. A medium-sized flask (T75) for cell culture contains approximately 0.6×10^7 cells. The cells were treated with trypsin, washed in phosphate-buffered saline (PBS) and suspended in 10 mls of PBS. From this stage the same protocol was followed for 10 mls blood and for the cells in 10 mls of PBS. Cell lysis was achieved by the addition of 500 μ l of proteinase K and 12 mls of buffer AL, followed by vortexing the sample 3 times for 5 seconds for

adequate mixing, and incubating at 70°C for 10 minutes. 10 mls of absolute ethanol was added, and the mixture vortexed to precipitate the DNA. Half the solution was then added to the QIAmp maxi column and centrifuged for 3 minutes at 1850 x g. The filtrate was discarded, and the remainder of the solution added to the QIAmp maxi column and centrifuged at 1850 x g for 3 minutes. As before, the filtrate was discarded. Five mls of buffer AW1 was then added to the QIAmp maxi column which was centrifuged at 4,500 x g for 1 minute. Five mls of buffer AW2 was then added and centrifuged at 4,500 x g for 15 minutes. The column was then placed inside a clean collecting tube, and 1ml of distilled water added and left to equilibrate for 5 minutes. The column was then centrifuged at 4,500 x g for 5 minutes. The filtrate was then re-loaded into the QIAmp column, again left for 5 minutes and centrifuged at 4,500 x g for 5 minutes. The concentration of the DNA in the filtrate was estimated using a spectrophotometer and stored at -20°C.

2.3 Metaphase CGH

CGH is a method for screening an entire genome for gains and losses of DNA. The CGH assay is based on the competitive hybridisation of fluorescently labelled test (tumour) and reference (normal) DNA onto human metaphase spreads and the subsequent measurement of the fluorescent signals along each chromosome. The relative values for normal and tumour DNA show the positions of the genomic losses and gains. Conventional CGH was performed using human metaphases from a normal male, broadly following standard methods (Kallioniemi *et al.*, 1992).

The probes were labelled directly by nick translation. One μg of each probe DNA was mixed on ice with 5 μl of nick translation buffer (10x nick translation buffer: 0.2 mM dATP, 0.2 mM dCTP, 0.2 mM dGTP in 500 mM Tris-HCl pH 7.8, 50 mM MgCl_2 , 100 μM ME, 100 μl BSA) and distilled water to make up the total volume to 50 μl , with 1 μl of FITC-12-dUTP or Texas Red-5-dUTP, 10 μl of DNA polymerase/DNase mix and 1 μl of DNA polymerase I. The reaction mixture was incubated at 16°C for 2 hours (or until the labelled fragments were 500-2000 base-pairs). The mixture was stored on ice while 5 μl of the mixture was run on a 1% agarose gel to measure the size of the labelled fragments. When the fragments were the appropriate size, 2 μl of EDTA was added and the mixture heated to 70°C for 5 minutes to denature the enzymes. The probes were then stored at -20°C until ready for hybridisation.

Labelled test (1 μg) and control (1 μg) DNA were mixed with 50 μl of human Cot1 DNA (1mg/ml), 0.1 volume of 3M sodium acetate and two volumes of absolute alcohol. The Cot1 DNA was added to inhibit the binding of labelled DNA to repetitive sequences in the target DNA (Kallioniemi *et al.*, 1992). The mixture was then placed onto dry ice for 30 minutes to precipitate the DNA. The mixture was centrifuged at 13,000 rpm for 15 minutes and the supernatant aspirated. The DNA pellet was air dried, re-suspended in 5 μl of deionised formamide and incubated at 37°C for 30 minutes. 5 μl of 2x hybridisation buffer (20% dextran sulphate, 4x SSC pH 7.0) was added and mixed. The DNA was then denatured at 75°C for 5 minutes and incubated for 1 hour at 37°C. During this incubation the target metaphases on the slide (Vysis) were denatured by placing the slide into 50mls of denaturation solution (70% deionised formamide, 2x SSC pH 7.0) heated to 73°C in a

water bath for 4 minutes. The slide was then placed in an ethanol series (70% ethanol (4°C), 95% ethanol and absolute ethanol, each for 2 minutes) to dehydrate the metaphases, and the slide then dried in air. Once the probe had incubated for an hour, the slide was placed on a hot plate (37°C) and 10µl of denatured probe applied to the area of the slide with the denatured metaphases. A 22 x 22 mm coverslip was placed over the target area, and rubber sealant applied to seal the edges. The slides were placed in a humidified chamber and incubated for 72 hours at 37°C.

Post-hybridisation, in low lighting conditions, the rubber cement and coverslip were removed and the slide was taken through a series of washes, 3 x 5 minutes in 50% formamide, 2 x SSC pH 7.0, then 3 x 5 minutes in 2 x SSC pH 7.0. These washes were performed in a Coplin jar placed in a shaking waterbath at 37°C. This was followed by a 5 minute wash in SSCT (4 x SSC, 0.05 % Tween 20 pH 7.0). The metaphases on the slide were then dehydrated in a further ethanol series. The slides were air-dried, 30µl of mounting solution applied (DAPI, Citfluor and antifade), and covered with a 22 x 50 mm coverslip.

Images were captured using a Zeiss Axioplan epifluorescence microscope equipped with a Photometrics KAF 14500-500 cooled charge-coupled device (CCD) camera and triple colour epifluorescence filter (selective for DAPI, FITC and rhodamine) connected to an Apple G3 computer. The image analysis was performed using software from QUIPS™. The automated karyotyping was checked manually.

To define the fluorescence ratio levels for CGH, DNA from a normal male and female were used in control experiments. The fluorescence from each metaphase was captured (Figure 2.1). In these experiments, male DNA labelled with Texas Red and female DNA labelled with FITC were co-hybridised onto normal metaphases. The images were captured using different filters specific for DAPI, Texas Red and FITC. Panel A shows the DAPI counterstain. Panel B shows the inverted DAPI image with the classical G banding pattern. Panel C shows the Texas Red image. Panel D shows the FITC image. Panel E shows the composite CGH image in which the Y chromosome can be seen excessively red and the X chromosome is excessively green. The data in panel E are then collated to give the composite representation (Figure 2.2). The threshold was selected so that there were no changes detected on the autosomes. The threshold was set at gain if the ratio was greater than 1.1 and at loss if the ratio was less than 0.9.

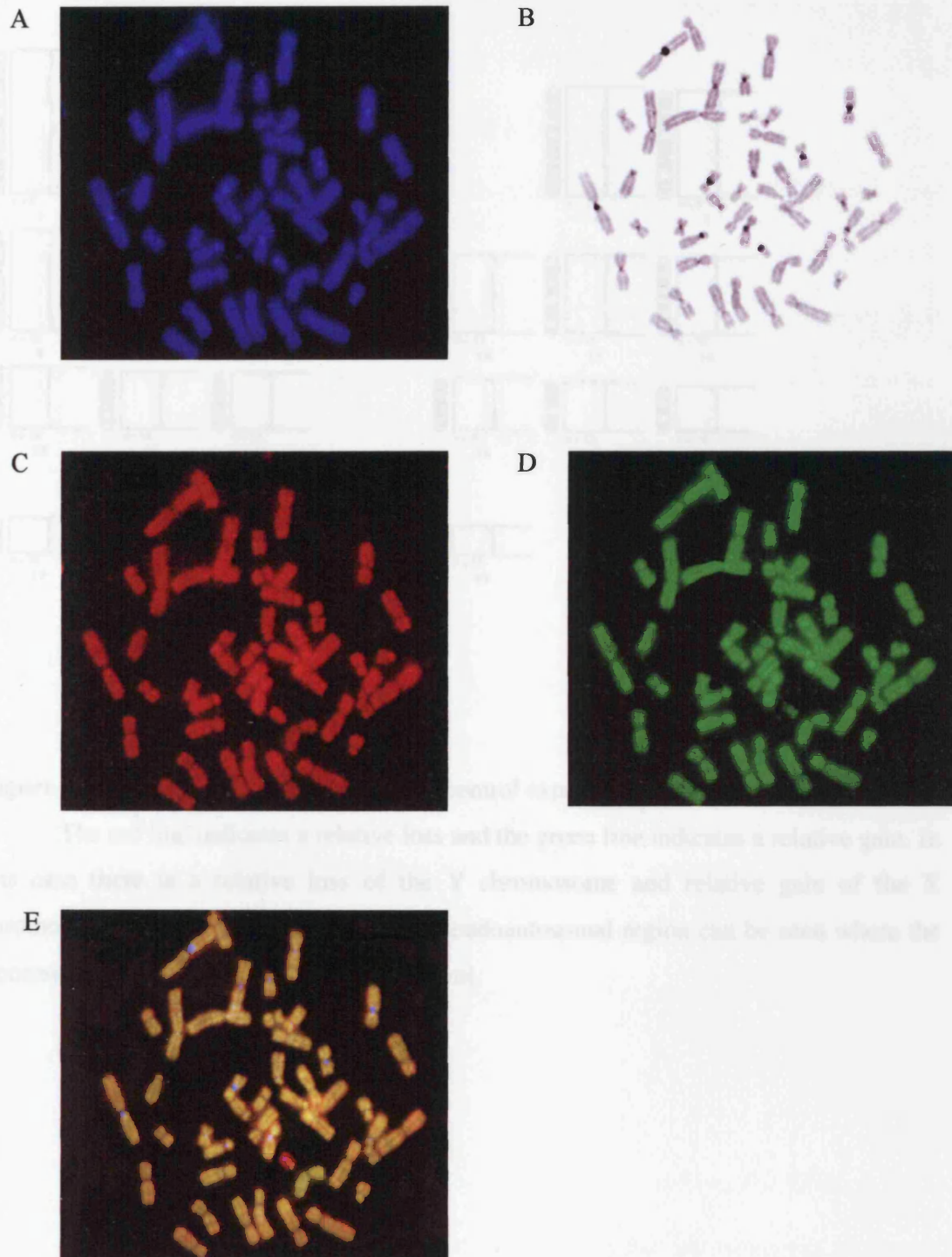


Figure 2.1 Composite images showing the same metaphase in a male versus female CGH control experiment

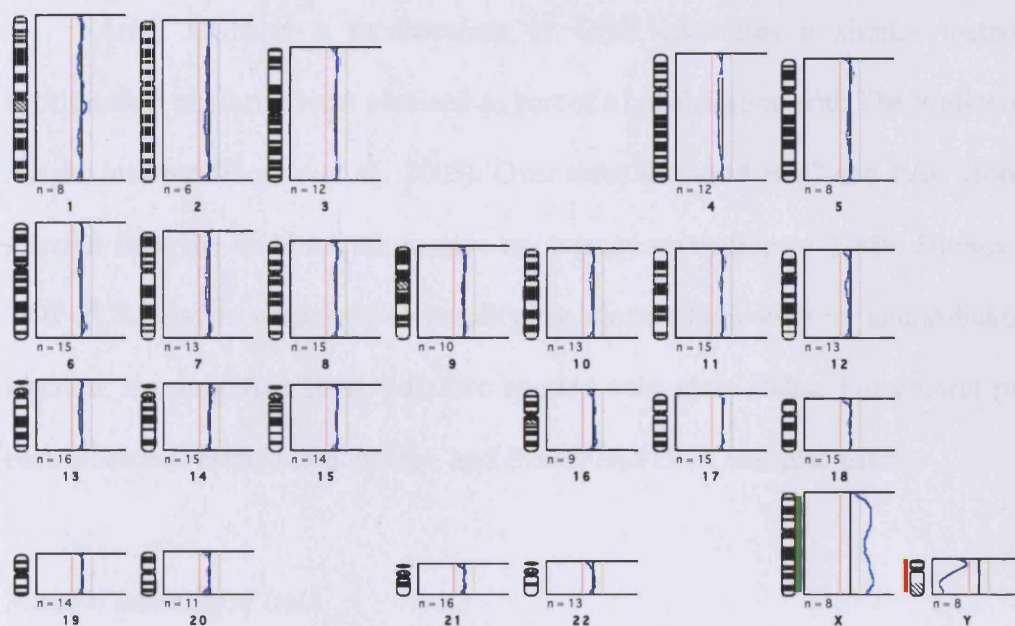


Figure 2.2 CGH of male versus female control experiment.

The red line indicates a relative loss and the green line indicates a relative gain. In this case there is a relative loss of the Y chromosome and relative gain of the X chromosome. On the Y chromosome the pseudoautosomal region can be seen where the fluorescence ratio is nearer to the normal level.

2.4 Array CGH

Array CGH is a modification of CGH and uses a similar method. The hybridisation platforms were obtained as part of a collaboration with The Wellcome Trust Sanger Institute (Fiegler *et al.*, 2003). Over three thousand BAC and PAC clones were selected from the Golden Path to give an average separation of 1 Mb. Human-specific DOP-PCR primers were used to amplify the clones. Following an amino-linking PCR reaction, the amplified DNA was then spotted onto glass slides. For control purposes, each clone was printed in duplicate, and *Drosophila* DNA was also used.

Random labelling of DNA

DNA extracted from the patient samples and cell lines was labelled with Cy5 and normal male DNA was labelled with Cy3, using a Bioprime Labelling kit (Invitrogen). 60µl of Random Primer Solution was added to 0.45µg of DNA and made up to 126µl with water. The solution was incubated at 100°C for ten minutes and then cooled on ice to denature the DNA. Fifteen µl of 10 x dNTP mix, 6µl of either Cy3 or Cy5 labelled dCTP and 3µl of Klenow Fragment were added to make a total volume of 150µl and the solution mixed gently. This solution was incubated at 37°C overnight and the reaction stopped by adding 15µl of EDTA.

Unincorporated labelled nucleotides were then removed from the labelled DNA using Micro-spin G50 columns. These columns were prepared by vortexing, with each placed in an Eppendorf tube and centrifuged in a microcentrifuge for one minute at 4,000 rpm. The columns were then placed in new Eppendorf tubes and used to clean the

labelled DNA. An aliquot (5µl) of each labelled DNA sample was then run on a 1% agarose gel to check the relative concentrations of test and reference DNA.

Preparations for hybridisation

Prior to hybridisation it is necessary to block repetitive sequences both in the clones on the hybridisation platform and in the labelled DNA. Repetitive sequences were blocked in the arrays with Cot1 and Herring Sperm DNA and in the labelled DNA with Cot1 DNA. The Pre-hybridisation Mixture (Herring sperm DNA, 135µl human Cot1 DNA, 23µl 3M NaAc (pH 5.2) and 400µl of cold absolute ethanol) and Hybridisation Mixture (180µl Cy3 labelled DNA, 180µl Cy5 labelled DNA, 135µl human Cot1 DNA, 55µl 3M NaAc (pH 5.2) and 1ml cold absolute ethanol) were precipitated at -20°C overnight.

To prepare the slide for hybridisation, a wall of rubber cement was placed around the area of the slides with the clones to create a well for the Pre-Hybridisation and Hybridisation mixture.

The precipitated Pre-Hybridisation mixture DNA was then washed in ethanol, and dried and re-suspended in 160µl Hybridisation buffer (70°C). The Pre-hybridisation Mixture was then applied to the slide within the well created by the rubber cement wall. The slide was then placed in a humidity chamber (slide box containing a 2 x SSC/40% formamide mix on a Whatman paper strip), which was placed on a rocking table for 60 minutes (5 rpm). Meanwhile, the precipitated Hybridisation Mixture DNA was then

washed in ethanol and dried and re-suspended in 60 µl of Hybridisation Buffer and 6µl yeast tRNA (100µg/µl, dissolved in H₂O at 70°C).

Hybridisation

The slide was removed from the humidity chamber and the Pre-Hybridisation Mixture removed with a pipette. The Hybridisation Mixture was then applied to the slide. It was important to ensure there were no bubbles and that there was even coverage of solution. The slide was then placed into a slide mailer humidified with 20% formamide/2 x SSC, sealed with Parafilm and placed into a hybridisation oven at 37°C. The slide was incubated with gentle rocking (5 rpm) for 48 hours, with a turn of 90° after 24 hours.

Washing

The slide was then removed from the incubator, the rubber cement removed, and placed into a tall glass trough containing PBS/0.05% Tween 20 to wash off any excess hybridisation solution. It was then transferred to another glass trough and washed in PBS/0.05% Tween 20 for 10 minutes at room temperature (shaking). It was then transferred to a 50% formamide/2 x SSC solution and incubated for 30 minutes (rocking, maximum speed) at 42°C. The slide was then placed in fresh PBS/0.05% Tween 20 and washed for 10 minutes at room temperature. The slide was then removed and placed in a metal rack and centrifuged at 1000 rpm for 2 minutes to dry it. The slide was now ready to scan.

Scanning

The fluorescent output from each fluorescent dye was measured in a confocal scanner ScanArray® 4000 (GSI Lumonics). This generated two images, one for the test and one for the reference. Figure 2.3 shows the output of one of the test samples (Cy 5 fluorescence of experiment using cell line CRL1620). The colours of the spots are not actual but representative of intensity of the signal. The optimal signal range is blue, but as the signal intensity increases beyond blue there is a change in colour from green to red to white.

Data processing

The relative intensities of Cy5 and Cy3 were extracted from the array images using Spot (Jain *et al.*, 2002). This generated a text file containing the data and a TIFF image, which gave a graphical representation of the data and was used to check if the test and reference images have been correctly overlaid. At this stage the data are in a text file and are then processed in an Excel file. The first processing step checked the test and reference values against the *Drosophila* clones. If the test and reference clones were less than twice the median *Drosophila* clone then the clones were rejected. The raw \log_2 ratios were normalised by dividing by the median raw ratio of the accepted values, and then the clones within each subarray were normalised using the median raw ratio of the subarray. There was then a check on the duplicate clone. The programme user could set an acceptable difference in these two values, and typically a value of 5-10% was used. If the difference was greater than this, the clone was excluded from further analysis. The clone ratios were then plotted against genomic location mapped against the July 2003

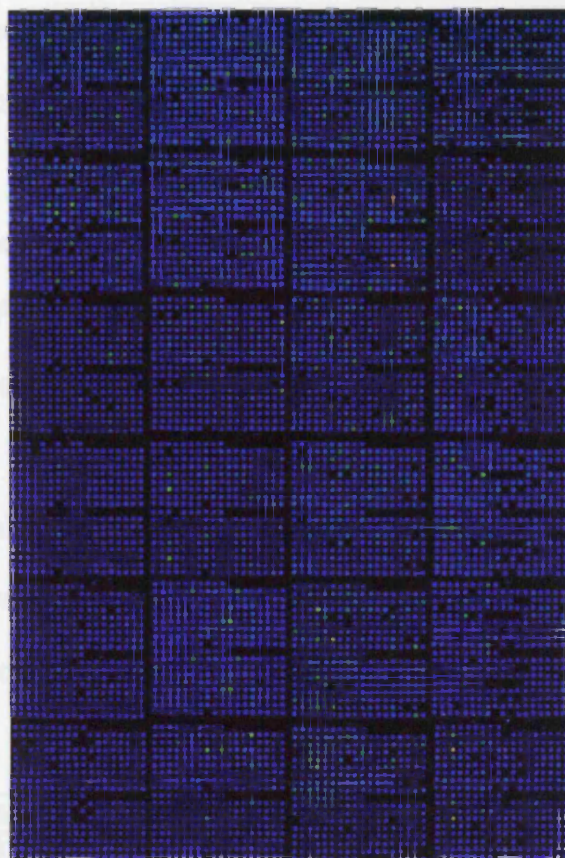


Figure 2.3 Cy 5 fluorescence from an array

The clones were arranged into blocks of 18 by 18 (subarrays).

The blocks were arranged on the slide into 24 blocks, which were 6 x 4.

The clones were spotted onto the array in duplicate with one clone in one half of the array and its duplicate in the other half. *Drosophila* clones were inserted for control purposes into two of the subarrays.

RP11-375	5p21.1	43.46 - 43.71
RP11-295.21	5p21.1	43.70 - 43.84
RP11-1447	5p21.1	43.89 - 43.96
		44.06 - 44.28
		44.29 - 44.38
RP11-1012	5p21.1	163.90 - 163.97
RP11-110	5p21.1	167.38 - 167.58
RP11-114	5p21.1	168.05 - 168.11
RP11-117116	5p21.1	19.31 - 19.42
RP11-199	5p21.1	21.89 - 22.00
RP11-845.18.1	5p21.1	23.37 - 23.55

Table 2.3: Probes obtained from Wellcome Trust Sanger Institute for FISH

freeze of the human genome sequence (NCBI133) within Ensembl (http://www.ensembl.org/Homo_sapiens/) to generate graphical representations of copy number for each chromosome (Figure 2.4).

2.5 Fluorescence *in-situ* hybridisation (FISH)

Standard FISH techniques were used (Senger *et al.*, 1993). The Clones for FISH were selected from the Sanger Institute website (http://www.ensembl.org/Homo_sapiens/) and requested from the Sanger Clone Library (<http://www.sanger.ac.uk/cgi-bin/humace/CloneRequest>) (Table 2.3). Additional probes for chromosomes 6, 7 and 9 and 10 centromeres, chromosome paints for 6p, 6q, 7p and 7q and a dual probe to detect EGFR and chromosome 7 centromere were all obtained from Vysis.

Probe	Cytogenetic location	Position (Mb)
RP3-337H4	6p21.1	43.56 - 43.66
RP11-22I24	6p21.1	43.66 - 43.71
RP1-261G23	6p21.1	43.70 - 43.88
RP11-344J7	6p21.1	43.88 - 43.96
RP11-227E22	6p21.1	43.96 - 44.05
RP11-346N8	6q16.1	93.89 - 94.09
RP11-557H15	6q23.2	134.78 - 134.97
RP11-448D5	6q23.3	137.23 - 137.23
RP11-368P1	6q24.1	142.22 - 142.36
RP11-86O4	6q24.2	143.50 - 143.62
RP11-13P5	6q25.3	159.46 - 159.57
RP3-495O10	6q26	163.59 - 163.78
RP1-51J12	6q26	163.85 - 163.97
RP11-517H2	6q27	167.48 - 167.58
RP11-471L1	6q27	168.05 - 168.11
RP11-513M16	9p22.1	19.31 - 19.42
RP11-149I2	9p21.3	21.89 - 22.00
RP11-495L19	9p21.3	23.37 - 23.55

Table 2.3 Probes obtained from Wellcome Trust Sanger Institute for FISH

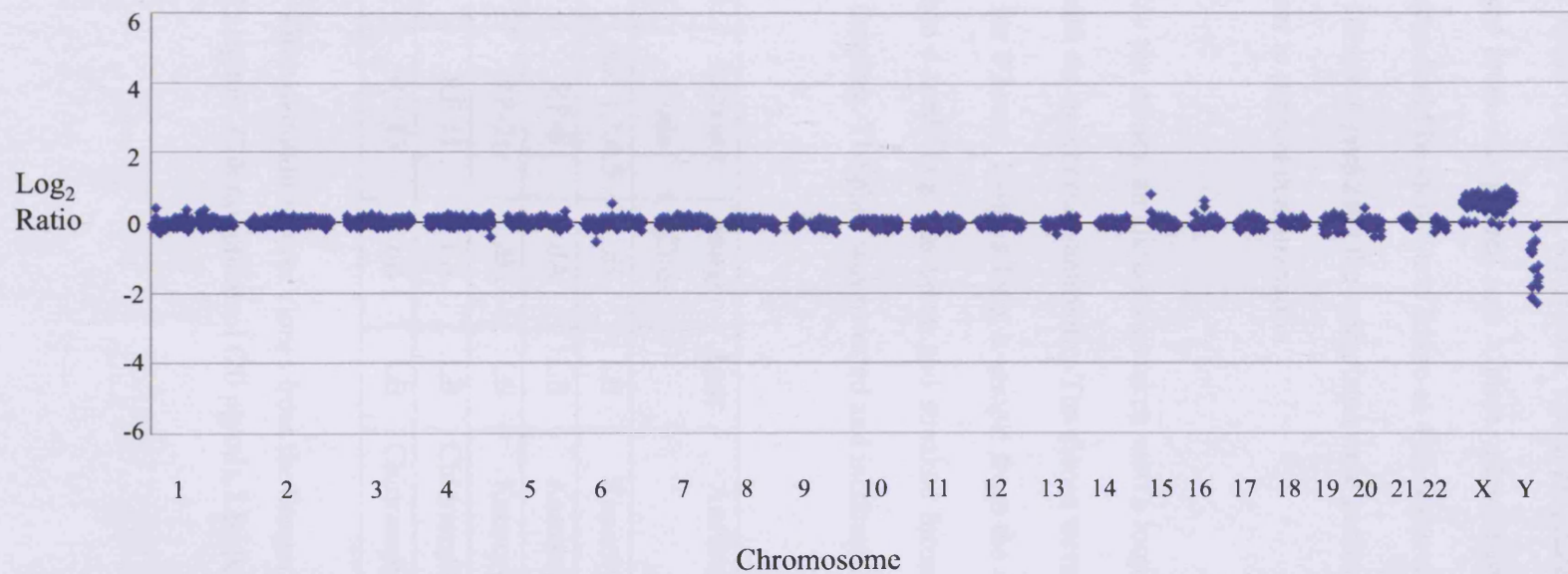


Figure 2.4 Whole genome array profile of a male versus female DNA control experiment.

The X axis shows the chromosome number and the Y axis is the fluorescence ratio on a log₂ scale. The male DNA was used as the control and the result shows relative gain of the X chromosome and loss of the Y chromosome.

The stabs of the clones could be stored for up to four weeks at 4°C until ready for use, but they were usually grown within a few days. The agar plates were prepared by heating liquid broth to 50°C in a water bath. The appropriate antibiotic was added (Table 2.4). The liquid broth was poured into a plate, allowed to set and then turned upside down. The plates could be stored in a fridge at 4°C covered with tin foil. All procedures involving the clones or preparing the agar plates were performed using a blue flame from a Bunsen burner to prevent contamination.

To grow the clones, an aliquot was taken with a loop from the stab, and placed in 10ml of LB with the appropriate antibiotic. The clones were then incubated in a shaking oven at 37°C for 8 hours. Using a loop, a sample from the culture was streaked onto an agar plate. Then a fresh loop was taken and streaked through the first streak, this time going around the plate. The plate was inverted and incubated at 37°C overnight.

Clone Type	Library Code	Sanger Code	Agar	Antibiotic	Growth Temperature
PAC	RP-1,3,4,5	dJ	LB	Kanamycin	37°C
PAC	RP-6	dA	LB	Kanamycin	37°C
PAC	RP-21	dM	LB	Kanamycin	37°C
BAC	RP-11	bA	LB	Chloramphenicol	37°C
BAC	RP-13	bB	LB	Chloramphenicol	37°C

Table 2.4 Growth conditions for clones from the Sanger Clone Library.
Kanamycin (25 µg/ml), Chloramphenicol (20 µg/ml), LB=liquid broth

The following morning a single colony was selected and inoculated into 10mls of LB and appropriate antibiotic and placed into a shaking oven at 37°C overnight. Glycerol stocks were prepared by adding 800µl of the culture to 200µl of glycerol. These were stored at -80°C. The remainder of the culture was placed in a centrifuge at 1,500 rpm for 5 minutes, the pellet was dried and a mini-preparation of plasmid DNA performed to extract the DNA. (The Equipment Park at Cancer Research UK performed the mini-preparations using a Qiagen kit).

To generate larger quantities of DNA, a sample was taken from the glycerol stock of a particular clone and inoculated into 10ml of LB with antibiotic. Eight hours later, 20 tubes containing 10ml of LB and antibiotic were prepared and inoculated with 200µl of culture. These were then incubated in a shaking oven at 37°C overnight. Each 10ml was centrifuged at 1,500 rpm for 5 minutes and the pellet dried prior to extraction of DNA.

Following DNA extraction, an estimation of the DNA concentration was made using a spectrophotometer. Digoxigenin labelling mixture (5µl) and 5µl of 10 x enzyme mixture were added to 1µg of probe DNA and made up to 40µl with water. The mixture was placed at 16°C until the fragments were the appropriate size (500 bp), which typically took 85 minutes. Five µl of the mixture was run on a 1% agarose gel to check the fragment size. EDTA (5µl) was then added and the mixture heated to 60°C for 5 minutes to inactivate the enzymes.

Hybridisation

Prior to hybridisation, the chromosomes on the slide were firstly aged in a microwave for 2.5 minutes. Denaturation Mixture (70% Formamide, 2 x SSC) (90µl) was then placed on the slide under a 22 x 50 mm coverslip, and the slide placed on a hot plate at 73°C for 3 minutes to denature the chromosomes. The slide was then washed in cool 2 x SSC and dehydrated in an ethanol series.

The probes were then prepared for hybridisation. Labelled DNA (300ng, 15µl) was precipitated with 5µl of human Cot1, 2µl salmon sperm DNA, 2µl of 3 M NaAc and 300µl of absolute alcohol on dry ice for 30 minutes (or -20°C overnight). The tube was then centrifuged at 15,000 rpm for 15 minutes at 4°C, dried in air and the DNA re-suspended in 11µl of Hybridisation Mixture (50% formamide (ultrapure), 2 x SSC, 10% dextran sulphate). The probe was denatured on a heating block at 85°C for 5 minutes and then incubated at 37°C for 30 minutes. Following this, the slide was pre-warmed on a heating block at 37°C and the denatured probe applied to a selected area of the slide. The hybridisation area was then sealed under a cover slip with rubber cement and the slide was placed in a moist chamber at 37°C overnight.

Post hybridisation washes & detection

The slide was washed in 50% formamide, 2 x SSC, pH 7.0 at 42°C three times for 5 minutes each with gentle shaking and then in 1 x SSC, pH 7.0 at 60°C three times for five minutes each. Then without allowing slides to dry, the hybridisation area was blocked in 90µl of SSCTM (4 x SSC, 0.1% Tween 20 (SSCT) + 5% Marvel) and

incubated at 37°C for 25 minutes. The blocking solution was drained from the slide and 90µl of the detection antibody (diluted in SSCTM) applied and covered with a coverslip (22 x 50 mm). Antibodies avidin-FITC 1:300 and anti-dig-rhodamine 1:100 were used for detection by incubating at 37°C for 45 minutes, followed by washing for 3 x 5 minutes in 4 x SSC, 0.1% Tween 20 (SSCT) at 42°C. The chromosomes were then counterstained with DAPI (0.3 µg/ml) in Citifluor and stored at 4°C in the dark. The images were captured with a Photometrics KAF 1400-500 cooled CCD camera attached to a Zeiss Axioskop epifluorescence microscope.

2.6 M-FISH

Pre-treatment of slide with metaphase spreads

The slide with the metaphase spreads needed to be treated to remove cellular debris. RNase working solution (100µl) was applied to the slide under a 22 x 50 mm cover slip at 37°C for 30 minutes to remove RNA. The slide was then washed in 2 x SSC at room temperature (2 x 5 minutes). It was then placed in pepsin working solution (pre-warmed to 37°C) for 5 minutes to remove proteins, cellular debris and cytoplasm. The slide was then washed in PBS at room temperature (2 x 5 minutes) and placed in formaldehyde fixation solution at room temperature for 2 minutes. The slide was again washed in PBS at room temperature (2 x 5 minutes), placed in an ethanol series to dehydrate the DNA and dried in air.

Hybridisation

The slide was placed in denaturation solution (70% deionised formamide, 2 x SSC pH 7.0) at 72°C for 1 - 3 minutes and then in an ethanol series and dried in air. The probe (10µl) was denatured in a 72°C water bath for 5 minutes and applied to the slide. A 22 x 22 mm coverslip was applied and sealed with rubber cement. The slide was placed in a warm chamber and incubated at 37°C overnight.

Post-hybridisation washes

The slide was placed in 0.4 x SSC, 0.3% NP-40 at 72°C for 5 minutes, washed in 2 x SSC, 0.1% NP-40 at room temperature for 3 minutes, then air dried in the dark. DAPI III counterstain (40µl) was applied under a 22 x 50 mm coverslip. The slide was then ready for image acquisition with a CCD camera and fluorescence microscope.

Chapter Three

Development of analysis parameters for array CGH

3.1 Introduction

Conventional or metaphase comparative genomic hybridisation (CGH) is a hybridisation-based method of assessing DNA sequence copy number across the whole genome (Kallioniemi *et al.*, 1992). Differentially labelled test and control DNAs are competitively co-hybridised onto metaphase chromosome spreads. The relative intensities of the fluorochromes across each target chromosome show the positions of genomic loss and gain. Since hybridisation of repetitive DNA sequences gives inconsistent data for assessing copy number change, unlabelled repetitive DNA is included in the hybridisation to block out this effect. Hence, within an individual experiment there are three elements competing to hybridise to the target DNA: labelled test and control DNA, and unlabelled Cot1 DNA containing repetitive sequence. Differences in experimental conditions cause variation in hybridisation efficiency, leading to variation around the true value of the hybridisation ratio of the two competing elements of labelled test and control DNA. To reduce the effects of variation across a slide, within an experiment, a composite CGH profile is derived from the averaging of at least five metaphase profiles.

Array CGH is a refinement of metaphase CGH, the main difference being the hybridisation platform. In metaphase CGH, the hybridisation platform consists of metaphase chromosomes, whereas in array CGH the chromosomes are replaced with

mapped fragments of DNA sequence arrayed onto a glass slide (Pinkel *et al.*, 1998; Solinas-Toldo *et al.*, 1997). There are two broad categories of hybridisation platform used in array CGH. The first has genomic sequence in bacterial artificial chromosome (BAC) and P1 artificial chromosome (PAC) clones (Pinkel *et al.*, 1998) and the second has complementary DNAs (cDNA) clones (Pollack *et al.*, 1999). (BAC and PAC are vectors used for cloning relatively large fragments of DNA. cDNAs are generated by converting RNA to DNA before insertion into a cloning vector.) The advantages of using cDNAs are that they give gene specific information and are not subject to mapping errors, as are genomic arrays. In addition, the probes are smaller and the array platforms are less labour intensive to produce. However, since cDNA clones are produced from RNA, they may have differences in sequence as a result of alternative intron splicing. The advantages of using genomic sequences are that these arrays cover non-expressed regions of the genome and have better hybridisation characteristics, as the probe and the target sequence have greater homology.

The challenges faced in array CGH are similar to those encountered with metaphase CGH. Array CGH is prone to both inter- and intra-experimental variation. The aims of this chapter are to gain a better understanding of experimental variability in array CGH and to devise a method of formulating a threshold to define regions of gain and loss in experimental samples.

3.1.1 Thresholds and experimental variation

In metaphase CGH two numerical thresholds are set. One threshold is used to define gain and the other to define loss. The convention in metaphase CGH is to set the thresholds based on control experiments, the ideal thresholds being values that optimise the balance between false positives and false negatives. The ratio of normal copy number is 1. The threshold for copy number change varies between users, but in general, thresholds of gain are set from 1.1 to 1.15 and loss from 0.85 to 0.9. Array CGH is a more sensitive technique with a ratio being given for each datum point on the array. Array CGH is sufficiently sensitive to determine amplification, where the ratio will be very high. For this reason the ratios are expressed as \log_2 ratios (Table 3.1). Hence, regions of normal copy number in a diploid nucleus (2:2) and a tetraploid nucleus (4:4) have a ratio of 1 and a \log_2 value of 0. Aneuploidy makes CGH analysis more complicated as, for example, a single copy loss in a tetraploid cell line has a 3:4 ratio, which is a \log_2 ratio of -0.41.

Copy number		Ratio	\log_2 ratio
Diploid	Tetraploid		
0:2	0:4	0	-Infinity
-	1:4	0.25	-2
1:2	2:4	0.5	-1
-	3:4	0.75	-0.41
2:2	4:4	1	0
-	5:4	1.25	0.32
3:2	6:4	1.5	0.58
-	7:4	1.75	0.81
4:2	8:4	2	1
10:2	20:4	5	2.32
20:2	40:4	10	3.32

Table 3.1 Ideal fluorescence ratios with corresponding \log_2 values.

In conventional CGH there is averaging of results between metaphases, but variation is still apparent (Kallioniemi *et al.*, 1992). Array CGH is a more sensitive technique than conventional CGH, and this generates its own challenges in interpreting results. While conventional CGH tests copy number of regions of a chromosome, array CGH tests copy number change of individual regions that are limited by the size of the probe.

In the control experiments where normal male and female DNA were used as the test and reference DNA, the autosomal clones should have a \log_2 ratio of zero. However deviation from zero is apparent (Figure 3.1). If thresholds of ± 0.2 were selected then regions of the chromosome would be incorrectly called gain and regions incorrectly called loss (false positives).

In a female versus male DNA control experiment, the X chromosome ratio is 2:1, which should give a \log_2 ratio of 1. Again, variation from the expected value across the chromosome is apparent (Figure 3.2). If the threshold for gain is set at \log_2 of 1 (\log_2 ratio of 2:1=1) then no region of the chromosome would be classed as gain (false negative). Even if the threshold were reduced to \log_2 0.5, although most of the chromosome would be called gain, there would still be regions classed as no copy number change.

The clone-to-clone variation within a region of change also contributes to the problem of defining thresholds between normal and change in copy number. However

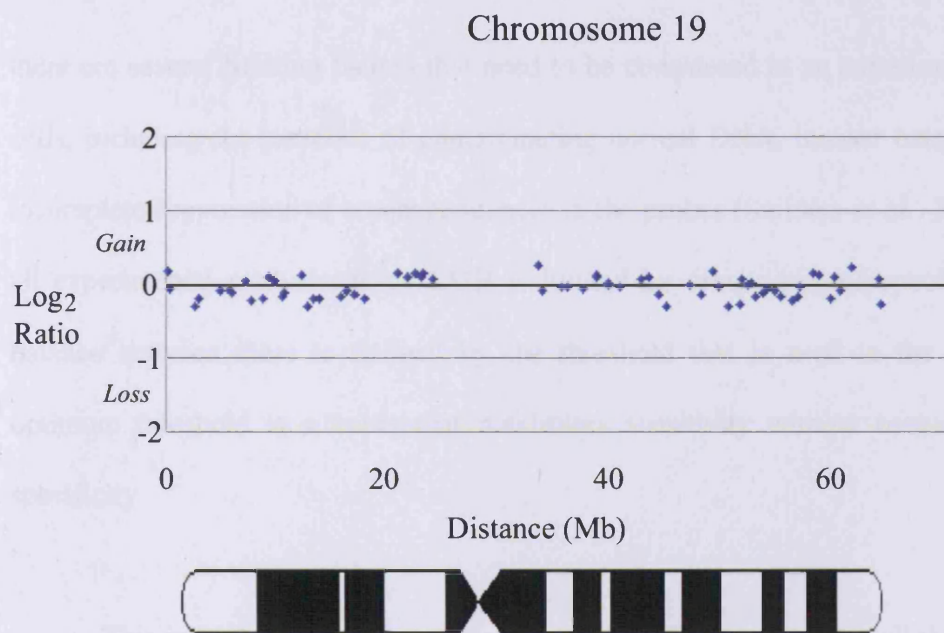


Figure 3.1 Array CGH profile of chromosome 19 in a female (test) versus male (control) experiment. Chromosome 19 consistently showed the greatest variability from the expected ratio in control experiments.

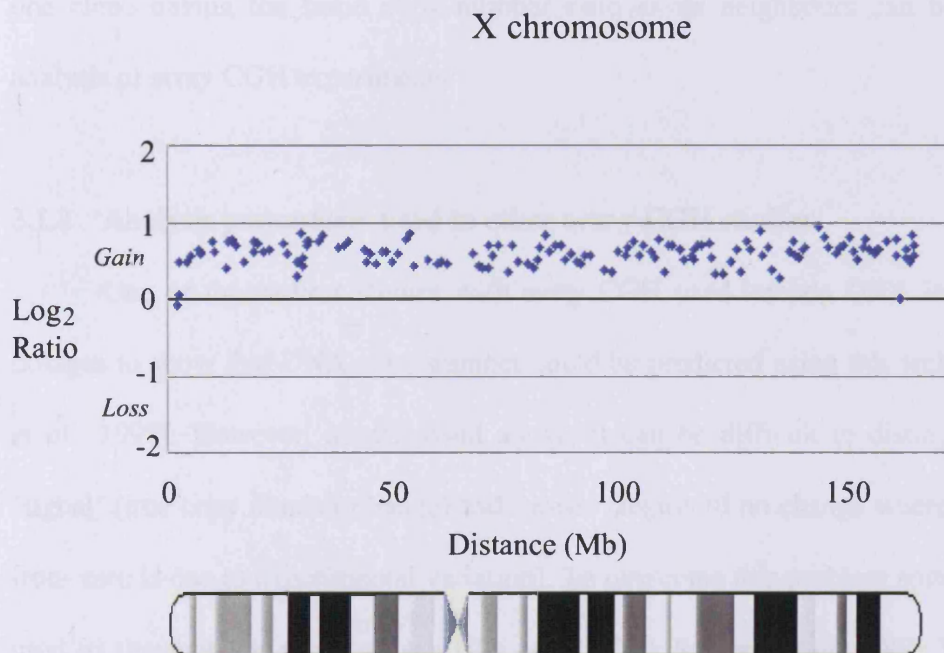


Figure 3.2 Array CGH profile of the X chromosome in a female (test) versus male (control) experiment.

there are several limiting factors that need to be considered in an experiment on tumour cells, including the presence of contaminating normal DNA, tumour heterogeneity and incomplete suppression of repeat sequences in the probes (Snijders *et al.*, 2001). As with all experimental methods, array CGH is limited by sensitivity and specificity and the balance between these is defined by the threshold that is used in the analysis. The optimum threshold is a value that maximises sensitivity without over-compromising specificity.

This intra-experimental variation makes it difficult to interpret all the data from an experiment. What is needed is a method of analysis that will compensate for this variation. Although in array CGH, each clone gives an independent \log_2 ratio, the results are linked in that all the clones in a region of change (for example the X chromosome in the female/male DNA control experiment) should show change. Thus, the likelihood of one clone having the same copy number ratio as its neighbours can be used in the analysis of array CGH experiments.

3.1.2 Analysis parameters used in other array CGH studies

One of the earliest studies with array CGH used lambda DNA in different test dosages to show that DNA copy number could be predicted using this technique (Pinkel *et al.*, 1998). However, as discussed above, it can be difficult to distinguish between 'signal' (true copy number change) and 'noise' (region of no change where the deviation from zero is due to experimental variation). To overcome this problem some groups have used set thresholds in their analysis (Cai *et al.*, 2002; Snijders *et al.*, 2001; Veltman *et al.*,

2003), while others have used moving thresholds that change according to the value of the neighbouring clones (Clark *et al.*, 2003; Clark *et al.*, 2002; Pollack *et al.*, 2002).

One study using set thresholds for detecting copy number change in bladder tumours, selected \log_2 thresholds of 0.2 for gain and -0.2 for loss (Veltman *et al.*, 2003). It is not transparent how these figures were reached except that they were based on eight, sex-mismatched, control experiments. It is inferred that the thresholds, for what are described as homozygous deletion or amplification, were based on the numerical value of the \log_2 value of the 2:1 ratio. Hence, scores above 1 were considered amplification and those below -1 as homozygous deletion. Analysis of homozygous deletion of *CDKN2A* by quantitative real-time PCR showed that fourteen of the tumours had a homozygous deletion of this gene and these had a mean \log_2 ratio of -2.16. (However, 3 tumours had \log_2 ratios of -0.63, -0.68 and -0.74). Twenty tumours showed normal copy number of *CDKN2A* by PCR, but the array for one of these gave a \log_2 ratio of -0.21.

A different study using an array of 960 BACs from the mouse genome set the thresholds at 1.2 and -0.8. These thresholds were based on autosomal chromosome variation of 0.85-1.15 with a coefficient of variation of 8% (Cai *et al.*, 2002).

Snijders *et al* examined breast tumours with array CGH (Snijders *et al.*, 2001). Figure 3.3 is taken from this study and it demonstrates that a threshold of \log_2 ratio -0.5 excludes some clones within regions of what appear to be loss. If the threshold is reduced

to -0.25, still not all the clones are included and there is overlap with clones from other regions, which may be normal.

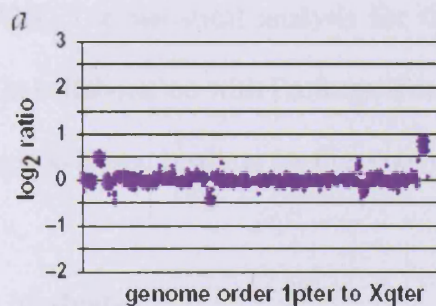


Figure 3.3 Array profile from Snijders *et al* (Snijders *et al.*, 2001).

To address the problems in using set thresholds some groups have used moving thresholds, where the value of the surrounding clone is taken into account in interpreting the results (Clark *et al.*, 2003; Clark *et al.*, 2002; Pollack *et al.*, 2002).

3.1.3 Aims

As yet there is no firm consensus as to how the results from array CGH experiments should be analysed. The simplest approach is to present data from selected regions only, showing for example, homozygous deletions and amplifications, which are easy to identify. Although single copy changes are more difficult to distinguish from normal, especially within a tetraploid genome, they may be very relevant. The array CGH platform used here facilitates a genome-wide survey of copy number change and I wished to present all the data. Therefore, a pragmatic and objective approach was needed to allow rational comparisons to be made between data sets. The aims of this chapter are firstly, to examine both inter- and intra-experimental variation in control experiments of

array CGH. Secondly, to examine the effect of altering thresholds on the interpretation of results. And thirdly, to use these investigations to devise an objective analytical tool for genome-wide array CGH. The statistical analysis for the interpretation of array CGH results was performed in collaboration with Professor Peter Sasieni, Cancer Research UK Centre for Epidemiology, Wolfson Institute for Preventive Medicine, London.

3.2 Materials and Methods

Six control array CGH experiments were performed using DNA from normal males and females. The fluorescence ratio of each clone was plotted on an Excel graph against its position along the chromosome. These test hybridisations provide three models for interpreting genetic changes in cancer. The autosomal clones represent the behaviour of normal regions of DNA, in a male versus female experiment the Y chromosome clones represent homozygous deletions, and in a female versus male DNA experiment the X chromosome clones represent a single copy loss in a diploid nucleus.

3.2.1 Additional pre-processing

Each experiment had a different experimental quality depending on factors such as the batch the slides came from, the production batch of Cot1 DNA and whether the slide dried out during hybridisation. A poor quality experiment gives fluorescence ratios that deviate from the true value more than for good experiments. In practice, it was straightforward to see when an experiment had not worked sufficiently well because there was variation in noise intensity across the slide and an increase in background signal. Methods of quantifying this variation were considered. For example, the spread of the

data could be measured. The spread is the difference between the greatest value and the least. As the spread of data can give a skewed view of the data due to outlying values, the inter-quartile range of locally centred values was used to measure variation. The inter-quartile range is the difference between the 75th percentile and the 25th percentile. If this value was greater than 0.275 then the experimental results were not used and the experiment was repeated.

The data in each included experiment were re-scaled so as to take account of the variable variability of the results. The effect of this is to use thresholds specific for each experiment. We determined the difference between each marker's \log_2 ratio and the local average (from the 5 down-stream and the 5 up-stream markers), and then scaled all \log_2 ratios by the inter-quartile range of these differences for the 22 autosomal chromosomes. Each experiment was normalised to an inter-quartile range of 1.

A further re-scaling was made using a chromosome specific factor obtained from the six control experiments. The chromosome specific factors were derived from the inter-quartile range of each individual chromosome, after the control data were normalised.

3.2.2 Sensitivity and specificity

The sensitivity of a test is the proportion of actual gains and losses identified. The specificity is the proportion of actual nulls identified. In the six control experiments, the autosomes were the known null and the mismatched sex chromosomes were the known

gain and the known loss. Table 3.2 shows the hypothetical results from known results and test results and how this can be quantified.

	Test results			
	Loss	Null	Gain	Totals
Actual Loss	A=True positive	B=False negative	C=False positive	A+B+C
Actual Null	D=False positive	E=True negative	F=False positive	D+E+F
Actual Gain	G=False positive	H=False negative	I=True positive	G+H+I

Table 3.2 Table of results from a hypothetical experiment

$$\text{Sensitivity} = (A+I) / (A+B+C+G+H+I)$$

$$\text{Specificity} = E / (D+E+F)$$

A receiver operating characteristic (ROC) curve plots the sensitivity against 'one hundred minus the specificity (%)' at different thresholds and this curve is then used to select the optimum threshold criteria.

3.3 Results

Three sets of results were obtained from this analysis of the control experiments. Firstly the list of clones that were discarded due to inconsistent or aberrant hybridisation characteristics, secondly the chromosome specific scaling factors and, thirdly, the ROC from which the threshold for the analysis can be selected.

3.3.1 Discarded clones

The clones representing the autosomes in male versus female DNA experiments that do not show a \log_2 ratio of around 0 were excluded from the analysis, i.e. markers that consistently gave large positive or negative results, or both, in the control samples (Table 3.3).

Chr	Clone position (Mb)	Clone name	Chr	Clone position (Mb)	Clone name
1	0.2	CTB-14E10	13	113.8	RP11-245B11
2	190.0	CTC-444N24	14	81.1	PR11-406A9
4	3.5	RP11-492123	15	19.7	RP11-2F9
4	191.3	CTC-963K6	15	87.9	RP11-233C13
5	10.4	CTD-2274H20	16	1.0	RP11-161M6
5	14.5	RP1-29O12	16	2.1	CTB-121I4
5	27.3	CTD-2219P12	16	89.6	CTC-240G10
5	162.2	RP11-505G12	16	89.7	RP11-533D19
6	33.4	RP11-175A4	17	4.8	RP5-1050D4
6	169.3	RP1-137D17	17	37.2	RP5-906A24
7	0.7	RP11-449P15	17	80.7	GSI-50C4
7	99.7	RP11-44M6	17	81.2	RP11-567O16
8	144.1	RP5-1118A7	18	73.9	RP11-234N1
8	144.2	RP11-472K18	18	76.9	RP11-315M18
9	132.5	RP11-83N9	18	77.2	RP11-154H12
10	135.0	RP11-122K13	19	5.0	CTC-482H14
11	64.1	RP11-424O11	19	13.1	CTC-250I14
11	65.1	CTB-184C17	19	18.2	CTC-251H24
12	49.0	RP11-302B13	20	61.1	RP5-1107C24
12	133.3	CTC-221K18	21	43.6	RP11-351D2
13	56.6	RP11-279F15	22	39.4	RP3-355C18

Table 3.3 List of discarded clones

3.3.2 Chromosome scaling factors

The following figures were calculated from a measure of the inter-quartile range of the \log_2 ratios of each chromosome when collated from all six control experiments

(Table 3.4). Chromosome 19 is the chromosome with greatest variability and therefore has the largest scaling factor. The inter-quartile range of chromosome 19 in the normalised samples was 2.2. These inter-quartile ranges were then used as scaling factors. For example, each normalised \log_2 ratio on chromosome 19 was divided by 2.2.

Chromosome	Scaling factor	Chromosome	Scaling factor
1	1.15807	12	1.108734
2	1.034719	13	1.087662
3	1.078727	14	1.190092
4	1.175389	15	1.028538
5	1.069797	16	1.209821
6	1.032107	17	1.249908
7	1.177455	18	1.157617
8	1.091517	19	2.210811
9	0.986733	20	1.23505
10	1.108118	21	1.201608
11	1.192114	22	1.414799

Table 3.4 Chromosome-specific scaling factors used in the statistical analysis

3.3.3 Identification of thresholds from the ROC

3.3.3.1 Dual thresholds

The first method for analysing copy number change used two separate thresholds for gain and two separate thresholds for loss based on control experiments (Figure 3.4, Algorithm A). The standard deviation of the autosomal clone \log_2 ratios was 0.09 in the control experiments. For loss the more stringent threshold was set at (-3SD -0.01) and a less stringent threshold was set as (-1SD -0.1). This translated into a more stringent threshold of \log_2 -0.28, $[(-0.09 \times 3) -0.01]$ and a less stringent threshold of \log_2 -0.1, $(-0.09 -0.01)$. Hence, when defining a region of loss the value of -3 SD from the zero

ROC curve

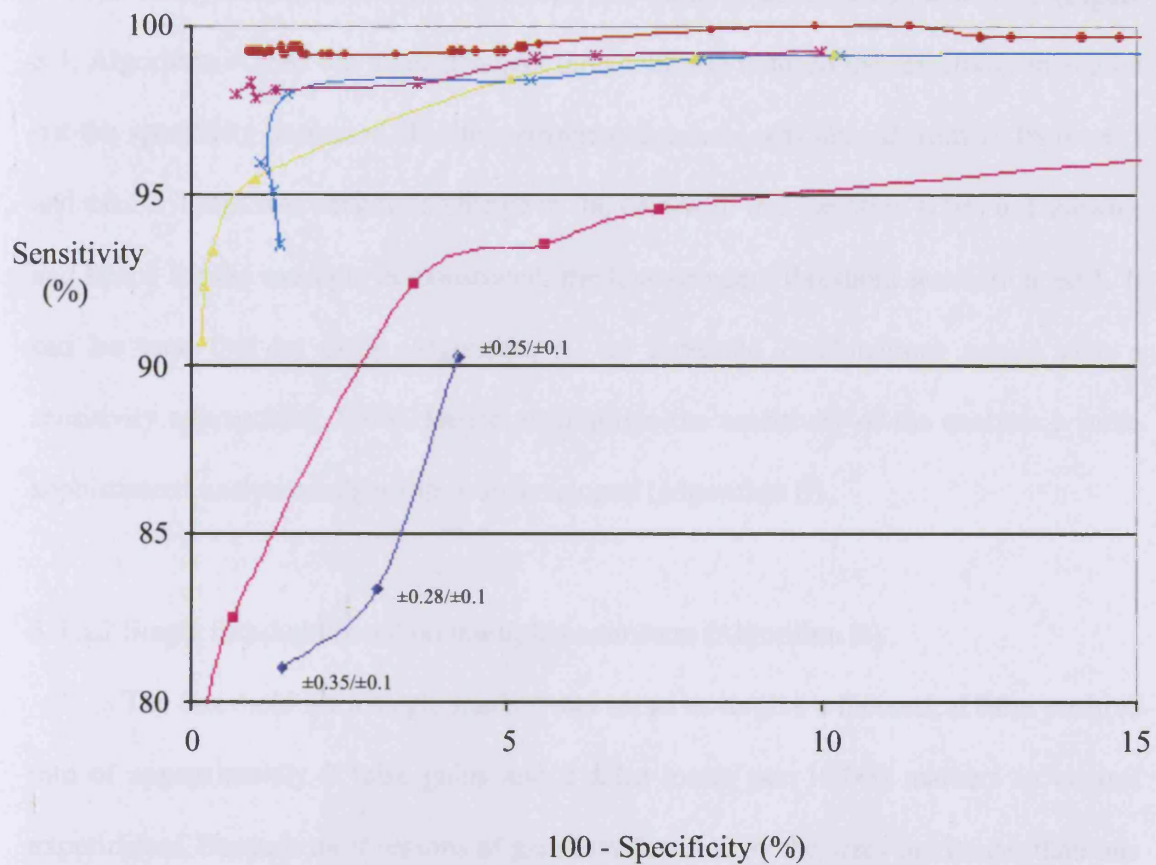
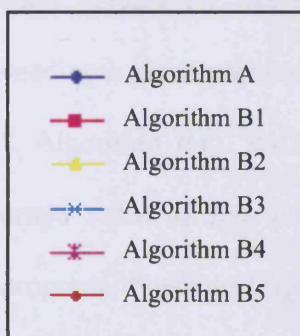


Figure 3.4 ROC curve. Different thresholds were selected to test the effect on sensitivity and specificity.



-0.1, needed to be achieved and the surrounding clones were also considered to be loss if the value was less than -0.1. The converse rules were applied for gain (Figure 3.4, Algorithm A). To assess how altering the more stringent threshold affected the sensitivity and specificity, the more stringent threshold was varied to ± 0.25 , ± 0.28 and ± 0.35 (Figure 3.4, Algorithm A). As the more stringent threshold was reduced the sensitivity increased but the specificity decreased. The less stringent threshold was altered from ± 0.08 to ± 0.1 and ± 0.14 . There was very little change in the data with this variation (Data not shown), and hence for the example demonstrated, the less stringent threshold was left at ± 0.1 . It can be seen that by using Algorithm A, no threshold combinations would give a sensitivity approaching 100%. Hence, to improve the sensitivity of the analysis a more sophisticated analytical algorithm was developed (Algorithm B).

3.3.3.2 Single threshold based on multiple parameters (Algorithm B)

The threshold for a single marker was set so as to give a theoretical false positive rate of approximately 2 false gains and 2 false losses per 10,000 markers in control experiments. Because most regions of gain/loss detected by the array are longer than one mega-base, we used less stringent thresholds for consecutive markers. Thus we also used theoretical thresholds (using the Normal distribution and independence of consecutive marker values) for the minimum (maximum) of 2, 3, 4 or 5 consecutive markers exceeding a given positive (negative) value so as to detect a gained or lost region (Figure 3.4, Algorithm B1). We also classified longer regions as being gained or lost if the average value of five consecutive markers consistently (over 25 clones) crossed an appropriate threshold (Figure 3.4, Algorithm B2). We defined all clones with \log_2 ratios

close to zero as null. At this stage there are regions defined as loss, gain, null or other. The values of regions defined as other were then averaged and classified as either gain, loss or null depending on the mean value of the number of clones involved (Figure 3.4, Algorithm B3). All markers have now been assigned a value of loss, gain or null. The next stage then determined if these classifications were correct. An average value of null regions was taken to assess if they are similar to the surrounding regions and if they were similar then they were re-classified. Following this all regions of loss or gain were then assessed and at least one quarter of all the clones in a particular region had to cross one threshold value, and three quarters have to cross another threshold and if not they are classified as null (Figure 3.4, Algorithm B4). Finally, we merged regions if the \log_2 -ratios of the markers between two markers showing gain or deletion were consistent with continued gain or loss across the extended region (Figure 3.4, Algorithm B5). Professor Sasieni automated this method of analysis using a programme written in STATA. The programme is currently being written in Excel format to facilitate wider use.

Using the full Algorithm B (including all steps B1 - B5), 229 (1.26%) of 18175 control markers were falsely identified as losses and 288 (1.58%) as gains, with an overall specificity of 97.2% (three markers were on the boundary between regions of loss and gain and were included in both categories). The sensitivity in regions of known loss was 98.7% (for 624 markers). It was 99.7% for areas of known gain (309 markers).

3.4 Discussion

This chapter has described the development of an automated method of analysis of array CGH that can be used to provide an objective assessment of results thus allowing comparisons between experimental sets. Examination of multiple tumour samples allows the frequency of genetic changes to be calculated and also minimal regions of deletion and gain to be defined. However, it should be remembered that a single genetic change in a single tumour might be significant in that tumour.

3.4.1 Errors

False positive results can be classified into two categories, statistical errors or errors relating to the characteristics of the reporter clone.

3.4.1.1 Statistical issues

Depending on the thresholds used, different levels of sensitivity and specificity are obtained. With 99% specificity, one null clone in a hundred will be a false positive. Hence, for a 3000-clone array (with little loss or gain) 30 clones will give false positive results. This may be an acceptable number of false positives, but if the array had 30,000 clones and the specificity was 99% then there would be 300 false positive results. With any method of analysis there are invariably going to be some false positives due to the analytical methodology and it is up to the individual user to decide which thresholds should be set, depending on the aims of the experiment.

3.4.1.2 Clone characteristics

In a control experiment, if a clone fails to give the expected \log_2 ratio, it may be that the clone is mis-labelled or mis-mapped, or contain a large proportion of repetitive sequence or sequence polymorphism. If a clone is mis-labelled or mis-mapped, as a clone in an autosomal region but is in fact a clone from the X chromosome, in a male versus female control experiment, the clone will consistently give a result indicating copy number change and therefore should be removed from the analysis. If a clone is mis-labelled or mis-mapped and both the true and false clone positions are within the autosomes, then this will not be detected by the sex mismatch controls. FISH mapping clones showing copy number changes to normal human metaphases will confirm their genomic positions. Sequencing the clones and comparison with the sequence database could also be used as a check. Clones with a high content of repetitive sequence give unreliable hybridisation characteristics, as the effect of repetitive sequences may not be completely suppressed by the Cot1 DNA

3.4.1.3 Genetic heterogeneity

Individuals show sequence variation between their genomes. Variation ranges from the level of the individual nucleotide where variation from single nucleotide polymorphisms (SNPs) is found, up to variation in copy number of hundreds of kilobases, termed large-scale copy number variation (LCV) (Iafrate *et al.*, 2004; Sebat *et al.*, 2004). The significance of LCV is not known, however it is conceivable that it may play a role in cancer susceptibility. The effects of variation such as LCV in genomes in

array CGH could be overcome by using DNA derived from the blood of the test individual as the control.

In summary, this chapter has raised some of the difficulties in interpreting array CGH results and has described a method of analysis to objectify this interpretation. The next chapter uses this method of interpretation in the array CGH analysis of high-grade astrocytic glioma cell lines and patient samples.

Chapter Four

DNA Copy Number Changes in High-Grade Astrocytic Gliomas

4.1 Introduction

Array CGH is a rapidly evolving method, and the utilisation of this technology is increasing. The first study published using array CGH had low resolution, but demonstrated the potential of the method (Solinas-Toldo *et al.*, 1997). Array CGH was used again in 1998 in the analysis of four breast tumours, and showed gain on chromosome 20, which was confirmed by FISH (Pinkel *et al.*, 1998). A low resolution array CGH system developed by Vysis was used to examine seven cell lines and seven tumours from patients with astrocytic glioma grade IV with only 58 clones specific for known oncogenes (Hui *et al.*, 2001). No novel findings were described.

This chapter describes the copy number changes detected by array CGH, with examples of confirmation of results by metaphase CGH in ten astrocytic glioma grade IV patient samples and ten high-grade astrocytic glioma cell lines. The array CGH platforms used in this study were developed as part of a collaboration between the Sanger Institute and Cancer Research UK. The resulting hybridisation platforms had 3000 BAC and PAC clones with an average separation of 1Mb (Fiegler *et al.*, 2003).

4.2 Results

Array CGH was performed on ten astrocytic glioma grade IV tumour samples and ten high-grade astrocytic glioma cell lines (Chapter 2.1.2). In addition, conventional CGH were performed on the cell lines. Multiple regions of copy number change across the genome were revealed by array CGH. Array CGH revealed, on average, 5.2% of the autosomal genome was deleted in the primary tumours and 14.9% in the cell lines. The corresponding figures for gain were 5.2% and 11.7%, respectively. By comparison, the percentages of deletions and gains (false positives) in control samples were 0.5% and 0.1%, respectively.

Conventional CGH identifies regions on the chromosome by cytogenetic banding. Array CGH identifies regions by chromosome number and nucleotide position, which are given in megabases (Mb). To assist in the interpretation of the data, the size of each chromosome and the positions of the centromeres are set out in Table 4.1. However heterochromatic regions are refractory to array CGH analysis and are therefore excluded from the results. The sex chromosomes are excluded from the analysis, as the samples were not sex matched.

Chromosome	Length (Mb)	Centromere (Mb)	Chromosome	Length (Mb)	Centromere (Mb)
1	245	123	12	133.4	36.0
2	243	93.4	13	114.1	16.0
3	199.3	91.4	14	105.3	15.6
4	191.6	50.9	15	100.1	17.0
5	190.0	47.7	16	90.0	37.4
6	170.7	60.4	17	81.6	23.7
7	158.4	58.5	18	77.8	16.7
8	145.9	44.8	19	63.8	28.4
9	134.5	46.5	20	63.6	27.7
10	135.4	40.3	21	47.0	12.3
11	135.0	53.6	22	49.4	11.8

Table 4.1 Chromosome size and position of the centromere in megabases (Mb).

4.2.2 Copy number changes presented in numerical chromosome order

Selected findings are presented in chromosome order and, in particular, affected genes involved in neural development or in known pathways in cancer are highlighted. The genetic locations of the changes are also given. When delineating the region involved in a copy number change, the flanking normal clones are used as the boundaries and each breakpoint is therefore between an aberrant clone and the adjacent normal clone. In the composite figures for each chromosome, the positions of the flanking normal clones are given for each aberrant genomic region.

Chromosome 1

Multiple gains and losses were found across the whole length of the chromosome (Figure 4.1). The distal short arm of chromosome 1 is a complex area of loss. The cell line U87 shows loss between 0.2 and 6 Mb. There is gain in chromosome 1p in seven patient tumour samples and seven cell lines. Tumour T1 shows a discrete loss between 5 and 10 Mb and tumour T5 has a discrete loss between 5 and 11 Mb. This region is encompassed by larger deletions in tumour T6 and cell lines CRL1620 and CRL2611. Chromodomain Helicase DNA-binding Protein 5 (*CHD5*) (1p36.31; 5.9 Mb), which plays a role in neural development maps within these deletions (Thompson *et al.*, 2003).

A discrete gain of RP5-1108M17 (1p21.1; 103 Mb), flanked by clones RP11-202K23 and RP1-118, was found in tumours T7 and T10 and cell line Htb138. Larger deletions involving this region were found in tumour T3 and cell lines CRL2365 and U87. Genes in this minimal region are the Amylase genes *AMY1A*, *AMY2A* and *AMY2B*.

A discrete gain was present in CRL2020 between 200 and 203 Mb, which contains the *MDM4* and Phosphatidylinositol 3-kinase, class 2, beta (*PIK3C2B*) (1q32). A discrete amplification was present in tumour T5 between 238 and 240 Mb, which contains the v-akt murine thymoma viral oncogene homolog 3 (*AKT3*) (1q43-44). The distal long arm had deletions between 224 and 245 Mb in four cell lines. The Fumarate Hydratase (*FH*) tumour suppressor gene (1q42.1), which is mutated in multiple leiomyomatosis and in renal cancer, maps within this deletion (Alam *et al.*, 2003).

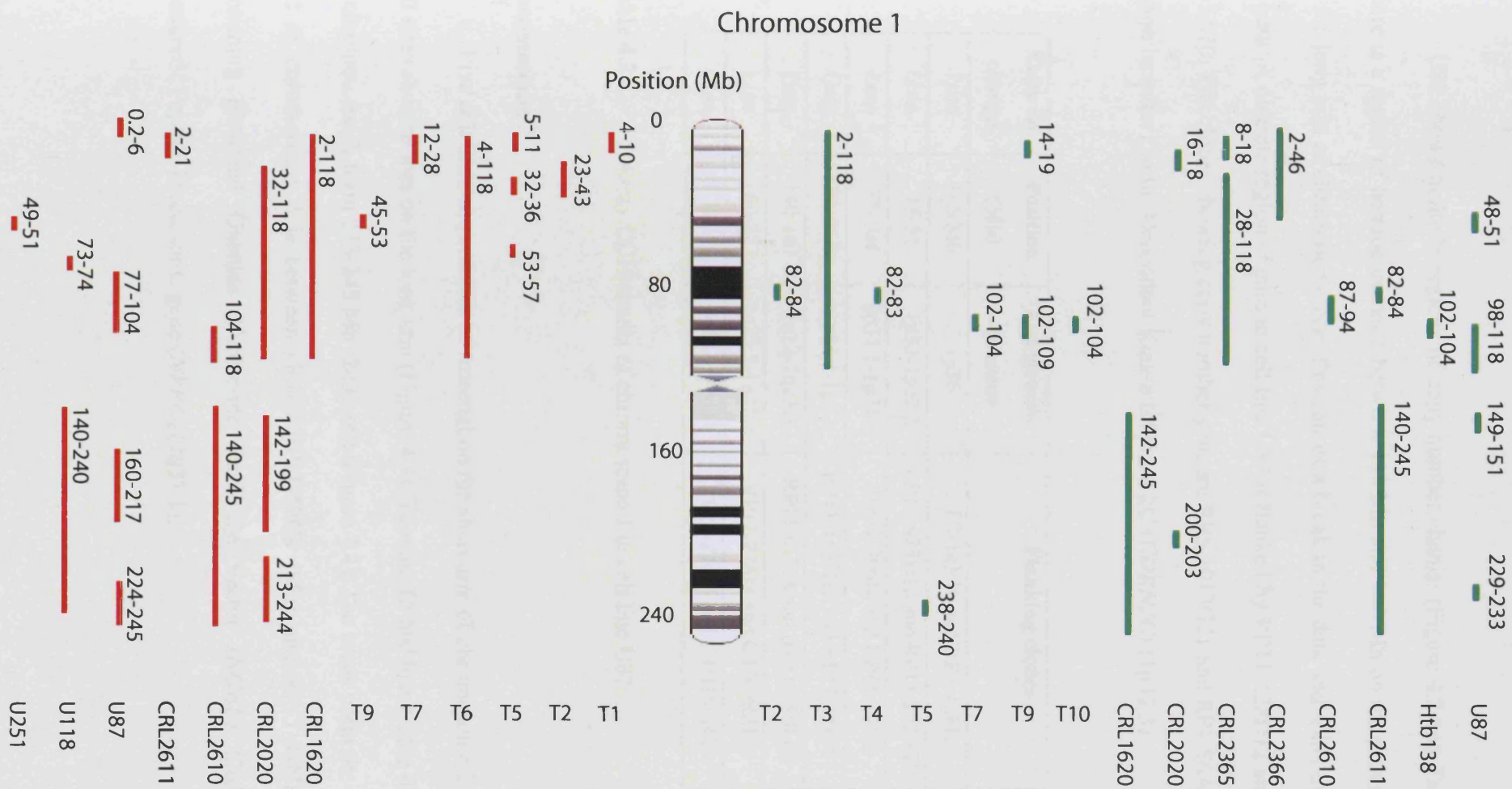


Figure 4.1 Composite array CGH profile of chromosome 1

U87 shows multiple regions of copy number change (Figure 4.2 and Table 4.2). There is a region of heterochromatin between 118 Mb and 140 Mb on the proximal part of the long arm of chromosome one, this causes a break in the data and splits the region of gain. A discrete region of gain in cell line U87 is flanked by RP11-428D12 and RP11-253A20. The clones showing copy number gain are RP5-1013G21 and RP1-86A18. This region includes Cyclin-Dependent Kinase Inhibitor 2C (*CDKN2C*) (1p32.3).

Copy no. change	Position (Mb)	Cytogenetic location	Flanking clones
Loss	0-6 Mb	1p36	CTB-14E10 and RP3-438L4
Gain	48-51	1p33-1p32.3	RP11-428D12 and RP11-253A20
Loss	77-104	1p31.1-1p21.3	RP11-306I4 and RP11-17C2
Gain	98-118	1p31.1-1p12	RP11-143H12 and RP11-418J17
Gain	140-161	1q12-1q23.3	RP11-417J8 and RP11-180L13
Loss	160-217	1q23.3-1q42.2	RP11-276J4 and CTB160H23
Loss	224-245	1q42.13-1q44	RP11-276J4 and CTB160H23

Table 4.2 Array CGH results of chromosome 1 in cell line U87

Chromosome 2

Five cell lines showed loss of material on the short arm of chromosome 2 and five cell lines showed loss on the long arm (Figure 4.3). Tumour T5 had loss on the distal end of chromosome 2, from 233-245 Mb (2q37-tel) (Figure 4.4). The break point the terminal end of chromosome 2 is between clones RP11-52C8 (Mb) and RP11-91N19 (Mb) containing Neuronal Guanine Nucleotide Exchange Factor (*NGEF*) (2q37) and Natriuretic Peptide Precursor C gene (*NPPC*) (2q37.1).

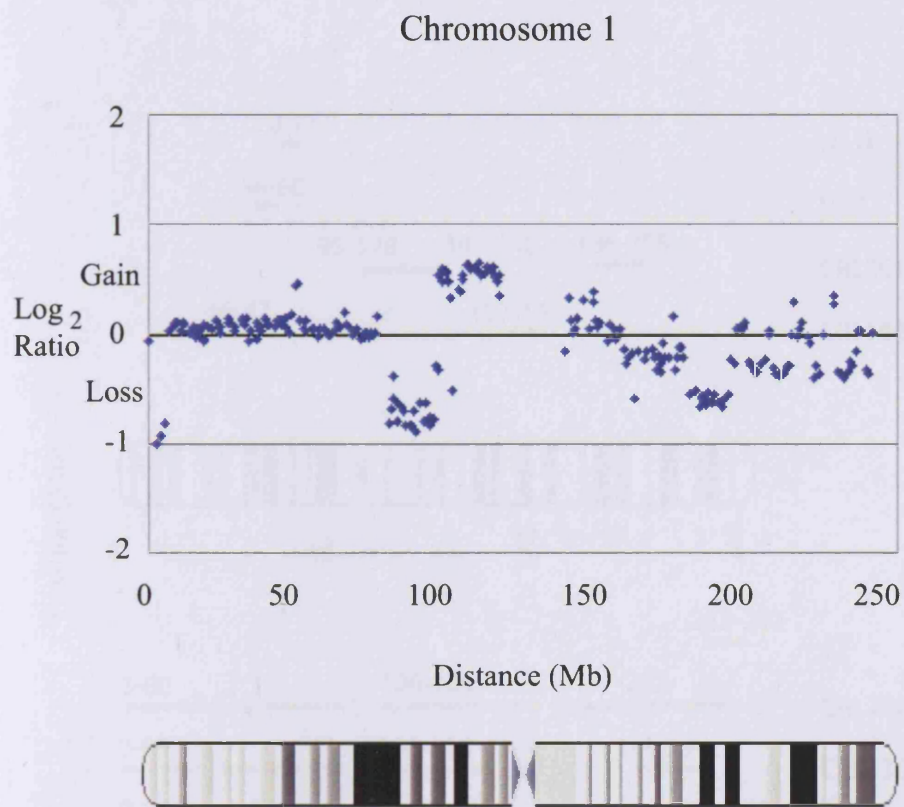


Figure 4.2 Array CGH profile of chromosome 1 in U87

Chromosome 1p shows two regions of loss and a region of copy number gain. 1q followed by a region of gain and two regions of loss. The heterochromatin on 1q gives a gap in the data.

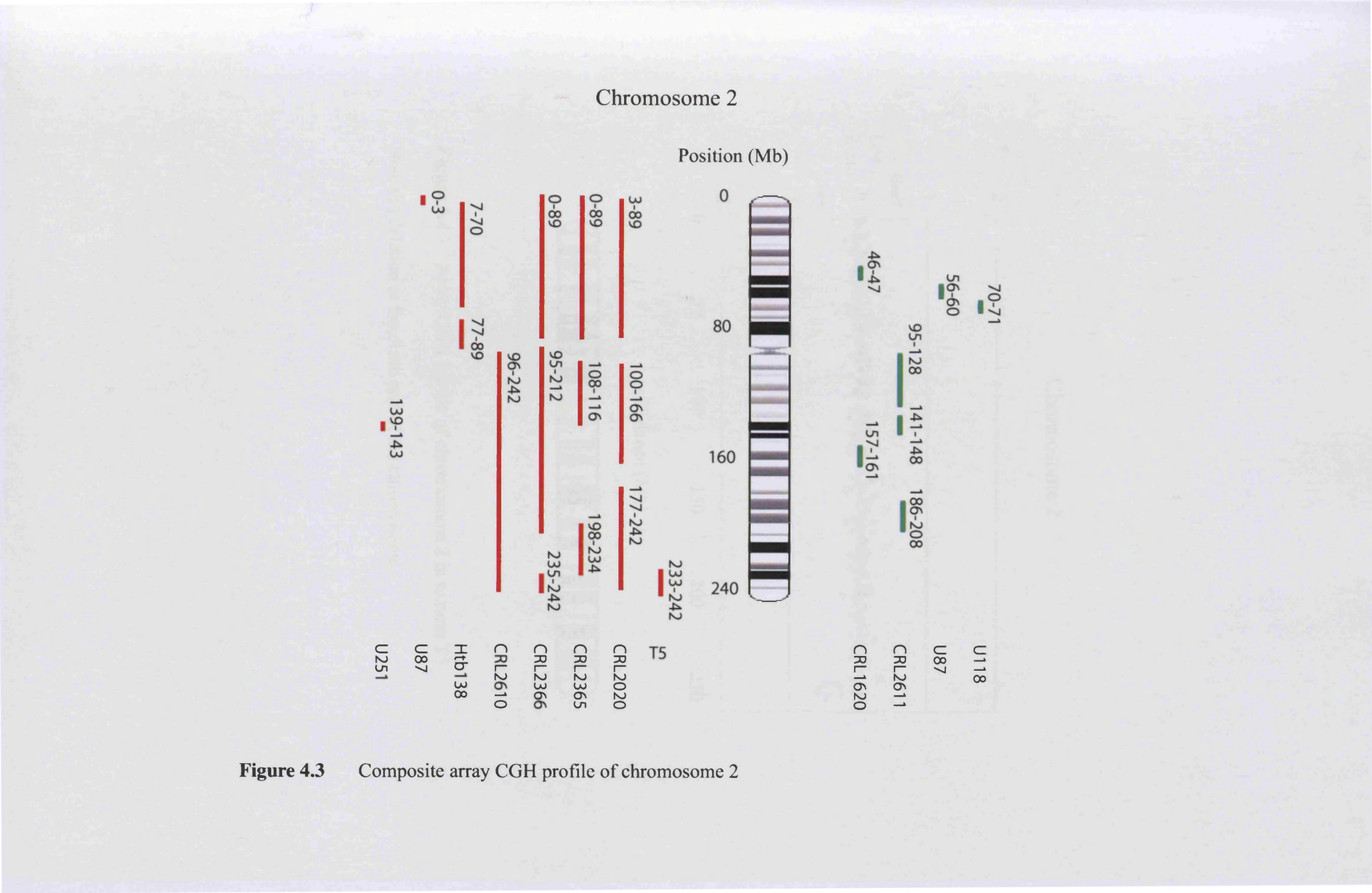


Figure 4.3 Composite array CGH profile of chromosome 2

Chromosome 2

Many copy number changes have been identified in this chromosome. The following table shows a single copy deletion of 8P11-12.3 (Cytoband 8p11-12.3) linked to chromosome 8P11-12.3 (Cytoband 8p11-12.3).

When the 8P11-12.3 region is deleted, the 8P11-12.3 region is lost. This deletion is associated with a loss of heterozygosity (LOH) at the 8P11-12.3 region.

The data shows a single copy deletion of 8P11-12.3 (Cytoband 8p11-12.3) linked to chromosome 8P11-12.3 (Cytoband 8p11-12.3).

When the 8P11-12.3 region is deleted, the 8P11-12.3 region is lost. This deletion is associated with a loss of heterozygosity (LOH) at the 8P11-12.3 region.

The data shows a single copy deletion of 8P11-12.3 (Cytoband 8p11-12.3) linked to chromosome 8P11-12.3 (Cytoband 8p11-12.3).

When the 8P11-12.3 region is deleted, the 8P11-12.3 region is lost. This deletion is associated with a loss of heterozygosity (LOH) at the 8P11-12.3 region.

The data shows a single copy deletion of 8P11-12.3 (Cytoband 8p11-12.3) linked to chromosome 8P11-12.3 (Cytoband 8p11-12.3).

When the 8P11-12.3 region is deleted, the 8P11-12.3 region is lost. This deletion is associated with a loss of heterozygosity (LOH) at the 8P11-12.3 region.

The data shows a single copy deletion of 8P11-12.3 (Cytoband 8p11-12.3) linked to chromosome 8P11-12.3 (Cytoband 8p11-12.3).

When the 8P11-12.3 region is deleted, the 8P11-12.3 region is lost. This deletion is associated with a loss of heterozygosity (LOH) at the 8P11-12.3 region.

The data shows a single copy deletion of 8P11-12.3 (Cytoband 8p11-12.3) linked to chromosome 8P11-12.3 (Cytoband 8p11-12.3).

When the 8P11-12.3 region is deleted, the 8P11-12.3 region is lost. This deletion is associated with a loss of heterozygosity (LOH) at the 8P11-12.3 region.

The data shows a single copy deletion of 8P11-12.3 (Cytoband 8p11-12.3) linked to chromosome 8P11-12.3 (Cytoband 8p11-12.3).

When the 8P11-12.3 region is deleted, the 8P11-12.3 region is lost. This deletion is associated with a loss of heterozygosity (LOH) at the 8P11-12.3 region.

The data shows a single copy deletion of 8P11-12.3 (Cytoband 8p11-12.3) linked to chromosome 8P11-12.3 (Cytoband 8p11-12.3).

When the 8P11-12.3 region is deleted, the 8P11-12.3 region is lost. This deletion is associated with a loss of heterozygosity (LOH) at the 8P11-12.3 region.

The data shows a single copy deletion of 8P11-12.3 (Cytoband 8p11-12.3) linked to chromosome 8P11-12.3 (Cytoband 8p11-12.3).

When the 8P11-12.3 region is deleted, the 8P11-12.3 region is lost. This deletion is associated with a loss of heterozygosity (LOH) at the 8P11-12.3 region.

The data shows a single copy deletion of 8P11-12.3 (Cytoband 8p11-12.3) linked to chromosome 8P11-12.3 (Cytoband 8p11-12.3).

When the 8P11-12.3 region is deleted, the 8P11-12.3 region is lost. This deletion is associated with a loss of heterozygosity (LOH) at the 8P11-12.3 region.

The data shows a single copy deletion of 8P11-12.3 (Cytoband 8p11-12.3) linked to chromosome 8P11-12.3 (Cytoband 8p11-12.3).

When the 8P11-12.3 region is deleted, the 8P11-12.3 region is lost. This deletion is associated with a loss of heterozygosity (LOH) at the 8P11-12.3 region.

The data shows a single copy deletion of 8P11-12.3 (Cytoband 8p11-12.3) linked to chromosome 8P11-12.3 (Cytoband 8p11-12.3).

When the 8P11-12.3 region is deleted, the 8P11-12.3 region is lost. This deletion is associated with a loss of heterozygosity (LOH) at the 8P11-12.3 region.

The data shows a single copy deletion of 8P11-12.3 (Cytoband 8p11-12.3) linked to chromosome 8P11-12.3 (Cytoband 8p11-12.3).

Chromosome 2

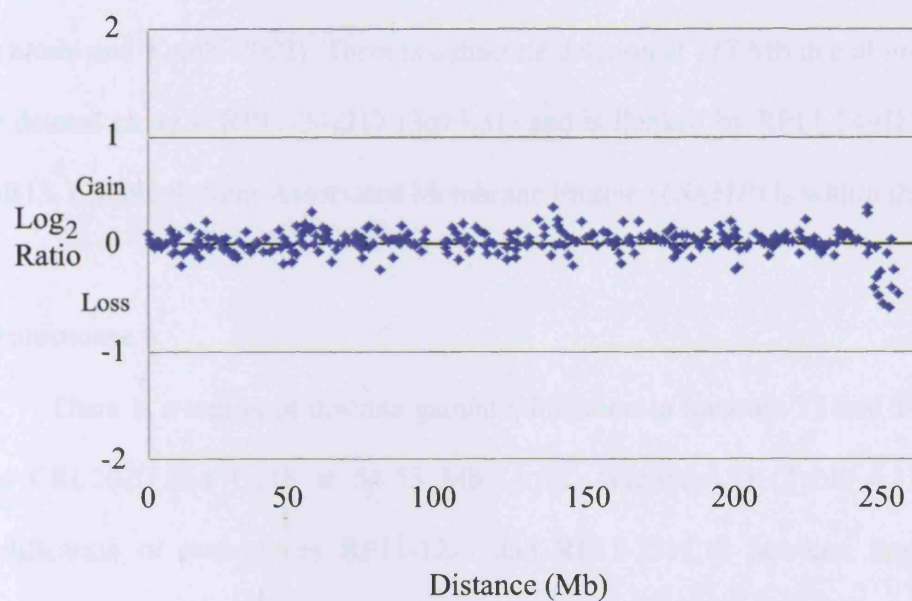


Figure 4.4 Array CGH profile of chromosome 2 in tumour T5

Note the deletion at the distal end of the chromosome.

Chromosome 3

Many copy number gains and losses were detected on chromosome 3 (Figure 4.5). A single clone deletion, RP11-165B2 at 13 Mb (3p25.1), flanked by clones RP11-488M6 and RP11-316A10, was deleted in cell line CRL1620 (Figure 4.6). This deletion contains Wingless-Type MMTV Integration site family member 7A gene (*WNT7A*) (3p25) (Kirikoshi and Katoh, 2002). There is a discrete deletion at 117 Mb in cell line CRL2611. The deleted clone is RP11-342J17 (3q13.31) and is flanked by RP11-249J17 and RP11-165B13. Limbic System-Associated Membrane Protein (*LSAMP*) is within this deletion.

Chromosome 4

There is a region of discrete gain/amplification in tumours T3 and T4 and in cell lines CRL2020 and U118 at 54-55 Mb (4q12) (Figure 4.7) (Table 4.3). T3 shows amplification of two clones RP11-12J3 and RP11-231C18 between flanking clones RP11-18M17 and RP11-148K14 (54.3-56.1 Mb) (Figure 4.8). Genes within this region are Cysteine-Rich Hydrophobic Domain 2 (*CHIC2*), Platelet Derived Growth Factor Receptor Alpha (*PDGFRA*), KIT oncogene (*KIT*) and Kinase Insert Domaine Receptor (*KDR*).

Sample	RP11-157C8	RP11-18M17	RP11-12J3	RP11-231C18	RP11-148K14
T3	-0.04	0.03	1.48	1.9	0.09
T4	0.24	0.20	0.36	0.14	0.11
CRL2020	0.18	0.18	0.92	0.09	0.18
U118	-0.20	-0.09	0.47	0.04	0.00

Table 4.3 Log₂ ratios of clones in tumour samples and cell lines showing gain or amplification at 4q12.

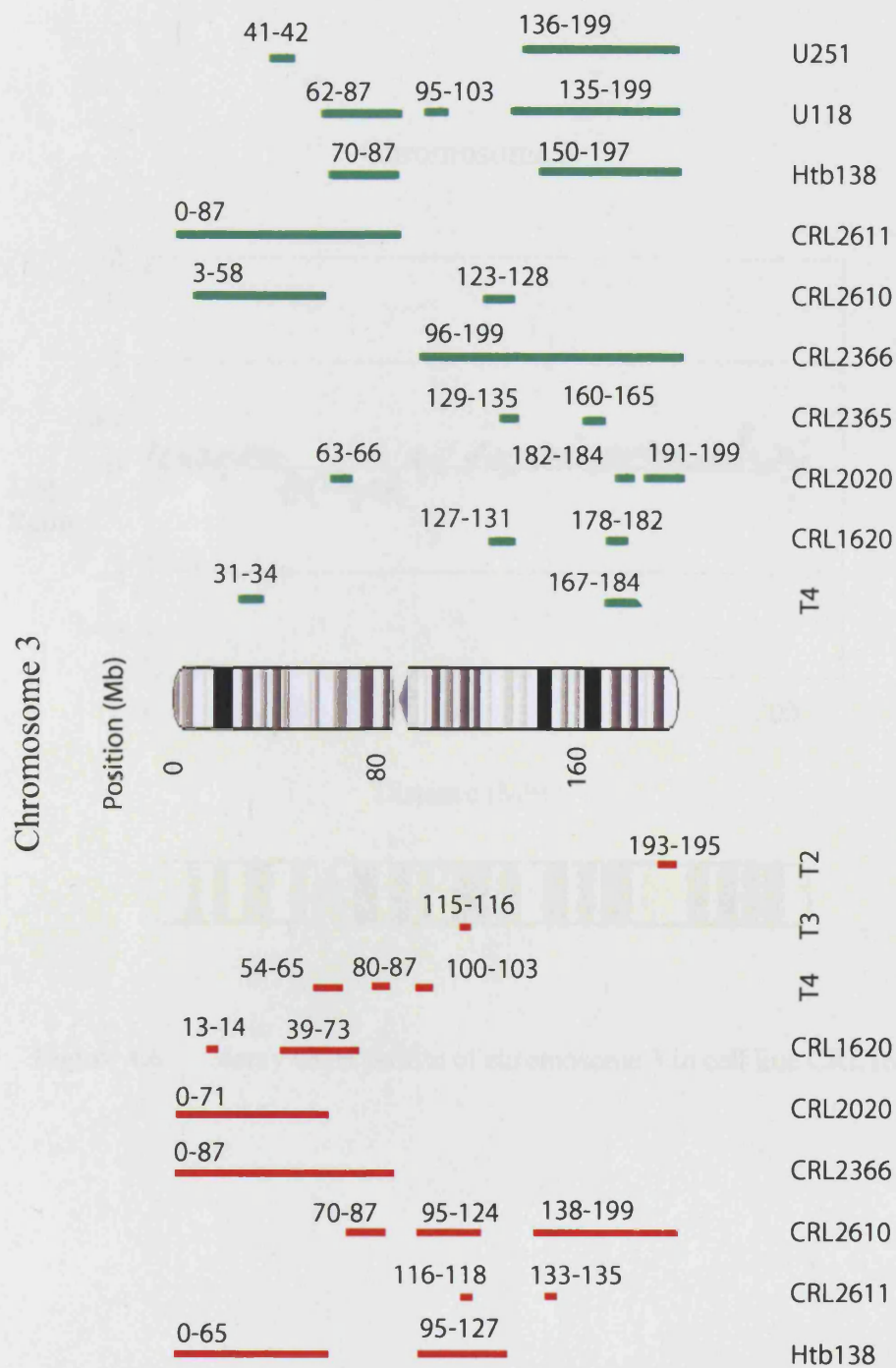


Figure 4.5 Composite array CGH profile of chromosome 3

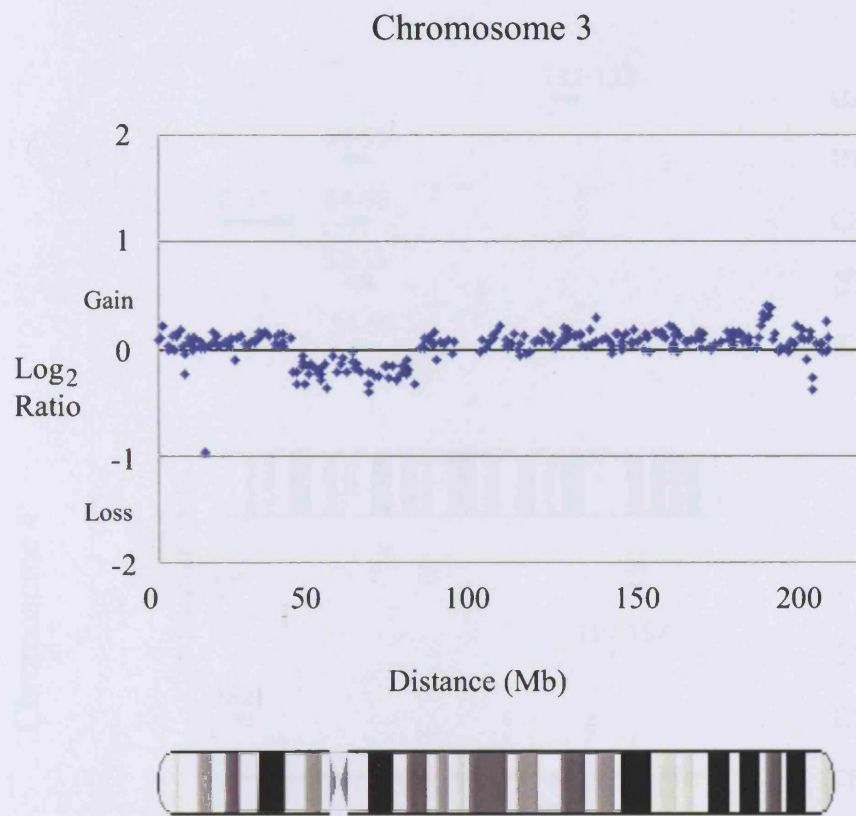


Figure 4.6 Array CGH profile of chromosome 3 in cell line CRL1620

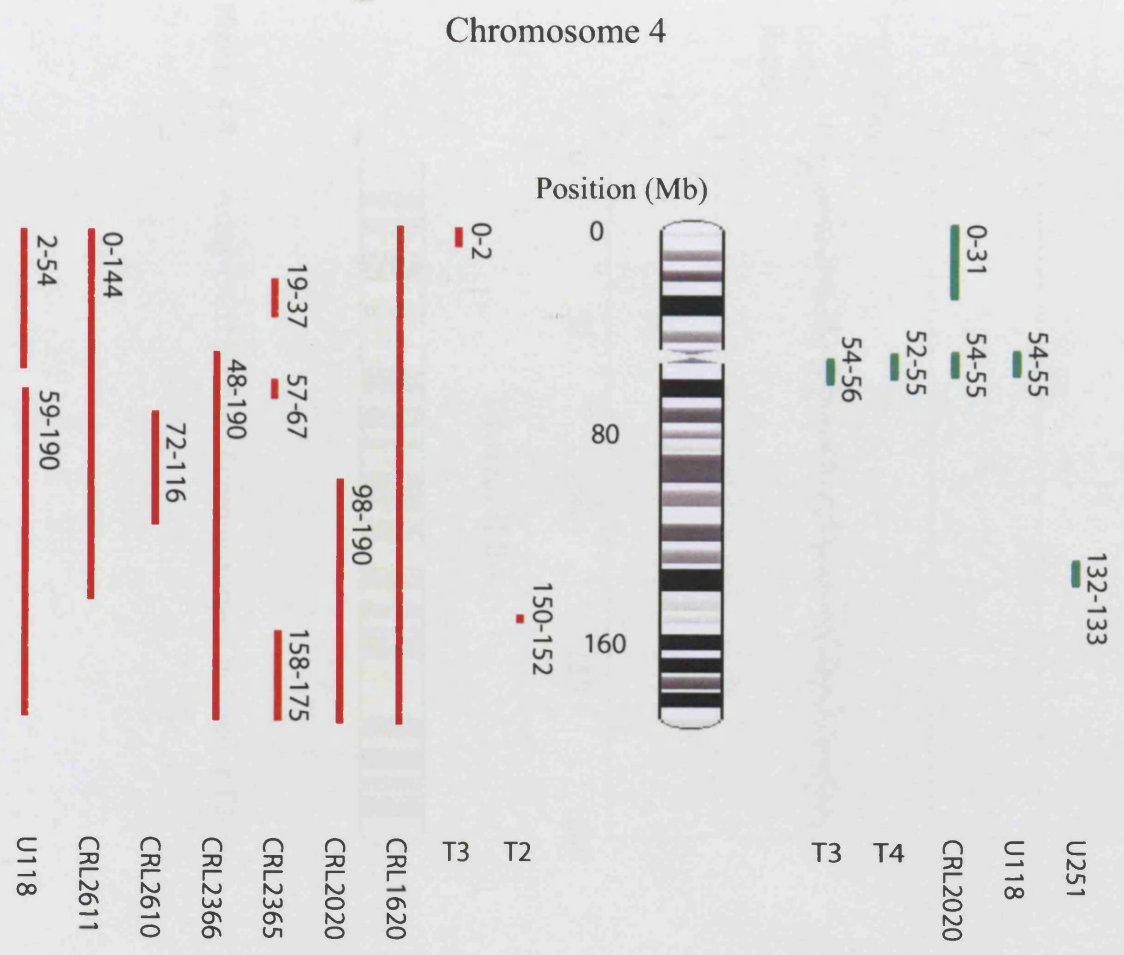


Figure 4.7 Composite array CGH profile of chromosome 4

Chromosome 5

Gain of 82-86 Mb (5q21) was found in tumours T2, T3 and T4 and in cell lines CRL2611 and Htb138 and this gain was encompassed by larger region of gain in cell line CRL2610 (Figure 4.9). Genes in this region of gain include Heparanase (*HPSE*), CPD-Diacylglycerol Synthase 1 (*CDS1*), Heterogeneous Nuclear Ribonucleoprotein D (*HNRPD*) and Protein Kinase CGMP-dependent, type II (*PRKG2*).

Chromosome 6

Chromosome 6 shows numerous regions of copy number change (Figure 4.10). The short arm of chromosome 6 had deletions in one tumour and four cell lines. The minimal region of deletion in tumour T2 was between 17 and 19 Mb (6p22.3) and contains the Spinocerebellar Ataxia 1/ataxin-1 gene (*SCA1*). The long arm of chromosome 6 had numerous copy number aberrations, the majority of changes being loss. Two patient samples, T5 and T8 show loss of 6q. The cell lines have a more complex set of changes.

CRL2365 and CRL2366 are derived from the same patient sample and they have the same DNA copy number profile on chromosome 6. The array CGH shows gain at 6p and two areas of loss, 6q14.3 (86 Mb) - 6q16.3 (100 Mb) and 6q21 (114 Mb) - 6q22.31 (122 Mb) (Figure 4.11). The flanking clones are bA30P6, bA117M4 and bA346K2, bA95G17. The deletion between 86 and 100 Mb, contains the Ephrin Receptor A7 gene (*EPHA7*) (6q16.1, 93.9Mb). A further deletion between 99 and 104 Mb (6q16.3), containing Cyclin C (*CCNC*) and Single Minded (*SIMI*) was seen in U87.

Chromosome 5

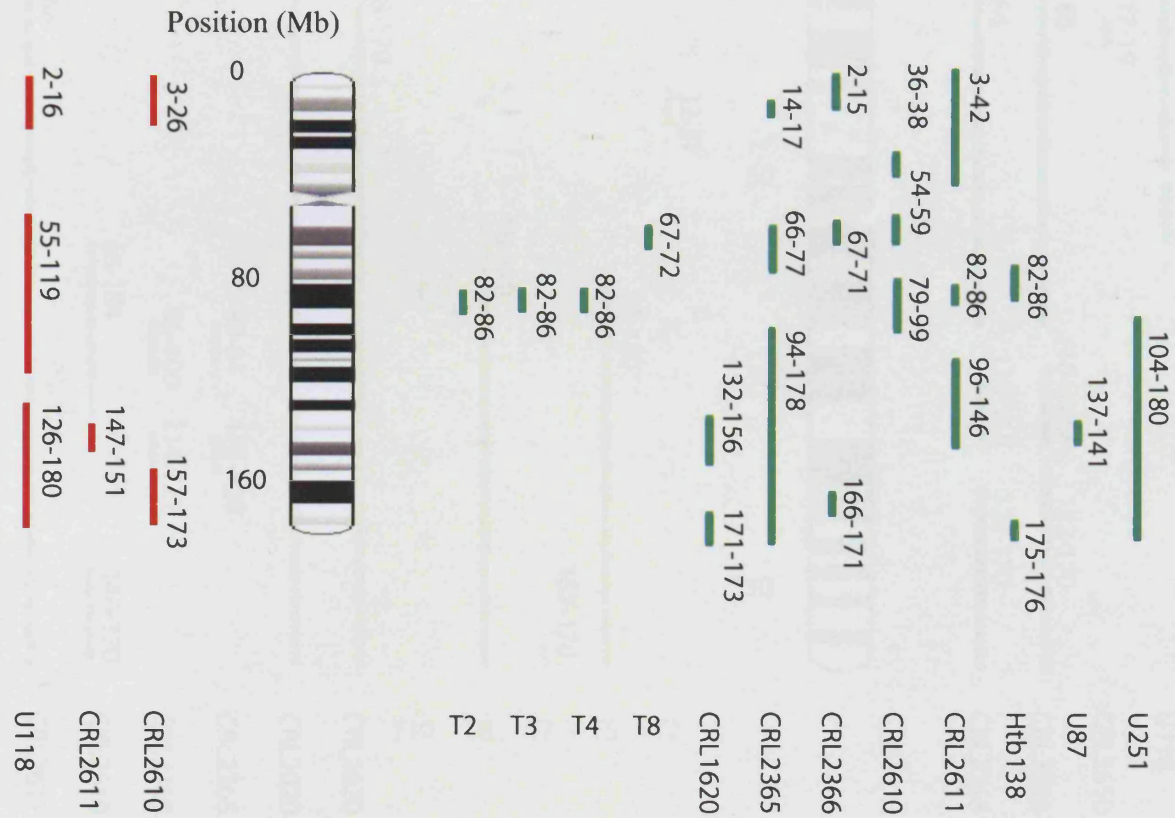


Figure 4.9 Composite array CGH profile of chromosome 5

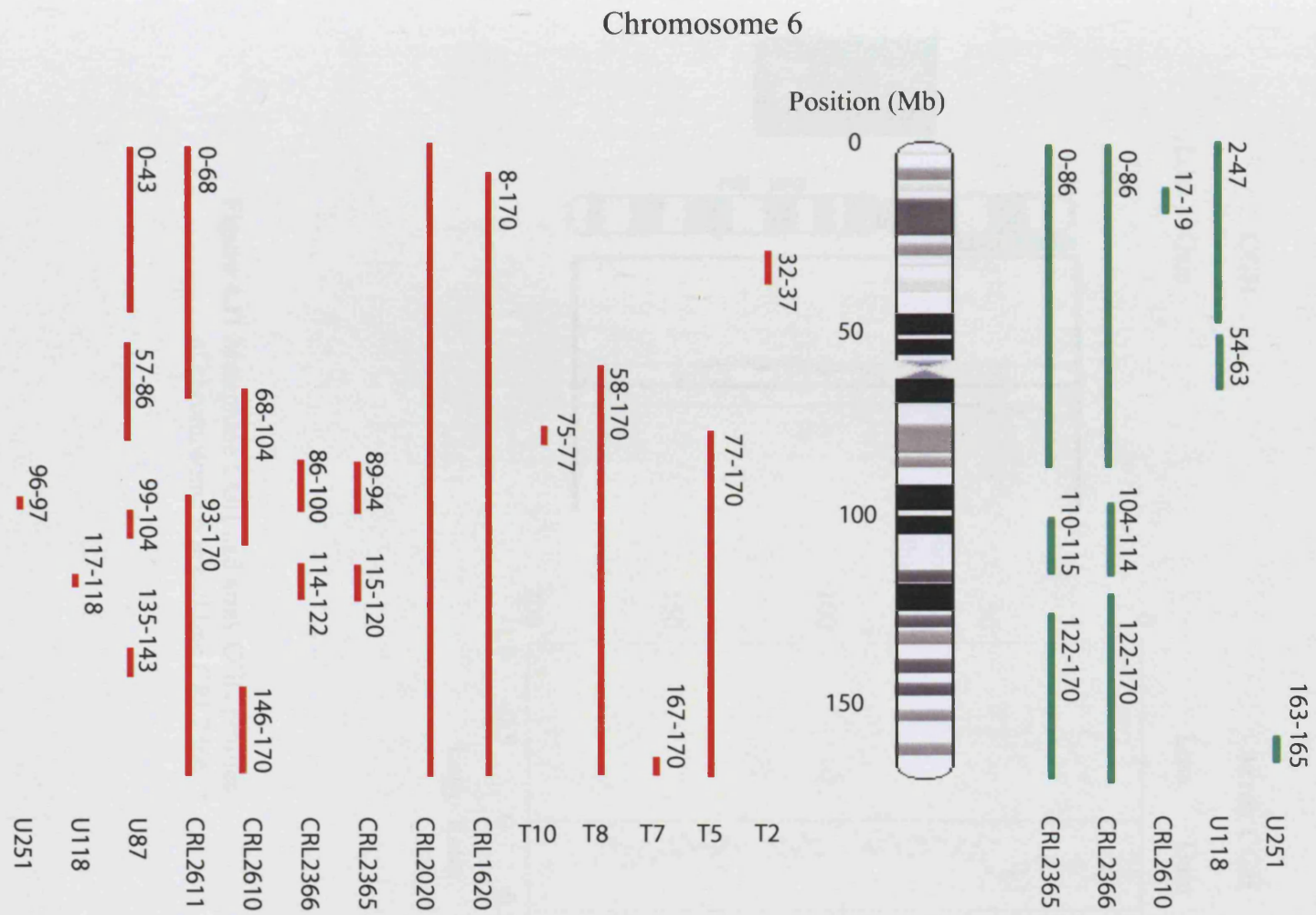


Figure 4.10 Composite array CGH profile of chromosome 6

Chromosome 6

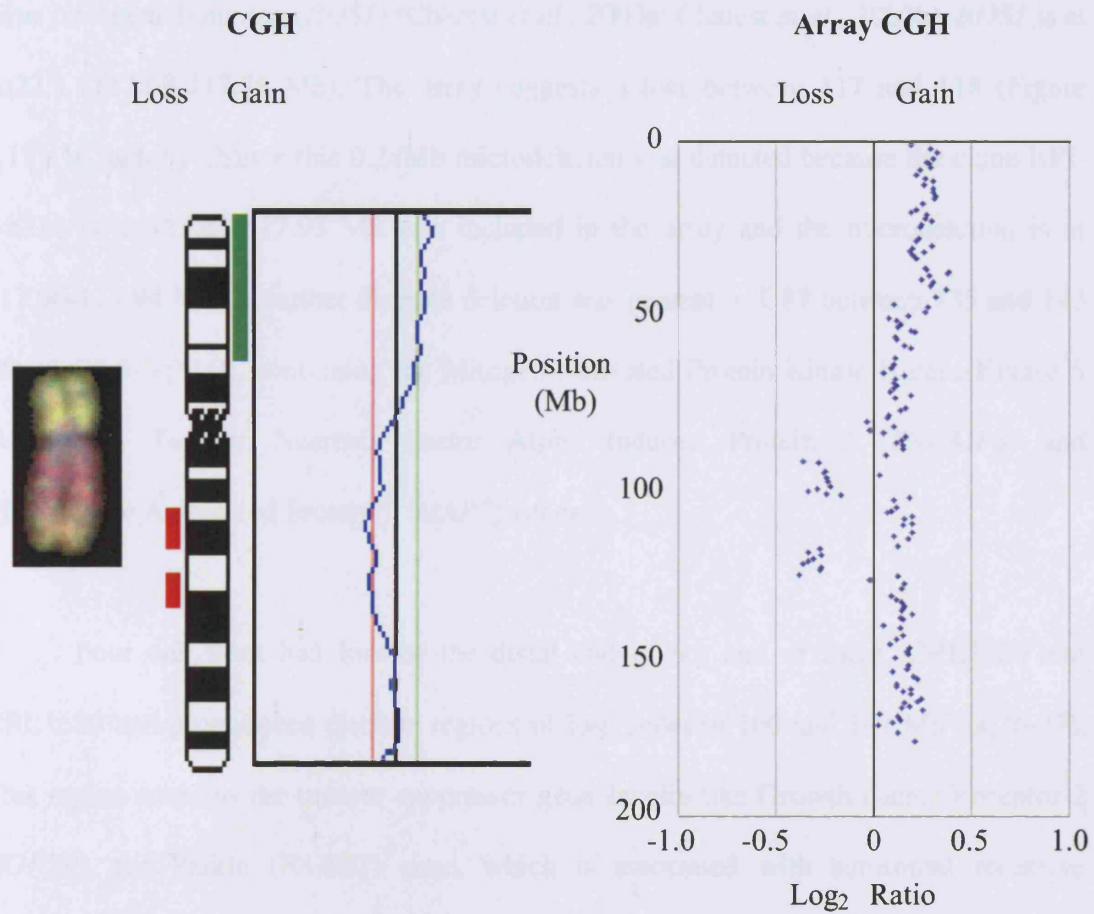


Figure 4.11 Metaphase CGH and array CGH profiles of chromosome 6 in cell line CRL2366

A discrete deletion was found between 117 and 118 Mb (6q22.1) in U118 (Figure 4.10), which encompasses a previously described microdeletion. This microdeletion causes a fusion between two genes, Fused in Glioma (*FIG*) and v-ros avian UR2 sarcoma virus oncogene homolog (*ROS1*) (Charest *et al.*, 2003a; Charest *et al.*, 2003b). *ROS1* is at 6q22.1 (117.63-117.76 Mb). The array suggests a loss between 117 and 118 (Figure 4.12). In fact, by chance this 0.24Mb microdeletion was detected because the clone RPI-94G16 is at 117.83-117.93 Mb was included in the array and the microdeletion is at 117.90-117.94 Mb. A further discrete deletion was present in U87 between 135 and 143 Mb (6q23.3-6q24.2), containing the Mitogen-Activated Protein Kinase-Kinase-Kinase 5 (*MAP3K5*), Tumour Necrosis Factor Alpha Induced Protein 3 (*TNFAIP3*) and Microtubule Associated Protein 7 (*MAP7*) genes.

Four cell lines had loss of the distal end of 6q, and of these, CRL2020 and CRL1620 had pronounced discrete regions of loss between 160 and 167 Mb (6q26-27). This region contains the tumour suppressor gene Insulin-like Growth Factor Receptor 2 (*IGF2R*), the Parkin (*PARK2*) gene, which is associated with autosomal recessive juvenile parkinsonism, Parkin Co-Regulated Gene (*PACRG*) and Quaking Isoform gene (*QKI*) (Figure 4.13).

Minimal regions of loss were seen at 75-77 Mb in tumour T10 and at 167-170 Mb in tumour T7. A discrete deletion was found in U251 between 96 and 97 Mb (6q16.1).

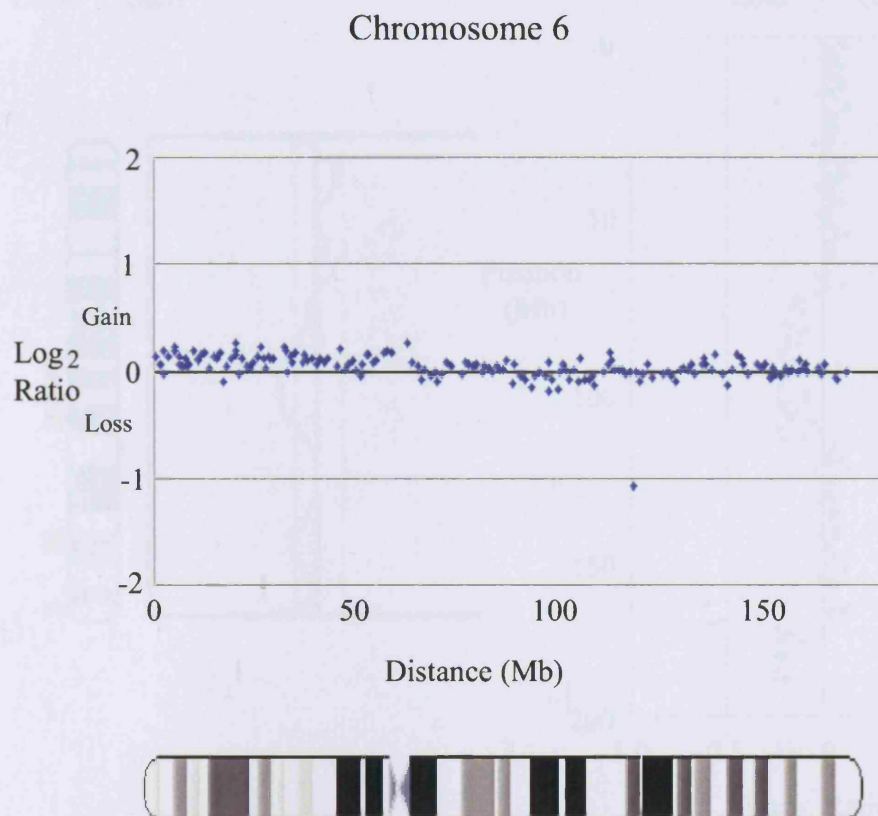


Figure 4.12 Array CGH profile of chromosome 6 in cell line U118

Clone RP1-94G16 shows a deletion at 117 Mb.

Chromosome 6

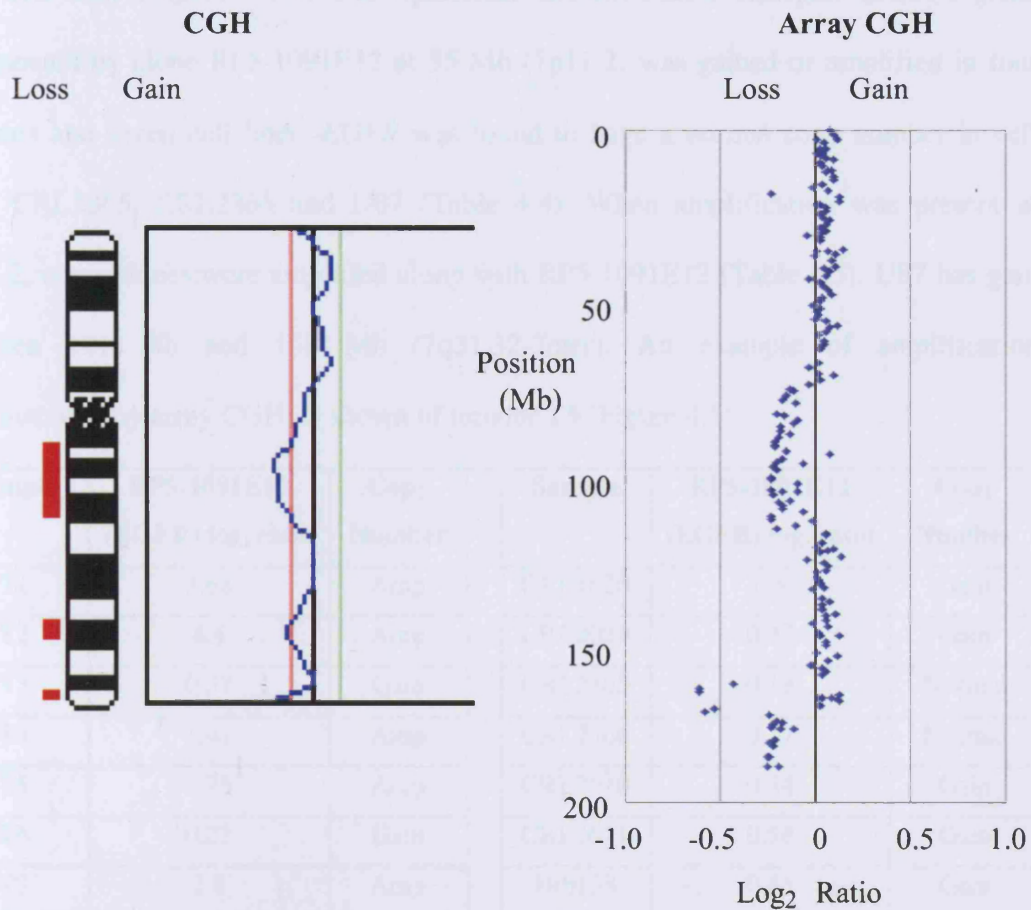


Figure 4.13 Metaphase CGH and array CGH profiles of chromosome 6 in cell line CRL2610

Chromosome 7

Gain of genetic material from chromosome 7 was seen in all tumour samples and nine cell lines (Figure 4.14). The Epidermal Growth Factor Receptor (*EGFR*) gene, represented by clone RP5-1091E12 at 55 Mb (7p11.2) was gained or amplified in four tumours and seven cell lines. *EGFR* was found to have a normal copy number in cell lines CRL2365, CRL2366 and U87 (Table 4.4). When amplification was present at 7p11.2, other clones were amplified along with RP5-1091E12 (Table 4.5). U87 has gain between 121 Mb and 158 Mb (7q31.32-7qter). An example of amplification demonstrated by array CGH, is shown of tumour T5 (Figure 4.15).

Sample	RP5-1091E12 (EGFR) log ₂ ratio	Copy Number	Sample	RP5-1091E12 (EGFR) log ₂ ratio	Copy Number
T1	3.68	Amp	CRL1620	0.8	Gain
T2	4.4	Amp	CRL2020	0.37	Gain
T3	0.37	Gain	CRL2365	0.13	Normal
T4	1.47	Amp	CRL2366	0.27	Normal
T5	3.75	Amp	CRL2610	0.34	Gain
T6	0.22	Gain	CRL2611	0.58	Gain
T7	2.8	Amp	Htb138	0.45	Gain
T8	2.2	Amp	U87	0.00	Normal
T9	2.3	Amp	U118	0.42	Gain
T10	0.26	Gain	U251	0.47	Gain

Table 4.4 Log₂ value of clone RP5-1091E12 representing *EGFR* in all the tumour samples and cell lines

In the literature, gain is more than two copies in a diploid state and amplification is four-five extra copies. Numerically it is possible to state how many copies a certain log₂ value represents, however in practice this is not so straightforward. In this study a

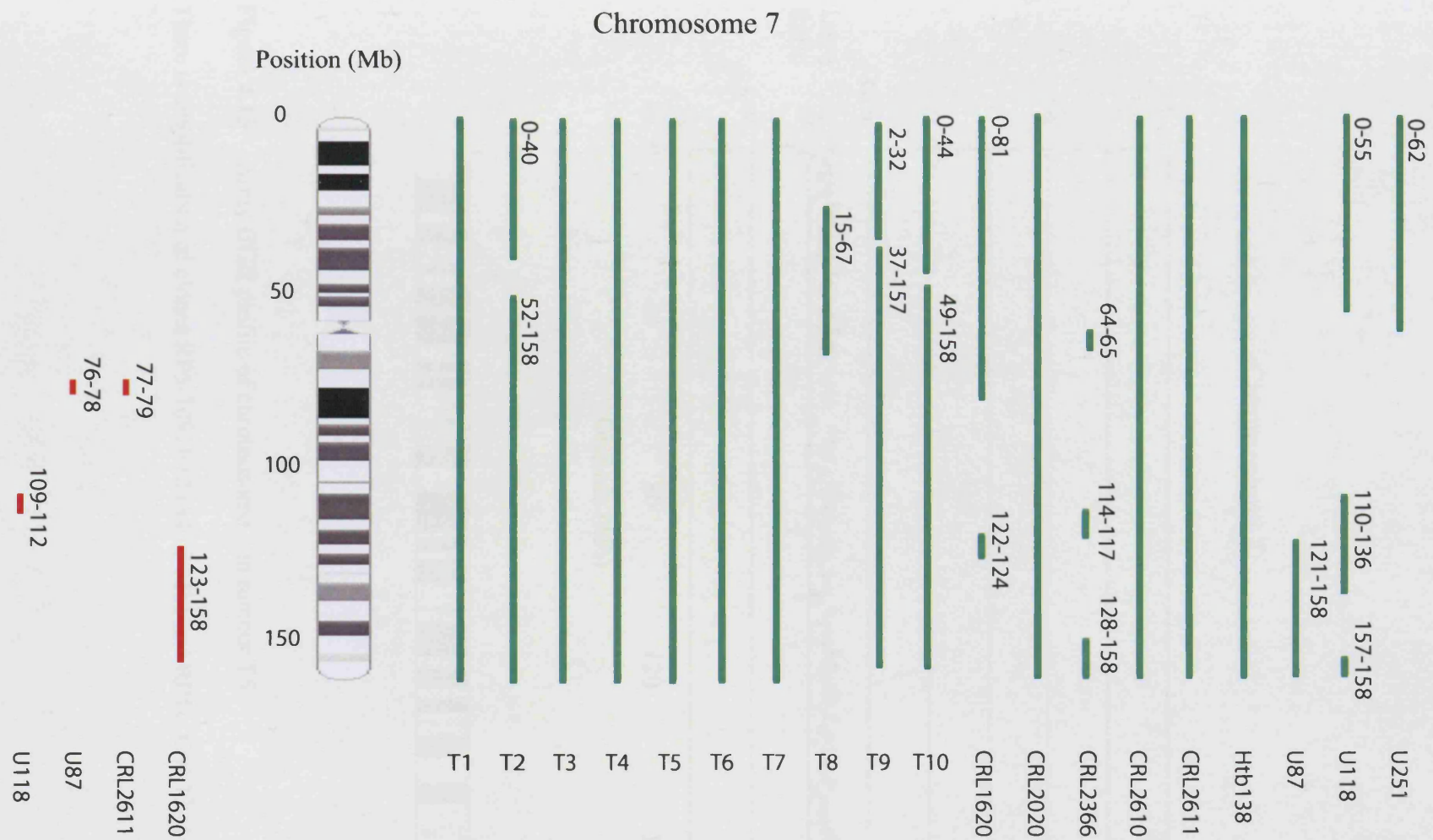


Figure 4.14 Composite array CGH profile of chromosome 7

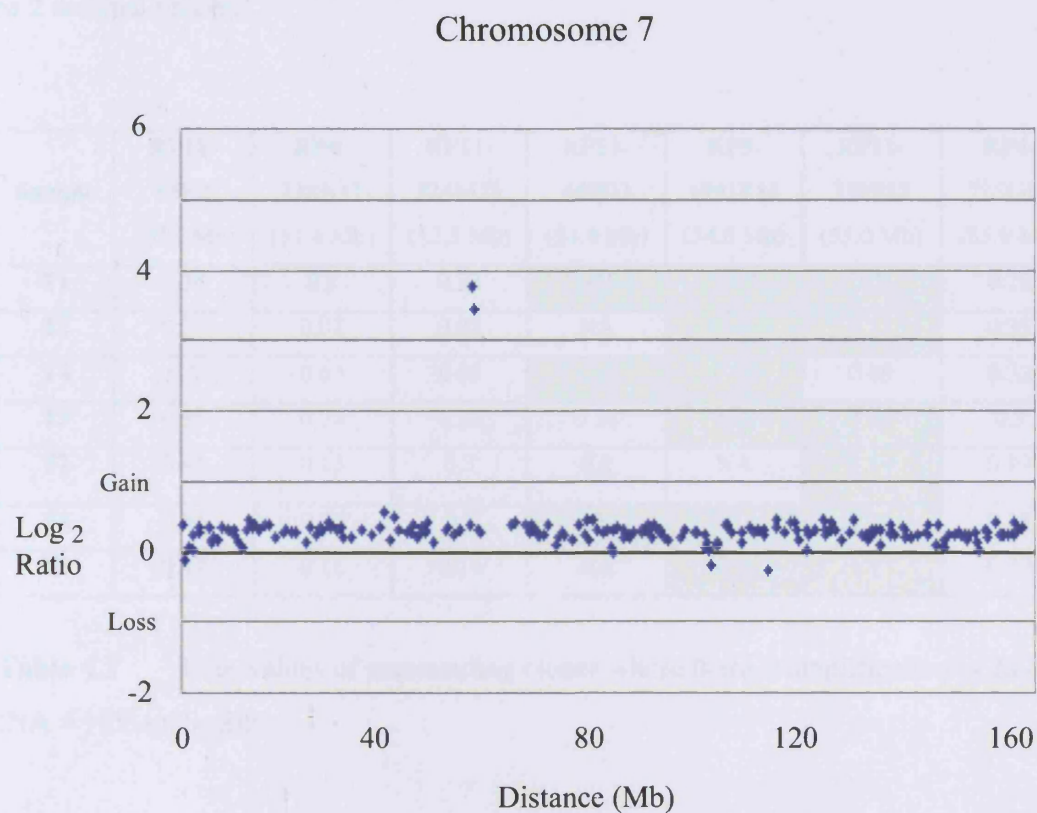


Figure 4.15 Array CGH profile of chromosome 7 in tumour T5

There is amplification of clones RP5-1091E12 (54.63 Mb) and RP11-339F13 (54.78 Mb).

\log_2 value of greater than 1 has been called amplification. Table 4.5 shows the \log_2 values of the surrounding clones where there is amplification of EGFR. \log_2 values are rounded to 2 decimal places.

Sample	RP11- 95E2 (50.2 Mb)	RP4- 718N17 (51.4 Mb)	RP11- 324M21 (52.5 Mb)	RP11- 449G3 (54.4 Mb)	RP5- 1091E12 (54.8 Mb)	RP11- 339F13 (55.0 Mb)	RP4- 725G10 (55.9 Mb)
T1	0.38	0.2	0.23	3.85	3.69	3.2	0.28
T2	0.04	0.02	0.07	NA	4.5	4.23	0.35
T4	0.6	0.63	0.88	1.25	1.48	0.88	0.32
T5	0.36	0.24	0.32	0.38	3.76	3.45	0.3
T7	0.43	0.13	0.3	0.8	NA	2.18	0.19
T8	0.37	0.25	0.2	2.27	2.27	1.28	0.28
T9	0.47	0.18	0.14	NA	2.3	1.55	0.23

Table 4.5 \log_2 values of surrounding clones where there is amplification of *EGFR* (NA = Not applicable)

Chromosome 8

There were deletions in chromosome 8, in eight cell lines but not in any tumour samples (Figure 4.16). There was a discrete gain of RP1-144M5 at 34 Mb (8p12) in tumour T3 and cell line CRL1620. This region, flanked by clones RP11-75P13 and RP1-155L11, contains no genes. Cell line U87 has two discrete deletions on the long arm. The first is from 87-90 Mb and is flanked by clones RP11-2F15 and RP5-1098O20. Included in this region of loss is the Matrix Metalloproteinase 16 gene (*MMP16*) (8q21.3). The second deletion from 141-145 Mb involves loss of clone RP11-370K2 (8q24.3) and is flanked by RP11-65A5 and RP5-118A7. Protein-Tyrosine Phosphatase type 4 A3 gene (*PTP4A3*) (8q24.3) is included in this deletion.

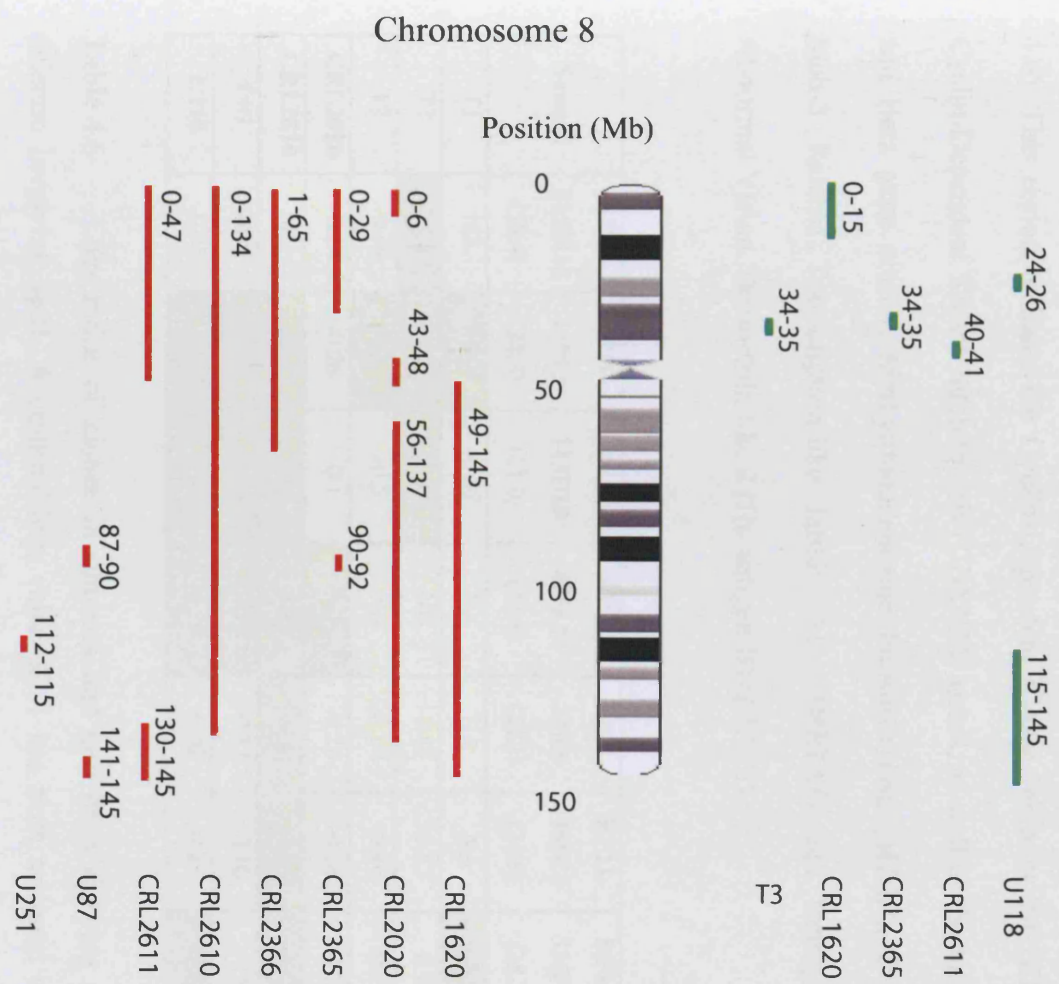


Figure 4.16 Composite array CGH profile of chromosome 8

Chromosome 9

Loss of 9p material was seen in nine tumour samples and six cell lines (Figure 4.17). Homozygous deletions were found on the short arm between 21 and 24 Mb (9p21) in tumour T2 and in cell lines CRL2020, CRL2610, U87 and U118 (Figure 4.18) (Table 4.6). This region includes the Cyclin-Dependent Kinase Inhibitor 2A (*CDKN2A*) and Cyclin-Dependent Kinase Inhibitor 2B (*CDKN2B*) genes, as well as the Interferon Alpha and Beta gene cluster, Methylthioadenosine Phosphorylase (*MTAP*), Doublesex and Mab-3 Related Transcription-like family A1 (*DMRTA1*) and Embryonic Lethal, Abnormal Vision, Drosophila-like 2 (Hu antigen B) (*ELAV2*).

Sample	RP11- 513M16 (19.4)	RP11- 15P13 (20.2)	RP11- 113D19 (21.0)	RP11- 495L19 (23.4)	RP11- 33K8 (24.1)	RP11- 468C2 (24.9)	RP11- 33G16 (25.7)	RP11- 5P15 (26.5)
T1	NA	-1.0	-0.37	NA	NA	NA	-1.3	-0.2
T2	2.37	-1.23	-1.35	NA	-0.85	-0.82	-0.95	-0.57
T7	-0.48	-1.15	-0.5	NA	-0.24	-0.46	-0.21	-0.38
CRL2020	-0.24	-0.26	-0.1	-1.39	-0.28	-0.24	-0.79	-0.42
CRL2610	-0.2	-3.03	-2.93	-3.77	-1.9	-1.85	-1.66	-0.39
U87	-0.72	-3.49	-3.08	-2.29	-0.12	-0.76	-0.8	-0.76
U118	-0.47	-1.84	-1.09	-1.29	-0.92	-0.84	-1.05	-1.45

Table 4.6 Log₂ ratios of clones in tumours and cell lines showing homozygous deletion involving 9p21. A nominal log₂ value of -1 has been assigned to describe a homozygous deletion.

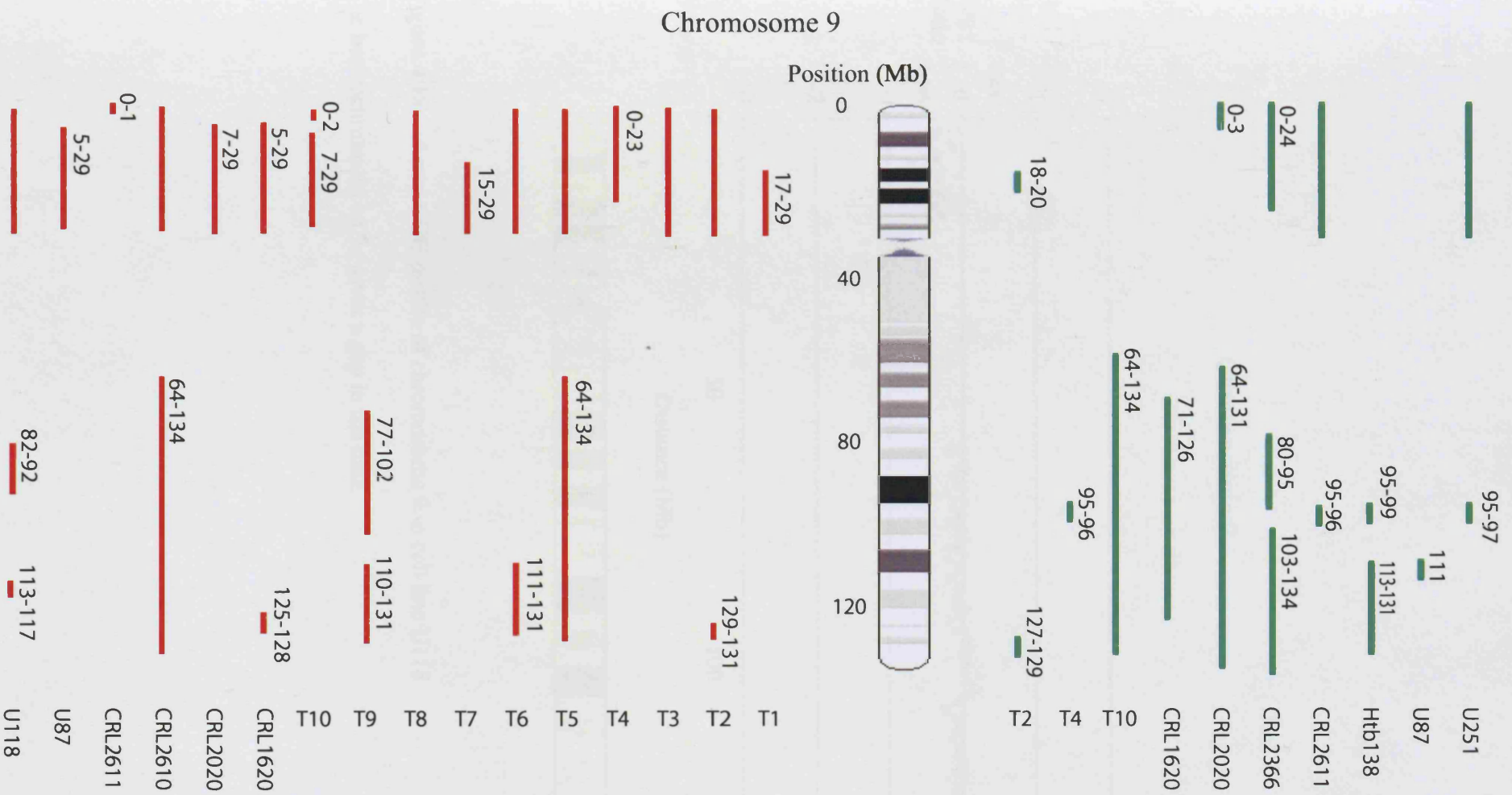


Figure 4.17 Composite array CGH profile of chromosome 9

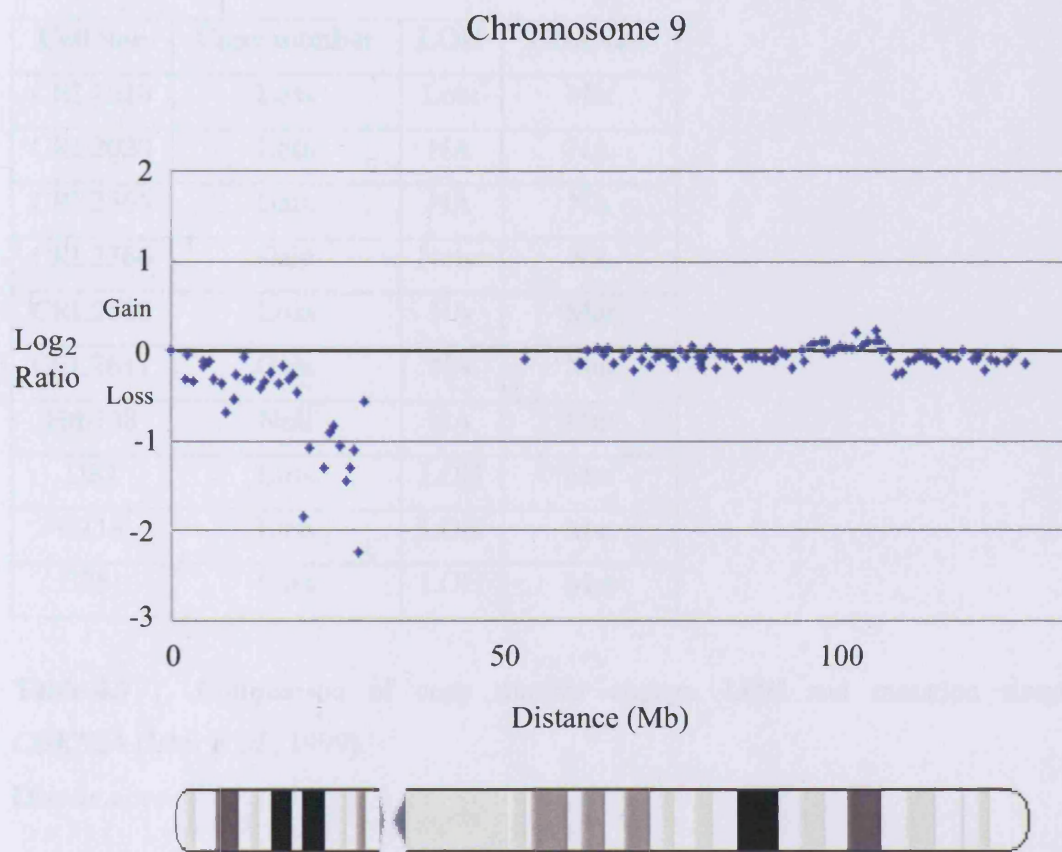


Figure 4.18 Array CGH profile of chromosome 9 in cell line U118

The heterochromatin on 9q gives a gap in the data.

The copy number data in the cell lines in the region involving *CDKN2A* was correlated with LOH status and mutation status of *CDKN2A* (Table 4.7).

Cell line	Copy number	LOH	<i>CDKN2A</i>
CRL1620	Loss	Loss	Mut
CRL2020	Loss	NA	NA
CRL2365	Gain	NA	NA
CRL2366	Gain	None	NA
CRL2610	Loss	NA	Mut
CRL2611	Gain	NA	Mut
Htb138	Null	NA	Mut
U87	Loss	LOH	Mut
U118	Loss	LOH	Mut
U251	Gain	LOH	Mut

Table 4.7 Comparison of copy number change, LOH and mutation status of *CDKN2A* (Ishii *et al.*, 1999).

DN=*de novo*

Cell line CRL1620 shows a probable homozygous deletion from 125-128 Mb (9q34). This deletion is flanked by clones RP11-373J8 and RP11-5N16 and includes the gene Abelson Murine Leukemia Viral Oncogene Homologue 1 (*ABL1*) (Figure 4.19).

Figure 4.19

And the one of the human samples was at the end of the chromosome 9. The data was processed (Figure 4.20), showing the results in Figure 4.21. The data was processed (Figure 4.20), showing the results in Figure 4.21. The data was processed (Figure 4.20), showing the results in Figure 4.21.

Figure 4.21 shows the results of the array CGH analysis. The data was processed (Figure 4.20), showing the results in Figure 4.21. The data was processed (Figure 4.20), showing the results in Figure 4.21.

The data was processed (Figure 4.20), showing the results in Figure 4.21. The data was processed (Figure 4.20), showing the results in Figure 4.21. The data was processed (Figure 4.20), showing the results in Figure 4.21.

The data was processed (Figure 4.20), showing the results in Figure 4.21. The data was processed (Figure 4.20), showing the results in Figure 4.21. The data was processed (Figure 4.20), showing the results in Figure 4.21.

The data was processed (Figure 4.20), showing the results in Figure 4.21. The data was processed (Figure 4.20), showing the results in Figure 4.21. The data was processed (Figure 4.20), showing the results in Figure 4.21.

The data was processed (Figure 4.20), showing the results in Figure 4.21. The data was processed (Figure 4.20), showing the results in Figure 4.21. The data was processed (Figure 4.20), showing the results in Figure 4.21.

The data was processed (Figure 4.20), showing the results in Figure 4.21. The data was processed (Figure 4.20), showing the results in Figure 4.21. The data was processed (Figure 4.20), showing the results in Figure 4.21.

The data was processed (Figure 4.20), showing the results in Figure 4.21. The data was processed (Figure 4.20), showing the results in Figure 4.21. The data was processed (Figure 4.20), showing the results in Figure 4.21.

The data was processed (Figure 4.20), showing the results in Figure 4.21. The data was processed (Figure 4.20), showing the results in Figure 4.21. The data was processed (Figure 4.20), showing the results in Figure 4.21.

The data was processed (Figure 4.20), showing the results in Figure 4.21. The data was processed (Figure 4.20), showing the results in Figure 4.21. The data was processed (Figure 4.20), showing the results in Figure 4.21.

The data was processed (Figure 4.20), showing the results in Figure 4.21. The data was processed (Figure 4.20), showing the results in Figure 4.21. The data was processed (Figure 4.20), showing the results in Figure 4.21.

The data was processed (Figure 4.20), showing the results in Figure 4.21. The data was processed (Figure 4.20), showing the results in Figure 4.21. The data was processed (Figure 4.20), showing the results in Figure 4.21.

The data was processed (Figure 4.20), showing the results in Figure 4.21. The data was processed (Figure 4.20), showing the results in Figure 4.21. The data was processed (Figure 4.20), showing the results in Figure 4.21.

Chromosome 9

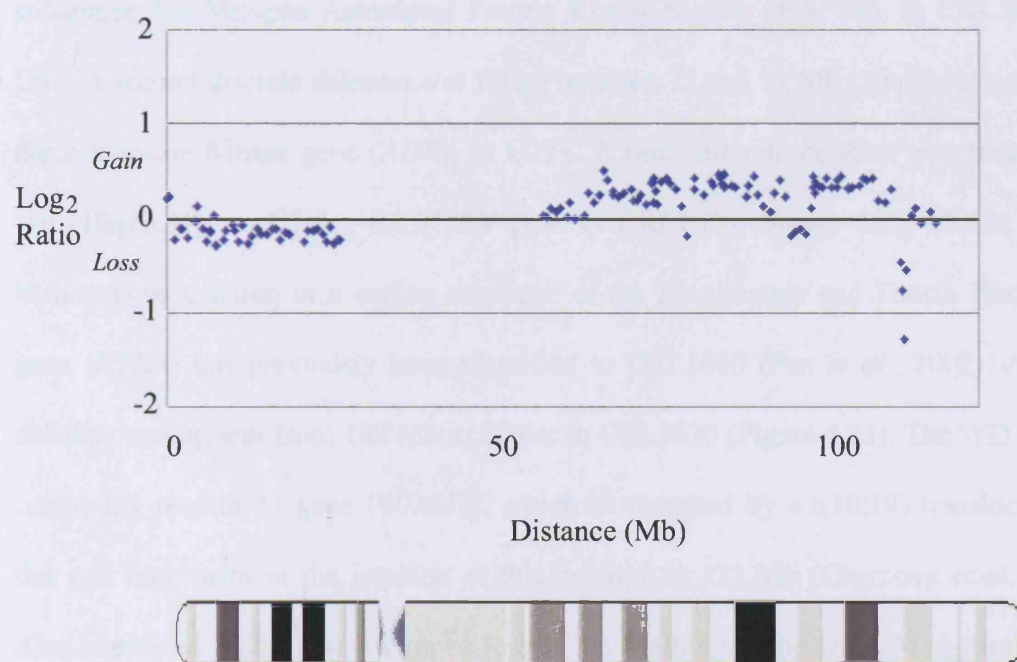


Figure 4.19 Array CGH profile of chromosome 9 in cell line CRL1620

Chromosome 10

All but one of the tumour samples and all the cell lines had some loss of chromosome 10 material (Figure 4.20), involving either the short (Figure 4.21) or long arm or both. The entire chromosome 10 was lost in three patient samples and four cell lines. A discrete deletion was found between 48 and 49 Mb (10q11.22-q11.23), containing the Mitogen Associated Protein Kinase 8 gene (*MAPK8*), in CRL2020 and U87. A second discrete deletion was found between 75 and 77 Mb (10q22.2), containing the Adenosine Kinase gene (*ADK*), in U251. A third discrete deletion was found at 89 Mb (10q23.31), containing the *PTEN* gene in CRL1620 (Figure 4.22) (Table 4.8). A homozygous deletion in a coding sequence of the Phosphatase and Tensin Homologue gene (*PTEN*) has previously been identified in CRL1620 (Fan *et al.*, 2002). A fourth deletion was present from 122 Mb to 10qter in CRL1620 (Figure 4.21). The WD Repeat-containing protein 11 gene (*WDR11*), which is disrupted by a t(10;19) translocation in this cell line, maps at the junction of this deletion at 122 Mb (Chernova *et al.*, 2001). Also contained within this region of loss is the Methylguanine-DNA Methyltransferase gene (*MGMT*) (Esteller *et al.*, 2000).

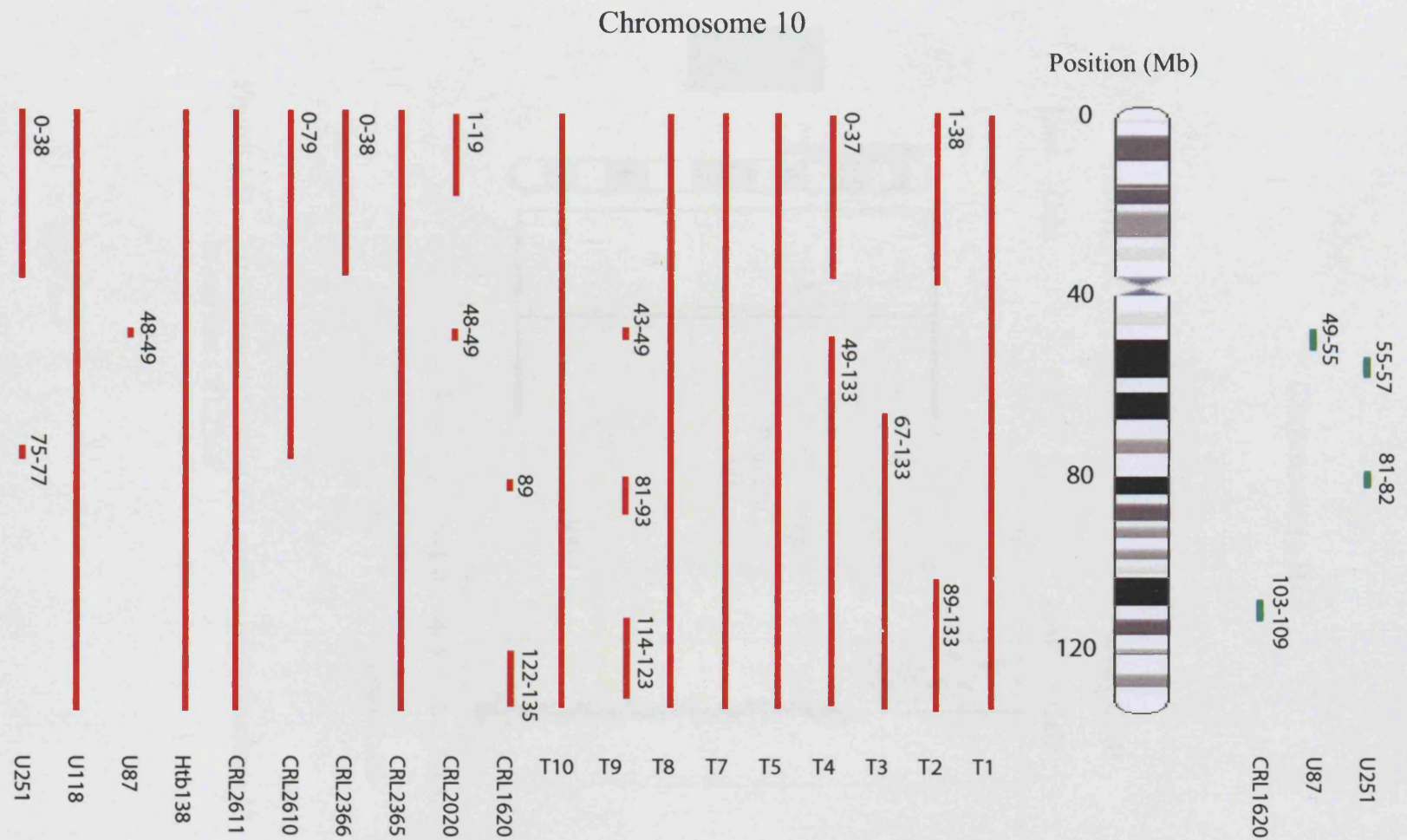


Figure 4.20 Composite array CGH profile of chromosome 10

Chromosome 10

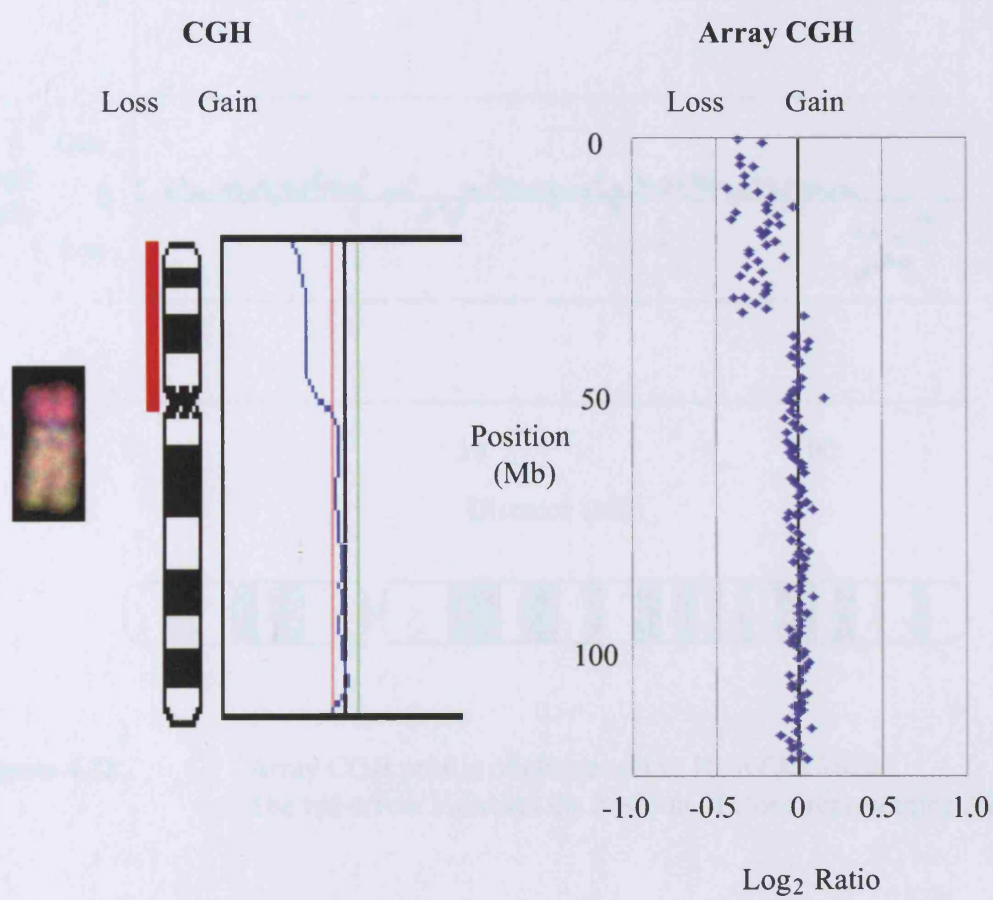


Figure 4.21 Metaphase and array CGH profiles of chromosome 10 in cell line CRL2366

Sample	Copy number RP11-380G5 (<i>PTEN</i>)	LOH	<i>PTEN</i> Mutation
CRL1620	Loss	NA	Mutant
CRL2020	Null	NA	NA
CRL2365	Null	LOH	NA
CRL2366	Null	NA	NA
CRL2610	Null	NA	Wild-type
CRL2611	Loss	NA	Wild-type
Htb138	Loss	NA	Wild-type
U87	Null	NA	Mutant
U118	Loss	LOH	Mutant
U251	Null	LOH	Mutant

Table 4.8 Comparison of copy number change, LOH and mutation of *PTEN* (Cox *et al.*, 2005; Huang *et al.*, 2004; Ishii *et al.*, 1999).

Chromosome 11

Loss of 11q material was seen in four cell lines and two tumours (Figure 4.23). Tumour T3 has a terminal deletion from 114-134 Mb (Figure 4.24). Tumour T5 has loss from 110-119 Mb and includes the genes Myeloid/Lymphoid or Mixed Lineage Leukaemia (*MLL*), Melanoma Cell Adhesion Molecule (*MCAM*) and Immunoglobulin Superfamily Member 4 (*IGSF4*). Htb138 has a discrete gain from 129-132 Mb (11q24-q25). This gain involves RP11-567M21 and PAC1064E20 and is flanked by clones RP11-264E20 and RP11-340L13. Friend Leukaemia Virus Integration 1 gene (*FLI1*) is included in this region.

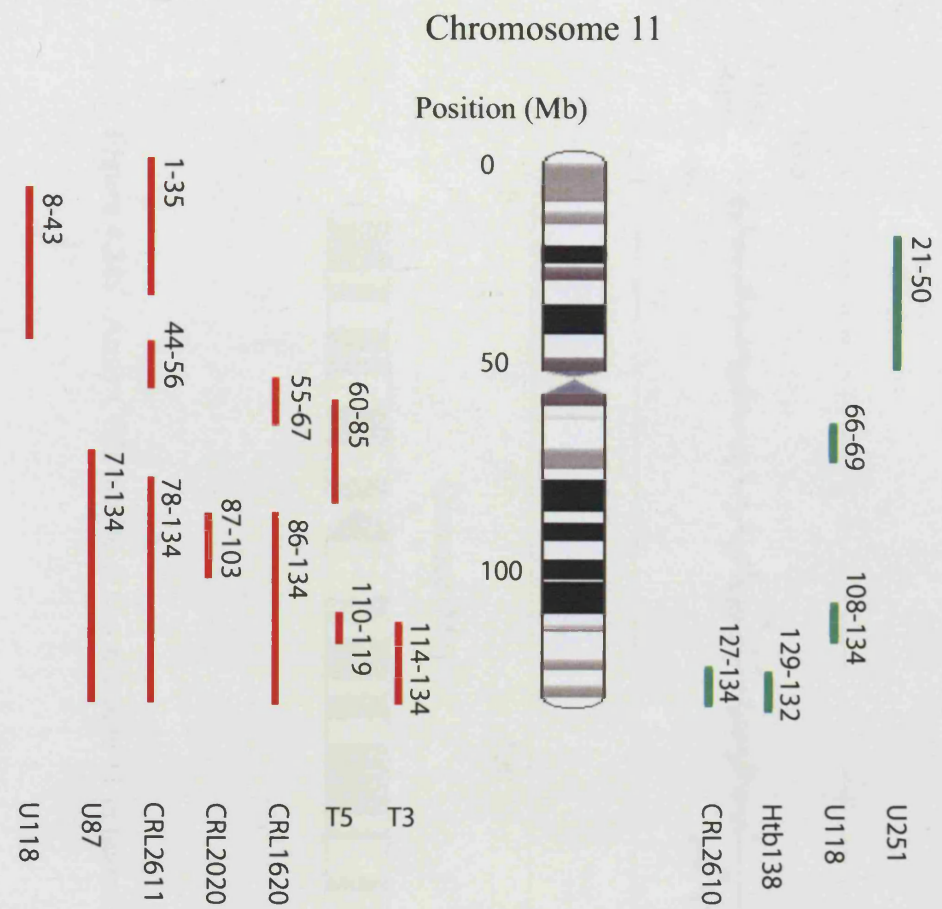
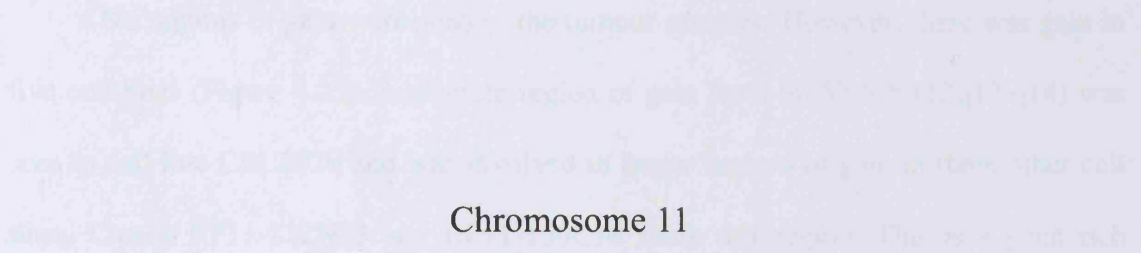


Figure 4.23 Composite array CGH profile of chromosome 11



Chromosome 12

No regions of gain were seen in the tumour samples. However, there was gain in five cell lines (Figure 4.25). A discrete region of gain from 50-59 Mb (12q13-q14) was seen in cell line CRL2020 and was involved in larger regions of gain in three other cell lines. Clones RP11-112N23 and RP11-150C16 flank this region. This is a gene rich region that includes Insulin-like Growth Factor Binding Protein 6 gene (*IGFBP6*), Homeo box C (*HOXC*) gene cluster, Cyclin-Dependent Kinase 2 gene (*CDK2*) (12q13), Cyclin-Dependent Kinase 4 gene (*CDK4*)(12q14) and the glioma-associated oncogene homologue 1 gene (*GLI*) (12q13). A discrete deletion in tumour T2 from 119-122 Mb (12q24.13) was included in larger regions of loss in cell lines CRL1620, CRL2366 and CRL2611. RP11-322N7 and RP11-87C12 are the clones with normal copy number ratio flanking this region. The gene B-cell CLL/Lymphoma 7A (*BCL7A*) is included in this deletion.

Chromosome 13

Nine cell lines and four tumours have loss on chromosome 13, and three cell lines show gain (Figure 4.26). Cell line U87 has two regions of loss at 19-32 Mb and 47-62 Mb, demonstrated on conventional CGH and array CGH (Figure 4.27). The flanking clones of the deletion 47-62 Mb are RP11-408L13 and RP11-234O23. The gene Retinoblastoma (*RBI*) is encompassed by this deletion. A minimal region of deletion 87-91 Mb (13q31.1) was defined by cell line U251 (Figure 4.28). The clones flanking this loss are RP11-478H12 and RP1-267D11. This region has low gene density but contains

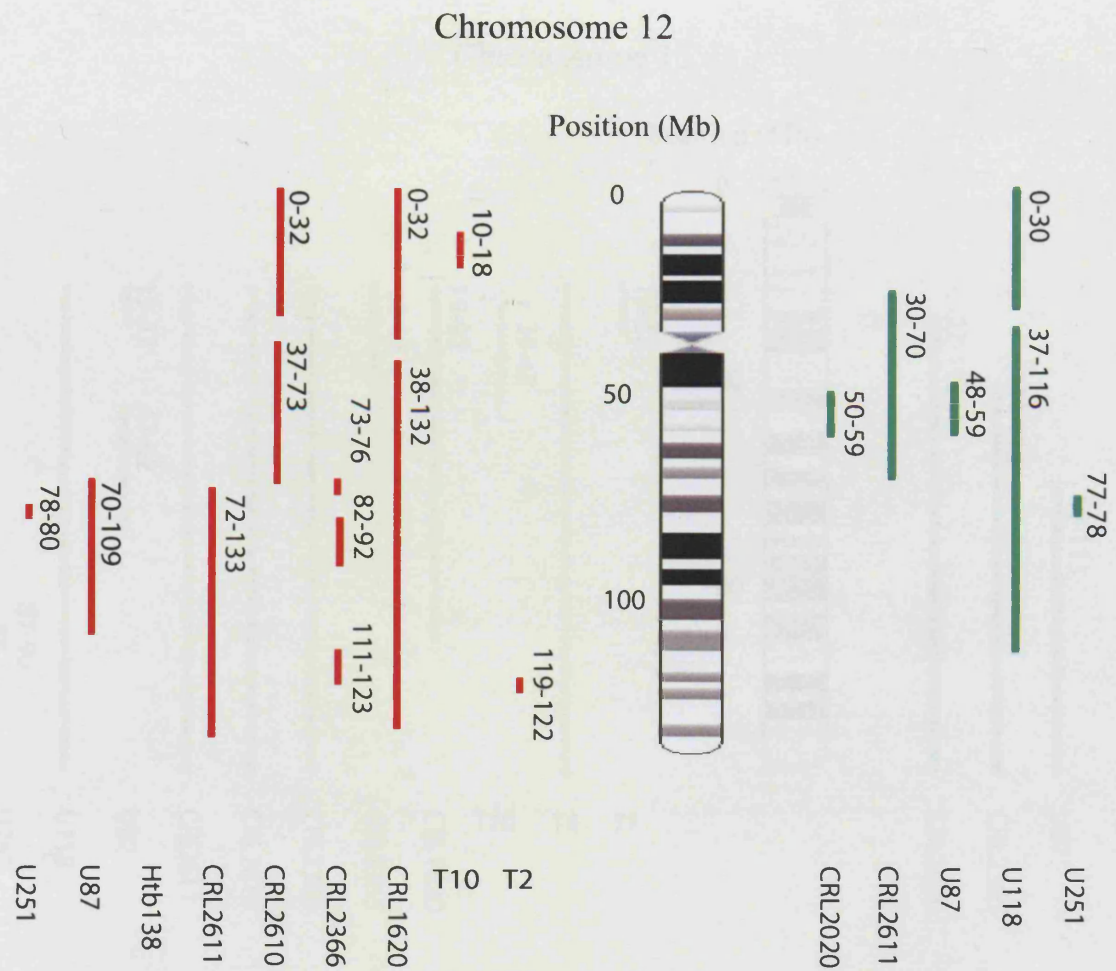


Figure 4.25 Composite array CGH profile of chromosome 12

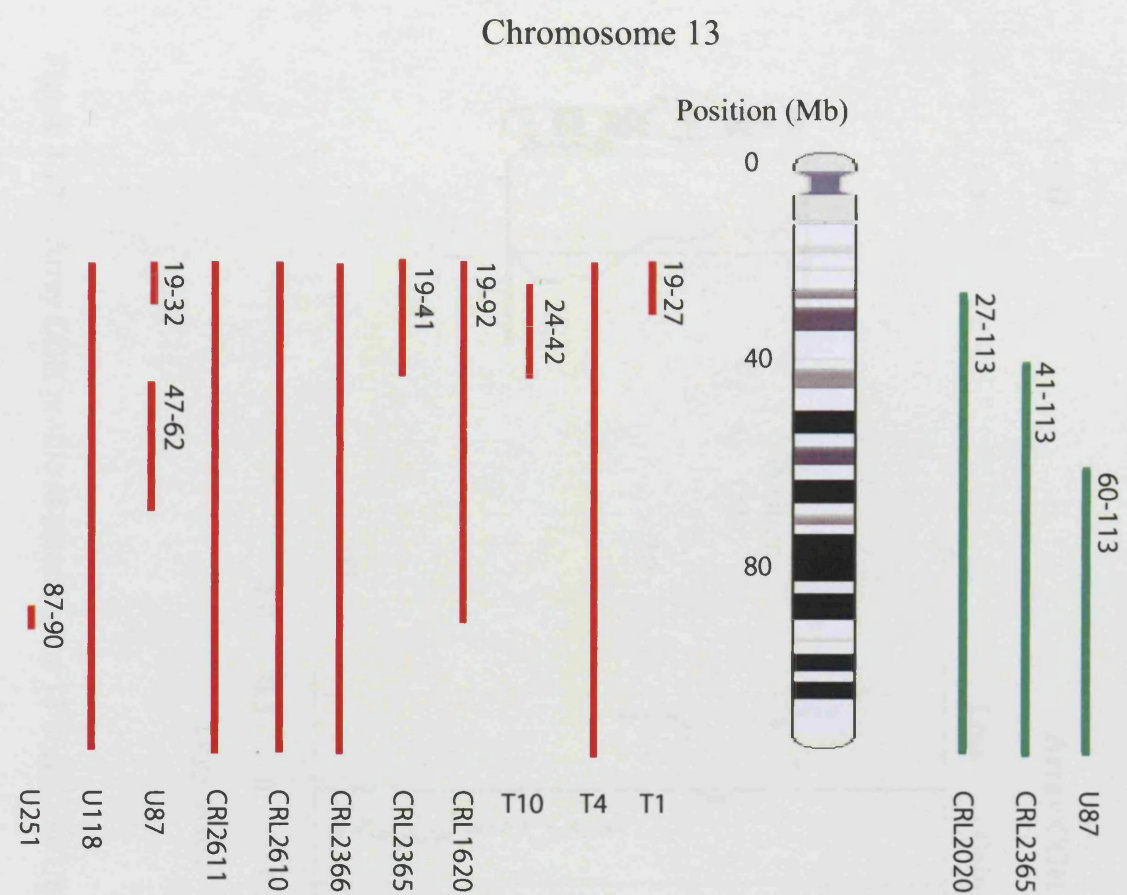


Figure 4.26 Composite array CGH profile of chromosome 13

Chromosome 13

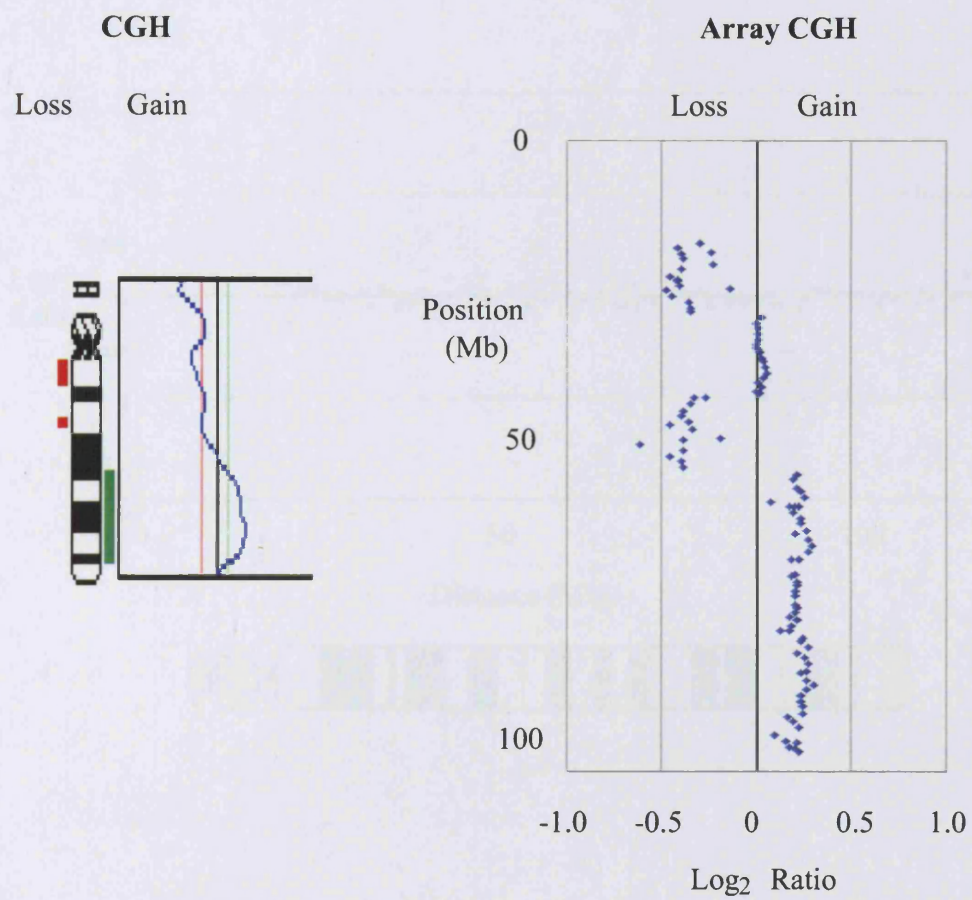


Figure 4.27 Array CGH profile of chromosome 13 in cell line U87

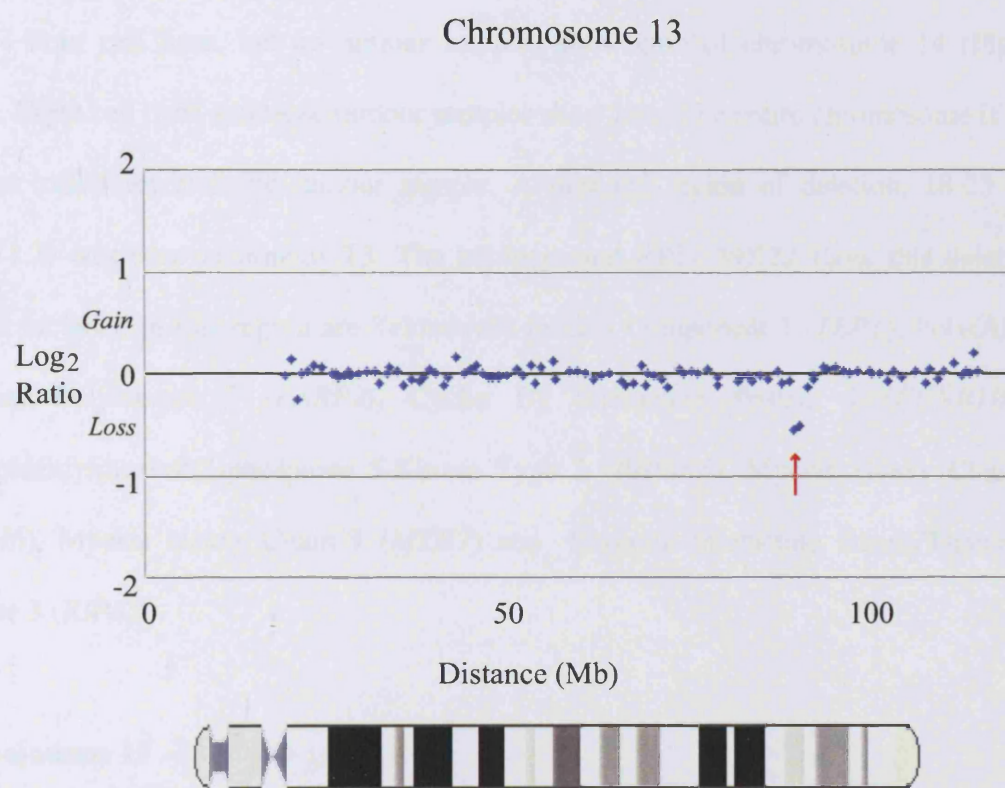


Figure 4.28 Array CGH profile of chromosome 13 in cell line U251
Red arrow indicates deletion from 87-91 Mb

the gene SLIT and Neutrotrophic Tyrosine Kinase Receptor-like family member 5 (*SLITRK5*).

Chromosome 14

Four cell lines, but no tumour samples show gain of chromosome 14 (Figure 4.29). Eight cell lines and three tumour samples show loss. The entire chromosome is lost in four cell lines and one tumour sample. A minimal region of deletion, 18-23 Mb (14q11.2) was seen in tumour T3. The telomere and RP11-89K22 flank this deletion. Genes included in this region are Telomerase Protein Component 1 (*TEP1*), Poly(ADP-Ribose) Polymerase 2 (*PARP2*), Cyclin B1 Interacting Protein 1 (*CCNB1IP1*), Phosphatidylinositol-3-phosphate 5-Kinase Type 3 (*PIP5K3*), Myosin Heavy Chain 6 (*MYH6*), Myosin Heavy Chain 7 (*MYH7*) and Receptor-Interacting Serine/Threonine Kinase 3 (*RIPK3*).

Chromosome 15

Loss was seen from chromosome 15 in six cell lines and one tumour sample (Figure 4.30). Gain was seen in four cell lines, but no tumour samples. There are two discrete regions of deletion on chromosome 15 in two cell lines U251 and Htb138. U251 has a discrete deletion between 25 and 27 Mb (15q13). The deleted clone is RP11-408F10 and is flanked by PR11-322N14 and RP11-164K24. Genes included in this deletion are hect domain and RLD 2 (*HERC2*), Amyloid Beta (A4) Precursor Protein-Binding Family A Member 2 (*APBA2*), Melanoma-Associated Antigen G1 (*MAGGI*), Kruppel-Like Factor 13 (*KLF13*) and Transient Receptor Potential Cation Channel

Chromosome 14

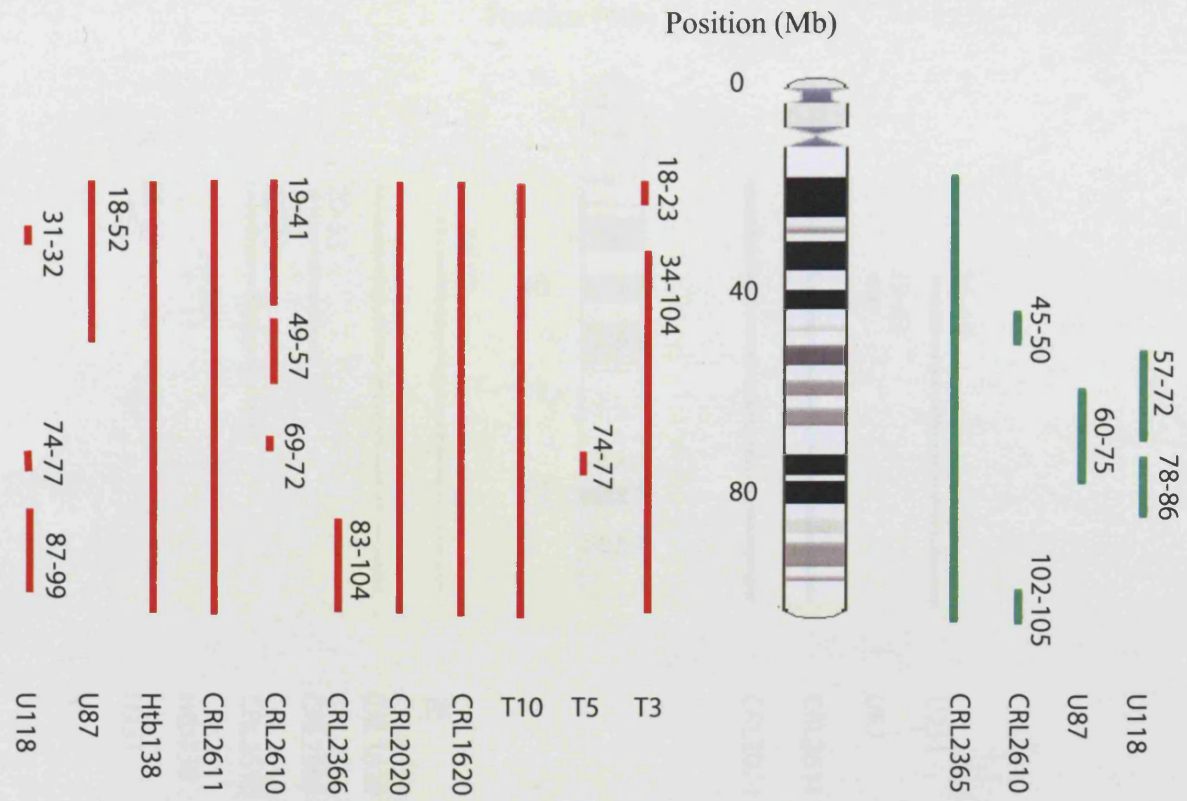


Figure 4.29 Composite array CGH profile of chromosome 14

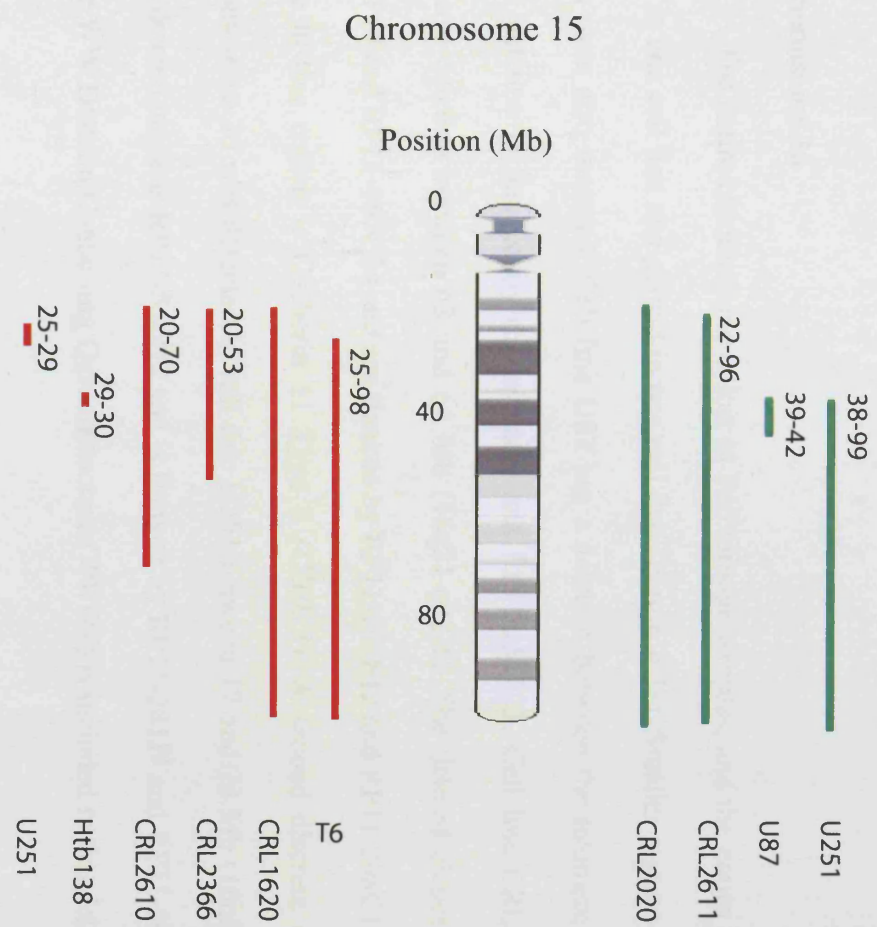


Figure 4.30 Composite array CGH profile of chromosome 15

Subfamily M Member 1 (*TRPM1*). Htb138 has a discrete deletion between 29 and 30 Mb (15q13.3). The deleted clone is RP11-E12 and is flanked by RP11-164K24 and RP11-250G15. Genes included in this deletion are cholinergic receptor, nicotinic, alpha polypeptide 7 (*CHRNA7*), Rho GTPase Activating Protein 11A (*ARHGAP11A*), Secretory Granule Neuroendocrine Protein 1 (*SGNE1*) and Gremlin 1 Homologue Cysteine Knot Superfamily (*GREM1*).

Chromosome 16

The entire chromosome is lost in two tumour samples, and the entire long arm is lost in one cell line and gained in one cell line (Figure 4.31). Smaller regions of loss and gain were also detected. Cell line U87 has a deletion between the telomere and 8 Mb. This deletion is flanked by the telomere and RP11-152P23. Cell line CRL1620 has a discrete deletion between 63 and 64 Mb (16q21-q22.1). The deleted clones are RP11-370P15 and RP11-467C24 and are flanked by RP11-148F12 and RP11-298C15. The only gene in this region is Cadherin 11 Type 2 (*CDH11*). A second discrete deletion on chromosome 16 was detected in cell line U251 between 77 and 78 Mb (16q23.1-q23.2). The deleted clone is RP11-556H2 and is flanked by RP11-281J9 and RP11-303E16. The gene WW Domain Containing Oxidoreductase (*WWOX*) is included in this deletion.

Chromosome 17

Three cell lines had loss of material on the short arm of chromosome 17, and five tumour samples and three cell lines had loss of material from the long arm (Figure 4.32). Cell line Htb138 has a discrete deletion between 6 and 7 Mb (17p13.2-p13.1) (Figure

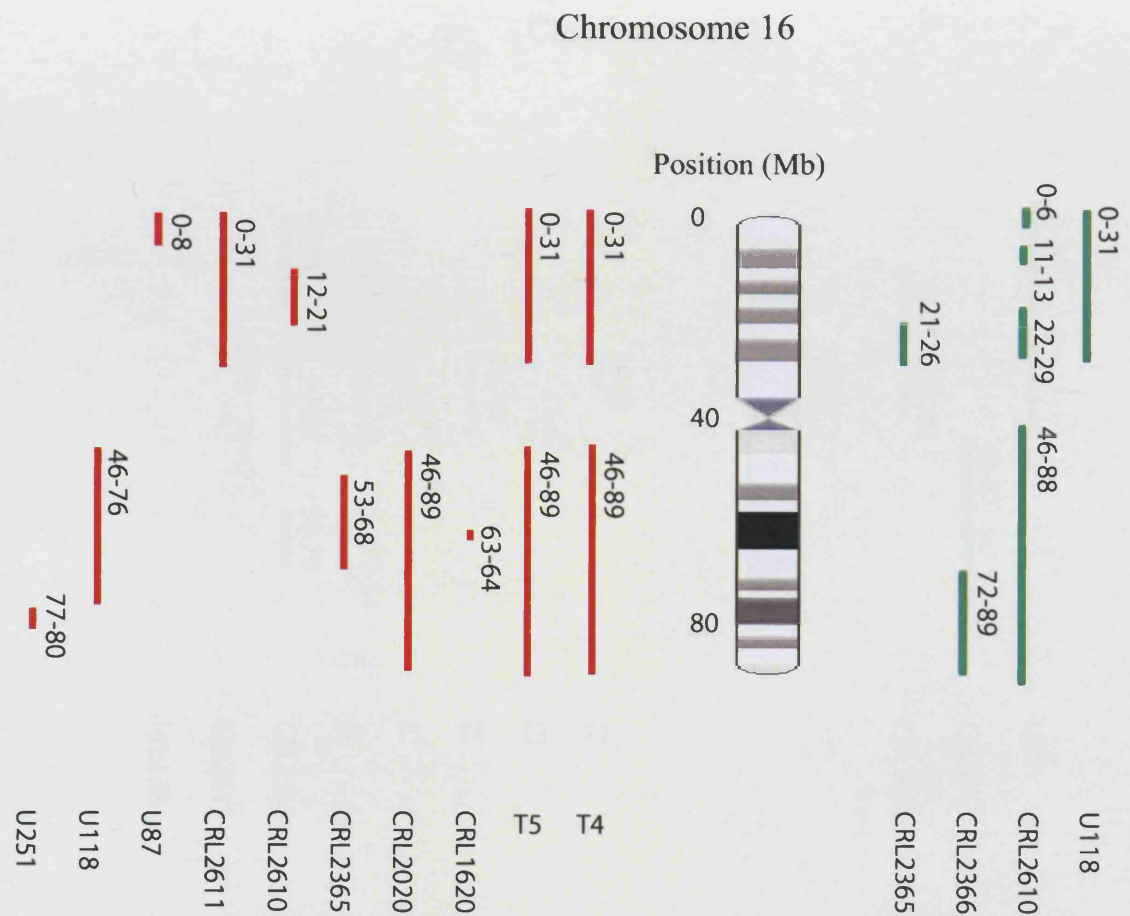


Figure 4.31 Composite array CGH profile of chromosome 16

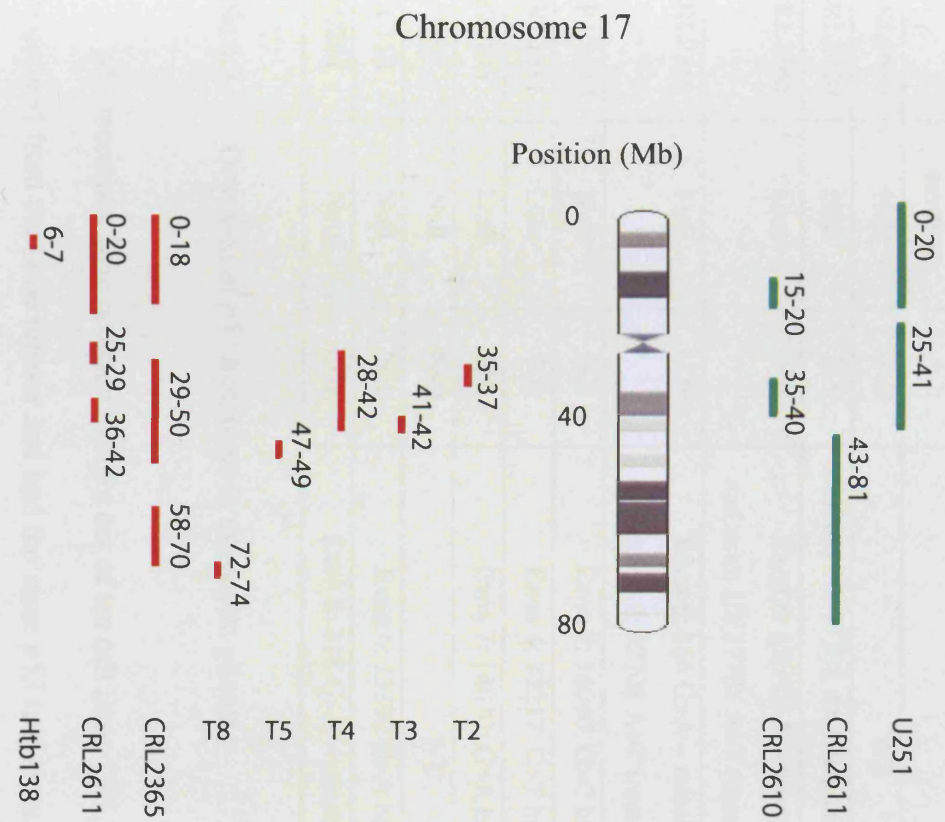


Figure 4.32 Composite array CGH profile of chromosome 17

4.33). The clones flanking this deletion are RP11-243K12 and RP11-404G1. The gene *p53* is included in this deletion. Eleven exons of *p53* were screened by SSCP for mutations in the cell lines by the Cancer Research UK Mutation Detection Facility. Those exons showing an abnormal result were then sequenced (Table 4.9).

Cell line	Copy number	LOH	<i>p53</i>
CRL1620	Null	Null	WT
CRL2020	Null	NA	Exon 10: 17708 A>T (mutation not reported)
CRL2365	Loss	NA	Exon 8: 856 G>A – missense mutation and exon 10: 17708 A>T (mutation not reported)
CRL2366	Null	LOH	Exon 8: 856 G>A – missense mutation and exon 10: 17708 A>T (mutation not reported)
CRL2610	Null	NA	Exon 7: 14040: G>C homozygote
CRL2611	Loss	NA	Exon 4: 12217: C>T homozygote
Htb138	Loss	NA	Exon 7: 14070: G>A homozygote
U87	Null	Null	WT
U118	Null	Null	Exon 6: 13398 G>A homozygote
U251	Null	LOH	Exon 8: 818 G>A – missense mutation.

Table 4.9 Detection of *p53* mutations in astrocytic gliomas

p53 mutations were detected in eight out of ten cell lines. CRL2365 and CRL2366 were derived from the same tumour and had the same *p53* mutations. The two cell lines with no *p53* mutation had no copy number loss of 17p13. Of the eight cell lines with *p53* mutation, five had no loss of 17p13. Three cell lines CRL2365, CRL2611 and U87 showed copy number loss involving 17p13.1 and *p53* mutation.

Chromosome 17

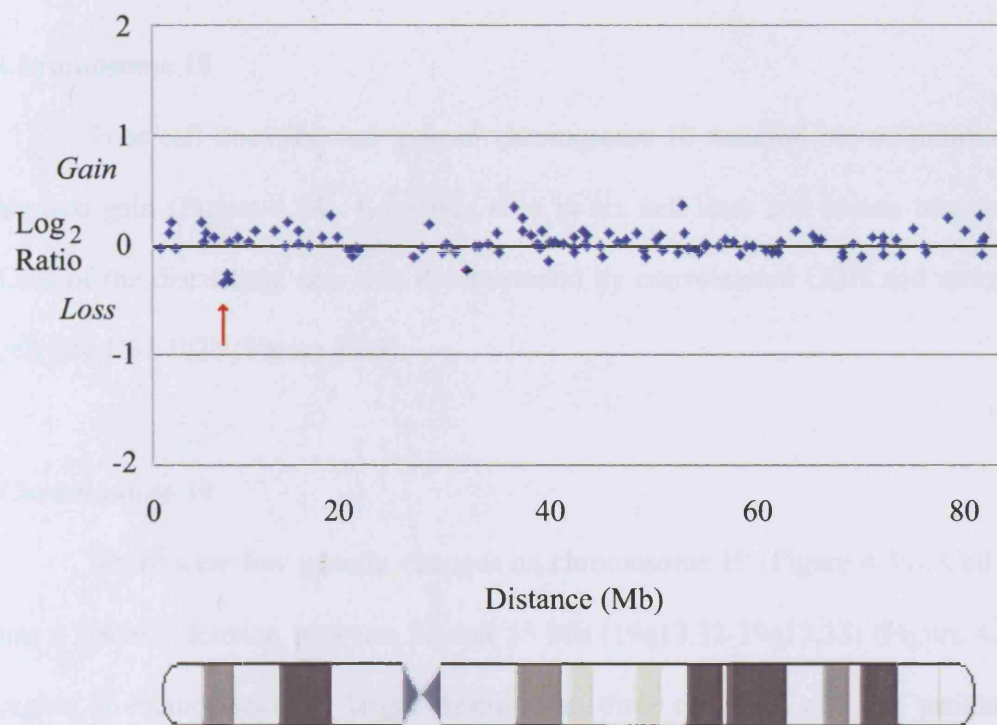


Figure 4.33 Array CGH profile of chromosome 17 in cell line Htb138
The red arrow indicates the clones representing *p53*

Tumour T3 has a discrete deletion between 41 and 42 Mb (17q21). The deleted clone is RP11-392O1 and is flanked by RP11-948G15 and RP5-905N1. The gene Breast Cancer 1 (*BRCA1*) is included within this deletion. Cell line U87 has a discrete deletion between 42 and 43 Mb (17q21.31).

Chromosome 18

Four cell lines showed gain of chromosome 18 material but no tumour samples showed gain (Figure 4.34). Loss was seen in six cell lines and in one tumour sample. Loss of the distal long arm was demonstrated by conventional CGH and array CGH in cell line CRL1620 (Figure 4.35).

Chromosome 19

There were few genetic changes on chromosome 19 (Figure 4.36). Cell line U87 has a discrete deletion between 52 and 55 Mb (19q13.32-19q13.33) (Figure 4.37). This region is encompassed by larger deletions in three cell lines and one patient sample. Clones CTC-483I11 and CTD-2545M3 flank this deletion. The gene Meis1 Myeloid Ecotropic Viral Integration Site 1 Homologue 3 (*MEIS3*) is included within this deletion.

Chromosome 20

The entire chromosome 20 was gained in four patient samples and seven cell lines. In addition, there is loss of 20q in two cell lines, and gain of 20p and the proximal part of 20q in one patient sample (Figures 4.38 and 4.39). The only region of loss on this chromosome is of the short arm of chromosome 20 in cell line U87 in which there is also

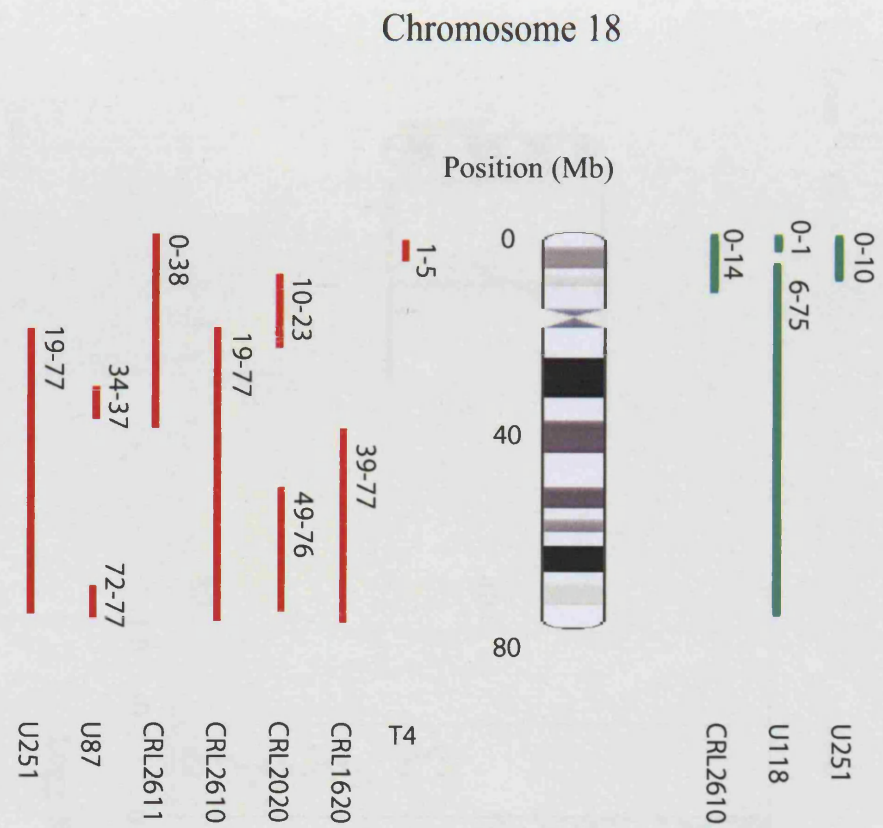


Figure 4.34 Composite array CGH profile of chromosome 18

Chromosome 18

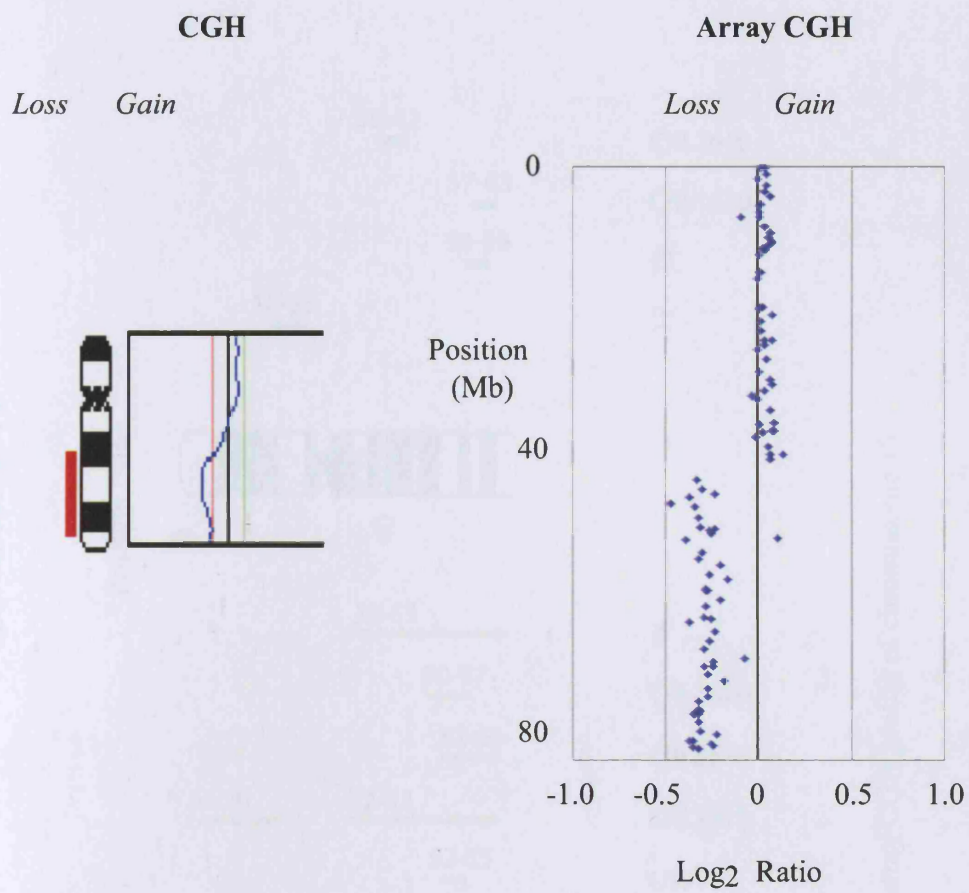


Figure 4.35 Array CGH profile of chromosome 18 in cell line CRL1620

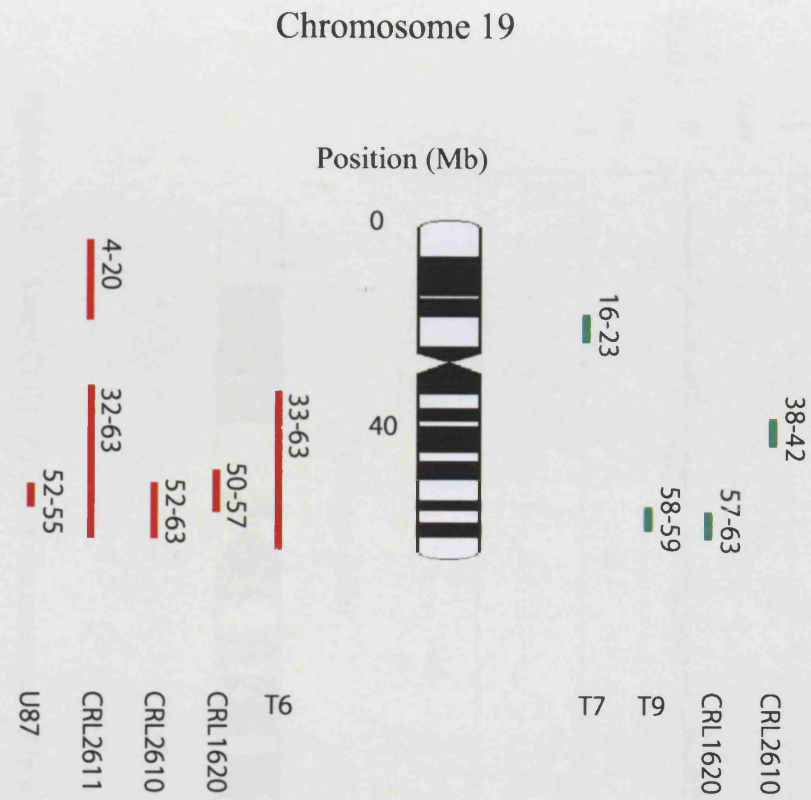


Figure 4.36 Composite array CGH profile of chromosome 19

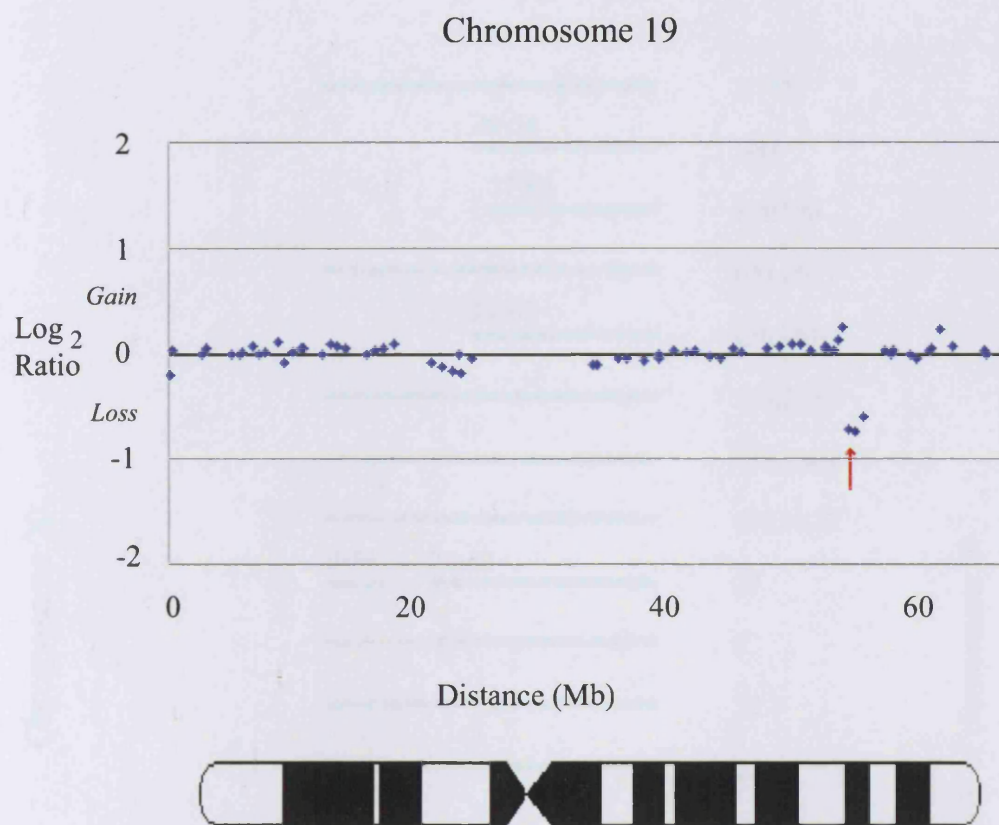


Figure 4.37 Array CGH profile of chromosome 19 in cell line U87

Red arrow indicates a deltion between 52 and 55 Mb

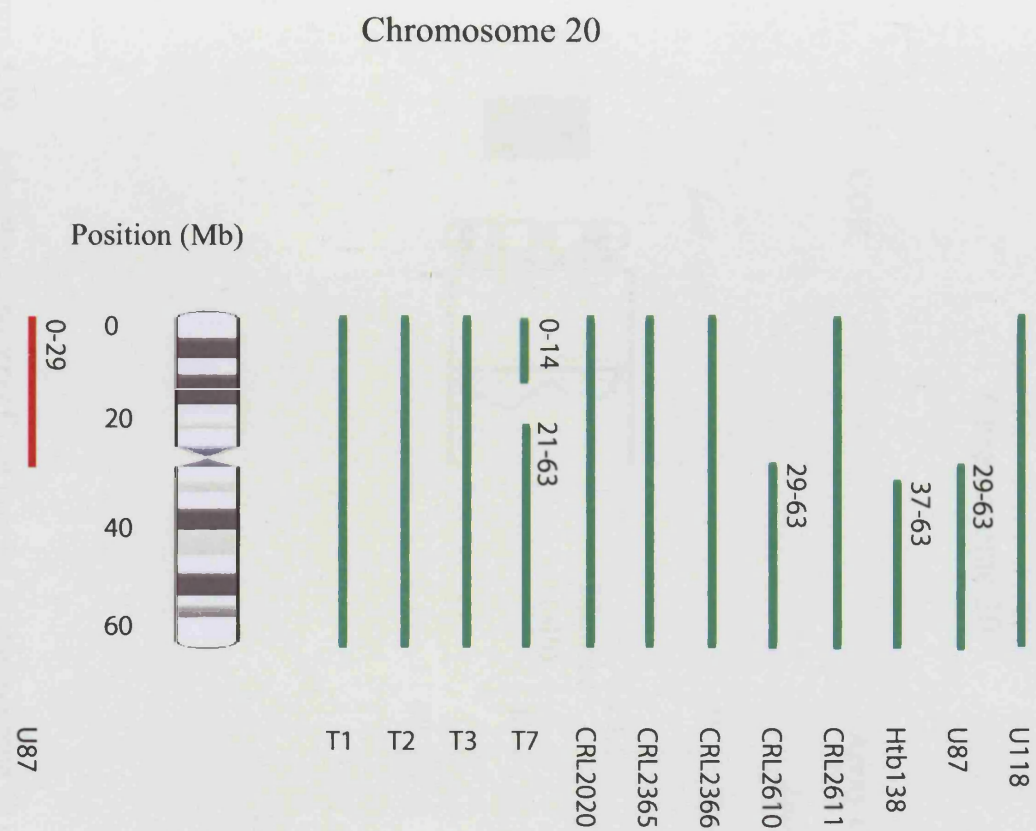


Figure 4.38 Composite array CGH profile of chromosome 20

gain of the long arm (Figure 4.40). 20q12-13 is a region often amplified in ovarian cancer. (Tanner *et al.*, 2000) Genes in this region include v-myb myeloblastosis viral oncogene homolog (avian)-like 2 (*MYBL2*) and Aurora Kinase A (*AURKA*).

Chromosome 21

Gain of material on chromosome 21 was seen in four cell lines and one patient sample (Figure 4.41). Loss of material was seen in one cell line and three patient samples.

Chromosome 22

Loss of the entire chromosome 22 was seen in one patient sample and two cell lines (Figure 4.42). Gain of the whole chromosome was seen in one cell line. Cell line CRL2610 has two discrete regions of loss on this chromosome (Figure 4.43). The first deletion is from the telomere and 24 Mb. This deletion is flanked by the telomere and CTA-125H2 (tel-22q12.1). The gene Breakpoint Cluster Region (*BCR*) is included in this deletion. The second region of loss is between 39 and 42 Mb (22q12.3-q13.2). The clones flanking this deletion are RP1-215F16 and RP3-388M5. This is a gene rich area, and genes of interest include Minichromosome Maintenance Deficient 5 (*MCM5*), E1A binding protein p300 (*EP300*), Myosin Heavy Polypeptide 9 (*MYH9*), SRY (sex Determining Region Y)-Box 10 (*SOX10*), GTP Binding Protein 1 (*GTPBP1*) and Mitogen-Activated Protein Kinase Kinase Kinase 7 Interacting Protein 1 (*MAP3K7IP1*).

Chromosome 20

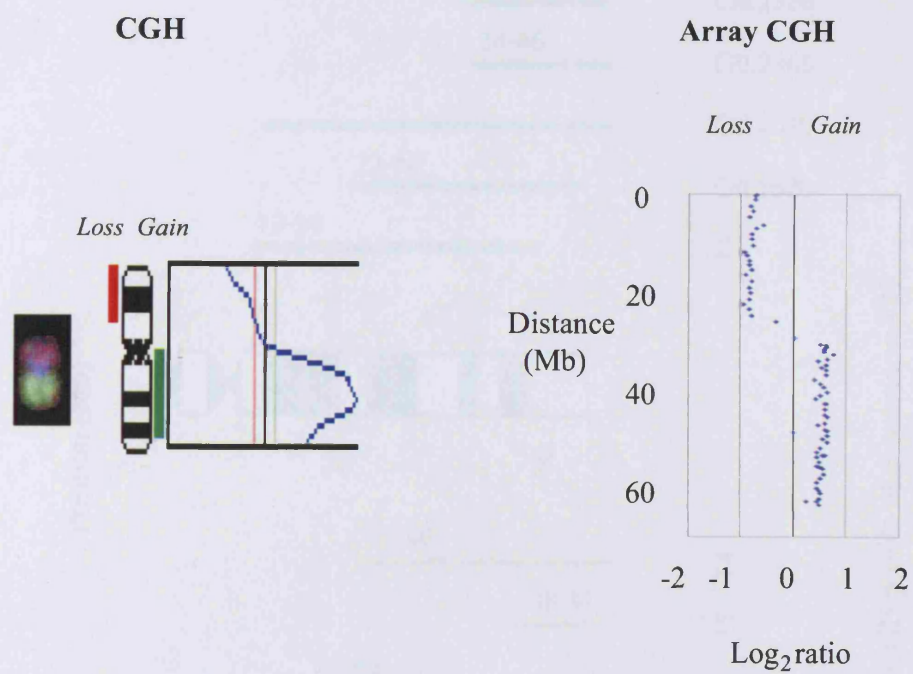


Figure 4.40 Metaphase and array CGH profiles of chromosome 20 in cell line U87

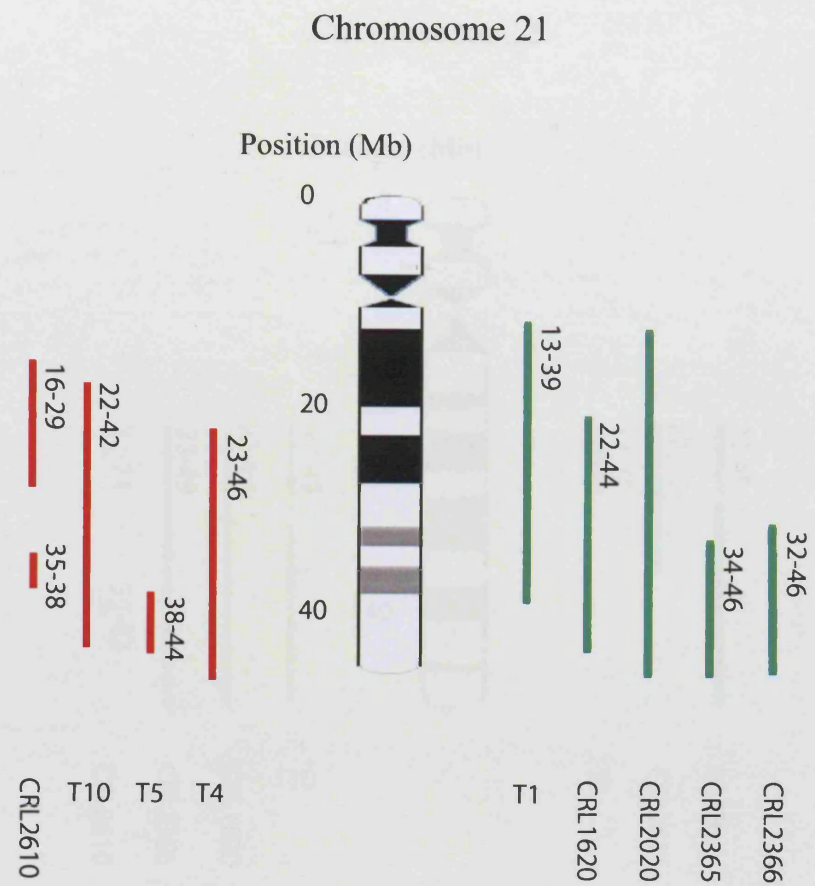


Figure 4.41 Composite array CGH profile of chromosome 21

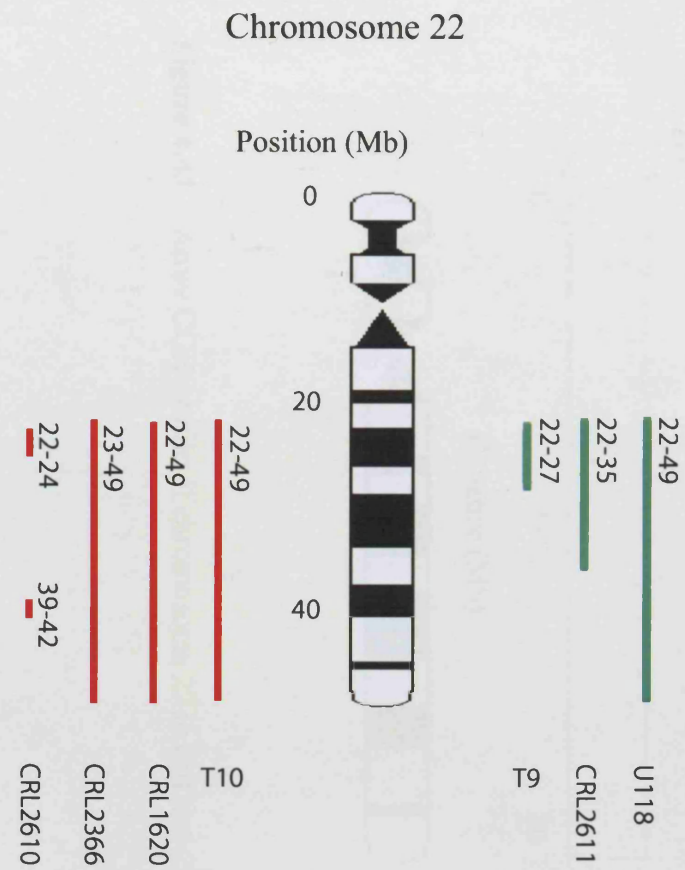


Figure 4.42 Composite array CGH profile of chromosome 22

4.4.2. Chromosome 22

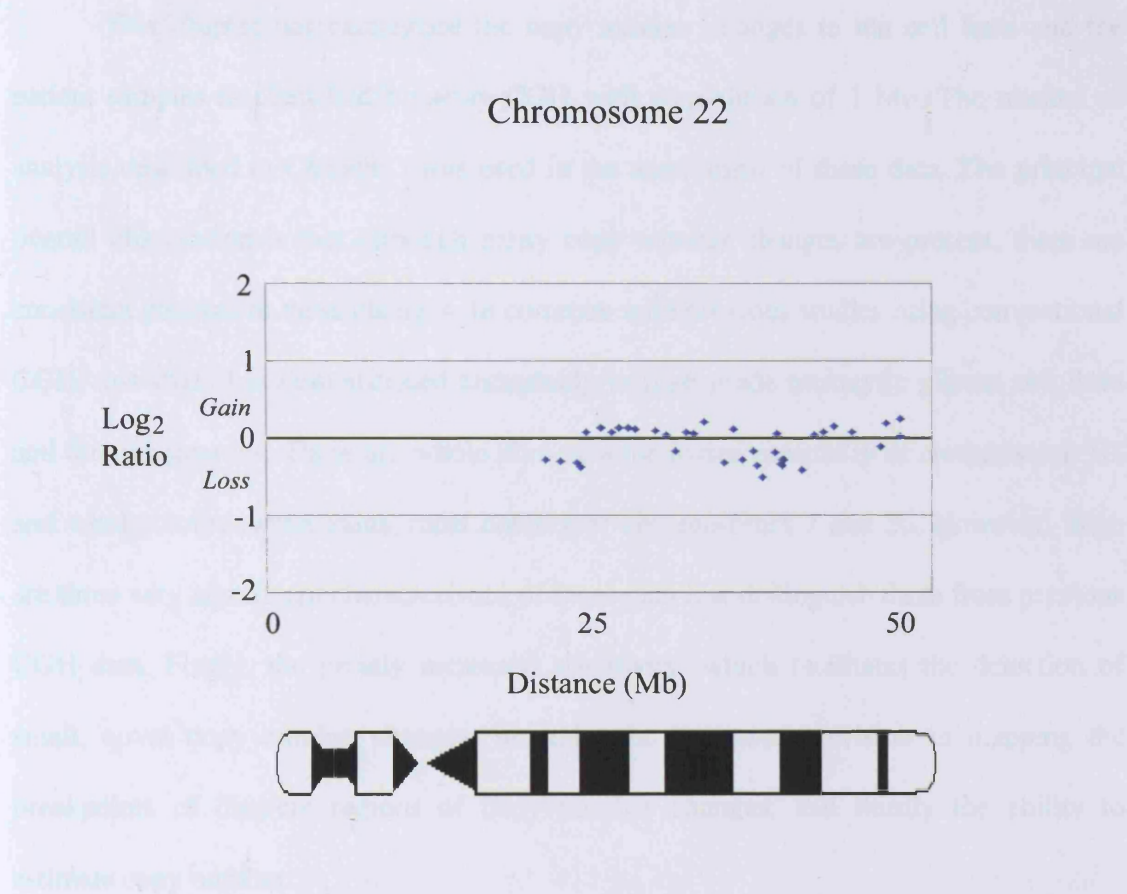


Figure 4.43 Array CGH profile of chromosome 22 in cell line CRL2610

4.3 Discussion

This chapter has catalogued the copy number changes in ten cell lines and ten patient samples as identified by array CGH with a resolution of 1 Mb. The method of analysis described in Chapter 3 was used in the assessment of these data. The principal overall observation is that although many copy number changes are present, there are consistent patterns in these changes. In common with previous studies using conventional CGH, this study has demonstrated aneuploidy in high-grade astrocytic glioma cell lines and tumour samples. There are whole chromosome losses especially of chromosome 10, and whole chromosome gains, most notably of chromosomes 7 and 20. However, there are three very significant characteristics of these data that distinguish them from previous CGH data. Firstly, the greatly increased sensitivity, which facilitates the detection of small, novel copy number changes, secondly the increased precision in mapping the breakpoints of discrete regions of copy number changes, and thirdly the ability to estimate copy number.

Conventional CGH cannot detect deletions that are less than 5-10 Mb. The greatly increased sensitivity with array CGH of detecting copy number changes is seen in discrete small regions of copy number change. Examples of regions with copy number changes detected by a single clone include clone RP11-165B2 on chromosome 3 in cell line CRL1620 (Figure 4.6) and RP1-94G16 on chromosome 6 in cell line U118 (Figure 4.12). Examples with copy number changes detected by two clones are amplification of the clones RP11-12J3 and RP11-231C18 on chromosome 4 in tumour T3 (Figure 4.8), and RP5-1091E12 and RP11-339F13 in tumour T5, chromosome 7 (Figure 4.15).

Examples where two clones show a deletion are RP11-165M8 and RP11-380G5 on chromosome 10 in cell line CRL1620 (Figure 4.22), and RP11-275J18 and RP11-388D4 on chromosome 13 in cell line U251 (Figure 4.28).

The precision in mapping breakpoints is also greatly enhanced. The breakpoints are defined between two clones with an average separation of approximately 1 Mb. Previous CGH studies would have defined the breakpoint only within the cytogenetic band. This is demonstrated in comparisons of conventional CGH and array CGH. Examples include chromosome 6 in CRL2366 (Figure 4.11), chromosome 6 in CRL2610 (Figure 4.13), chromosome 13 in U87 (Figure 4.27) and chromosome 18 in CRL1620 (Figure 4.35). Other examples demonstrating the increased precision in breakpoint mapping will be discussed further in Chapter 5, and include a deletion on the short arm of chromosome 6, from the telomere to 43 Mb in cell line U87. The actual breakpoint is between RP11-501I18 (42.9 Mb) and RP11-227E22 (44.0 Mb). Genes within this region include Vascular Endothelial Growth Factor (*VEGF*), Polymerase DNA ETA (*POLH*) and GTP Binding Protein 2 (*GTPBP2*). Another example is seen in an interstitial deletion between 135 and 143 Mb, on the long arm of chromosome 6 in U87. The proximal breakpoint is between RP11-323N12 (135.6 Mb) and RP11-448D5 (137.2 Mb) and the distal part of the deletion is between RP11-368P1 (142.3 Mb) and RP11-86O4 (143.5 Mb).

In addition to the additional sensitivity and precision in array CGH, the \log_2 ratios of the individual clones enable an estimate of relative levels of gain or loss to be made,

i.e. regions of amplification (Tables 4.4 and 4.5) and homozygous deletion (Table 4.6). The data from these tables will be further discussed in Chapter 6. On chromosome 6 in cell line CRL2020, the increased sensitivity of detection and increased precision, together with the knowledge of relative changes in copy number high-lighted a region of interest at 6q26. In this example, there is relative loss of the whole of chromosome 6, but in addition there appears to be an interstitial deletion at the distal end of the chromosome. This is discussed further in Chapter 5.

Array CGH is a new method of analysis and therefore the full significance of the data generated using this method needs to be explored. Knowledge of what a region of copy number change detected by array CGH indicates, will determine how these data are used to further understand these tumours. However, observations of how known genetic changes are represented by this method will facilitate a greater understanding of the method, which may be applied to novel regions of change. Particular regions where there are copy number changes that are known to be associated with gene mutations include *PTEN*, *CDKN2A*, *FIG-ROS*, *EGFR* and *PDGFR*. Gain or amplification on chromosome 4 between 54 and 55 Mb (4q12) was detected in cell lines U118 and U251 and in tumours T3 and T4 (Figure 4.7 and Table 4.3). *PDGFR* is contained within this region. As with amplification of *EGFR*, there is co-amplification of surrounding genes. Activating mutations in *PDGFR* have not been described in astocytic glioma, however mutations in *PDGFR* have been detected in another tumour type, gastrointestinal stromal tumours (Heinrich *et al.*, 2003). The 0.24 Mb interstitial deletion in cell line U118 on chromosome 6 leads to the fusion of two genes, *FIG* and *ROS1*, to produce a novel oncogene (Charest

et al., 2003a; Charest *et al.*, 2003b) (Figure 4.12). Therefore, this deletion detected by array CGH does not indicate the presence of a tumour suppressor gene, but the presence on an oncogene. The region demonstrating the most extreme loss in terms of \log_2 ratio and in the number of samples involved is the short arm of chromosome 9. Table 4.6 shows the \log_2 values for the clones in this region in those samples showing a deletion. The lowest values for \log_2 ratios are centred in the region of the tumour suppressor gene *CDKN2A*. The tumour suppressor gene *PTEN* is at 89 Mb on chromosome 10. Cell line CRL1620 has a homozygous deletion in this region. The \log_2 ratio of the clone representing this homozygous deletion is RP11-380G5 is -0.46. As with the case of the FIG-ROS microdeletion in cell line U118, the homozygous deletion does not cover the entire clone and hence this is reflected in the \log_2 ratio.

One consideration in assessing the significance of a region of copy number change is that of genetic heterogeneity (Section 3.4.1.3). LCVs in the genome have recently been mapped (Iafrate *et al.*, 2004). Areas identified in this study which correspond to areas of LCV as identified by Iafrate *et al* are shown in Table 4.10

Region of copy number change	Genes
1p21.1	Amylase gene cluster
1q43-44	<i>AKT3</i>
10q11.22	<i>MAPK8</i>
12q24.13	<i>BCL7A</i>
13q31.1	<i>SLITRK5</i>

Table 4.10 Regions of copy number change identified by array CGH, which are LCVs

Genes encompassed by a region of copy number change and those genes at the breakpoints are all candidate tumour suppressor genes or oncogenes. Apart from the expected findings involving *EGFR* and *PDGFR* other growth factors or genes affecting growth factor signalling were identified including *KIT* (4q12), *KDR* (4q12), *ROS1* (6q22.1), *IGF2R* (6q25-26) and *IGFBP6* (12q13). Regions of copy number change encompassed many signalling molecules including *PTEN* (10q23.31), *PIK3C2B* (1q32), *MAP3K5* (6q23) and *MAP3K7IP1* (22q13.1). Candidate genes with a more direct role in cell cycle control and apoptosis include *CDKN2A*, *CDKN2B* (9p22), *MDM4* (1q32), *CDKN2C* (1p32.3), *CCNC* (6q21), *CDK2* (12q13), *CDK4* (12q14) and *MCM5* (22q13.1). Involved genes with a role in maintenance of genome integrity include *p53* (17p13), *RBI* (13q14) and *EP300* (22q13).

In conclusion, this chapter has identified regions of copy number change, containing many candidate tumour suppressor genes and oncogenes, in high-grade astrocytic glioma cell lines and tumour samples. The frequency of each genetic change is scored, as theoretically it could be considered that the most frequently occurring changes are the most significant. This argument follows from the concept that if a genetic change gives a growth advantage to the cell then the cells with these changes will be selected for and so will predominate in the cell population. Also, the more frequent a genetic change then the more likely this change is intrinsic to the original tumour from which the cell line was derived. The relationship between selected copy number changes and translocation breakpoints are investigated in Chapter 5. A wider view of the significance of copy number changes in tumours is discussed in Chapter 6.

Chapter Five

Molecular Cytogenetic Analysis of High-Grade Astrocytic Glioma Cell Lines

5.1 Introduction

Having assessed the astrocytic glioma tumour samples and cell lines for regions of copy number change, the next step was to confirm selected regions of copy number change by FISH. Following this, I investigated the relationship between the copy number data obtained by array CGH and the positional data as identified by FISH. Comparing the array data from this study and data from a paper published in 2001 about a translocation breakpoint in cell line CRL1620, indicated that array CGH might be used to map translocation breakpoints (Chernova *et al.*, 2001). Chernova *et al* detected a reciprocal translocation t(10;19) in cell line CRL1620, which resulted in the formation of a chimeric fusion protein between WDR11 and ZNF320. The function of WDR11 is not known, but it is a member of the WD-repeat protein family and these are involved in cell functions such as signal transduction, cell cycle progression and apoptosis. Examination of the array profile of chromosome 10 in cell line CRL1620 (Figure 4.20 and 4.22) shows a breakpoint between 122 and 123 Mb, with a loss of the distal region of chromosome 10. The breakpoint is between clones RP11-323P17 (122.6 Mb) and RP11-62L18 (123.4 Mb) and contains *WDR11*. Hence, this suggests that regions of copy number change identified by array CGH may be used to map translocation breakpoints.

When interpreting FISH data the ploidy of the cell should be considered. Hence, the first step was to determine the ploidy of each cell line using karyotyping and M-FISH. In array CGH the control is normal human DNA, which has a $2n$ ploidy. The same quantity of DNA is used for the test and reference. Therefore, if a sample with a $4n$ ploidy was used with the control of $2n$, there would be no changes detected by array CGH. Secondly, the array CGH data is considered from the perspective of three model situations of copy number change. These are DNA gain or amplification, homozygous deletion and reduced copy number. Using FISH to confirm copy number change requires that two probes are used, one from within the region of interest and one from a region of normal copy number.

5.2 Results

The M-FISH experiments described in this section were performed in collaboration with Radost Vatcheva and the FISH experiments were obtained in collaboration with Tania Jones, Pat Gorman and Chrysanthos Poullikas.

5.2.1 M-FISH karyotypes of the cell lines

All the cell lines in the study were karyotyped by M-FISH, except for Htb138 and U118, which have previously been described. A summary of the ploidy is shown in Table 5.1, and following this there is a full description of each karyotype with representative images (Figures 5.1-5.8). Chromosomal translocations are specified in the M-FISH karyotypes.

Cell Line	Chromosome Range	Mode
CRL 1620	75 – 82 Hypotetraploid	82
CRL 2020	75 – 101 Near-tetraploid	93
CRL 2365	68 – 99 Near-tetraploid	Bimodal 88 or 92
CRL 2366	76 – 96 Near-tetraploid 149 – 196 Near-octaploid	93
CRL 2610	50 – 71 Hypotriploid	61
CRL 2611	69 – 99 Hypertriploid - hypertetraploid	86
U87	41 – 47 Near-diploid 85 – 87 Near-tetraploid	44-47
U251	47 – 54 Hyperdiploid	49

Table 5.1 Chromosome range and modal number of chromosomes in cell lines

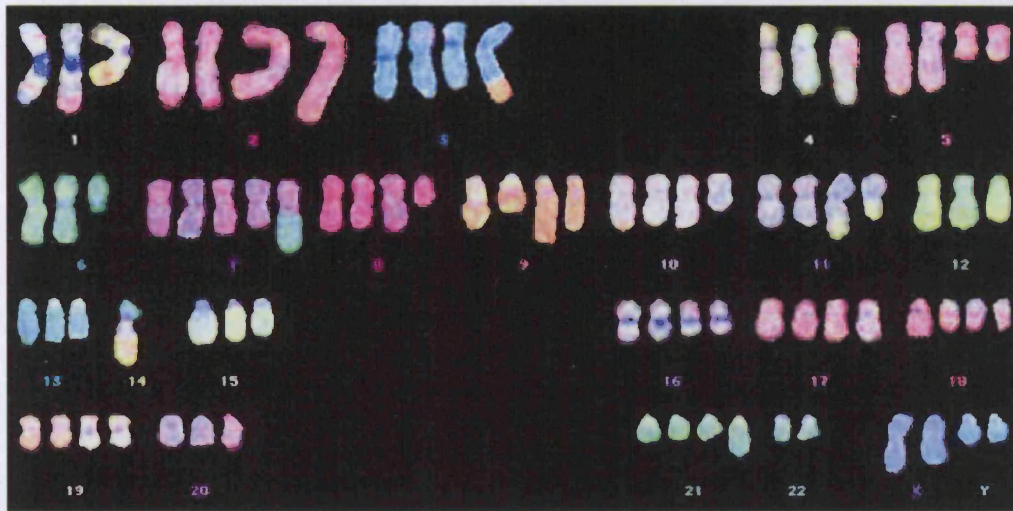


Figure 5.1 M-FISH karyotype of CRL1620

A range of 71 - 83 chromosomes, with a mode of 82, was found in 30 cells counted.

M-FISH analysis showed a male karyotype with the following aberrations:

der(1)t(1;14)[6], dic(1)t(1;X)[8], der(1)t(1;18)(q32;?)[8], der(2)(2;5)[8],
 der(3)t(3;9)(q27;?)[6], del(5)(q13) x 2[6], del(6)(?)[8], del(6)(-p)[1],
 der(7)t(6;7)(q14;q11)[8], del(8)(q?)[8], del(9)(p11.2)[8], dic(9)x 2[6], del(10)(q?)[1],
 der(11)t(1;11)[8], -13[8], -14 x 3[8], del(16)[8], der(18)t(1;18) x 3[8], der(21)t(13;21)[8],
 -22 [8], der(?)t(14;22) [1] [cp 8]

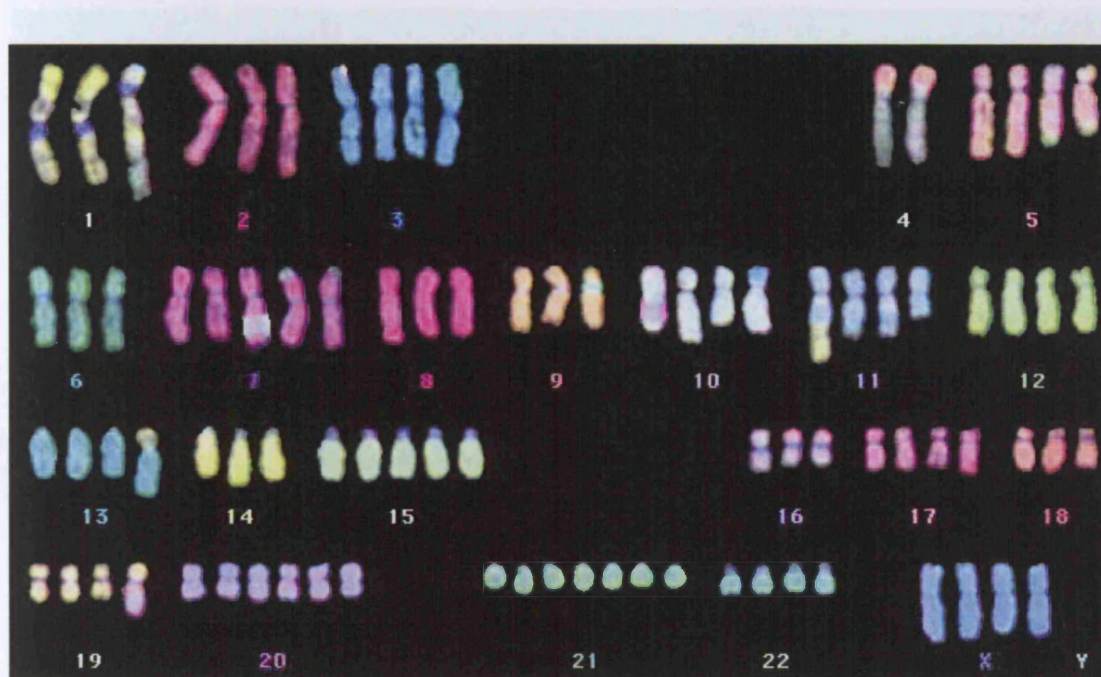


Figure 5.2 M-FISH karyotype of CRL2020

A range of 75-101 chromosomes, with a mode of 93, was found in thirty cells counted.

M-FISH analysis showed a female karyotype with the following aberrations:

-1 x 2[9], der(1)t(1;4)t(1;9)t(9;11)[3], t(1;4)x 2[6], -2[6], der(3)(3;13)(q13;q12)[3],
der(4)t(4;5)(p14;?)x2[6], der(5)t(5;16;17)(p13;?;?) [5], der(5)t(4;5;19)[6], +7[4],
der(7) t(6;7)(?; p22)[5], t(8;13)[1] 6 ins(9) (6;9)(?;p13)[6], der(10)t(X;10)t(?;p11.2)[6],
der(11)t(1;11)t(?;q23)[5], der(13)t(13;14)[2], del(13) [1], der(16)t(5;16)x2[6], -18[5],
der(19)t(19;5;16)(q12;?;?) [6], +20[6] +21 x 2[6], -22[2] [cp6]

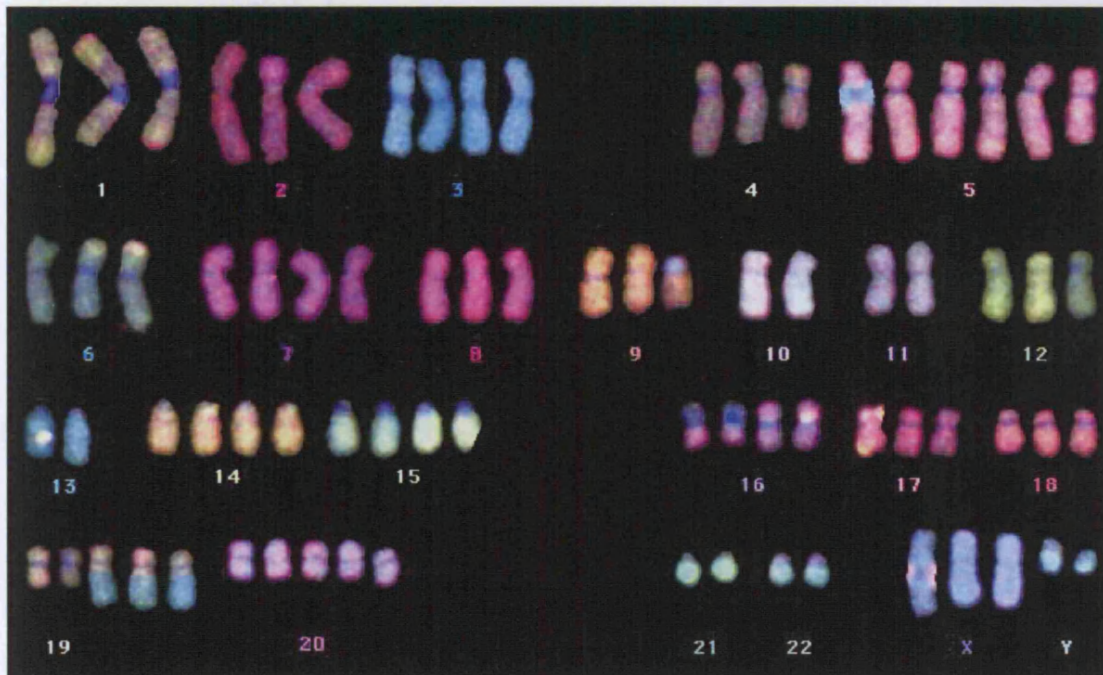


Figure 5.3 M-FISH karyotype of CRL2365

A range of 68 – 184 chromosomes, with a mode of 88-92, was found in thirty cells counted.

M-FISH analysis showed a male karyotype with the following aberrations:

t(1;14)[1], t(1;7)[1], t(7;6;1;7)[1], der(1)t(1;5)(p36;?)[1], der(1)t(1;17)t(p36;?)[5],
 der(1)t(1;7)[1], +3[4], der(3)t(3;4)(q13;?)[1], -4[6], der(4)t(4;5)[2], del(5)(q32)[5],
 der(6)t(6;19)(p24;?) x 2-3[6], dic(6)[1], -7[3], del(9)[1], -10 x 2[4], del(10)(q?)[1], -13[4],
 i(14)(q10)[1], der(16)t(6;16) x 2 [6], der(19)t(13;19)(q12;q13)[6], del(19)[1], +20[4],
 +21[4], -22[6] [cp 6]

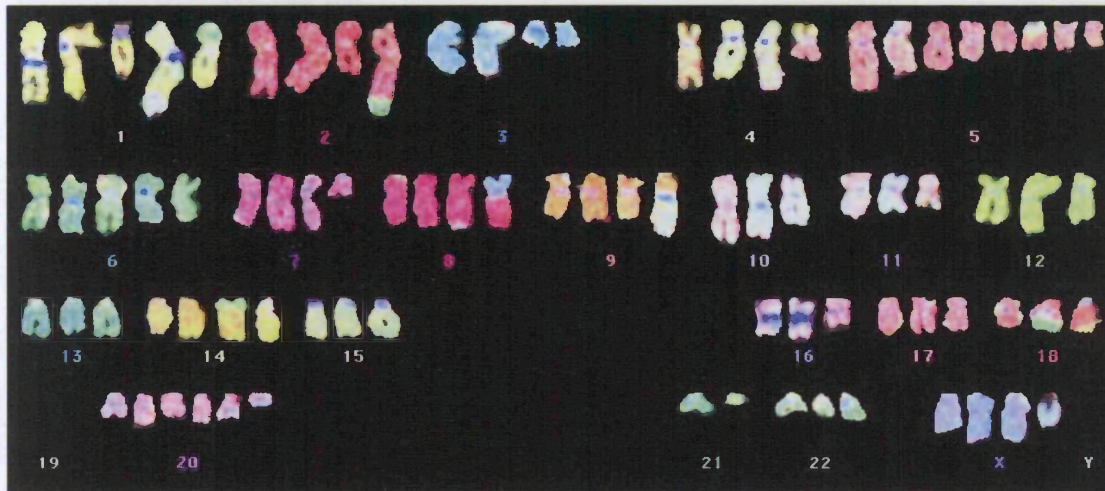


Figure 5.4 M-FISH karyotype of CRL2366

A range of 76-196 chromosomes, with a mode of 93, was found in thirty cells counted.

M-FISH analysis showed a male karyotype with the following aberrations:

der(1)t(1;10)[2], der(1)t(1;7)[1], t(1;21)[1], der(2)t(2;6)(q33;?)[4], del(3) x 2 [2],
 der(4)t(4;5)[2], +5[5], del(5) [5], del(7)[2], der(8)t(X;8)[4], del(9)[4], der(11)t(11;17)[4],
 der(14)t(14;21)[1], der (15)t(15;18)(p12;?)[2], der(18)t(18;21)[1], -19[4], +21[2], -Y [1]
 [cp5]

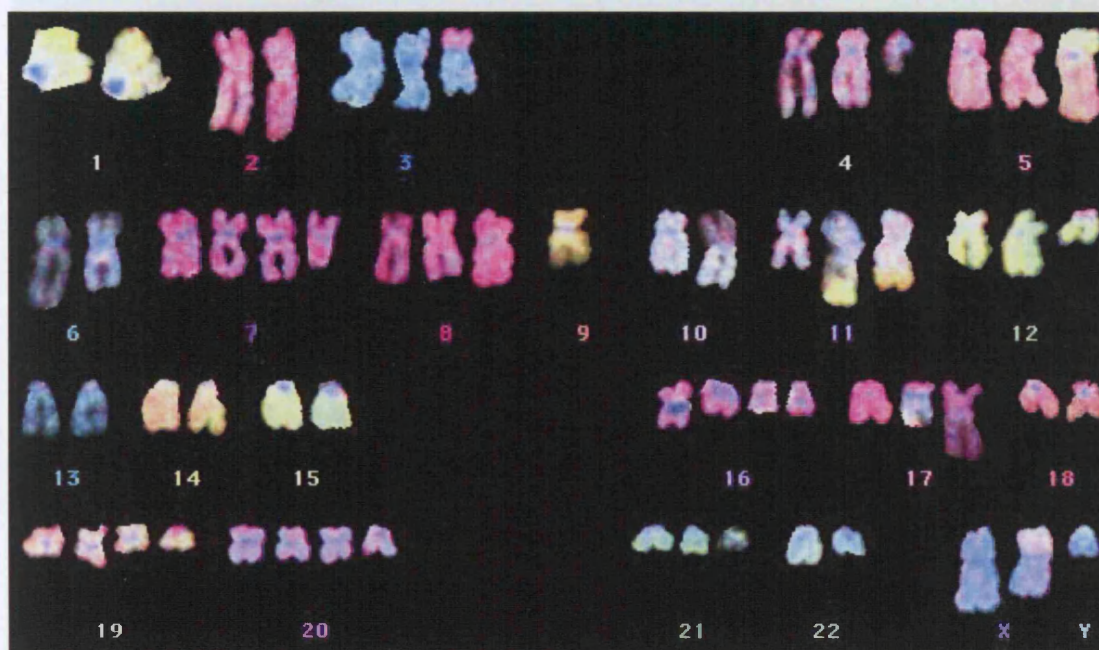


Figure 5.5 M-FISH karyotype of CRL2610

A range of 50 – 71 chromosomes, with a mode of 61, was found in thirty cells counted.

M-FISH analysis of showed a male karyotype with the following aberrations:

del(1)[4], t(2;5)[1], der(2)t(1;2)[2], der(3)t(1;3)[1], der(3)(3;16)[2], del(4)[4],

der(5)t(1;5)[6], del(6)[2], der(6)t(6;16)[1], del(8)[3], der(8)t(3;8)[1],

der(10)t(4;10)(?;p11)[7], der(10)t(X;10)(?;q10)[1], der(11)t(11;14)(q25;?)[7],

der(11)(1;11)[5] der(12)t(12;18)[7], der(13)t(8;13)[2], der(19)t(20;19;6)[3] [cp8]

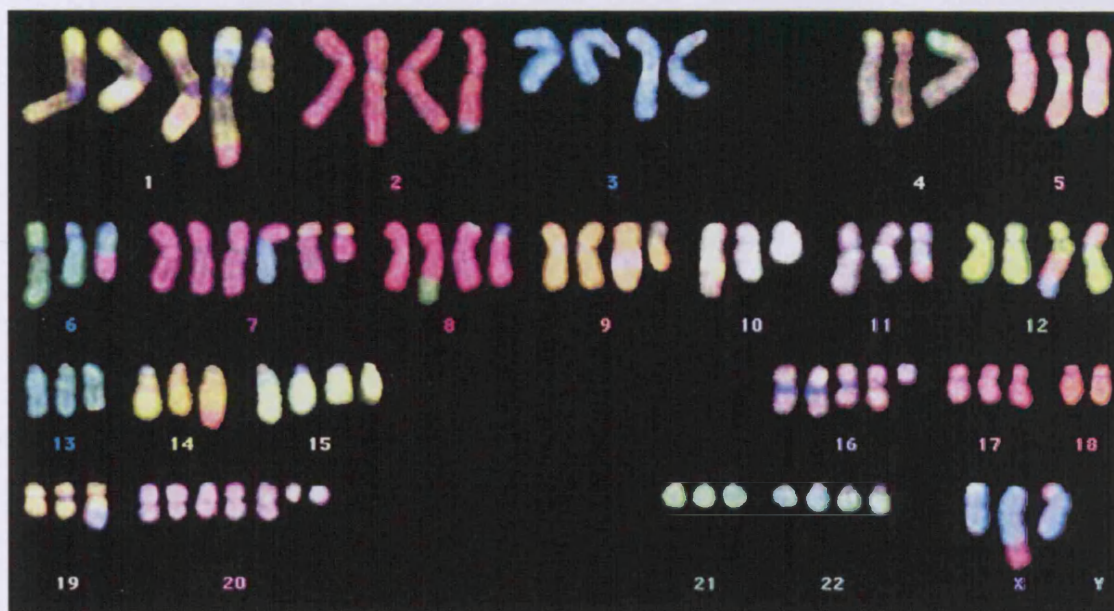


Figure 5.6 M-FISH karyotype of CRL2611

A range of 75 – 167 chromosomes, with a mode of 86, was found in thirty cells counted.

M-FISH analysis showed a female karyotype with the following aberrations:

der(1)t(1;17)[5], der(1)t(1;18)[2], del(1)[5], der(2)t(2;11)[2], der(2)t(X;2), t(3;20)[1],
 der(4)t(4;6)(p16;6?)[5], der(5)t(3;5)(?;p12)[2], der(5)t(5;8)[2], del(6)[4], t(6;7)[3],
 der(7)t(5;7)x2[2], der(8)t(6;8)(6;q24)[4], der(8)t(8;17)[3], del(8)[2], del(9)[2],
 der(10)t(10;17)[1], der(11)t(11;17)(q21;?)[3], der(12)t(5;12)t(5;X)[4], der(12)t(5;12)[2],
 der(14)t(14;18)(q32;?)[4], del(16)[2], der(17)t(17;19)[1], der(19)t(X;19)(?;q13)[4],
 +20[5], del(20)x2[1], der(20)t(16;20)[1], der(22)t(15;22)[2], der(X)t(X;2)[4],
 der(X)t(X;10)(X;10)[5], t(X;7),[2] [cp 5]



Figure 5.7 M-FISH karyotype of U87

A range of 41-87 chromosomes, with a mode of 44-47, was found in thirty cells counted.

M-FISH analysis showed a female karyotype with the following aberrations:

der(1)del(1)t(1;13)[6], der(6)t(6;7)(p21;q31)[6], der(6)t(6;12)t(q23-24;?)[7],
 der(9)ins(9;13)(?;?)[6], del(10)(q11)[5], del(11)[6], der(12)t(6;12)[2],
 der(12)del(12)t(6;12)(q23-24;q23)[4], der(13)t(10;13)[1], der(16)t(1;16)(?;p13)[7],
 del(20)(p10)[5], der(20)t(1;14)t(1;20) [7], i(21)(q10)[1], der(22)t(10;22)(?;q13)[4];
 der(21)t(17;21)[1] [cp 7]

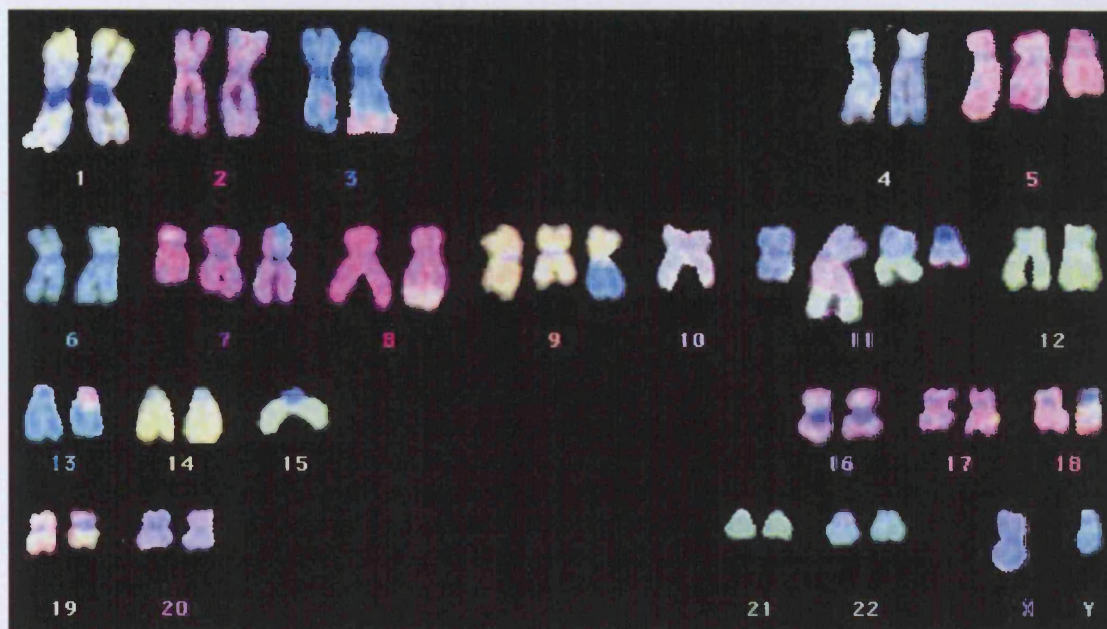


Figure 5.8 M-FISH karyotype of U251

A range of 47 – 54 chromosomes, with a mode of 49, was found in thirty cells counted.

M-FISH analysis showed a male karyotype with the following aberrations:

-X,[5], der(5)t(5;8)(q31;?)[3], del(5)(q?)[1], +7[4], der(8)t(5;8)(?:q22)[5],
der(9)t(3;9)(?:q21)[5], -10[5], der(11)t(11;10)t(10;15)[5] or
der(11,10,15)(11?::10?::15?::)[5], der(17)t(5;17)[5], der(11)t(11;15)(q12;q12)[5],
del(11)(?)[5], del(18)(q11)[5] [cp5]

5.2.2 Confirmation of copy number change

5.2.2.1 Amplification

Gene amplification was detected by array CGH predominantly in the patient tumour samples. However, I wished to confirm amplification in a cell line with FISH. The best model for an amplified gene in the cell lines was *EGFR* in CRL1620. This cell line shows a region of amplification on chromosome 7 between clones RP11-449G3 (54 Mb) and RP4-725G10 (55 Mb), which contains *EGFR* (Figure 5.9 a). A dual probe for the centromere of chromosome 7 and *EGFR* confirmed *EGFR* copy number gain in cell line CRL1620. This hypotetraploid cell line was found to have 4-5 centromeres of chromosome 7, each associated with *EGFR*. However, copies of *EGFR* were also integrated into 1-2 copies of chromosome 11 (Figure 5.9 b).

5.2.2.2 Homozygous deletion

A discrete deletion was detected in cell line CRL2610 between 21 and 24 Mb (9p21), containing *CDKN2A/CDKN2B* (Figure 5.10). This region was included in larger deletions in six cell lines and all patient samples. Array CGH log₂ ratios suggested homozygous loss at 21-22 Mb (9p21-p22) in tumour T2 and cell lines CRL2020, CRL2610, U87 and U118. FISH was used to investigate the homozygous deletion in CRL2610. The control probe RP11-513M16 (19.3 Mb; 9p22.1), labelled with Texas Red was co-hybridised with each of the test probes, RP11-149I2 (21.9Mb; 9p21.3) and RP11-495L19 at (22.3 Mb; 9p21.3), both labelled with FITC.

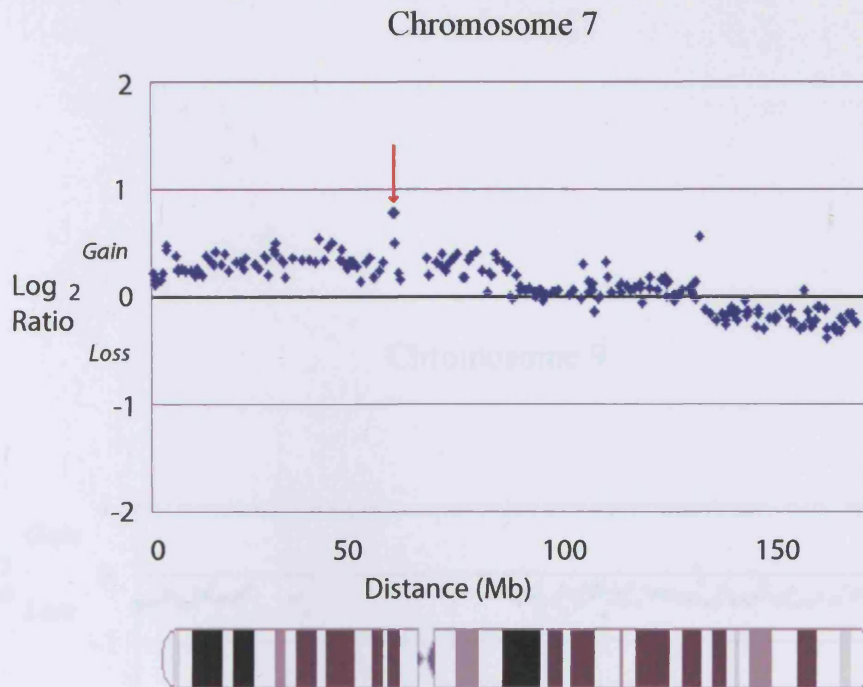


Figure 5.9 a Array CGH profile of chromosome 7 in CRL1620. Red arrow indicates the clone containing *EGFR*.

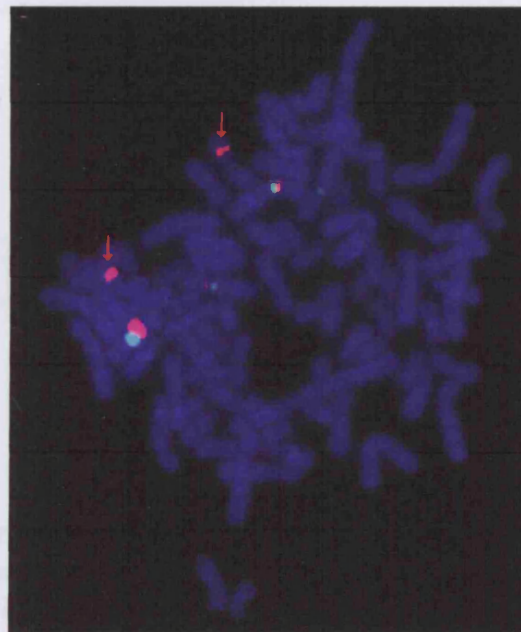


Figure 5.9 b FISH analysis of CRL1620 with a dual probe for *EGFR* (red) and the centromere of chromosome 7 (green). Red arrows show *EGFR* inserted into chromosome 11.

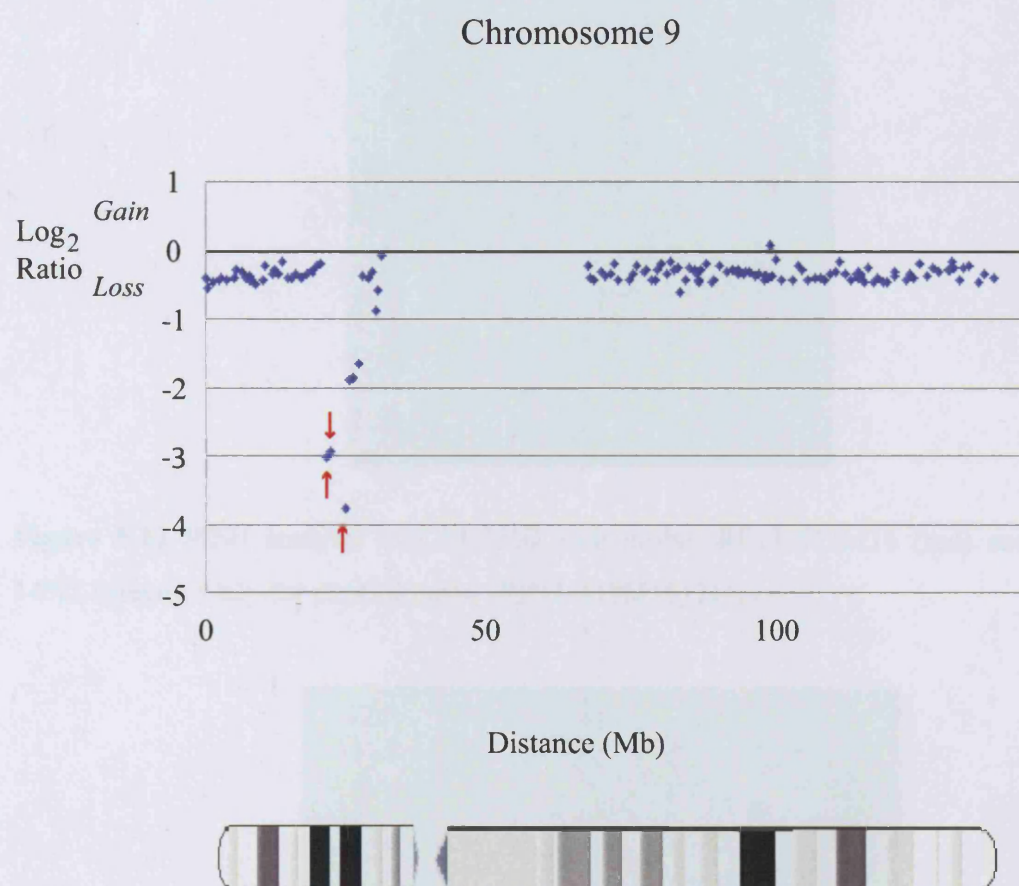


Figure 5.10 Array CGH profile of chromosome 9 in cell line CRL2610. Reduced copy number of chromosome 9 is seen, with a homozygous deletion involving clones RP11-113D19 (21.0 Mb), RP11-15P13 (20.2 Mb) and RP11-495I19 (23.4 Mb). These clones are indicated with red arrows.

Most cells analysed had two copies of chromosome 9. The control probe was found to be present on each copy of chromosome 9, but no signal is present on either chromosome 9 for either of the test probes, indicating a homozygous deletion of these probes (Figures 5.11 and 5.12).

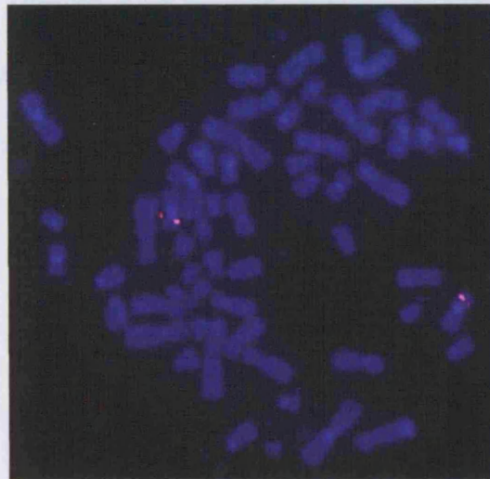


Figure 5.11 FISH analysis of CRL2610 with probes RP11-513M16 (red) and RP11-149I2 (green). Only the control probe (RP11-513M16) is seen.

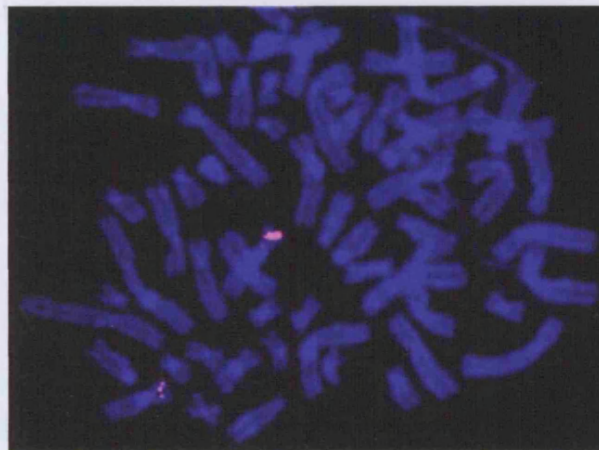


Figure 5.12 FISH analysis of CRL2610 with probes RP11-513M16 (red) and RP11-495L19 (green). Only the control probe (RP11-513M16) is seen.

5.2.2.3 Reduced copy number

The array CGH results from CRL2356 and CRL2366 suggested that there were two discrete deletions on chromosome 6, one between 89 and 94 Mb and the other between 115 and 120 Mb (Figure 5.13 a). The deletion between 89 and 94 Mb was confirmed by FISH using a test probe RP11-346N8 (93 Mb, 6q16) containing the gene *EPHA7*, together with a control probe RP11-517H2 (167 Mb, 6q27) (Figure 5.13 b).

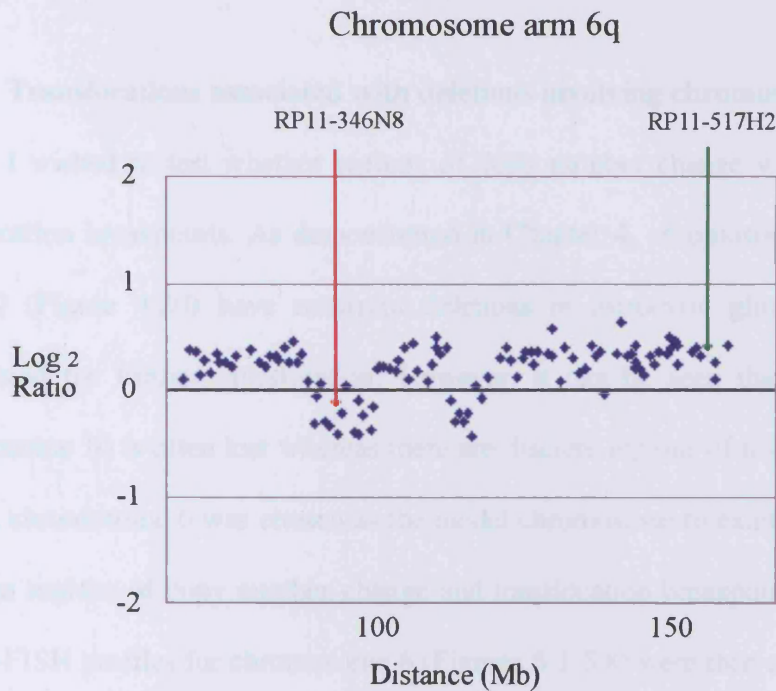


Figure 5.13 a Array CGH profile of chromosome arm 6q in cell line CRL2365. Two deletions are demonstrated. The positions of two probes are shown with arrows RP11-346N8 (red) and RP11-517H2 (green).

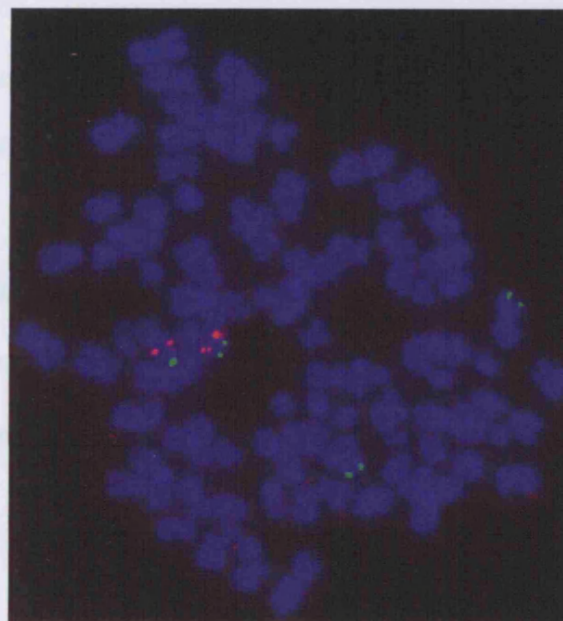


Figure 5.13 b FISH analysis of the chromosome 6 deletion between 89 and 94 Mb in CRL2365. Loss of the *EPHA7* gene was shown using RP11-346N8 (red) and RP11-517H2 (green). In this tetraploid cell line four copies of RP11-517H2 are present, but only two copies of RP11-346N8.

5.2.3 Translocations associated with deletions involving chromosome 6

I wished to test whether regions of copy number change were associated with translocation breakpoints. As demonstrated in Chapter 4, chromosomes 6 (Figure 4.10) and 10 (Figure 4.20) have recurrent deletions in astrocytic gliomas and could be considered for further investigation. However, it can be seen that the whole of the chromosome 10 is often lost whereas there are discrete regions of loss in chromosome 6. Hence, chromosome 6 was chosen as the model chromosome to examine the relationship between regions of copy number change and translocation breakpoints. The array CGH and M-FISH profiles for chromosome 6 (Figures 5.1-5.8) were then used to choose three cell lines for further analysis by FISH, U87, CRL2020 and CRL2610.

5.2.3.1 Cell line U87

In U87, the array CGH profile shows four regions of copy number loss on chromosome 6 (Table 5.2). The M-FISH profile of U87 (Figure 5.7) shows three aberrant chromosomes with chromosome 6 material. These were derived from one chromosome 6 translocated to chromosome 7, $\text{der}(6)\text{t}(6;7)(\text{p}21;\text{q}31)$, and a reciprocal translocation between chromosomes 6 and 12, $\text{der}(6)\text{t}(6;12)(\text{q}23-24;\text{q}?)$ and $\text{der}(12)\text{t}(6;12)(\text{q}23-24;\text{q}?)$. The FISH experiments are shown first, followed by a diagrammatic representation of the findings.

Genetic change	Clones flanking deletion	Position (Mb)	Cytogenetic location
Loss	RP11-227E22	0- 43	6pter - 6p21.1
Loss	RP3-422B11, RP11-30P6	57 - 86	6p11.2 - 6q14.3
Loss	RP11-98I9, RP1-244F1	99 - 104	6q16.2 - 6q16.3
Loss	RP1-32B1, RP11-86O4	135 - 143	6q23.3 - 6q24.2

Table 5.2 Deletions of chromosome 6 in U87

5.2.3.1.1 Characterisation of der(6)t(6;7)(p21;q31)

The array CGH profiles for chromosomes 6 and 7 in cell line U87 and the proposed translocation breakpoints, marked with red arrows, are shown in Figure 5.14. FISH, using five probes (Table 5.3), was used to investigate the proposed breakpoint at 6p21.1.

Clone	Position (Mb)	Test or Control
RP3-337H4	43.5	Test
RP11-22I24	43.6	Test
RP1-261G23	43.7	Test (<i>VEGF</i>)
RP11-344J7	43.8	Test (<i>VEGF</i>)
RP11-227E22	43.9	Control

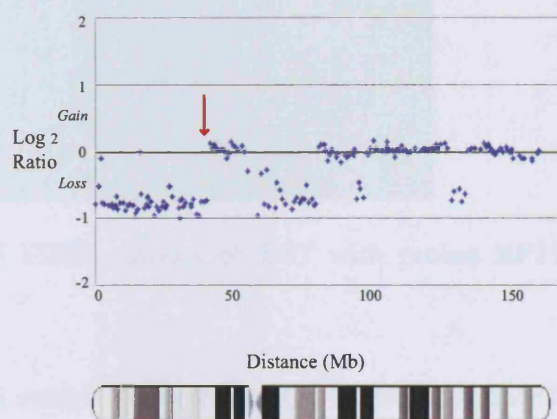
Table 5.3 Probes used to test the 6p21.1 breakpoint in U87

A



B

Chromosome 6



C

Chromosome 7

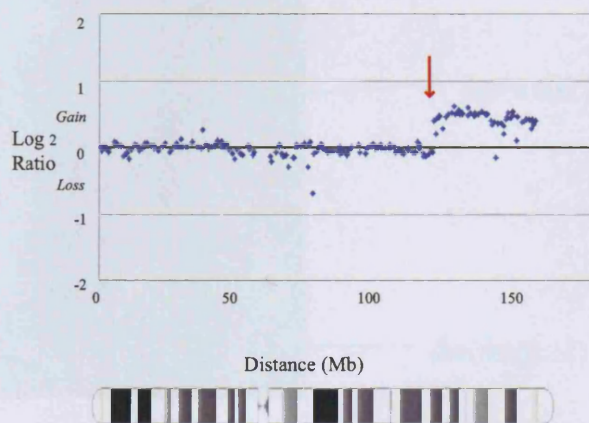


Figure 5.14 Characterisation of der(6)t(6;7) in cell line U87

A M-FISH of der(6)t(6;7) (p21;q31)

B Array CGH profile of chromosome 7 in U87

The red arrow indicates the breakpoint at 6p21

C Array CGH profile of chromosome 6 in U87

The red arrow indicates the breakpoint at 7q31

FISH analysis with probes RP11-227E22 and RP11-344J7 showed both probes to be present on the der(6)t(6;12) and on the der(6)t(6;7). The breakpoint is therefore telomeric to RP11-344J7 (Figure 5.15).

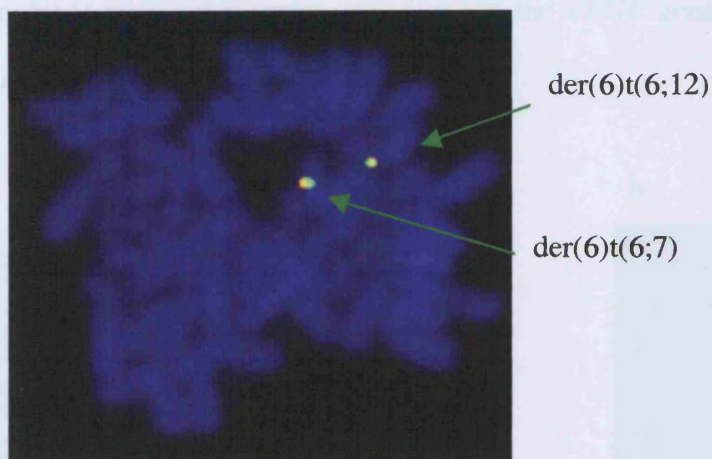


Figure 5.15 FISH analysis of U87 with probes RP11-227E22 (red) & RP11-344J7 (green).

FISH analysis with probes RP11-227E22 and RP1-261G23 showed both probes to be present on the der(6)t(6;12) and the der(6)t(6;7). The breakpoint is therefore telomeric to RP1-261G23 (Figure 5.16).

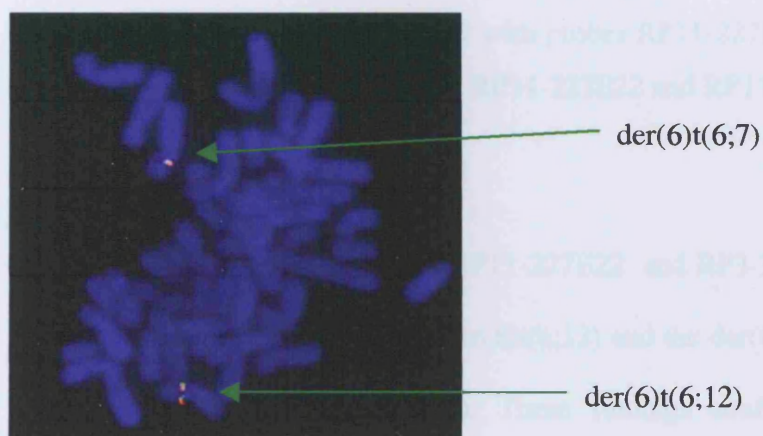


Figure 5.16 FISH analysis of U87 with probes RP11-227E22 (red) and RP1-261G23 (green).

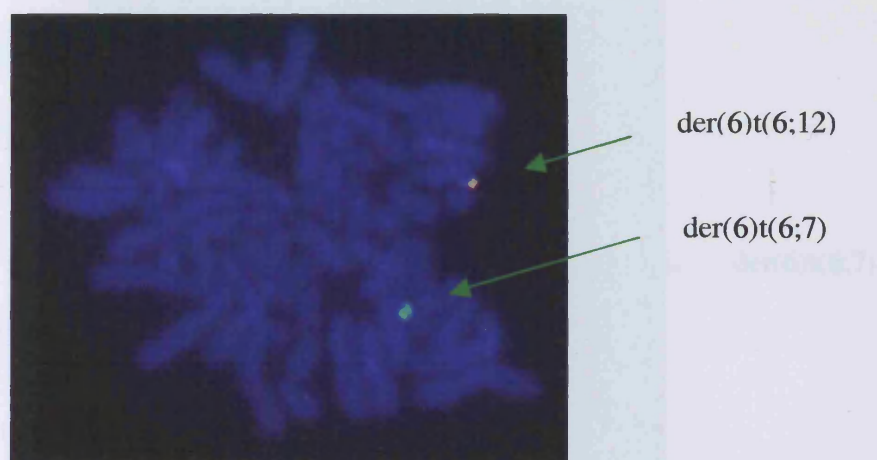


Figure 5.18 FISH analysis of U87 with probes RP11-227E22 (green) & RP3-337H4 (red)

FISH using a chromosome 7q arm specific paint was performed on U87 to determine whether the translocation involved the long or short arm of this chromosome. There was signal on two copies of chromosome 7 as well as the der(6)t(6;7) (Figure 5.19) indicating that the translocation breakpoint is on the long arm of chromosome 7. The array profile of U87 shows a gain from 7q31 to 7qter, with a breakpoint between 120.2 and 122.4 Mb (Figure 5.14). Further FISH studies with probes from 7q31 are needed to confirm the location of the translocation breakpoint.

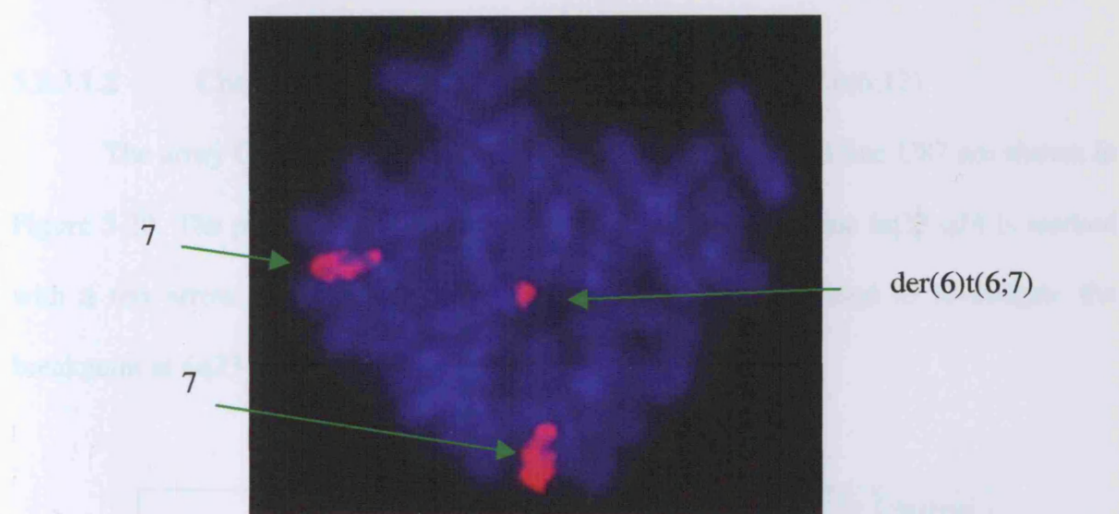


Figure 5.19 FISH analysis of U87 with a paint for chromosome arm 7q

5.2.3.1.2 Characterisation of the der(6)t(6;12) and the der(12)t(6;12)

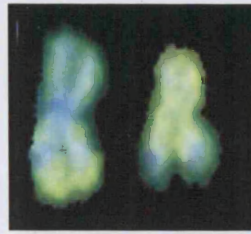
The array CGH profiles for chromosomes 6 and 12 in cell line U87 are shown in Figure 5.20. The proposed translocation breakpoint at chromosome 6q23-q24 is marked with a red arrow. FISH, using the probes in Table 5.4 was used to investigate the breakpoint at 6q23-q24.

Clone	Position (Mb)	Test or Control
RP11-557H15	134.8	Control
RP11-448D5	137.2	Test
RP11-368P1	142.2	Test
RP11-86O4	143.5	Test

Table 5.4 Probes used to test the chromosome 6 breakpoints in t(6;12) in U87

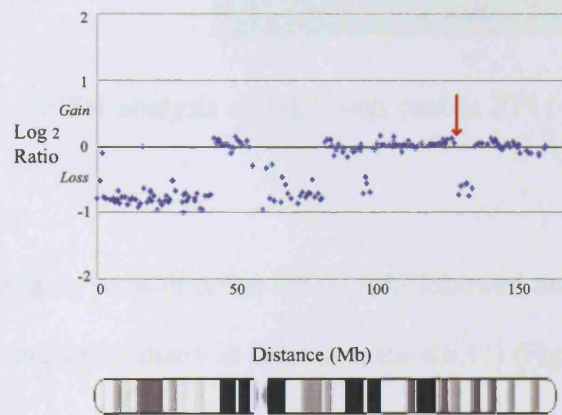
FISH analysis with probes RP11-557H15 and RP11-448D5 showed RP11-557H15 to be present on both the der(6)t(6;12) and the der(6)t(6;7), indicating that it is centromeric to the deletion (Figure 5.21). RP11-448D5 is present on the der(6)t(6;7), but not on the der(12)t(6;12) or the der(6)t(6;12), indicating that the probe is deleted in the t(6;12).

A



B

Chromosome 6



C

Chromosome 12

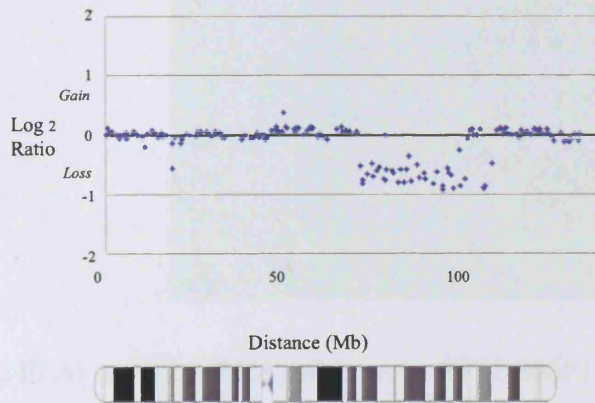


Figure 5.20 Characterisation of der(6)t(6;12) and der(12)t(6;12) in cell line U87

A M-FISH der(6)t(6;12) and der(12)t(6;12)

B Array CGH profile of chromosome 6 in U87

The red arrow indicates the translocation breakpoint at 6q23-q24

C Array CGH profile of chromosome 12 in U87

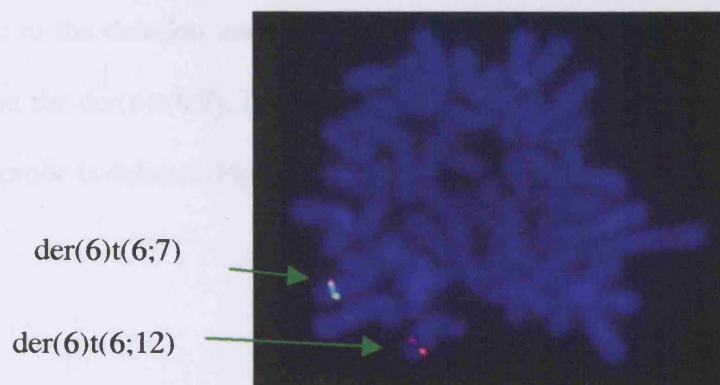


Figure 5.21 FISH analysis of U87 with probes RP11-557H15 (red) and RP11-448D5 (green).

FISH analysis with probe RP11-368P1 showed the probe to be present only on the der(6)t(6;7) indicating that it is deleted in the t(6;12) (Figure 5.22).

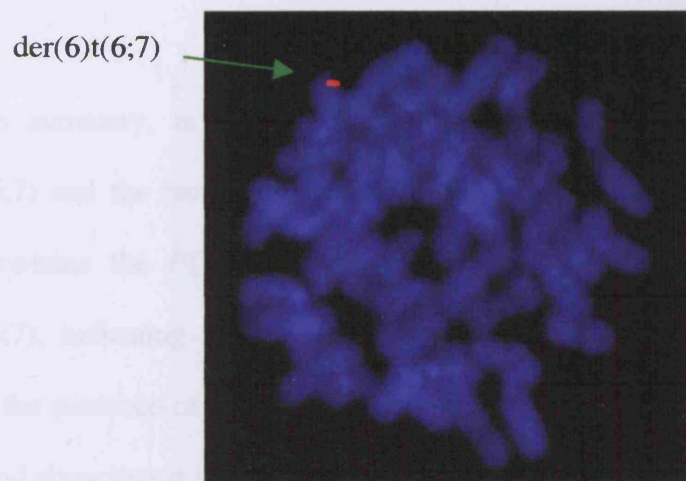


Figure 5.22 FISH analysis of U87 with probe RP11-368P1 (red).

FISH analysis with probes RP11-448D5 and RP11-86O4 showed RP11-86O4 to be present on both the der(12)t(6;12) and the der(6)t(6;7), indicating that this probe is telomeric to the deletion and has been translocated to chromosome 12. RP11-448D5 is present on the der(6)t(6;7), but not on the der(12)t(6;12) or the der(6)t(6;12), confirming that this probe is deleted (Figure 5.23).

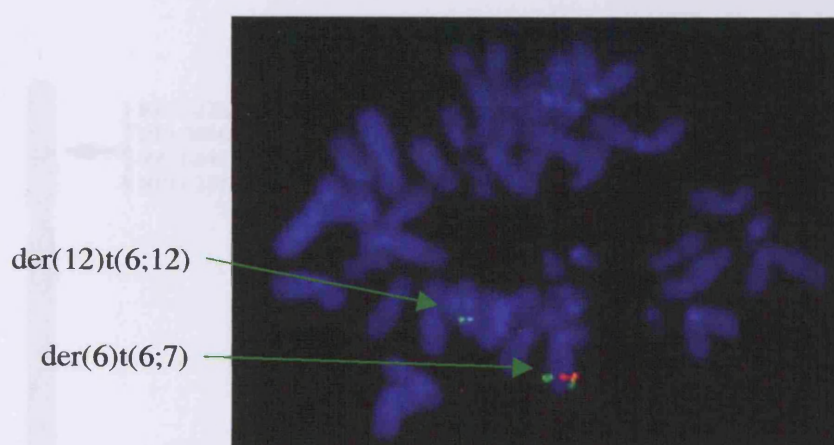


Figure 5.23 FISH analysis of U87 with probes RP11-448D5 (red) and RP11-86O4 (green).

In summary, in U87 I characterised the chromosome 6 breakpoints in the der(6)t(6;7) and the reciprocal t(6;12) translocation (Figure 5.24). Probe RP11-22I24, which contains the *POLH* and *GTPBP2* genes, gave a very small signal on the der(6)t(6;7), indicating that it is intersected by the translocation. These experiments confirm the presence of a deletion of chromosome 6 within and distal to probe RP11-22I24, and show that it is associated with a translocation between chromosomes 6 and 7. In addition, FISH analysis of the t(6;12), confirms a deletion between RP11-557H15 and RP11-86O4, and shows that it is associated with a translocation between chromosomes 6 and 12.

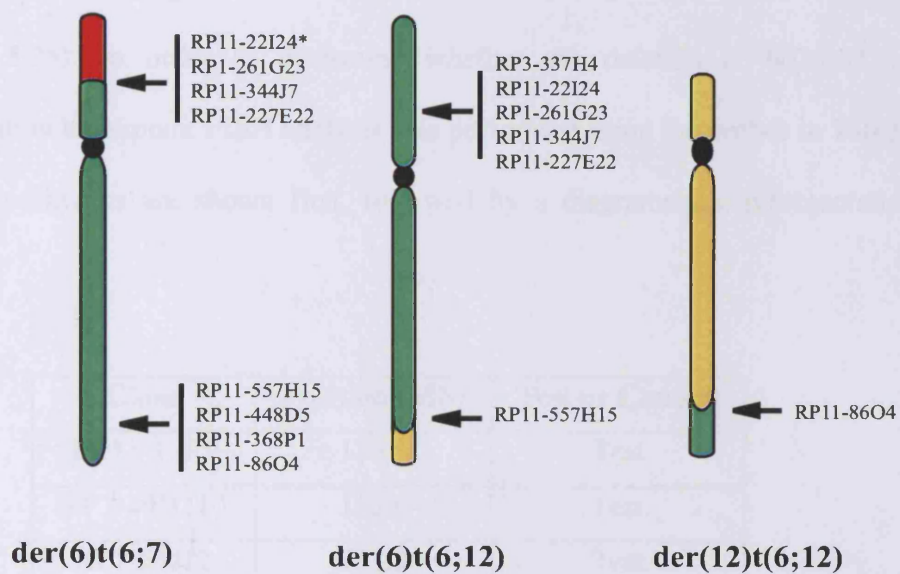


Figure 5.24

Summary of FISH analysis of chromosome 6 aberrations in U87. Chromosome 6 is shown in green, chromosome 7 in red, and chromosome 12 in yellow. RP11-22I24* signifies a smaller signal for this probe on the der(6)t(6;7) than on the der(6)t(6;12) suggesting that the breakpoint intersects this probe.

5.2.3.2 Cell line CRL2020

M-FISH shows that cell line CRL2020 is near-tetraploid with three copies of chromosome 6, in most cells, and a translocation of a fragment of chromosome 6 to chromosome 7. In the karyotype shown, three apparently normal copies of chromosome 7 are present, and two copies of the der(7)t(6:7) (6?:p22) (Figure 5.2). The array CGH profile confirms the gain of the whole of chromosome 7 and a deletion at 6q26-q27 (Figure 5.25). In order to determine whether the deletion at 6q26-q27 was the translocation breakpoint FISH analysis was performed using the probes in Table 5.5. The FISH experiments are shown first, followed by a diagrammatic representation of the findings.

Clone	Position (Mb)	Test or Control
RP11-13P5	159.5	Test
RP3-495O10	163.6	Test
RP1-51J12	163.9	Test
RP11-517H2	167.5	Test
RP11-471L1	168.0	Control

Table 5.5 Probes used to test the 6q26-q27 breakpoint in CRL2020

FISH analysis with probes RP11-13P5 and RP3-495O10 showed RP11-13P5 to be present on 2-3 copies of chromosome 6, while RP3-495O10 is present on only one of these, confirming a deletion of this probe (Figure 5.26).

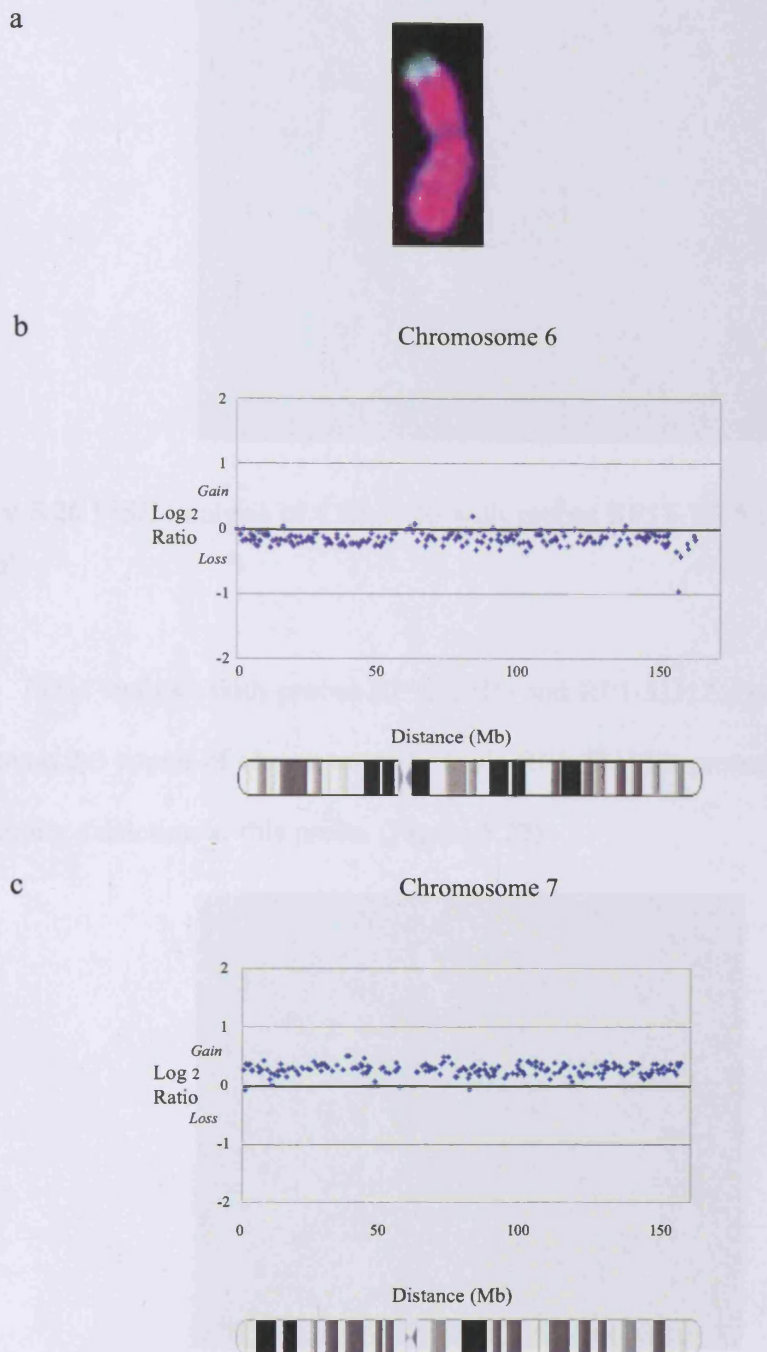


Figure 5.25

Deletion associated with a translocation, involving chromosome 6 in cell line CRL2020.

(a) M-FISH of der(7)t(6;7)

(b) Array CGH profile of chromosome 6 in CRL2020

(b) Array CGH profile of chromosome 7 in CRL2020

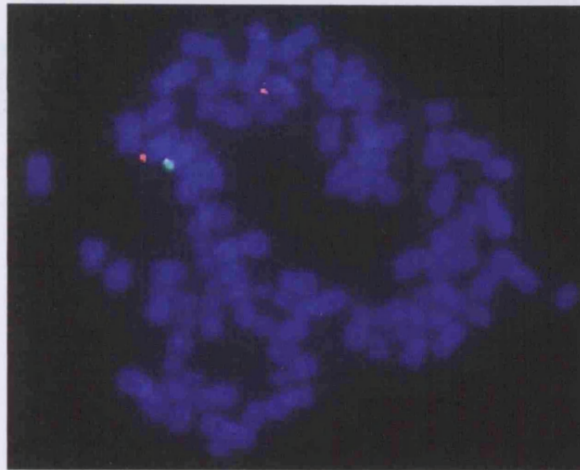


Figure 5.26 FISH analysis of CRL2020 with probes RP11-13P5 (red) and RP3-495O10 (green).

FISH analysis with probes RP11-13P5 and RP1-51J12 showed RP11-13P5 to be present on 2-3 copies of chromosome 6, while RP1-51J12 is present on only one of these, confirming a deletion of this probe. (Figure 5.27)



Figure 5.27 FISH analysis of CRL2020 with probes RP11-13P5 (red) and RP1-51J12 (green). Only 2 copies of chromosome 6 are present on this partial metaphase spread.

FISH analysis with probe RP1-51J12 and 6q paint showed three copies of 6q to be present, only one of which has RP1-51J12, confirming the deletion of this probe from 6q (Figure 5.28).

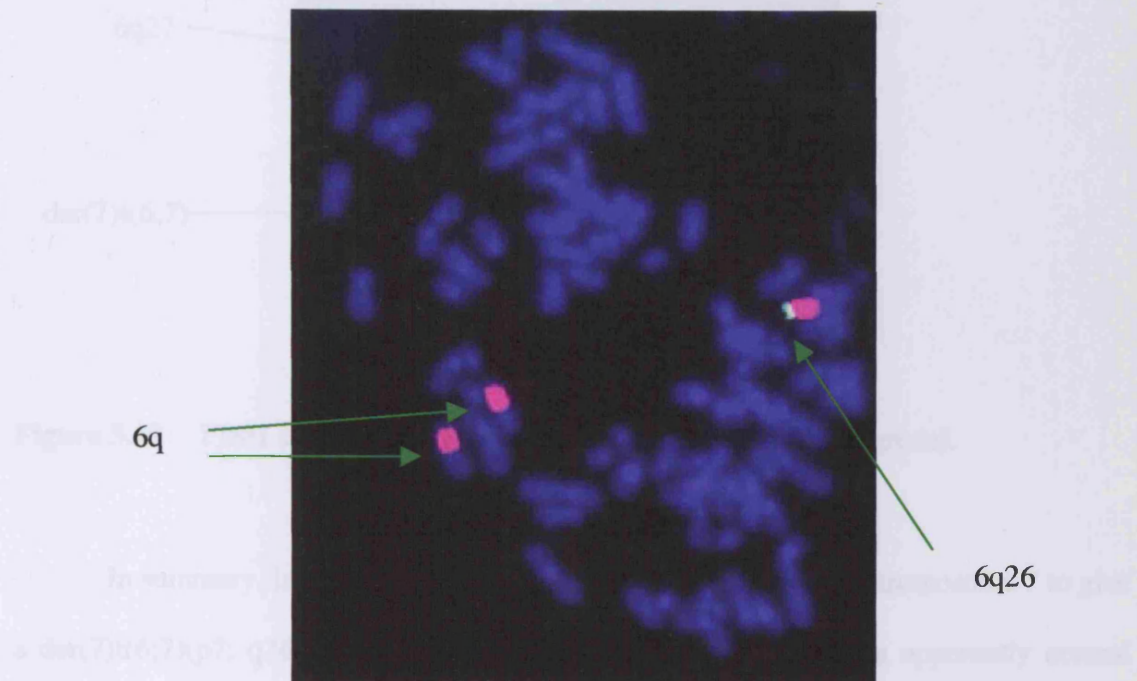


Figure 5.28 FISH analysis of CRL2020 with probe RP1-51J12 (green) and 6q paint (red).

FISH analysis of CRL2020 with probe RP11-471L1 showed this distal 6q probe to be present on the long arm of one chromosome 6 and on the terminal short arm of each of the der(7)t(6;7) (Figure 5.29).

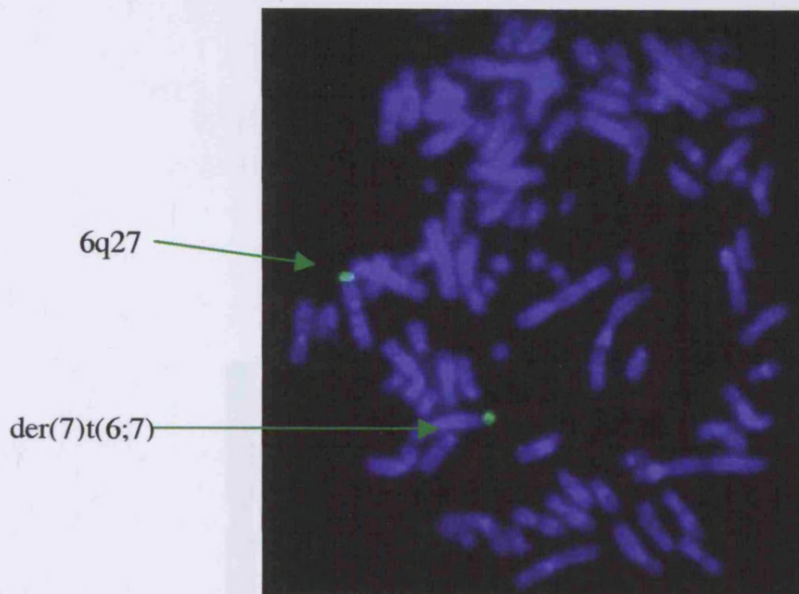


Figure 5.29 FISH analysis of CRL2020 with probe RP11-471L1 (green).

In summary, in CRL2020, chromosome 6 is translocated to chromosome 7 to give a $\text{der}(7)\text{t}(6;7)(\text{p?}; \text{q}26\text{-}27)$ and $\text{del}(6)(\text{q}26\text{-}27) \times 2$ (Figure 5.30). An apparently normal copy of chromosome 6 is also present. A discrete deletion detected by array CGH between 160 and 167 Mb was investigated by FISH using probes RP11-13P5 (159.4 Mb), RP3-495O10 (163.6 Mb), RP1-51J12 (163.8 Mb) and RP11-471L1 (168 Mb). All four probes were present on the normal chromosome 6. Of the other chromosome 6 derivatives, RP11-13P5 was present on the $\text{del}(6)(\text{q}26\text{-}27)$ while RP11-471L1 was present on the $\text{der}(7)\text{t}(6;7)$. Therefore, it appears that the segment of chromosome 6 distal to RP11-13P5 became translocated to the short arm of chromosome 7, but sequences including RP3-495O10 (PACRG) and RP1-51J12 (QKI) became deleted so that only the terminal probe from 6qter, RP11-471L1, is present on the $\text{der}(7)\text{t}(6;7)$. The chromosome 6 from which the segment translocated became duplicated after the translocation. These experiments confirm the presence of a deletion between 160 and 168 Mb, including the

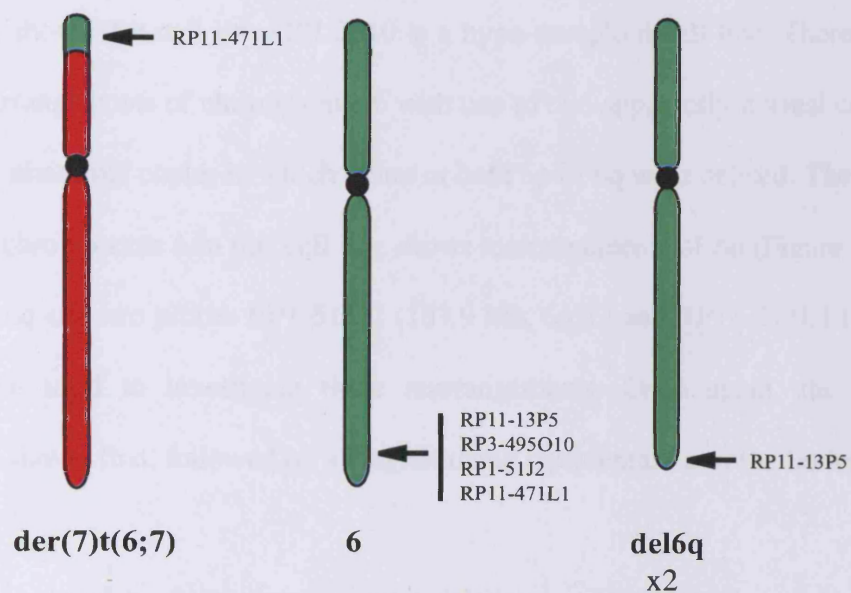


Figure 5.30

Summary of FISH analysis of the chromosome 6 deletion in CRL2020. Chromosome 6 is shown in green and chromosome 7 in red.

PARK2, *PACRG* and *QKI* genes, and show that it is associated with a translocation between chromosomes 6 and 7.

5.2.3.3 Cell line CRL2610

M-FISH shows that cell line CRL2610 is a hypo-tetraploid cell line. There were complicated rearrangements of chromosome 6 with one to two apparently normal copies, and one to three abnormal copies in which either or both 6p or 6q were deleted. The array CGH profile of chromosome 6 in this cell line shows rearrangements of 6q (Figure 5.31). FISH paints for 6q and two probes RP1-51J12 (163.9 Mb, 6q26) and RP11-471L1 (168.0 Mb, 6q27) were used to investigate these rearrangements. Once again, the FISH experiments are shown first, followed by a diagrammatic representation of the findings.

FISH analysis of the distal chromosome 6 deletion in CRL2610 using probe RP1-51J12 and 6q paint showed RP1-51J12 to be present on the distal end of one 6q, but not on the other (Figure 5.32). Instead, the probe is on a small and as yet unidentified chromosome.

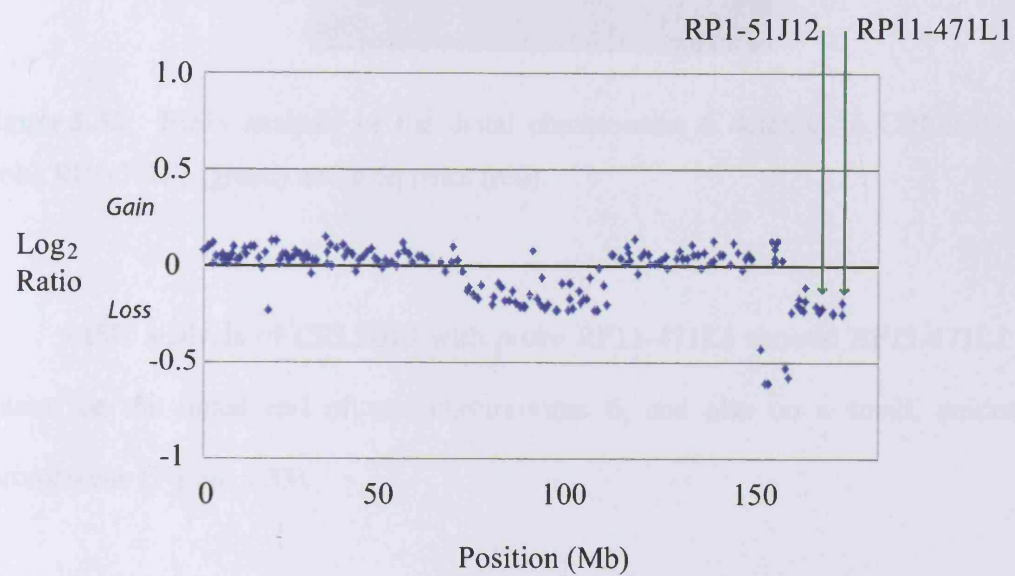


Figure 5.31 Array CGH profile of chromosome 6 in cell line CRL2610. The green lines indicate the position of the probes used in the FISH experiments. The probe names are also indicated.

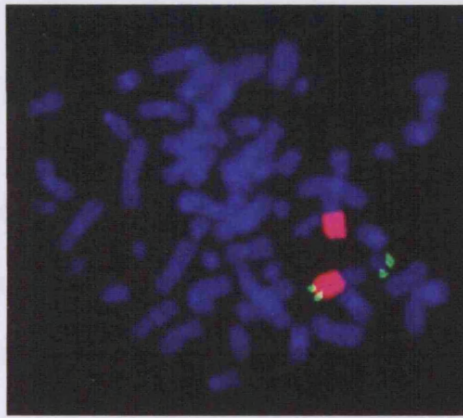


Figure 5.32 FISH analysis of the distal chromosome 6 deletion in CRL2610, using probe RP1-51J12 (green) and a 6q paint (red).

FISH analysis of CRL2610 with probe RP11-471L1 showed RP11-471L1 to be present on the distal end of one chromosome 6, and also on a small, unidentified chromosome (Figure 5.33).

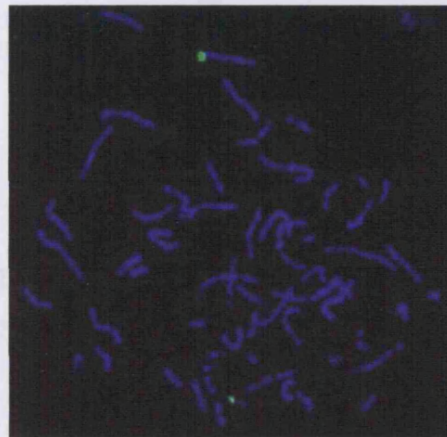


Figure 5.33 FISH analysis of CRL2610 with probe RP11-471L1 (green).

In summary, in cell line CRL2610, a distal deletion was identified using probes RP1-51J12 and RP11-471L1 (Figure 5.34). These probes were both found to be at the distal end of 6q on one chromosome and on a very small chromosome, but missing from a second 6q segment. These findings indicate a translocation at the distal end of chromosome 6 with the breakpoint centromeric to these two probes.

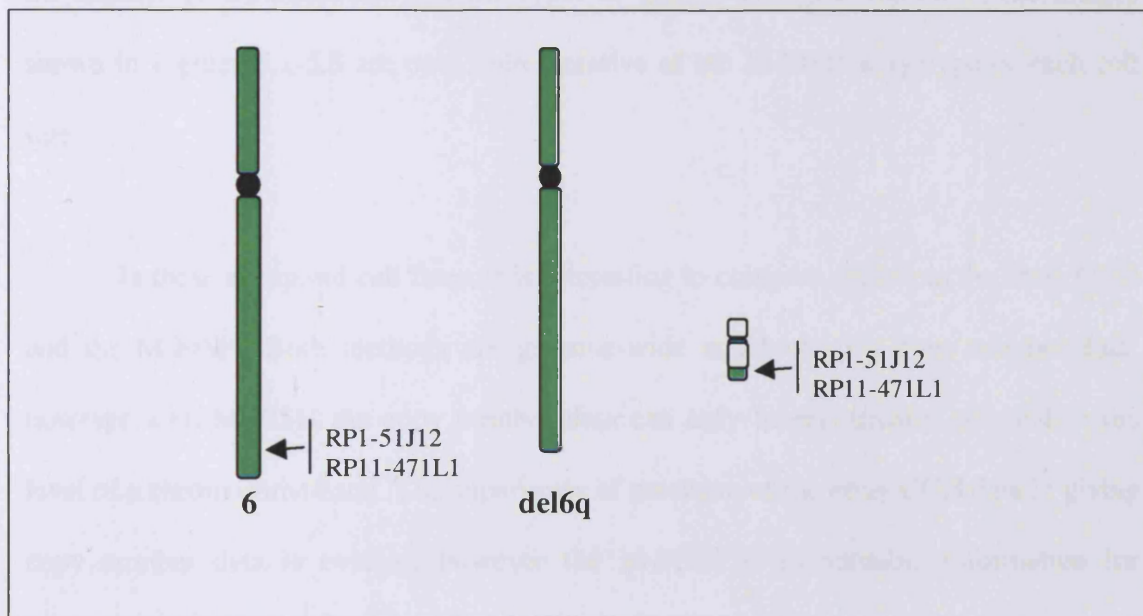


Figure 5.34 Summary of FISH analysis of the distal chromosome 6q deletion in CRL 2610. Chromosome 6 is shown in green.

5.3 Discussion

This chapter showed the M-FISH analysis of eight of the cell lines used in this study. The cell lines were found to have complex karyotypes, with duplication of the genome and many genetic changes. On reviewing the whole chromosome changes, taking the cell lines as tetraploid, it can be seen that there is relative loss of chromosomes 6, 9 and 10 and gain of chromosomes 7 and 20. Although the constituent cells in each cell line are clonal, cell-to-cell variation is observed using M-FISH, and hence there is a range in the number of chromosomes and the types of genetic changes. Therefore, the images shown in Figures 5.1-5.8 are only representative of the M-FISH karyotype of each cell line.

In these aneuploid cell lines, it is interesting to compare data from the array CGH and the M-FISH. Both methods are genome-wide and both give copy number data, however with M-FISH the copy number data can only be realistically assessed to the level of a chromosome band. The superiority of precision of the array CGH data in giving copy number data is evident, however the M-FISH gives valuable information for karyotyping. In regard of positional data, when interpreting array CGH it is assumed each clone is in the position of the normal karyotype, it is M-FISH that gives information regarding aberrant genomic position such as in relation to a translocation.

The initial FISH experiments were performed to confirm selected regions of copy number change detected by array CGH. Examples selected were of amplification, homozygous deletion and a clone with reduced copy number. There is no precise

definition of amplification. However, if there is greater than a five-fold increase in copy number it is generally interpreted as amplification, rather than just gain of DNA. The example that was selected for amplification was that of *EGFR* (Figure 5.9). From the FISH analysis, it was possible to state that there was an increase in *EGFR* copy number, as the number of signals of *EGFR* was detected in excess of the control centromere probe. Also the strength of the signal was greater for *EGFR* than in the control experiments. However, quantification of copy number using FISH signal intensity can only be described as an estimate, as signal intensity varies with probe hybridisation and detection efficiency.

FISH proved to be more effective in assessing deletions than in quantifying copy number gain. Incorporating a control probe for comparison, FISH was used to confirm a homozygous deletion of the probe containing *CDKN2A* in cell line CRL2610. Here, the number of signals was important rather than strength of signal. In patient samples, there will be a mixture of normal and tumour cells. Therefore, dual-probe interphase FISH may be a more reliable method of detecting a homozygous deletion than PCR.

FISH was also used to assess relative copy number loss. The region assessed is an interstitial deletion in cell lines CRL2365 and CRL2366. A probe containing *EPHA7* was selected for confirmation. *EPHA7* is part of the EPH family of protein tyrosine kinase receptors. The EPH family are involved in neurulation, control of axon guidance and in blood vessel development (Holder and Klein, 1999; Holmberg *et al.*, 2000). Further studies have suggested that *EPHA7* is an effector of *HOXA13* (Stadler *et al.*, 2001). The

probe representing this gene was co-hybridised with a probe from a region on the same chromosome with normal copy number as assessed by array CGH. The relative loss of this DNA was confirmed.

Following a comparison of the array CGH data and the M-FISH data, three translocations were selected for further analysis. Translocations involving chromosome 6 were considered particularly interesting, as this chromosome has previously been reported to have frequent LOH and reduced copy number in these tumours. Also the deletions of 6 were discrete deletions as opposed to the deletions of chromosome 10, which tended to involve the whole chromosome. These selected translocations were der(6)t(6;7) in cell line U87, a reciprocal translocation der(6)t(6;12) and der(12)t(6;12) again in cell line U87, and translocations in two cell lines CRL2020 and CRL2610 involving a deletion in band 6q26. These translocations were characterised for the chromosome 6 components. Work is ongoing to characterise the chromosome 7 component of der(6)t(6;7) and the chromosome 12 breakpoints in the reciprocal translocation der(6)t(6;12) and der(12)t(6;12), and the translocation partners of chromosome 6 in cell lines CRL2020 and CRL2610.

Having characterised these translocations with array CGH and M-FISH and then further defined them with FISH, the next question is what is the significance of these translocations. From the view of gene theory, if these translocations engender a growth or survival advantage to the cell, then the presumption is that the translocation results in an alteration in the function of a gene or genes in the region. The classical view of a

functional translocation is that of *BCR-ABL*, which results in a fusion oncoprotein. This may well be the case in at least some of the translocations described in this thesis. Namely, the translocation breakpoints are within two genes and result in the fusion of their coding sequences, changing their activity. However, the array CGH data gives a wider perspective in that it shows that these translocations are associated with regions of copy number change. It may be that genomic aberrations within these regions of copy number change are giving the growth advantage to the cell and the translocations are merely a by-product of the mechanism of genetic change that has effected this copy number change. How the data from this thesis may give information about mechanisms of genetic change are discussed in Chapter 6.

Examination of the copy number changes associated with each of the characterised translocations shows that there are both deletions and gains and that some of the copy number changes are discrete, interstitial changes. The der(6)t(6;7) in cell line U87 has a deletion from the telomere of the short arm of chromosome 6 to the breakpoint at 43.6 Mb. The question raised here is whether the critical event is deletion of one or more tumour suppressor genes on 6p? Alternatively, or possibly in addition, the translocation itself is important, with a fusion gene being generated at the breakpoint. It remains to be established whether the key gene in this translocation is DNA polymerase eta (*POLH*) or *GTPBP2* on chromosome 6 or it could be that the aberrant gene is on chromosome 7. Genes in the region of the breakpoint on chromosome 7 include Protein tyrosine phosphatase receptor type 2 (*PTPZRI*) (121.2 Mb) and Alpha aminoacidic semialdehyde synthase (*AASS*) (121.3 Mb). *POLH* is a low fidelity polymerase and is

involved in post-replicative DNA repair (Kusumoto *et al.*, 2004; Matsuda *et al.*, 2000). Defects in this gene are responsible for the Xeroderma Pigmentosum Variant (Broughton *et al.*, 2002; Masutani *et al.*, 1999). GTP binding proteins, also termed G proteins are activated by binding GTP and inactivated by the hydrolysis of GTP to GDP. This “on” and “off” switch mechanism enables these varied proteins perform a wide range of biological activities (Bourne *et al.*, 1990). *GTPBP2* is a novel member of the G protein family, at 6p21, its function is yet to be characterised (Watanabe *et al.*, 2000). *PTPRZ1* is involved in oligodendrocyte differentiation (Canoll *et al.*, 1996; canRanjan and Hudson, 1996). Using a mouse model of multiple sclerosis, Harroch *et al* suggested that *PTPRZ1* has a role in oligodendrocyte survival and recovery (Harroch *et al.*, 2002). AASS is an enzyme which catalyses the first steps of the degradation of the essential amino acid, lysine. Inactivating mutations of AASS have been found in patients with hyperlysinaemia (Sacksteder *et al.*, 2000).

The other translocations characterised here are associated with discrete, interstitial deletions on the long arm of chromosome 6. The first interstitial deletion between 137.2 Mb and 143.5 Mb contains a large number of genes. What can be considered here is whether a translocation breakpoint is the critical change in the tumour or if it is the deletion of a tumour suppressor gene? The same consideration can be applied to the translocations involving 6q25-26. Does the deletion at 6q25-26 harbour a tumour suppressor gene?

Genes involved in the deletion associated with translocation at 6q26 include *IGF2R*, *PARK2*, *PACRG* and *QKI*. Insulin-like growth factor II receptor (*IGF2R*) activates the potent growth inhibitor, transforming growth factor beta, and is involved in the degradation of the mitogen insulin-like growth factor 2 (*IGF2*). Mutation in *IGF2R*, in association with LOH, has been identified in hepatocellular carcinoma and non-small cell lung cancer (De Souza *et al.*, 1995; Kong *et al.*, 2000). Parkinson's disease is a neurodegenerative illness where there is loss of a cell population in the mid-brain, the substantia nigra. Mutations in *PARK2* (Parkin) are associated with autosomal recessive juvenile parkinsonism, especially in exons 2, 3, 4 and 7 (Giasson and Lee, 2001; Hedrich *et al.*, 2004). *PARK2* is involved in protein degradation as an E3 ubiquitin ligase (Zhang *et al.*, 2000). Inactivating mutations have been identified in *PARK2* in other tumour types including ovarian cancer, hepatocellular carcinoma and non-small cell lung cancer (Cesari *et al.*, 2003; Denison *et al.*, 2003; Picchio *et al.*, 2004; Wang *et al.*, 2004). Parkin coregulated gene (*PACRG*) shares the same promoter as *PARK2* (West *et al.*, 2003). *PACRG* is also thought to be involved in protein degradation (Imai *et al.*, 2003). Mutant mice, called Quaking have an abnormal gait and defects in myelination (Sidman *et al.*, 1964). The mice with this deficit were found to have mutation in *QKI* (Cox *et al.*, 1994; Ebersole *et al.*, 1992; Justice and Bode, 1988). This assumption has recently been complicated, by the finding that mice with Quaking phenotype, have both mutation of *QKI* and absent *PARK2* expression (Lorenzetti *et al.*, 2004).

5.3.1 Further work

Having characterised the chromosome 6 components of the selected translocations, the translocation partners should now be characterised. In respect of der(6)t(6;7) in cell line U87, the array CGH profile of chromosome 7 shows a region of gain from 121 Mb (7q31.32) to the telomere of the long arm (Figure 5.14c). Probes from 7q31.32 can be used in FISH to investigate this proposed translocation breakpoint (Table 5.6).

Clone	Cytogenetic location	Position (Mb)
RP11-384A20	7q31.32	121.2
RP5-1049N15	7q31.32	121.3
RP11-560I19	7q31.32	121.4
RP5-1101C3	7q31.32	121.6
RP5-850I1	7q31.32	121.7
RP11-350G10	7q31.32	121.8
RP11-395G17	7q31.32	121.9
RP5-1166A24	7q31.32	122.0
RP4-589D8	7q31.32	122.1
RP11-61D3	7q31.32	122.2
RP11-85N14	7q31.32	122.3
RP11-560I19	7q31.32	122.4

Table 5.6 Tiling path probes which can be used to investigate chromosome 7 breakpoint of der(6)t(6;7) in cell line U87

Regarding the reciprocal translocation der(6)t(6;12) and der(12)t(6;12) in cell line U87, the array CGH profile of chromosome 12 shows an interstitial deletion on the long arm (Figure 5.20c). Probes from the breakpoints around this interstitial deletion can now

be selected and these should lead to the identification of the translocation breakpoint (Table 5.7).

Clone	Cytogenetic location	Position (Mb)
RP11-11G4	12q15	68.8
RP11-320P7	12q15	68.8
RP11-396J13	12q15	68.9
RP11-566H23	12q15	69.0
RP11-785D18	12q15	69.2
RP11-130E17	12q15	69.3
RP11-654D6	12q15	69.4
RP11-158O11	12q15	69.5
CTD-2021H9	12q15	69.6
RP11-934P3	12q15	69.7
RP11-101K2	12q15	69.8

Clone	Cytogenetic location	Position (Mb)
RP11-575G13	12q23.1	99.4
RP11-427C3	12q23.1	99.5
RP11-252G12	12q23.1	99.6
RP11-263E1	12q23.1	99.7
RP11-447N23	12q23.1	99.7
RP11-350G24	12q23.1	99.8
RP11-426H24	12q23.1	99.9

Table 5.7 Tiling path probes which can be used to investigate the chromosome 12 breakpoints of the reciprocal translocation der(6)t(6;12) and der(12)t(6;12) in cell line U87

The breakpoint on the short arm of chromosome 7 from the der(7)t(6;7) in cell line CRL2020 has not been identified. On examining the array CGH profile of chromosome 7, it can be seen there is gain of the whole chromosome but no obvious deletion. It could be that the material from chromosome 6 has translocated to the telomere of the short arm of chromosome 7. FISH using a telomeric probe from 7 would confirm this supposition. The translocation partner of chromosome 6q material in cell line CRL2610 has not yet been identified, M-FISH being unsuccessful in this respect.

Undoubtedly, one of the contributing factors for this is that the material from chromosome 6 is small. Individual chromosome-specific FISH paints in conjunction with a probe from the long arm of chromosome 6 (labelled in a different fluorescence probe) could solve the problem.

Genes affected by the translocations, or close to the breakpoints have been selected for further investigation, based on their involvement in other tumours, in cell growth control or their specific role in neural cells (Table 5.8). Firstly I propose that the expression of the genes is assessed with real-time PCR and then selected genes are sequenced.

5.3.2 Conclusion

This chapter has demonstrated that genomic positional changes demonstrated by M-FISH are associated with copy number changes as detected by array CGH. FISH was used to confirm and further refine the breakpoints of selected translocations associated with deletions on chromosome 6. A detailed description on how to continue in the investigation of the genes at selected translocations was also given. Chapter 6 gives a wider view of this body of work and places it into the broader field of genetics. It also discusses its potential impact on medical therapies.

Gene symbol	Gene name	Cytogenetic location	Position (Mb)
GTPBP2	GTP-Binding protein 2	6p21.1	43.7
POLH	Polymerase	6p21.1	43.7
PTPRZ1	Protein-tyrosine phosphatase receptor-type zeta-1	7q31.32	121.1
AASS	Alpha-aminoadipic semialdehyde synthase	7q31.32	121.3
MAP3K5	Mitogen-activated protein kinase kinase kinase 5	6q23.3	136.9
MAP7	Microtubule-associated protein 7	6q23.3	136.7
CITED2	CBP/p300-interacting transactivator, with glu/asp-rich c-terminal domain 2	6q24.1	139.7
IGF2R	Insulin-like growth factor receptor 2	6q25.1	160.4
PARK2	Parkin	6q26	161.7
PACRG	Parkin co-regulated gene	6q26	163.1
QKI	Quaking	6q26	163.8

Table 5.8 Selected genes from translocations

Chapter Six

Final Discussion

6.1 Review of the aims

This thesis focused on changes in DNA in high-grade astrocytic gliomas and in particular on copy number and positional changes and their inter-relationship. There were three main aims in this thesis. The first aim of this thesis was to gain a better understanding of the advantages of array CGH and to develop a method of analysis. The second aim was to assess copy number changes in high-grade astrocytic glioma cell lines and patient samples. And the third aim was to investigate the relationship between changes in copy number as detected by array CGH and positional changes in DNA, namely translocations detected by M-FISH.

6.2 Project methodology and results

6.2.1 Overview

The initial part of this thesis addressed the problem of variation in the assessment of array CGH results, and described the development of an automated analytical programme. This programme was then used to assess the array CGH results of ten high-grade astrocytic glioma cell lines and ten tumour samples. Each data point in each experiment was then designated gain, null or loss in relation to copy number. The method of analysis did not discriminate between levels of gain and levels of loss. For instance, using only this method it would not be possible to differentiate between a region of simple gain or high-level amplification. Likewise a homozygous deletion could not be

distinguished from reduced copy number. In this thesis, I overcame this problem by selecting the regions with the greatest copy number change and presented these data as individual profiles. An alternative method would be to use an Excel file to present the clones listed in order of their \log_2 values.

Chapter 4 displayed the results of the array CGH with examples of individual chromosome profiles. At the time of inception of the study, array CGH was a new technique with metaphase CGH being the conventional method. It was important to compare the results from these techniques in order to assess the greater sensitivity and precision of the array CGH. In particular, this thesis demonstrated the advantage of assessing each individual data point independently in each experiment. This facilitated the ability to define breakpoints in chromosomes precisely and in Chapter 5 these were then used to map translocation breakpoints.

6.2.2 Evolution of array technology

There was great inter-experimental variation arising from batch differences of printed slides and Cot1 DNA. As there are more users of this technology, sharing information on the performance of the printed slides and Cot1 DNA and can iron out these issues. In my experience, keeping inter-experimental variation to a minimum was key to having reliable results. This is why I rejected experiments with an inter-quartile range of greater than \log_2 of 0.275. Greater confidence in the data would come from experimental replicates and combining data. Also, inter-experimental replicates would give a greater confidence in the data. In the arrays that were available, there were two

copies of each clone in different regions of the slide. It would be preferable to have more replicates for analysis of the data. This is becoming feasible as the technology is evolving and more data points are being printed onto the slides. Currently this increase in capacity is being used to increase the resolution of the arrays (Ishkanian *et al.*, 2004). This thesis has highlighted the problem of analysing large data sets and the issues relating to variation. My experience suggests that when designing the array CGH slides, these issues should be addressed and adequate controls and replicates included. For instance, if there were the same control probe in each sub-array then this would enable an assessment of experimental variation across the slide. Also, when designing experiments adequate slides should be allowed for sample repeats.

6.2.3 Advantages and disadvantages of using cell lines and patient samples

Cell lines were used in this study as they are a renewable resource and can be used as a model system for experiments. Metaphase spreads can be prepared from cell lines and so can be studied more easily by FISH than the primary tumours. The main disadvantages are cross contamination and artefact genetic changes. Cell lines are clonal, however in a genetically unstable cell there is evolution in the karyotype and the new genetic changes will not represent the original tumour. The primary tumour samples avoid the artefact of multiple passages and the accumulation of the subsequent cell line artefact genetic changes. The disadvantage of primary tumour samples is that they are infiltrated with normal cells, either from normal brain cells or white cells, which enter the area as part of an inflammatory response. Also there are different populations of tumour cells in the patient samples. These cells may be of different grades of tumour and even if

the same grade there may be sub-populations with different genetic aberrations. Cell lines have the advantage of having no contaminating normal cells and are clonal, although the genetic profile differs from cell to cell. Therefore, a homozygous deletion will remain a homozygous deletion, and there is no dilution. With the advent of laser capture microdissection it is now possible to select as little as one cell for analysis (Bonner *et al.*, 1997). Hence, the cell lines and tumour samples are different model systems each with their own advantages.

A further disadvantage in using cell lines is the problem of cross contamination. This problem was addressed in the research community when certain cell lines were shown by DNA fingerprinting to be cross-contaminated with HeLa cells. It was suggested that new cell lines should have a source sample kept for later verification and there should be more accurate and complete documentation (Drexler and Matsuo, 1999; MacLeod *et al.*, 2002; Stacey, 2000). Cross contamination in astrocytic glioma cell lines has occurred between Htb16 and U118. There has also been cross contamination between astrocytic glioma cell lines U251, SNB-19 and U373, which was detected in a study identifying mutations in *p53*, *CDKN2A*, *p14^{ARF}* and *PTEN* in 34 glioma cell lines. Cell lines were found to display different results when sourced from different laboratories (Ishii *et al.*, 1999).

It is clear the cell lines have many more copy number changes than the patient samples. It is assumed that this is due to changes that have arisen in cell culture of the lines. From this point of view, the copy number changes present in both the tumour

samples and the cell lines are considered the most relevant. Of the expected changes the tumour samples the tumour samples demonstrated amplification of *EGFR* and *PDGFR*, whereas the \log_2 values of the clone representing *EGFR* tended to suggest gain rather than amplification in the cell lines. Mutations in *EGFR* have not been found in non-amplified DNA (Ekstrand *et al.*, 1992; Frederick *et al.*, 2000). However, it may be that there may be activating mutations of *EGFR* in the cell lines that were associated with amplification of *EGFR*, however the amplification of *EGFR* has been lost with repeated passages. Conversely, the homozygous deletion of *CDKN2A* is detected with greater deviation of \log_2 value by the cell lines. This may be because the cell lines are clonal and not contaminated by normal tissue. In detecting changes at *PTEN* and *p53* again the cell lines proved to be more powerful. In the case of *PTEN*, the deletion was defined to 1 Mb in cell line CRL1620 as opposed to the minimum region of deletion of 4 Mb in T9, in the tumour samples. The tumour samples did not demonstrate copy number change involving *p53* (17p13), however three cell lines showed loss, involving *p53*. The minimal region of deletion was defined to 1 Mb in cell line Htb138. The cell lines were important for the molecular cytogenetic studies as metaphase spreads could be obtained. Interphase cytogenetic studies could be performed on the tumour samples, however the results would be more difficult to interpret and many more nuclei are needed for examination. By using the cell lines and patient samples, the advantages of each can be selected and the disadvantages recognised and given due consideration in reaching conclusions

6.3 Significance of thesis

Various questions are raised when considering the significance of regions of copy number change in high-grade astrocytic gliomas. The thesis focused on one aspect of the copy number change, the relationship to translocations. This forms only part of a wider view of what a region of copy number change may signify. Does a region of copy number change indicate the presence of an underlying mutation? Is the copy number change itself contributing to the tumour? Is it possible that the change contributed to the tumour at one time but is now redundant? How can the patterns of change seen be related to mechanisms of genetic change? And why are there so many and varied genetic changes in these tumours?

6.3.1 Copy number change and underlying mutation

The identification of a tumour suppressor gene or oncogene within a region of change is supportive evidence that the particular genetic change is pertinent to the tumour. However, the identification of a tumour suppressor gene or oncogene is in itself a process which builds upon numerous and independent lines of evidence. For example, in a region of deletion, all the genes in that particular region can be considered candidate tumour suppressor genes. Further evidence as to which is a tumour suppressor gene is if there is functional loss of the gene. Functional studies, such as replacing the lost gene product in a tumour and monitoring its effect on tumour growth build on the evidence that a particular gene is a tumour suppressor gene. Through independent studies, a gene will gain a body of evidence as to whether it is a tumour suppressor gene, as each stage and method has its own merit and inherent problems of interpretation.

For the model of tumour suppressor genes proposed by Knudson, the presence of a region of deletion may indicate the presence of a mutation in the remaining allele. Subsequent studies have supported this model and have added complexity, in that along with a mutation in the remaining allele, loss of function of the remaining allele can occur through alternative mechanisms such as homozygous deletion and gene silencing. One effect is that it can alter gene expression (Fodde and Smits, 2002)

An amplification of a region of DNA containing an oncogene is a straightforward example of how identifying a genetic change can help in the search for genes involved in cancer development. To identify a single base-pair change in the 3000,000,000 base pairs of code, in the human genome is a mammoth task. At present it is not feasible to sequence the whole genome of each individual and compare it to the whole sequence within their tumour, so we need to identify hot spots. Our current understanding leads us toward coding sequences. The presence of a genetic change does not mean that it will be causal to the formation of the tumour. Indeed the genetic change may have contributed to the development of the tumour and now be present and no longer required, so it is conceivable that returning its function to normal at this stage will not be useful.

Undoubtedly astrocytic glioma genetics are complex, and amongst the genetic changes that are present some will be not be relevant to the tumour or may not be relevant at that time or in the cellular environment. Of the relevant changes three points should be considered. Firstly that multiple genetic changes are required for each tumour,

Secondly at a genetic level, a gene can have loss of function through a number of mechanisms including homozygous deletion, loss of heterozygosity and mutation. Gain of function can be through mutation, deletion of regulatory regions, and translocation of regulatory regions. Finally locus heterogeneity describes the situation where the same disease can be caused by defects in different genes. This can be understood at a molecular level as different genes co-operating or acting in the same cellular pathway, where a defect in any one of the genes leads to the same end-point.

6.3.2 Temporal relationship between development of copy number change and underlying mutation

Certain copy number changes are associated with underlying gene mutations. Loss of the short arm of chromosome 17 is associated with *p53* mutation in the remaining allele, as is deletion of chromosome 10 and *PTEN* mutation. A deletion of a chromosome will not be detected by copy number studies if there is duplication of the remaining allele, however this will be detected by LOH studies. One question that remains unanswered is what comes first, the mutation or the change in copy number?

In this thesis the relationship between copy number change, LOH and *p53* mutation is examined (Table 4.8). In eight cell lines, there are mutations of *p53* and one of these cell lines, U118, is not associated with copy number change or LOH at 17p13. Of the two samples with wild-type *p53*, neither demonstrated a deletion at 17p13. Further to this, when examining CRL2365 and CRL2366, which are both derived from the same tumour, it can be seen that CRL2366 has no copy number loss but CRL2365 has a

deletion involving 17p13. Both cell lines had the same *p53* mutations. It is interesting that none of the tumour samples show a copy number loss at 17p13. Three of the cell lines show a loss at this region. This raises the possibility that cell lines lose material in regions of LOH following culture. On examining the relationship between *PTEN* mutation and deletion (Table 4.7), two samples with wild-type *PTEN* were found to have a deletion involving 10q11.

These examples in this study provide conflicting results on which comes first, the mutation or chromosome deletion. Explanations for these results include that both processes are going on in parallel, in that there is not a linear relationship between mutation and copy number change/LOH. The other explanation is that different mechanisms are operating for different genes. Further larger studies are required to gain a clearer picture.

6.3.3 Patterns of genetic change

The arrays demonstrate interstitial copy number changes; these may be discrete regions of gain or loss. The example of chromosome 6 in cell line CRL2020 is interesting because the array CGH suggested deletion of the whole chromosome. However, in addition to this there was a more marked loss seen at 6q26. Molecular cytogenetic studies showed loss of a whole chromosome 6 in this tetraploid cell line and that there was also a deletion at 6q26 of one of the chromosomes.

Interstitial deletions may be better tolerated than, for instance, losing the whole chromosome arm, as along with the tumour suppressor gene there may be other genes necessary for the survival of the tumour. Hence, following the double strand break and loss of the region containing the tumour suppressor gene, the remaining fragment containing essential genes can be either rejoined causing an interstitial deletion or may be joined to another region of DNA, which has either been broken or joined to the end of a chromosome with telomere attrition. If this shuffling of the genome gives the cell a growth advantage then this cell will survive and divide, i.e. it is selected.

In considering mechanisms of genetic change, some insights can be gained from the patterns of change and the sites of change. Interesting regions are 7p12 (*EGFR*) and 9p21 (*CDKN2A*). Amplification of *EGFR* tends to be found only with gain of chromosome 7 (Figure 4.14 and Table 4.5). However, the \log_2 values of the gain and amplification in the region suggest that there are populations of differently sized amplicons containing *EGFR*. If these amplicons were generated by BFB cycles then it would suggest that there were not defined breakpoints in this cycle, or if there were defined breakpoints there has been attrition of the borders of the amplicons. The amplification of *EGFR* was seen in the patient samples but not in the cell lines. This suggests that the cell lines may lose the amplicons containing *EGFR*, which tend to be found as double minutes. Cell line CRL1620 maintained amplification of *EGFR* through stable integration of amplicons containing *EGFR* into chromosomes (Figure 5.9 b). The story of *EGFR* as an oncogene is further complicated by the presence of mutations in *EGFR* (Discussed later).

In this study, the most striking region of gain or amplification was seen on the short arm of chromosome 7. The highest log₂ ratios were for the clone RP5-1091E12, which represents *EGFR* (Table 4.4), it can be seen that the tumour samples showed much higher values than the cell lines. It is known that *EGFR* is amplified in astrocytic gliomas, but here it is shown that not just the clone representing *EGFR* is amplified but also the surrounding clones. From Table 4.5 it could be suggested that three clones, RP11-449G3, RP5-1091E12 and RP11-339F13, are co-amplified. The flanking clones are RP11-324M21 and RP4-725G10. Apart from *EGFR*, the genes encompassed by these flanking clones include Sec61 Gamma Subunit (*SC61G*), LanC Antibiotic Synthetase Component C-Like 2 (*LANCL2*), Mitochondrial Ribosomal Protein S17 (*MRPS17*), Glioblastoma Amplified Sequence (*GBAS*), Sulfatase-Modifying Factor 2 (*SUMF2*), Chaperonin Containing T-Complex Polypeptide 1 Subunit 6A (*CCT6A*), Phosphorylase Kinase Muscle Gamma-1 (*PHKG1*), Coiled-coil-Helix-Coiled-coil-Helix Domain Containing 2 (*CHCHD2*) and some novel proteins. The co-amplification of one or more of these genes may be necessary for tumour development.

Amplification of the clone representing *EGFR* is seen in the patient samples but not in the cell lines, although the entire chromosome 7 is gained in four cell lines and the short arm of chromosome 7 is gained in a further three cell lines. It is possible that there is amplification DNA, containing *EGFR* and as the cell line undergoes more passages it losses this additional material. Different patterns of amplification are seen (Section 1.2.5). Inverted tandem repeats of the gene, the proposed mechanism for this being the

BFB cycle. The second is that multiple copies of the gene can be inserted into the genome at alternative sites, not the normal gene locus. The third is that sections of DNA can be amplified as double minutes, which do not have a centromere. Hence, at cell division there is unequal division of the double minutes and perhaps following selection there is loss of the amplified gene.

Homozygous deletion at 9p21 was found in the presence of loss of the short arm of chromosome 9. The patterns of loss are variable. For instance, in cell line CRL2610 there appears to be a distinct change in \log_2 values demarcating the homozygous deletion, but in U87 the change is more gradual. Again this is a reflection of sub-populations of cells with varying deletions.

The pattern of interstitial loss is interesting as current understanding of these regions is that there is likely to be a tumour suppressor gene in this region. In this study the smaller the deletion, the more likely the gene of interest will be identified. Hence, from this perspective the most interesting changes will be single copy deletions with a \log_2 value suggestive of a homozygous deletion. This is corroborated by the examples of *PTEN* in cell line CRL2610 and the *FIG-ROS* deletion in cell line U118. However, it may be the region that is retained that is equally as interesting. For example, in the translocations associated with deletion at 6q26, it may be that there are important genes for survival of the cell of the material distal to the deletion.

6.3.4 Fragile sites

This study demonstrated regions of deletion at fragile sites including 6q26, 1p36, 9p22 and 16q23. Fragile sites are chromosomal regions that are prone to breaks when cells are grown in medium that inhibits DNA replication. There are 89 common fragile sites and these are present in the majority of the population. Chromosome breaks at common fragile sites can be induced by aphidicolin, 5-azacytidine or bromodeoxyuridine (BrdU). There are 28 rare fragile sites. These occur in less than 5% of the population and display Mendelian inheritance. Chromosome breaks at rare fragile sites can be induced by low folate and/or thymidine, or distamycin A or BrdU (Smith *et al.*, 1998).

Four regions of deletion associated with fragile sites were demonstrated in this study. These regions contain several candidate tumour suppressor genes (Table 6.1). This study has demonstrated translocations associated with 6q26 deletions. On examining the array CGH and M-FISH data on the cell lines, it is possible that translocations are also associated with deletions at 1p36 (cell line CRL2365) and 9p22 (cell line U87). This raises the question, are translocations at fragile sites part of the mechanism of deletion of certain tumour suppressor genes?

Genomic location	Fragile site	Candidate tumour suppressor genes
1p36	FRA1A	<i>p73</i>
6q26	FRA6E	<i>IGF2R, QKI, PARK2, PACRG</i>
9p22	FRA9A	<i>CDKN2A, CDKN2B</i>
16q23	FRA16D	<i>WWOX</i>

Table 6.1 Genomic regions associated with fragile sites in high-grade astrocytic gliomas. Candidate tumour suppressor genes from the regions are also suggested.

6.4 Clinical perspective of this thesis

The potential diagnostic application of array CGH has been demonstrated in renal cancer using an array with 235 clones (Wilhelm *et al.*, 2002). 33 out of 34 renal carcinomas were correctly identified through characterised genetic changes and 8 samples were correctly identified as being either normal or benign tumour (Wilhelm *et al.*, 2002). If a clinical decision is to be made using information based on array technology there has to be uniformity in analysing results. The analytical methods described in Chapter 3 of this thesis would contribute to this process. Expression arrays have been used in the classification of different histological subtypes of brain tumours and been able to predict prognosis in children with medulloblastoma (Pomeroy *et al.*, 2002). In the clinical setting, DNA is more convenient than RNA based-methods as DNA is more stable, and is more practical as formalin-fixed tissue can be used.

In breast cancer management molecular markers for predicting treatment response are already included in Pathology reports. Oestrogen receptor, progesterone receptor and c-erb B2 status are reported. Oestrogen receptor positive patients can be given endocrine-based therapies such as Tamoxifen. Trastuzumab is an antibody against the c-erb B2 receptor. The Pathology report of the next decade will include an increasing amount of pertinent genetic data. The development of biological markers for astrocytic gliomas needs to develop in parallel with targeted therapies.

This study suggested candidate tumour suppressor genes and oncogenes in a number of key cellular pathways, such as p53, Rb, and the receptor tyrosine kinases,

EGFR, PDGFR. One approach of controlling cancer that is under development is that of designing therapeutic agents to specifically target and reverse the effect of key molecular aberrations. There are many molecularly targeted agents in development and in clinical trials (<http://www.cancer.gov/trials>). These molecularly targeted agents need to be introduced into clinical use in parallel with better genetic characterisation of tumours.

There have been some successes in the treatment of cancer with molecularly targeted agents. One example is the use of small molecule inhibitors of receptor tyrosine kinases. In astrocytic gliomas, the receptor tyrosine kinase, *EGFR* is an attractive target for therapy as it is commonly has a gain of function in these tumours through, copy number changes or mutation. Gefitinib (4 - (3-chloro-4-fluoroanilino) - 7 - methoxy - 6 - (3-morpholinopropoxy) quinazoline) (also known as ZD1839 and Iressa) is a small molecule inhibitor of EGFR that has had demonstrable effect in non-small cell carcinoma of the lung (adenocarcinoma) (Fujiwara *et al.*, 2003).

Unfortunately, the success with Gefitinib was not repeated in high-grade astrocytic glioma patients (Rich *et al.*, 2004). One explanation for this could simply be that Gefitinib does not cross the blood-tumour barrier. However, a more complex explanation may be emerging from studies on the coding sequence of *EGFR*. Oncogenic activation of EGFR can occur by a number of different mechanisms, including DNA amplification and activating mutations. These two mechanisms are interrelated, as evidence suggest that rearrangements occur following amplification. Two independent studies demonstrated the relationship between response to Gefitinib in non-small cell

lung cancer and mutations in the EGFR of the patient's tumour (Lynch *et al.*, 2004; Paez *et al.*, 2004). The presence of EGFR mutations may be a predictive marker for response to Gefitinib therapy in adenocarcinoma of the lung. Hence, along with copy number studies to determine response to therapies, other methods of analysis can be combined including sequence analysis

6.5 Conclusions

This thesis has contributed to the understanding of the application of a new technology, array CGH, and has used this technique to catalogue copy number changes in high-grade astrocytic glioma cell lines and patient samples. This thesis will therefore also contribute to neuro-oncology research, in the identification of tumour suppressor genes and oncogenes. In addition, the relationship between copy number changes and positional changes was examined and translocations associated with deletions were detected. Therefore, this thesis has also raised interesting questions about mechanisms of genetic changes in cancer.

Array CGH examines a single modality of cell structure and function, copy number changes. There other changes which may be inter-related and inter-dependent such as changes in RNA and protein. The value of the copy number data will be greatly strengthened by combining the data with other genome-wide assessments of cellular physiology such as parental origin of DNA strands, DNA sequence data, RNA expression and functional protein (tissue arrays). This thesis has described the beginning of what can now become a larger study as described in the original aim (Figure 1.8).

References

- Abdel-Rahman, W.M., Katsura, K., Rens, W., Gorman, P.A., Sheer, D., Bicknell, D., Bodmer, W.F., Arends, M.J., Wyllie, A.H. and Edwards, P.A. (2001) Spectral karyotyping suggests additional subsets of colorectal cancers characterized by pattern of chromosome rearrangement. *Proc Natl Acad Sci U S A*, **98**, 2538-2543.
- Adelaide, J., Huang, H.E., Murati, A., Alsop, A.E., Orsetti, B., Mozziconacci, M.J., Popovici, C., Ginestier, C., Letessier, A., Basset, C., *et al.* (2003) A recurrent chromosome translocation breakpoint in breast and pancreatic cancer cell lines targets the neuregulin/NRG1 gene. *Genes Chromosomes Cancer*, **37**, 333-345.
- Alam, N.A., Rowan, A.J., Wortham, N.C., Pollard, P.J., Mitchell, M., Tyrer, J.P., Barclay, E., Calonje, E., Manek, S., Adams, S.J., *et al.* (2003) Genetic and functional analyses of FH mutations in multiple cutaneous and uterine leiomyomatosis, hereditary leiomyomatosis and renal cancer, and fumarate hydratase deficiency. *Hum Mol Genet*, **12**, 1241-1252.
- Alberts, B., Johnson, A.L., Lewis, J., Raff, M., Roberts, K. and Walter, P. (2002) *Molecular Biology of the Cell*.
- Amler, L.C. and Schwab, M. (1992) Multiple amplicons of discrete sizes encompassing N-myc in neuroblastoma cells evolve through differential recombination from a large precursor DNA. *Oncogene*, **7**, 807-809.
- Amler, L.C., Shibasaki, Y., Savelyeva, L. and Schwab, M. (1992) Amplification of the N-myc gene in human neuroblastomas: tandemly repeated amplicons within homogeneously staining regions on different chromosomes with the retention of single copy gene at the resident site. *Mutat Res*, **276**, 291-297.
- Ashley, D.J. (1969) The two "hit" and multiple "hit" theories of carcinogenesis. *Br J Cancer*, **23**, 313-328.
- Backlund, L.M., Nilsson, B.R., Goike, H.M., Schmidt, E.E., Liu, L., Ichimura, K. and Collins, V.P. (2003) Short postoperative survival for glioblastoma patients with a dysfunctional Rb1 pathway in combination with no wild-type PTEN. *Clin Cancer Res*, **9**, 4151-4158.

- Baker, S.J., Fearon, E.R., Nigro, J.M., Hamilton, S.R., Preisinger, A.C., Jessup, J.M., vanTuinen, P., Ledbetter, D.H., Barker, D.F., Nakamura, Y., *et al.* (1989) Chromosome 17 deletions and p53 gene mutations in colorectal carcinomas. *Science*, **244**, 217-221.
- Balesaria, S., Brock, C., Bower, M., Clark, J., Nicholson, S.K., Lewis, P., de Sanctis, S., Evans, H., Peterson, D., Mendoza, N., *et al.* (1999) Loss of chromosome 10 is an independent prognostic factor in high-grade gliomas. *Br J Cancer*, **81**, 1371-1377.
- Barlund, M., Monni, O., Weaver, J.D., Kauraniemi, P., Sauter, G., Heiskanen, M., Kallioniemi, O.P. and Kallioniemi, A. (2002) Cloning of BCAS3 (17q23) and BCAS4 (20q13) genes that undergo amplification, overexpression, and fusion in breast cancer. *Genes Chromosomes Cancer*, **35**, 311-317.
- Biernat, W., Aguzzi, A., Sure, U., Grant, J.W., Kleihues, P. and Hegi, M.E. (1995) Identical mutations of the p53 tumor suppressor gene in the gliomatous and the sarcomatous components of gliosarcomas suggest a common origin from glial cells. *J Neuropathol Exp Neurol*, **54**, 651-656.
- Bigner, S.H., McLendon, R.E., Fuchs, H., McKeever, P.E. and Friedman, H.S. (1997) Chromosomal characteristics of childhood brain tumors. *Cancer Genet Cytogenet*, **97**, 125-134.
- Bigner, S.H., Wong, A.J., Mark, J., Muhlbaier, L.H., Kinzler, K.W., Vogelstein, B. and Bigner, D.D. (1987) Relationship between gene amplification and chromosomal deviations in malignant human gliomas. *Cancer Genet Cytogenet*, **29**, 165-170.
- Bleehen, N.M. and Stenning, S.P. (1991) A Medical Research Council trial of two radiotherapy doses in the treatment of grades 3 and 4 astrocytoma. The Medical Research Council Brain Tumour Working Party. *Br J Cancer*, **64**, 769-774.
- Bogler, O., Huang, H.J. and Cavenee, W.K. (1995a) Loss of wild-type p53 bestows a growth advantage on primary cortical astrocytes and facilitates their in vitro transformation. *Cancer Res*, **55**, 2746-2751.
- Bogler, O., Huang, H.J., Kleihues, P. and Cavenee, W.K. (1995b) The p53 gene and its role in human brain tumors. *Glia*, **15**, 308-327.

- Bonner, R.F., Emmert-Buck, M., Cole, K., Pohida, T., Chuaqui, R., Goldstein, S. and Liotta, L.A. (1997) Laser capture microdissection: molecular analysis of tissue. *Science*, **278**, 1481,1483.
- Botstein, D., White, R.L., Skolnick, M. and Davis, R.W. (1980) Construction of a genetic linkage map in man using restriction fragment length polymorphisms. *Am J Hum Genet*, **32**, 314-331.
- Bourne, H.R., Sanders, D.A. and McCormick, F. (1990) The GTPase superfamily: a conserved switch for diverse cell functions. *Nature*, **348**, 125-132.
- Broughton, B.C., Cordonnier, A., Kleijer, W.J., Jaspers, N.G., Fawcett, H., Raams, A., Garritsen, V.H., Stary, A., Avril, M.F., Boudsocq, F., *et al.* (2002) Molecular analysis of mutations in DNA polymerase eta in xeroderma pigmentosum-variant patients. *Proc Natl Acad Sci U S A*, **99**, 815-820.
- Brunner, C., Jung, V., Henn, W., Zang, K.D. and Urbschat, S. (2000) Comparative genomic hybridization reveals recurrent enhancements on chromosome 20 and in one case combined amplification sites on 15q24q26 and 20p11p12 in glioblastomas. *Cancer Genet Cytogenet*, **121**, 124-127.
- Burton, E.C., Lamborn, K.R., Feuerstein, B.G., Prados, M., Scott, J., Forsyth, P., Passe, S., Jenkins, R.B. and Aldape, K.D. (2002) Genetic aberrations defined by comparative genomic hybridization distinguish long-term from typical survivors of glioblastoma. *Cancer Res*, **62**, 6205-6210.
- Cai, W.W., Mao, J.H., Chow, C.W., Damani, S., Balmain, A. and Bradley, A. (2002) Genome-wide detection of chromosomal imbalances in tumors using BAC microarrays. *Nat Biotechnol*, **20**, 393-396.
- Canoll, P.D., Petanceska, S., Schlessinger, J. and Musacchio, J.M. (1996) Three forms of RPTP-beta are differentially expressed during gliogenesis in the developing rat brain and during glial cell differentiation in culture. *J Neurosci Res*, **44**, 199-215.
- canRanjan, M. and Hudson, L.D. (1996) Regulation of tyrosine phosphorylation and protein tyrosine phosphatases during oligodendrocyte differentiation. *Mol Cell Neurosci*, **7**, 404-418.
- Carmeliet, P. and Jain, R.K. (2000) Angiogenesis in cancer and other diseases. *Nature*, **407**, 249-257.

- Cesari, R., Martin, E.S., Calin, G.A., Pentimalli, F., Bichi, R., McAdams, H., Trapasso, F., Drusco, A., Shimizu, M., Masciullo, V., *et al.* (2003) Parkin, a gene implicated in autosomal recessive juvenile parkinsonism, is a candidate tumor suppressor gene on chromosome 6q25-q27. *Proc Natl Acad Sci U S A*, **100**, 5956-5961.
- Charest, A., Kheifets, V., Park, J., Lane, K., McMahon, K., Nutt, C.L. and Housman, D. (2003a) Oncogenic targeting of an activated tyrosine kinase to the Golgi apparatus in a glioblastoma. *Proc Natl Acad Sci U S A*, **100**, 916-921.
- Charest, A., Lane, K., McMahon, K., Park, J., Preisinger, E., Conroy, H. and Housman, D. (2003b) Fusion of FIG to the receptor tyrosine kinase ROS in a glioblastoma with an interstitial del(6)(q21q21). *Genes Chromosomes Cancer*, **37**, 58-71.
- Chene, P. (2001) Targeting p53 in cancer. *Curr Med Chem Anti-Canc Agents*, **1**, 151-161.
- Chene, P. (2003) Inhibiting the p53-MDM2 interaction: an important target for cancer therapy. *Nat Rev Cancer*, **3**, 102-109.
- Chene, P. (2004) Inhibition of the p53-MDM2 Interaction: Targeting a Protein-Protein Interface. *Mol Cancer Res*, **2**, 20-28.
- Chernova, O.B., Hunyadi, A., Malaj, E., Pan, H., Crooks, C., Roe, B. and Cowell, J.K. (2001) A novel member of the WD-repeat gene family, WDR11, maps to the 10q26 region and is disrupted by a chromosome translocation in human glioblastoma cells. *Oncogene*, **20**, 5378-5392.
- Chernova, O.B., Somerville, R.P. and Cowell, J.K. (1998) A novel gene, LGI1, from 10q24 is rearranged and downregulated in malignant brain tumors. *Oncogene*, **17**, 2873-2881.
- Clark, J., Edwards, S., Feber, A., Flohr, P., John, M., Giddings, I., Crossland, S., Stratton, M.R., Wooster, R., Campbell, C., *et al.* (2003) Genome-wide screening for complete genetic loss in prostate cancer by comparative hybridization onto cDNA microarrays. *Oncogene*, **22**, 1247-1252.
- Clark, J., Edwards, S., John, M., Flohr, P., Gordon, T., Maillard, K., Giddings, I., Brown, C., Bagherzadeh, A., Campbell, C., *et al.* (2002) Identification of amplified and expressed genes in breast cancer by comparative hybridization onto microarrays of randomly selected cDNA clones. *Genes Chromosomes Cancer*, **34**, 104-114.

- Collins, V.P. (1999) Progression as exemplified by human astrocytic tumors. *Semin Cancer Biol*, **9**, 267-276.
- Collins, V.P. (2002) Cellular mechanisms targeted during astrocytoma progression. *Cancer Lett*, **188**, 1-7.
- Cox, C., Bignell, G., Greenman, C., Stabenau, A., Warren, W., Stephens, P., Davies, H., Watt, S., Teague, J., Edkins, S., *et al.* (2005) A survey of homozygous deletions in human cancer genomes. *Proc Natl Acad Sci U S A*, **102**, 4542-4547.
- Cox, R.D., Shedlovsky, A., Hamvas, R., Goldsworthy, M., Whittington, J., Connelly, C.S., Dove, W.F. and Lehrach, H. (1994) A 1.2-Mb YAC contig spans the quaking region. *Genomics*, **21**, 77-84.
- Dang, T.P., Gazdar, A.F., Virmani, A.K., Sepetavec, T., Hande, K.R., Minna, J.D., Roberts, J.R. and Carbone, D.P. (2000) Chromosome 19 translocation, overexpression of Notch3, and human lung cancer. *J Natl Cancer Inst*, **92**, 1355-1357.
- De Souza, A.T., Hankins, G.R., Washington, M.K., Orton, T.C. and Jirtle, R.L. (1995) M6P/IGF2R gene is mutated in human hepatocellular carcinomas with loss of heterozygosity. *Nat Genet*, **11**, 447-449.
- Deloukas, P., Earthrowl, M.E., Grafham, D.V., Rubenfield, M., French, L., Steward, C.A., Sims, S.K., Jones, M.C., Searle, S., Scott, C., *et al.* (2004) The DNA sequence and comparative analysis of human chromosome 10. *Nature*, **429**, 375-381.
- Deloukas, P., Matthews, L.H., Ashurst, J., Burton, J., Gilbert, J.G., Jones, M., Stavrides, G., Almeida, J.P., Babbage, A.K., Bagguley, C.L., *et al.* (2001) The DNA sequence and comparative analysis of human chromosome 20. *Nature*, **414**, 865-871.
- Denison, S.R., Wang, F., Becker, N.A., Schule, B., Kock, N., Phillips, L.A., Klein, C. and Smith, D.I. (2003) Alterations in the common fragile site gene Parkin in ovarian and other cancers. *Oncogene*, **22**, 8370-8378.
- Douglas, E.J., Fiegler, H., Rowan, A., Halford, S., Bicknell, D.C., Bodmer, W., Tomlinson, I.P. and Carter, N.P. (2004) Array comparative genomic hybridization

- analysis of colorectal cancer cell lines and primary carcinomas. *Cancer Res*, **64**, 4817-4825.
- Drexler, H.G. and Matsuo, Y. (1999) Guidelines for the characterization and publication of human malignant hematopoietic cell lines. *Leukemia*, **13**, 835-842.
- Dunham, A., Matthews, L.H., Burton, J., Ashurst, J.L., Howe, K.L., Ashcroft, K.J., Beare, D.M., Burford, D.C., Hunt, S.E., Griffiths-Jones, S., *et al.* (2004) The DNA sequence and analysis of human chromosome 13. *Nature*, **428**, 522-528.
- Dunham, I., Shimizu, N., Roe, B.A., Chisoe, S., Hunt, A.R., Collins, J.E., Bruskiewich, R., Beare, D.M., Clamp, M., Smink, L.J., *et al.* (1999) The DNA sequence of human chromosome 22. *Nature*, **402**, 489-495.
- Ebersole, T., Rho, O. and Artzt, K. (1992) The proximal end of mouse chromosome 17: new molecular markers identify a deletion associated with quakingviable. *Genetics*, **131**, 183-190.
- Ekstrand, A.J., Longo, N., Hamid, M.L., Olson, J.J., Liu, L., Collins, V.P. and James, C.D. (1994) Functional characterization of an EGF receptor with a truncated extracellular domain expressed in glioblastomas with EGFR gene amplification. *Oncogene*, **9**, 2313-2320.
- Ekstrand, A.J., Sugawa, N., James, C.D. and Collins, V.P. (1992) Amplified and rearranged epidermal growth factor receptor genes in human glioblastomas reveal deletions of sequences encoding portions of the N- and/or C-terminal tails. *Proc Natl Acad Sci U S A*, **89**, 4309-4313.
- Esteller, M., Garcia-Foncillas, J., Andion, E., Goodman, S.N., Hidalgo, O.F., Vanaclocha, V., Baylin, S.B. and Herman, J.G. (2000) Inactivation of the DNA-repair gene MGMT and the clinical response of gliomas to alkylating agents. *N Engl J Med*, **343**, 1350-1354.
- Fan, X., Aalto, Y., Sanko, S.G., Knuutila, S., Klatzmann, D. and Castresana, J.S. (2002) Genetic profile, PTEN mutation and therapeutic role of PTEN in glioblastomas. *Int J Oncol*, **21**, 1141-1150.
- Fearon, E.R., Cho, K.R., Nigro, J.M., Kern, S.E., Simons, J.W., Ruppert, J.M., Hamilton, S.R., Preisinger, A.C., Thomas, G., Kinzler, K.W., *et al.* (1990) Identification of a chromosome 18q gene that is altered in colorectal cancers. *Science*, **247**, 49-56.

- Fearon, E.R. and Vogelstein, B. (1990) A genetic model for colorectal tumorigenesis. *Cell*, **61**, 759-767.
- Ferrara, N. (2002) VEGF and the quest for tumour angiogenesis factors. *Nat Rev Cancer*, **2**, 795-803.
- Fiegler, H., Carr, P., Douglas, E.J., Burford, D.C., Hunt, S., Smith, J., Vetrie, D., Gorman, P., Tomlinson, I.P. and Carter, N.P. (2003) DNA microarrays for comparative genomic hybridization based on DOP-PCR amplification of BAC and PAC clones. *Genes Chromosomes Cancer*, **36**, 361-374.
- Fodde, R. and Smits, R. (2002) Cancer biology. A matter of dosage. *Science*, **298**, 761-763.
- Frederick, L., Wang, X.Y., Eley, G. and James, C.D. (2000) Diversity and frequency of epidermal growth factor receptor mutations in human glioblastomas. *Cancer Res*, **60**, 1383-1387.
- Friend, S.H., Bernards, R., Rogelj, S., Weinberg, R.A., Rapaport, J.M., Albert, D.M. and Dryja, T.P. (1986) A human DNA segment with properties of the gene that predisposes to retinoblastoma and osteosarcoma. *Nature*, **323**, 643-646.
- Fujiwara, K., Kiura, K., Ueoka, H., Tabata, M., Hamasaki, S. and Tanimoto, M. (2003) Dramatic effect of ZD1839 ('Iressa') in a patient with advanced non-small-cell lung cancer and poor performance status. *Lung Cancer*, **40**, 73-76.
- Fults, D., Pedone, C.A., Thomas, G.A. and White, R. (1990) Allelotype of human malignant astrocytoma. *Cancer Res*, **50**, 5784-5789.
- Giasson, B.I. and Lee, V.M. (2001) Parkin and the molecular pathways of Parkinson's disease. *Neuron*, **31**, 885-888.
- Gorre, M.E., Mohammed, M., Ellwood, K., Hsu, N., Paquette, R., Rao, P.N. and Sawyers, C.L. (2001) Clinical resistance to STI-571 cancer therapy caused by BCR-ABL gene mutation or amplification. *Science*, **293**, 876-880.
- Grimwood, J., Gordon, L.A., Olsen, A., Terry, A., Schmutz, J., Lamerdin, J., Hellsten, U., Goodstein, D., Couronne, O., Tran-Gyamfi, M., *et al.* (2004) The DNA sequence and biology of human chromosome 19. *Nature*, **428**, 529-535.
- Hahn, S.A., Schutte, M., Hoque, A.T., Moskaluk, C.A., da Costa, L.T., Rozenblum, E., Weinstein, C.L., Fischer, A., Yeo, C.J., Hruban, R.H., *et al.* (1996) DPC4, a

- candidate tumor suppressor gene at human chromosome 18q21.1. *Science*, **271**, 350-353.
- Hall, J.M., Lee, M.K., Newman, B., Morrow, J.E., Anderson, L.A., Huey, B. and King, M.C. (1990) Linkage of early-onset familial breast cancer to chromosome 17q21. *Science*, **250**, 1684-1689.
- Hamilton, S.R., Liu, B., Parsons, R.E., Papadopoulos, N., Jen, J., Powell, S.M., Krush, A.J., Berk, T., Cohen, Z., Tetu, B., *et al.* (1995) The molecular basis of Turcot's syndrome. *N Engl J Med*, **332**, 839-847.
- Hanahan, D. and Weinberg, R.A. (2000) The hallmarks of cancer. *Cell*, **100**, 57-70.
- Hanks, S., Coleman, K., Reid, S., Plaja, A., Firth, H., Fitzpatrick, D., Kidd, A., Mehes, K., Nash, R., Robin, N., *et al.* (2004) Constitutional aneuploidy and cancer predisposition caused by biallelic mutations in BUB1B. *Nat Genet*, **36**, 1159-1161.
- Harroch, S., Furtado, G.C., Brueck, W., Rosenbluth, J., Lafaille, J., Chao, M., Buxbaum, J.D. and Schlessinger, J. (2002) A critical role for the protein tyrosine phosphatase receptor type Z in functional recovery from demyelinating lesions. *Nat Genet*, **32**, 411-414.
- Hartmann, C., Numann, A., Mueller, W., Holtkamp, N., Simon, M. and von Deimling, A. (2004) Fine mapping of chromosome 22q tumor suppressor gene candidate regions in astrocytoma. *Int J Cancer*, **108**, 839-844.
- Hattori, M., Fujiyama, A., Taylor, T.D., Watanabe, H., Yada, T., Park, H.S., Toyoda, A., Ishii, K., Totoki, Y., Choi, D.K., *et al.* (2000) The DNA sequence of human chromosome 21. *Nature*, **405**, 311-319.
- Hayflick, L. and Moorhead, P.S. (1961) The serial cultivation of human diploid cell strains. *Exp Cell Res*, **25**, 585-621.
- Hedrich, K., Eskelson, C., Wilmot, B., Marder, K., Harris, J., Garrels, J., Meija-Santana, H., Vieregge, P., Jacobs, H., Bressman, S.B., *et al.* (2004) Distribution, type, and origin of Parkin mutations: review and case studies. *Mov Disord*, **19**, 1146-1157.
- Heilig, R., Eckenberg, R., Petit, J.L., Fonknechten, N., Da Silva, C., Cattolico, L., Levy, M., Barbe, V., de Berardinis, V., Ureta-Vidal, A., *et al.* (2003) The DNA sequence and analysis of human chromosome 14. *Nature*, **421**, 601-607.

- Heinrich, M.C., Corless, C.L., Demetri, G.D., Blanke, C.D., von Mehren, M., Joensuu, H., McGreevey, L.S., Chen, C.J., Van den Abbeele, A.D., Druker, B.J., *et al.* (2003) Kinase mutations and imatinib response in patients with metastatic gastrointestinal stromal tumor. *J Clin Oncol*, **21**, 4342-4349.
- Hellman, A., Zlotorynski, E., Scherer, S.W., Cheung, J., Vincent, J.B., Smith, D.I., Trakhtenbrot, L. and Kerem, B. (2002) A role for common fragile site induction in amplification of human oncogenes. *Cancer Cell*, **1**, 89-97.
- Hermanson, M., Funa, K., Hartman, M., Claesson-Welsh, L., Heldin, C.H., Westermark, B. and Nister, M. (1992) Platelet-derived growth factor and its receptors in human glioma tissue: expression of messenger RNA and protein suggests the presence of autocrine and paracrine loops. *Cancer Res*, **52**, 3213-3219.
- Hillier, L.W., Fulton, R.S., Fulton, L.A., Graves, T.A., Pepin, K.H., Wagner-McPherson, C., Layman, D., Maas, J., Jaeger, S., Walker, R., *et al.* (2003) The DNA sequence of human chromosome 7. *Nature*, **424**, 157-164.
- Hoeijmakers, J.H. (2001) Genome maintenance mechanisms for preventing cancer. *Nature*, **411**, 366-374.
- Holder, N. and Klein, R. (1999) Eph receptors and ephrins: effectors of morphogenesis. *Development*, **126**, 2033-2044.
- Holmberg, J., Clarke, D.L. and Frisen, J. (2000) Regulation of repulsion versus adhesion by different splice forms of an Eph receptor. *Nature*, **408**, 203-206.
- Huang, J., Wei, W., Zhang, J., Liu, G., Bignell, G.R., Stratton, M.R., Futreal, P.A., Wooster, R., Jones, K.W. and Shaperro, M.H. (2004) Whole genome DNA copy number changes identified by high density oligonucleotide arrays. *Hum Genomics*, **1**, 287-299.
- Hui, A.B., Lo, K.W., Yin, X.L., Poon, W.S. and Ng, H.K. (2001) Detection of multiple gene amplifications in glioblastoma multiforme using array-based comparative genomic hybridization. *Lab Invest*, **81**, 717-723.
- Humphray, S.J., Oliver, K., Hunt, A.R., Plumb, R.W., Loveland, J.E., Howe, K.L., Andrews, T.D., Searle, S., Hunt, S.E., Scott, C.E., *et al.* (2004) DNA sequence and analysis of human chromosome 9. *Nature*, **429**, 369-374.

- Iafrate, A.J., Feuk, L., Rivera, M.N., Listewnik, M.L., Donahoe, P.K., Qi, Y., Scherer, S.W. and Lee, C. (2004) Detection of large-scale variation in the human genome. *Nat Genet*, **36**, 949-951.
- Ichimura, K., Bolin, M.B., Goike, H.M., Schmidt, E.E., Moshref, A. and Collins, V.P. (2000) Deregulation of the p14ARF/MDM2/p53 pathway is a prerequisite for human astrocytic gliomas with G1-S transition control gene abnormalities. *Cancer Res*, **60**, 417-424.
- Ichimura, K., Schmidt, E.E., Goike, H.M. and Collins, V.P. (1996) Human glioblastomas with no alterations of the CDKN2A (p16INK4A, MTS1) and CDK4 genes have frequent mutations of the retinoblastoma gene. *Oncogene*, **13**, 1065-1072.
- Ichimura, K., Schmidt, E.E., Miyakawa, A., Goike, H.M. and Collins, V.P. (1998) Distinct patterns of deletion on 10p and 10q suggest involvement of multiple tumor suppressor genes in the development of astrocytic gliomas of different malignancy grades. *Genes Chromosomes Cancer*, **22**, 9-15.
- Imai, Y., Soda, M., Murakami, T., Shoji, M., Abe, K. and Takahashi, R. (2003) A product of the human gene adjacent to parkin is a component of Lewy bodies and suppresses Pael receptor-induced cell death. *J Biol Chem*, **278**, 51901-51910.
- Ishii, N., Maier, D., Merlo, A., Tada, M., Sawamura, Y., Diserens, A.C. and Van Meir, E.G. (1999) Frequent co-alterations of TP53, p16/CDKN2A, p14ARF, PTEN tumor suppressor genes in human glioma cell lines. *Brain Pathol*, **9**, 469-479.
- Ishkanian, A.S., Malloff, C.A., Watson, S.K., DeLeeuw, R.J., Chi, B., Coe, B.P., Snijders, A., Albertson, D.G., Pinkel, D., Marra, M.A., *et al.* (2004) A tiling resolution DNA microarray with complete coverage of the human genome. *Nat Genet*, **36**, 299-303.
- Jackson, S.P. (2002) Sensing and repairing DNA double-strand breaks. *Carcinogenesis*, **23**, 687-696.
- Jain, A.N., Tokuyasu, T.A., Snijders, A.M., Segreaves, R., Albertson, D.G. and Pinkel, D. (2002) Fully automatic quantification of microarray image data. *Genome Res*, **12**, 325-332.

- James, C.D., He, J., Carlbom, E., Mikkelsen, T., Ridderheim, P.A., Cavenee, W.K. and Collins, V.P. (1990) Loss of genetic information in central nervous system tumors common to children and young adults. *Genes Chromosomes Cancer*, **2**, 94-102.
- Jones, A.M., Douglas, E.J., Halford, S.E., Fiegler, H., Gorman, P.A., Roylance, R.R., Carter, N.P. and Tomlinson, I.P. (2005) Array-CGH analysis of microsatellite-stable, near-diploid bowel cancers and comparison with other types of colorectal carcinoma. *Oncogene*, **24**, 118-129.
- Justice, M.J. and Bode, V.C. (1988) Three ENU-induced alleles of the murine quaking locus are recessive embryonic lethal mutations. *Genet Res*, **51**, 95-102.
- Kallioniemi, A., Kallioniemi, O.P., Sudar, D., Rutovitz, D., Gray, J.W., Waldman, F. and Pinkel, D. (1992) Comparative genomic hybridization for molecular cytogenetic analysis of solid tumors. *Science*, **258**, 818-821.
- Kamb, A., Gruis, N.A., Weaver-Feldhaus, J., Liu, Q., Harshman, K., Tavitgian, S.V., Stockert, E., Day, R.S., 3rd, Johnson, B.E. and Skolnick, M.H. (1994) A cell cycle regulator potentially involved in genesis of many tumor types. *Science*, **264**, 436-440.
- Kan, Y.W. and Dozy, A.M. (1978) Polymorphism of DNA sequence adjacent to human beta-globin structural gene: relationship to sickle mutation. *Proc Natl Acad Sci U S A*, **75**, 5631-5635.
- Kinzler, K.W. and Vogelstein, B. (1997) Cancer-susceptibility genes. Gatekeepers and caretakers. *Nature*, **386**, 761, 763.
- Kirikoshi, H. and Katoh, M. (2002) Expression of WNT7A in human normal tissues and cancer, and regulation of WNT7A and WNT7B in human cancer. *Int J Oncol*, **21**, 895-900.
- Kleihues, P. and Cavenee, W.K. (2000) *Pathology and Genetics of Tumours of the Nervous System*. International Agency for Research on Cancer, World Health Organization, Lyon, France.
- Kleihues, P., Louis, D.N., Scheithauer, B.W., Rorke, L.B., Reifenberger, G., Burger, P.C. and Cavenee, W.K. (2002) The WHO classification of tumors of the nervous system. *J Neuropathol Exp Neurol*, **61**, 215-225; discussion 226-219.

- Kleihues, P. and Ohgaki, H. (1999) Primary and secondary glioblastomas: from concept to clinical diagnosis. *Neuro-oncol*, **1**, 44-51.
- Knobbe, C.B. and Reifenberger, G. (2003) Genetic alterations and aberrant expression of genes related to the phosphatidyl-inositol-3'-kinase/protein kinase B (Akt) signal transduction pathway in glioblastomas. *Brain Pathol*, **13**, 507-518.
- Knudson, A.G., Jr. (1971) Mutation and cancer: statistical study of retinoblastoma. *Proc Natl Acad Sci U S A*, **68**, 820-823.
- Kong, F.M., Anscher, M.S., Washington, M.K., Killian, J.K. and Jirtle, R.L. (2000) M6P/IGF2R is mutated in squamous cell carcinoma of the lung. *Oncogene*, **19**, 1572-1578.
- Kraus, J., Weber, R.G., Cremer, M., Seebacher, T., Fischer, C., Schurra, C., Jauch, A., Lichter, P., Bensimon, A. and Cremer, T. (1997) High-resolution comparative hybridization to combed DNA fibers. *Hum Genet*, **99**, 374-380.
- Krex, D., Hauses, M., Appelt, H., Mohr, B., Ehninger, G., Schackert, H.K. and Schackert, G. (2002) Physical and functional characterization of the human LGI1 gene and its possible role in glioma development. *Acta Neuropathol (Berl)*, **103**, 255-266.
- Kusumoto, R., Masutani, C., Shimmyo, S., Iwai, S. and Hanaoka, F. (2004) DNA binding properties of human DNA polymerase ϵ : implications for fidelity and polymerase switching of translesion synthesis. *Genes Cells*, **9**, 1139-1150.
- Lander, E.S., Linton, L.M., Birren, B., Nusbaum, C., Zody, M.C., Baldwin, J., Devon, K., Dewar, K., Doyle, M., FitzHugh, W., *et al.* (2001) Initial sequencing and analysis of the human genome. *Nature*, **409**, 860-921.
- Lane, D.P. (1992) Cancer. p53, guardian of the genome. *Nature*, **358**, 15-16.
- Lane, D.P. and Crawford, L.V. (1979) T antigen is bound to a host protein in SV40-transformed cells. *Nature*, **278**, 261-263.
- Lang, G.A., Iwakuma, T., Suh, Y.A., Liu, G., Rao, V.A., Parant, J.M., Valentin-Vega, Y.A., Terzian, T., Caldwell, L.C., Strong, L.C., *et al.* (2004) Gain of function of a p53 hot spot mutation in a mouse model of Li-Fraumeni syndrome. *Cell*, **119**, 861-872.
- Lewin, B. (2004) *Genes VIII*. Pearson Prentice Hall.

- Li, J., Yen, C., Liaw, D., Podsypanina, K., Bose, S., Wang, S.I., Puc, J., Miliaresis, C., Rodgers, L., McCombie, R., *et al.* (1997) PTEN, a putative protein tyrosine phosphatase gene mutated in human brain, breast, and prostate cancer. *Science*, **275**, 1943-1947.
- Li, Y.J., Sanson, M., Hoang-Xuan, K., Delattre, J.Y., Poisson, M., Thomas, G. and Hamelin, R. (1995) Incidence of germ-line p53 mutations in patients with gliomas. *Int J Cancer*, **64**, 383-387.
- Liang, B.C., Ross, D.A., Greenberg, H.S., Meltzer, P.S. and Trent, J.M. (1994) Evidence of allelic imbalance of chromosome 6 in human astrocytomas. *Neurology*, **44**, 533-536.
- Linzer, D.I. and Levine, A.J. (1979) Characterization of a 54K dalton cellular SV40 tumor antigen present in SV40-transformed cells and uninfected embryonal carcinoma cells. *Cell*, **17**, 43-52.
- Listernick, R., Charrow, J. and Gutmann, D.H. (1999) Intracranial gliomas in neurofibromatosis type 1. *Am J Med Genet*, **89**, 38-44.
- Loeb, L.A. (2001) A mutator phenotype in cancer. *Cancer Res*, **61**, 3230-3239.
- Lohrum, M.A., Ludwig, R.L., Kubbutat, M.H., Hanlon, M. and Vousden, K.H. (2003) Regulation of HDM2 activity by the ribosomal protein L11. *Cancer Cell*, **3**, 577-587.
- Lorenzetti, D., Antalffy, B., Vogel, H., Noveroske, J., Armstrong, D. and Justice, M. (2004) The neurological mutant quaking(viable) is Parkin deficient. *Mamm Genome*, **15**, 210-217.
- Lynch, T.J., Bell, D.W., Sordella, R., Gurubhagavatula, S., Okimoto, R.A., Brannigan, B.W., Harris, P.L., Haserlat, S.M., Supko, J.G., Haluska, F.G., *et al.* (2004) Activating Mutations in the Epidermal Growth Factor Receptor Underlying Responsiveness of Non-Small-Cell Lung Cancer to Gefitinib. *N Engl J Med*.
- MacLeod, R.A., Dirks, W.G. and Drexler, H.G. (2002) Persistent use of misidentified cell lines and its prevention. *Genes Chromosomes Cancer*, **33**, 103-105.
- Maher, E.A., Furnari, F.B., Bachoo, R.M., Rowitch, D.H., Louis, D.N., Cavenee, W.K. and DePinho, R.A. (2001) Malignant glioma: genetics and biology of a grave matter. *Genes Dev*, **15**, 1311-1333.

- Maity, A., Pore, N., Lee, J., Solomon, D. and O'Rourke, D.M. (2000) Epidermal growth factor receptor transcriptionally up-regulates vascular endothelial growth factor expression in human glioblastoma cells via a pathway involving phosphatidylinositol 3'-kinase and distinct from that induced by hypoxia. *Cancer Res*, **60**, 5879-5886.
- Marx, J. (2002) Telomeres. Chromosome end game draws a crowd. *Science*, **295**, 2348-2351.
- Masutani, C., Kusumoto, R., Yamada, A., Dohmae, N., Yokoi, M., Yuasa, M., Araki, M., Iwai, S., Takio, K. and Hanaoka, F. (1999) The XPV (xeroderma pigmentosum variant) gene encodes human DNA polymerase eta. *Nature*, **399**, 700-704.
- Matsuda, T., Bebenek, K., Masutani, C., Hanaoka, F. and Kunkel, T.A. (2000) Low fidelity DNA synthesis by human DNA polymerase-eta. *Nature*, **404**, 1011-1013.
- Miyakawa, A., Ichimura, K., Schmidt, E.E., Varmeh-Ziaie, S. and Collins, V.P. (2000) Multiple deleted regions on the long arm of chromosome 6 in astrocytic tumours. *Br J Cancer*, **82**, 543-549.
- Mohapatra, G., Bollen, A.W., Kim, D.H., Lamborn, K., Moore, D.H., Prados, M.D. and Feuerstein, B.G. (1998) Genetic analysis of glioblastoma multiforme provides evidence for subgroups within the grade. *Genes Chromosomes Cancer*, **21**, 195-206.
- Moolgavkar, S.H. and Knudson, A.G., Jr. (1981) Mutation and cancer: a model for human carcinogenesis. *J Natl Cancer Inst*, **66**, 1037-1052.
- Mungall, A.J., Palmer, S.A., Sims, S.K., Edwards, C.A., Ashurst, J.L., Wilming, L., Jones, M.C., Horton, R., Hunt, S.E., Scott, C.E., *et al.* (2003) The DNA sequence and analysis of human chromosome 6. *Nature*, **425**, 805-811.
- Nigg, E.A. (2002) Centrosome aberrations: cause or consequence of cancer progression? *Nat Rev Cancer*, **2**, 815-825.
- Nigro, J.M., Baker, S.J., Preisinger, A.C., Jessup, J.M., Hostetter, R., Cleary, K., Bigner, S.H., Davidson, N., Baylin, S., Devilee, P., *et al.* (1989) Mutations in the p53 gene occur in diverse human tumour types. *Nature*, **342**, 705-708.
- Nishikawa, R., Ji, X.D., Harmon, R.C., Lazar, C.S., Gill, G.N., Cavenee, W.K. and Huang, H.J. (1994) A mutant epidermal growth factor receptor common in human

- glioma confers enhanced tumorigenicity. *Proc Natl Acad Sci U S A*, **91**, 7727-7731.
- Olive, K.P., Tuveson, D.A., Ruhe, Z.C., Yin, B., Willis, N.A., Bronson, R.T., Crowley, D. and Jacks, T. (2004) Mutant p53 gain of function in two mouse models of Li-Fraumeni syndrome. *Cell*, **119**, 847-860.
- Olopade, O.I., Jenkins, R.B., Ransom, D.T., Malik, K., Pomykala, H., Nobori, T., Cowan, J.M., Rowley, J.D. and Diaz, M.O. (1992) Molecular analysis of deletions of the short arm of chromosome 9 in human gliomas. *Cancer Res*, **52**, 2523-2529.
- Paez, J.G., Janne, P.A., Lee, J.C., Tracy, S., Greulich, H., Gabriel, S., Herman, P., Kaye, F.J., Lindeman, N., Boggon, T.J., *et al.* (2004) EGFR Mutations in Lung Cancer: Correlation with Clinical Response to Gefitinib Therapy. *Science*.
- Pastan, I. and Gottesman, M. (1987) Multiple-drug resistance in human cancer. *N Engl J Med*, **316**, 1388-1393.
- Picchio, M.C., Martin, E.S., Cesari, R., Calin, G.A., Yendamuri, S., Kuroki, T., Pentimalli, F., Sarti, M., Yoder, K., Kaiser, L.R., *et al.* (2004) Alterations of the tumor suppressor gene Parkin in non-small cell lung cancer. *Clin Cancer Res*, **10**, 2720-2724.
- Pinkel, D., Seagraves, R., Sudar, D., Clark, S., Poole, I., Kowbel, D., Collins, C., Kuo, W.L., Chen, C., Zhai, Y., *et al.* (1998) High resolution analysis of DNA copy number variation using comparative genomic hybridization to microarrays. *Nat Genet*, **20**, 207-211.
- Pinkel, D., Straume, T. and Gray, J.W. (1986) Cytogenetic analysis using quantitative, high-sensitivity, fluorescence hybridization. *Proc Natl Acad Sci U S A*, **83**, 2934-2938.
- Pollack, J.R., Perou, C.M., Alizadeh, A.A., Eisen, M.B., Pergamenschikov, A., Williams, C.F., Jeffrey, S.S., Botstein, D. and Brown, P.O. (1999) Genome-wide analysis of DNA copy-number changes using cDNA microarrays. *Nat Genet*, **23**, 41-46.
- Pollack, J.R., Sorlie, T., Perou, C.M., Rees, C.A., Jeffrey, S.S., Lonning, P.E., Tibshirani, R., Botstein, D., Borresen-Dale, A.L. and Brown, P.O. (2002) Microarray analysis reveals a major direct role of DNA copy number alteration in the transcriptional program of human breast tumors. *Proc Natl Acad Sci U S A*, **99**, 12963-12968.

- Pomeroy, S.L., Tamayo, P., Gaasenbeek, M., Sturla, L.M., Angelo, M., McLaughlin, M.E., Kim, J.Y., Goumnerova, L.C., Black, P.M., Lau, C., *et al.* (2002) Prediction of central nervous system embryonal tumour outcome based on gene expression. *Nature*, **415**, 436-442.
- Pore, N., Liu, S., Haas-Kogan, D.A., O'Rourke, D.M. and Maity, A. (2003) PTEN mutation and epidermal growth factor receptor activation regulate vascular endothelial growth factor (VEGF) mRNA expression in human glioblastoma cells by transactivating the proximal VEGF promoter. *Cancer Res*, **63**, 236-241.
- Ramaswamy, S., Nakamura, N., Vazquez, F., Batt, D.B., Perera, S., Roberts, T.M. and Sellers, W.R. (1999) Regulation of G1 progression by the PTEN tumor suppressor protein is linked to inhibition of the phosphatidylinositol 3-kinase/Akt pathway. *Proc Natl Acad Sci U S A*, **96**, 2110-2115.
- Ransom, D.T., Ritland, S.R., Moertel, C.A., Dahl, R.J., O'Fallon, J.R., Scheithauer, B.W., Kimmel, D.W., Kelly, P.J., Olopade, O.I., Diaz, M.O., *et al.* (1992) Correlation of cytogenetic analysis and loss of heterozygosity studies in human diffuse astrocytomas and mixed oligo-astrocytomas. *Genes Chromosomes Cancer*, **5**, 357-374.
- Rasheed, A., Herndon, J.E., Stenzel, T.T., Raetz, J.G., Kendelhardt, J., Friedman, H.S., Friedman, A.H., Bigner, D.D., Bigner, S.H. and McLendon, R.E. (2002) Molecular markers of prognosis in astrocytic tumors. *Cancer*, **94**, 2688-2697.
- Rhei, E., Kang, L., Bogomolnii, F., Federici, M.G., Borgen, P.I. and Boyd, J. (1997) Mutation analysis of the putative tumor suppressor gene PTEN/MMAC1 in primary breast carcinomas. *Cancer Res*, **57**, 3657-3659.
- Rich, J.N., Reardon, D.A., Peery, T., Dowell, J.M., Quinn, J.A., Penne, K.L., Wikstrand, C.J., Van Duyn, L.B., Dancey, J.E., McLendon, R.E., *et al.* (2004) Phase II trial of gefitinib in recurrent glioblastoma. *J Clin Oncol*, **22**, 133-142.
- Robinson, D.R., Wu, Y.M. and Lin, S.F. (2000) The protein tyrosine kinase family of the human genome. *Oncogene*, **19**, 5548-5557.
- Roelofs, H., Schuurin, E., Wiegant, J., Michalides, R. and Giphart-Gassler, M. (1993) Amplification of the 11q13 region in human carcinoma cell lines: a mechanistic view. *Genes Chromosomes Cancer*, **7**, 74-84.

- Ross, M.T., Grafham, D.V., Coffey, A.J., Scherer, S., McLay, K., Muzny, D., Platzer, M., Howell, G.R., Burrows, C., Bird, C.P., *et al.* (2005) The DNA sequence of the human X chromosome. *Nature*, **434**, 325-337.
- Rous, P. (1911) Transmission of a malignant new growth by means of a cell-free filtrate. *Jama*, **56**, 198.
- Sacksteder, K.A., Biery, B.J., Morrell, J.C., Goodman, B.K., Geisbrecht, B.V., Cox, R.P., Gould, S.J. and Geraghty, M.T. (2000) Identification of the alpha-aminoacidic semialdehyde synthase gene, which is defective in familial hyperlysinemia. *Am J Hum Genet*, **66**, 1736-1743.
- Saitoh, Y., Bruner, J.M., Levin, V.A. and Kyritsis, A.P. (1998) Identification of allelic loss on chromosome arm 6p in human astrocytomas by arbitrarily primed polymerase chain reaction. *Genes Chromosomes Cancer*, **22**, 165-170.
- Sawyers, C.L. (2001) Research on resistance to cancer drug Gleevec. *Science*, **294**, 1834.
- Schena, M., Shalon, D., Davis, R.W. and Brown, P.O. (1995) Quantitative monitoring of gene expression patterns with a complementary DNA microarray. *Science*, **270**, 467-470.
- Schlegel, J., Stumm, G., Scherthan, H., Bocker, T., Zirngibl, H., Ruschoff, J. and Hofstadter, F. (1995) Comparative genomic in situ hybridization of colon carcinomas with replication error. *Cancer Res*, **55**, 6002-6005.
- Schmidt, E.E., Ichimura, K., Goike, H.M., Moshref, A., Liu, L. and Collins, V.P. (1999) Mutational profile of the PTEN gene in primary human astrocytic tumors and cultivated xenografts. *J Neuropathol Exp Neurol*, **58**, 1170-1183.
- Schmidt, E.E., Ichimura, K., Messerle, K.R., Goike, H.M. and Collins, V.P. (1997) Infrequent methylation of CDKN2A(MTS1/p16) and rare mutation of both CDKN2A and CDKN2B(MTS2/p15) in primary astrocytic tumours. *Br J Cancer*, **75**, 2-8.
- Schmutz, J., Martin, J., Terry, A., Couronne, O., Grimwood, J., Lowry, S., Gordon, L.A., Scott, D., Xie, G., Huang, W., *et al.* (2004) The DNA sequence and comparative analysis of human chromosome 5. *Nature*, **431**, 268-274.
- Schwab, M. (1999) Oncogene amplification in solid tumors. *Semin Cancer Biol*, **9**, 319-325.

- Schwab, M., Alitalo, K., Klemmner, K.H., Varmus, H.E., Bishop, J.M., Gilbert, F., Brodeur, G., Goldstein, M. and Trent, J. (1983) Amplified DNA with limited homology to myc cellular oncogene is shared by human neuroblastoma cell lines and a neuroblastoma tumour. *Nature*, **305**, 245-248.
- Sebat, J., Lakshmi, B., Troge, J., Alexander, J., Young, J., Lundin, P., Maner, S., Massa, H., Walker, M., Chi, M., *et al.* (2004) Large-scale copy number polymorphism in the human genome. *Science*, **305**, 525-528.
- Seeger, R.C., Brodeur, G.M., Sather, H., Dalton, A., Siegel, S.E., Wong, K.Y. and Hammond, D. (1985) Association of multiple copies of the N-myc oncogene with rapid progression of neuroblastomas. *N Engl J Med*, **313**, 1111-1116.
- Senger, G., Ragoussis, J., Trowsdale, J. and Sheer, D. (1993) Fine mapping of the human MHC class II region within chromosome band 6p21 and evaluation of probe ordering using interphase fluorescence in situ hybridization. *Cytogenet Cell Genet*, **64**, 49-53.
- Sheer, D. and Shipley, J.M. (2005) *Molecular Cytogenetics of Cancer, in: Introduction to the Cellular and Molecular Biology of Cancer*. Oxford University Press.
- Sherr, C.J. and McCormick, F. (2002) The RB and p53 pathways in cancer. *Cancer Cell*, **2**, 103-112.
- Sidman, R.L., Dickie, M.M. and Appel, S.H. (1964) Mutant Mice (Quaking and Jimpy) with Deficient Myelination in the Central Nervous System. *Science*, **144**, 309-311.
- Smith, D.I., Huang, H. and Wang, L. (1998) Common fragile sites and cancer (review). *Int J Oncol*, **12**, 187-196.
- Snijders, A.M., Nowak, N., Segreaves, R., Blackwood, S., Brown, N., Conroy, J., Hamilton, G., Hindle, A.K., Huey, B., Kimura, K., *et al.* (2001) Assembly of microarrays for genome-wide measurement of DNA copy number. *Nat Genet*, **29**, 263-264.
- Solinas-Toldo, S., Lampel, S., Stilgenbauer, S., Nickolenko, J., Benner, A., Dohner, H., Cremer, T. and Lichter, P. (1997) Matrix-based comparative genomic hybridization: biochips to screen for genomic imbalances. *Genes Chromosomes Cancer*, **20**, 399-407.

- Speicher, M.R., Gwyn Ballard, S. and Ward, D.C. (1996) Karyotyping human chromosomes by combinatorial multi-fluor FISH. *Nat Genet*, **12**, 368-375.
- Stacey, G.N. (2000) Cell contamination leads to inaccurate data: we must take action now. *Nature*, **403**, 356.
- Stadler, H.S., Higgins, K.M. and Capecchi, M.R. (2001) Loss of Eph-receptor expression correlates with loss of cell adhesion and chondrogenic capacity in Hoxa13 mutant limbs. *Development*, **128**, 4177-4188.
- Steck, P.A., Pershouse, M.A., Jasser, S.A., Yung, W.K., Lin, H., Ligon, A.H., Langford, L.A., Baumgard, M.L., Hattier, T., Davis, T., *et al.* (1997) Identification of a candidate tumour suppressor gene, MMAC1, at chromosome 10q23.3 that is mutated in multiple advanced cancers. *Nat Genet*, **15**, 356-362.
- Stehelin, D., Varmus, H.E., Bishop, J.M. and Vogt, P.K. (1976) DNA related to the transforming gene(s) of avian sarcoma viruses is present in normal avian DNA. *Nature*, **260**, 170-173.
- Stone, S., Jiang, P., Dayananth, P., Tavtigian, S.V., Katcher, H., Parry, D., Peters, G. and Kamb, A. (1995) Complex structure and regulation of the P16 (MTS1) locus. *Cancer Res*, **55**, 2988-2994.
- Storchova, Z. and Pellman, D. (2004) From polyploidy to aneuploidy, genome instability and cancer. *Nat Rev Mol Cell Biol*, **5**, 45-54.
- Stott, F.J., Bates, S., James, M.C., McConnell, B.B., Starborg, M., Brookes, S., Palmero, I., Ryan, K., Hara, E., Vousden, K.H., *et al.* (1998) The alternative product from the human CDKN2A locus, p14(ARF), participates in a regulatory feedback loop with p53 and MDM2. *Embo J*, **17**, 5001-5014.
- Strachan, T. and Read, P. (1999) *Human Molecular Genetics* 2.
- Tanner, M.M., Grenman, S., Koul, A., Johannsson, O., Meltzer, P., Pejovic, T., Borg, A. and Isola, J.J. (2000) Frequent amplification of chromosomal region 20q12-q13 in ovarian cancer. *Clin Cancer Res*, **6**, 1833-1839.
- Thiagalingam, S., Foy, R.L., Cheng, K.H., Lee, H.J., Thiagalingam, A. and Ponte, J.F. (2002) Loss of heterozygosity as a predictor to map tumor suppressor genes in cancer: molecular basis of its occurrence. *Curr Opin Oncol*, **14**, 65-72.

- Thiel, G., Losanowa, T., Kintzel, D., Nisch, G., Martin, H., Vorpahl, K. and Witkowski, R. (1992) Karyotypes in 90 human gliomas. *Cancer Genet Cytogenet*, **58**, 109-120.
- Thompson, P.M., Gotoh, T., Kok, M., White, P.S. and Brodeur, G.M. (2003) CHD5, a new member of the chromodomain gene family, is preferentially expressed in the nervous system. *Oncogene*, **22**, 1002-1011.
- Tognon, C., Knezevich, S.R., Huntsman, D., Roskelley, C.D., Melnyk, N., Mathers, J.A., Becker, L., Carneiro, F., MacPherson, N., Horsman, D., *et al.* (2002) Expression of the ETV6-NTRK3 gene fusion as a primary event in human secretory breast carcinoma. *Cancer Cell*, **2**, 367-376.
- Tohma, Y., Gratas, C., Biernat, W., Peraud, A., Fukuda, M., Yonekawa, Y., Kleihues, P. and Ohgaki, H. (1998) PTEN (MMAC1) mutations are frequent in primary glioblastomas (de novo) but not in secondary glioblastomas. *J Neuropathol Exp Neurol*, **57**, 684-689.
- Tomlinson, I.P., Novelli, M.R. and Bodmer, W.F. (1996) The mutation rate and cancer. *Proc Natl Acad Sci U S A*, **93**, 14800-14803.
- Vassilev, L.T., Vu, B.T., Graves, B., Carvajal, D., Podlaski, F., Filipovic, Z., Kong, N., Kammlott, U., Lukacs, C., Klein, C., *et al.* (2004) In Vivo Activation of the p53 Pathway by Small-Molecule Antagonists of MDM2. *Science*, **303**, 844-848.
- Veltman, J.A., Fridlyand, J., Pejavar, S., Olshen, A.B., Korkola, J.E., DeVries, S., Carroll, P., Kuo, W.L., Pinkel, D., Albertson, D., *et al.* (2003) Array-based comparative genomic hybridization for genome-wide screening of DNA copy number in bladder tumors. *Cancer Res*, **63**, 2872-2880.
- Venter, J.C., Adams, M.D., Myers, E.W., Li, P.W., Mural, R.J., Sutton, G.G., Smith, H.O., Yandell, M., Evans, C.A., Holt, R.A., *et al.* (2001) The sequence of the human genome. *Science*, **291**, 1304-1351.
- Vogelstein, B. and Kinzler, K.W. (1998) *The genetic basis of human cancer*.
- von Deimling, A., Bender, B., Jahnke, R., Waha, A., Kraus, J., Albrecht, S., Wellenreuther, R., Fassbender, F., Nagel, J., Menon, A.G., *et al.* (1994) Loci associated with malignant progression in astrocytomas: a candidate on chromosome 19q. *Cancer Res*, **54**, 1397-1401.

- von Deimling, A., Eibl, R.H., Ohgaki, H., Louis, D.N., von Ammon, K., Petersen, I., Kleihues, P., Chung, R.Y., Wiestler, O.D. and Seizinger, B.R. (1992a) p53 mutations are associated with 17p allelic loss in grade II and grade III astrocytoma. *Cancer Res*, **52**, 2987-2990.
- von Deimling, A., Louis, D.N., von Ammon, K., Petersen, I., Hoell, T., Chung, R.Y., Martuza, R.L., Schoenfeld, D.A., Yasargil, M.G., Wiestler, O.D., *et al.* (1992b) Association of epidermal growth factor receptor gene amplification with loss of chromosome 10 in human glioblastoma multiforme. *J Neurosurg*, **77**, 295-301.
- Vousden, K.H. (2000) p53: death star. *Cell*, **103**, 691-694.
- Wang, F., Denison, S., Lai, J.P., Philips, L.A., Montoya, D., Kock, N., Schule, B., Klein, C., Shridhar, V., Roberts, L.R., *et al.* (2004a) Parkin gene alterations in hepatocellular carcinoma. *Genes Chromosomes Cancer*, **40**, 85-96.
- Wang, S.I., Puc, J., Li, J., Bruce, J.N., Cairns, P., Sidransky, D. and Parsons, R. (1997) Somatic mutations of PTEN in glioblastoma multiforme. *Cancer Res*, **57**, 4183-4186.
- Wang, T.L., Diaz, L.A., Jr., Romans, K., Bardelli, A., Saha, S., Galizia, G., Choti, M., Donehower, R., Parmigiani, G., Shih Ie, M., *et al.* (2004b) Digital karyotyping identifies thymidylate synthase amplification as a mechanism of resistance to 5-fluorouracil in metastatic colorectal cancer patients. *Proc Natl Acad Sci U S A*, **101**, 3089-3094.
- Watanabe, K., Sato, K., Biernat, W., Tachibana, O., von Ammon, K., Ogata, N., Yonekawa, Y., Kleihues, P. and Ohgaki, H. (1997) Incidence and timing of p53 mutations during astrocytoma progression in patients with multiple biopsies. *Clin Cancer Res*, **3**, 523-530.
- Watanabe, K., Tachibana, O., Sata, K., Yonekawa, Y., Kleihues, P. and Ohgaki, H. (1996) Overexpression of the EGF receptor and p53 mutations are mutually exclusive in the evolution of primary and secondary glioblastomas. *Brain Pathol*, **6**, 217-223; discussion 223-214.
- Watanabe, M., Yoshida, K., Hida, M., Kato, H., Uchida, K., Yamaguchi, R., Tateyama, S. and Sugano, S. (2000) Cloning, expression analysis, and chromosomal mapping of GTPBP2, a novel member of the G protein family. *Gene*, **256**, 51-58.

- Weber, R.G., Sabel, M., Reifenberger, J., Sommer, C., Oberstrass, J., Reifenberger, G., Kiessling, M. and Cremer, T. (1996) Characterization of genomic alterations associated with glioma progression by comparative genomic hybridization. *Oncogene*, **13**, 983-994.
- West, A.B., Lockhart, P.J., O'Farrell, C. and Farrer, M.J. (2003) Identification of a novel gene linked to parkin via a bi-directional promoter. *J Mol Biol*, **326**, 11-19.
- Wilhelm, M., Veltman, J.A., Olshen, A.B., Jain, A.N., Moore, D.H., Presti, J.C., Jr., Kovacs, G. and Waldman, F.M. (2002) Array-based comparative genomic hybridization for the differential diagnosis of renal cell cancer. *Cancer Res*, **62**, 957-960.
- Wong, A.J., Bigner, S.H., Bigner, D.D., Kinzler, K.W., Hamilton, S.R. and Vogelstein, B. (1987) Increased expression of the epidermal growth factor receptor gene in malignant gliomas is invariably associated with gene amplification. *Proc Natl Acad Sci U S A*, **84**, 6899-6903.
- Zhang, Y., Gao, J., Chung, K.K., Huang, H., Dawson, V.L. and Dawson, T.M. (2000) Parkin functions as an E2-dependent ubiquitin- protein ligase and promotes the degradation of the synaptic vesicle-associated protein, CDCrel-1. *Proc Natl Acad Sci U S A*, **97**, 13354-13359.
- Zhou, H., Kuang, J., Zhong, L., Kuo, W.L., Gray, J.W., Sahin, A., Brinkley, B.R. and Sen, S. (1998) Tumour amplified kinase STK15/BTAK induces centrosome amplification, aneuploidy and transformation. *Nat Genet*, **20**, 189-193.
- Zhu, Y. and Parada, L.F. (2002) The molecular and genetic basis of neurological tumours. *Nat Rev Cancer*, **2**, 616-626.

Appendices

Appendix A Reagents

QiampDNA Blood Maxi Kit (Qiagen, 51192)
Fluorescein isothiocyanate-12-dUTP (FITC) (NEN Life Science, NEL-413)
Texas Red-5-dUTP (TR) (NEN Life Science, NEL-417)
2-mercaptoethanol (2-ME) (Sigma, M-3148)
Bioprime Labelling kit (Invitrogen 18094-011)
10x dNTP mix (0.5 mM dCTP, 2 mM dATP, 2 mM dGTP, 2 mM dTTP in TE buffer)
1mM Cy3-dCTP (NEN Life Science, NEL 576)
1mM Cy5-dCTP (NEN Life Science, NEL 577)
Micro-spin G50 columns (Pharmacia Amersham, 275330-01)
Dextran sulphate
Tween 20
SSC
Sodium acetate (Na Ac)
Human Cot1 DNA (Invitrogen or Roche)
Herring sperm DNA (Sigma D7290)
Ethanol (100% and 80%)
Yeast tRNA (Invitrogen 15401-029)
Bionick kit (Invitrogen 18247 015)
Digoxigenin-11-dUTP (Roche Diagnostics 1093 088).
dATP (Amersham pharmacia biotech 27-2050-01)
dCTP (Amersham pharmacia biotech 27-2060-01)
dGTP (Amersham pharmacia biotech 27-2070-01)
dTTP (Amersham pharmacia biotech 27-2080-01)
Fluorescein-avidin DCS (Vector labs A2011)
anti-digoxigenin-rhodamine (Roche Diagnostics 1207 750)
Formamide (International Biotechnologies INC 72024)
Tween 20 (Pierce 28320)
Citifluor (Glycerol/PBS) (Citifluor Ltd)

RNase (Sigma R-5000)

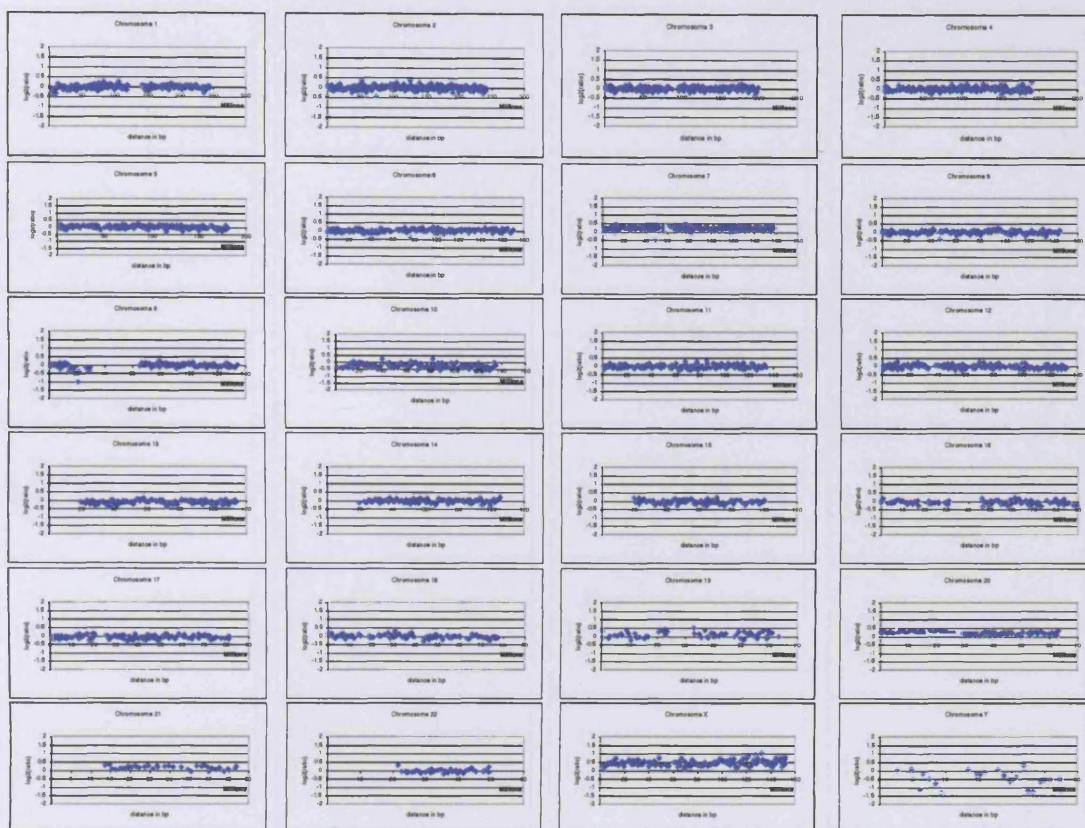
Pepsin (Vysis MK262957)

NP-40 (CALBIOCHEM)

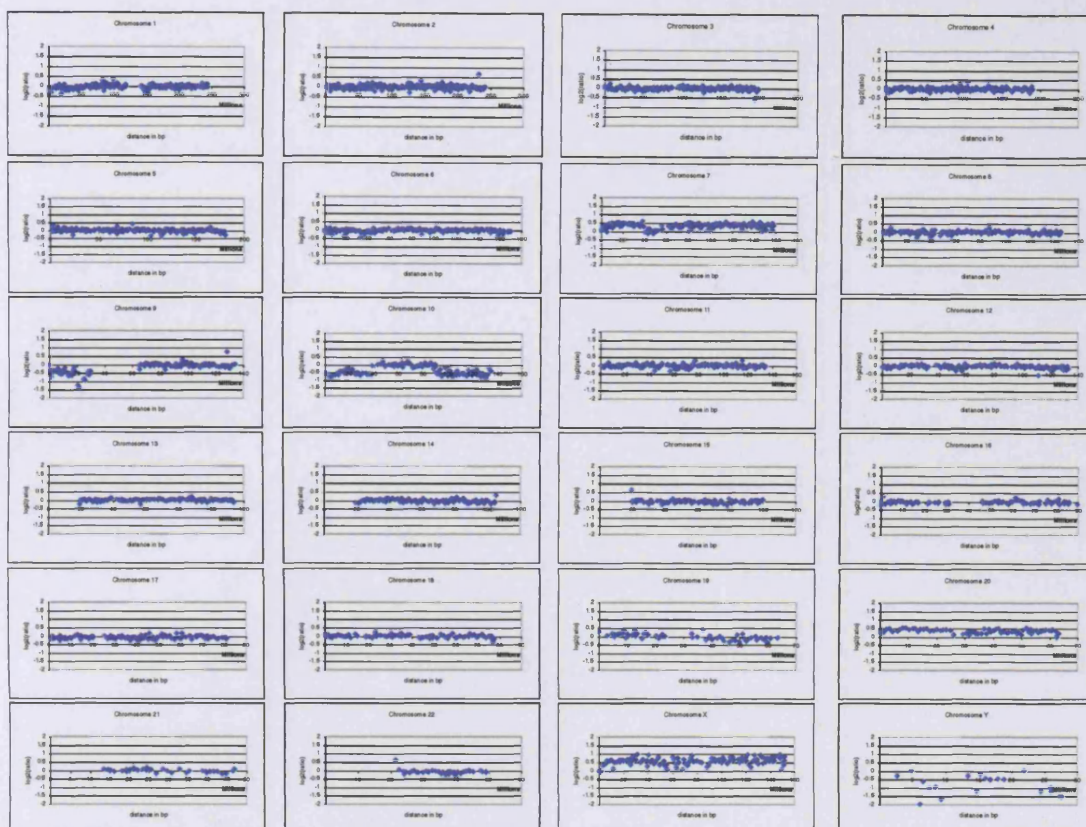
DAPI III

Appendix B Cytogenetic nomenclature

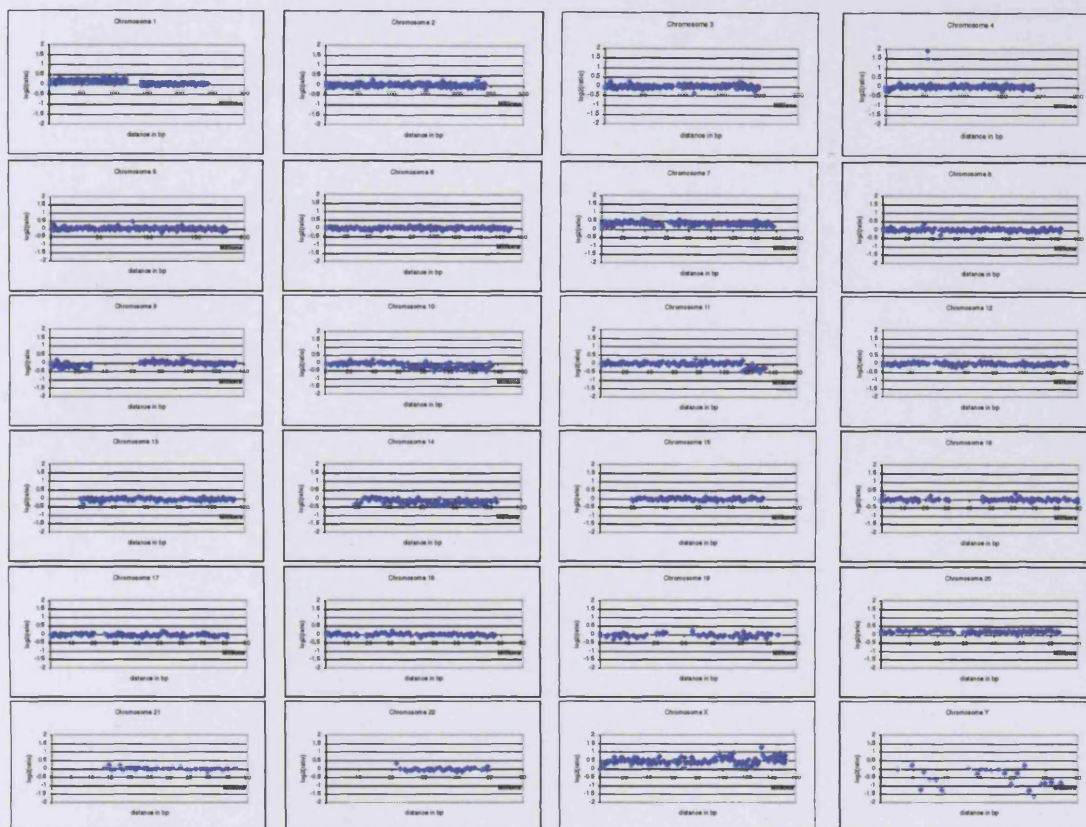
p	Short arm of the chromosome
q	long arm of the chromosome
del	Deletion
der	Derivative chromosome
dup	Duplication
I	Isochromosome
Ins	Insertion
Inv	Inversion
t	Translocation
ter	Terminal (can also be written pter or qter)
+	If placed before a chromosome it indicates gain of the chromosome, if placed after the chromosome it indicates gain of part of the chromosome
-	If placed before a chromosome it indicates loss of the chromosome, if placed after the chromosome it indicates loss of part of the chromosome



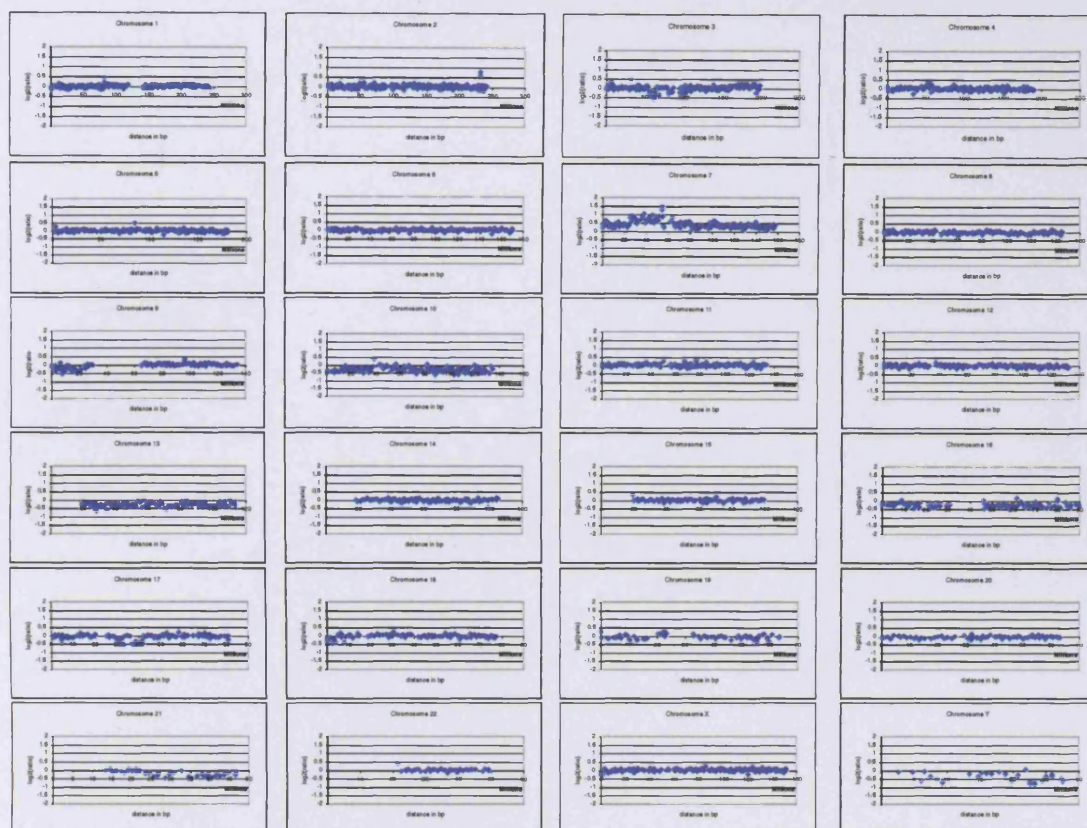
Appendix C1 Array CGH profile of Tumour T1



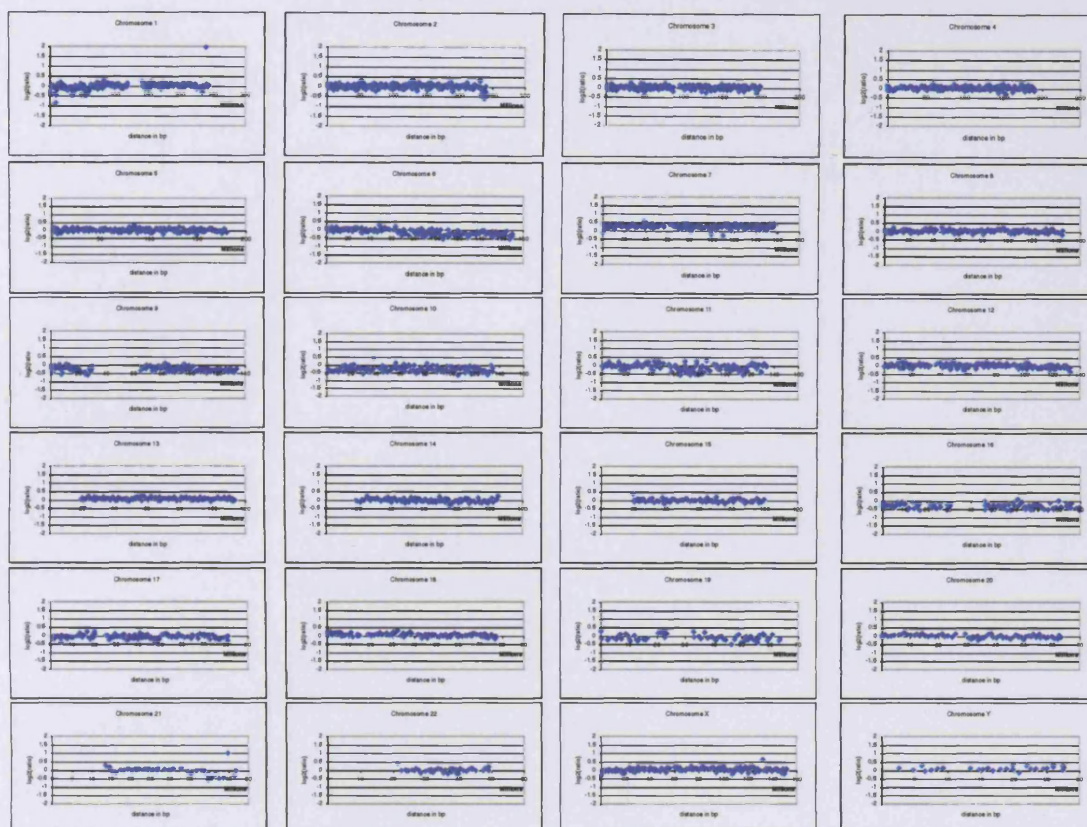
Appendix C2 Array CGH profile of Tumour T2



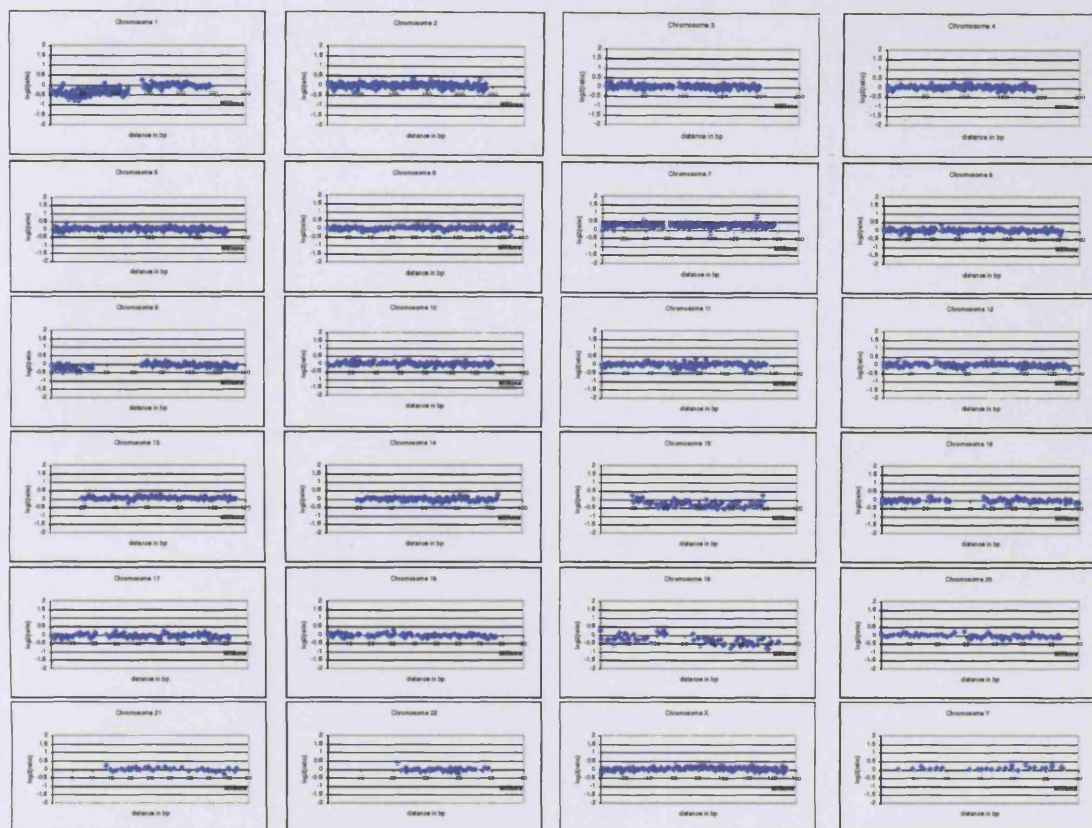
Appendix C3 Array CGH profile of Tumour T3



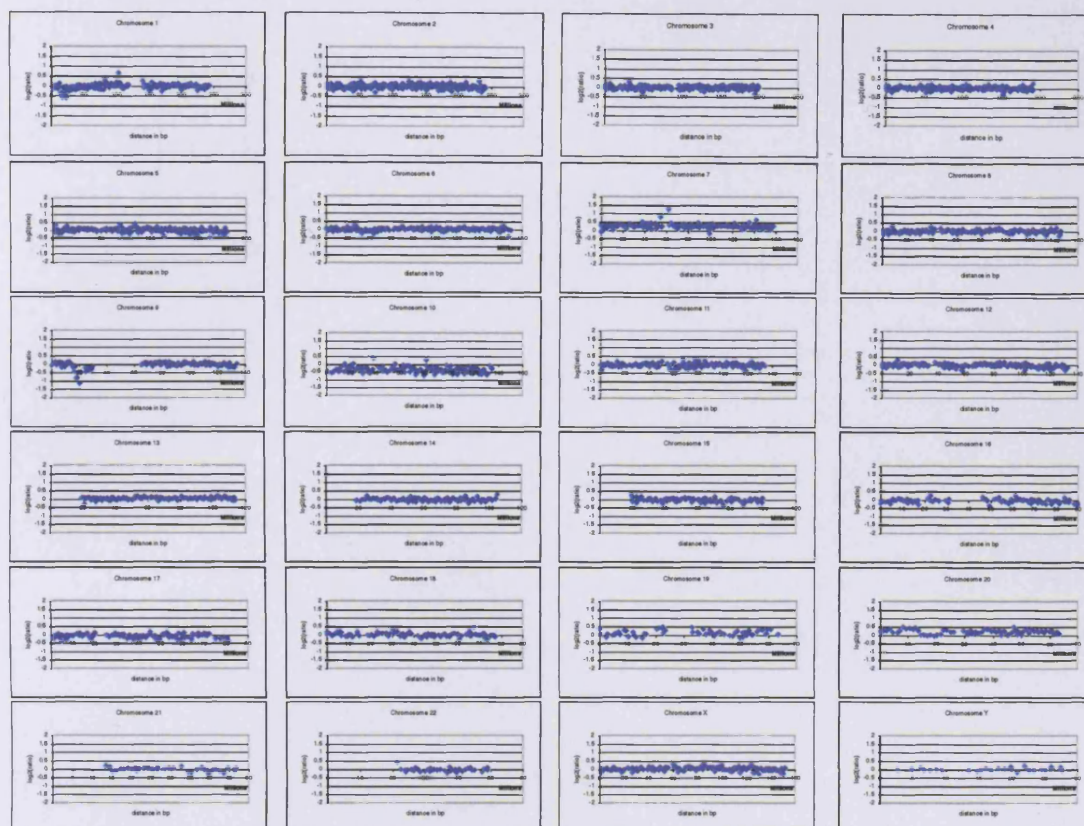
Appendix C4 Array CGH profile of Tumour T4



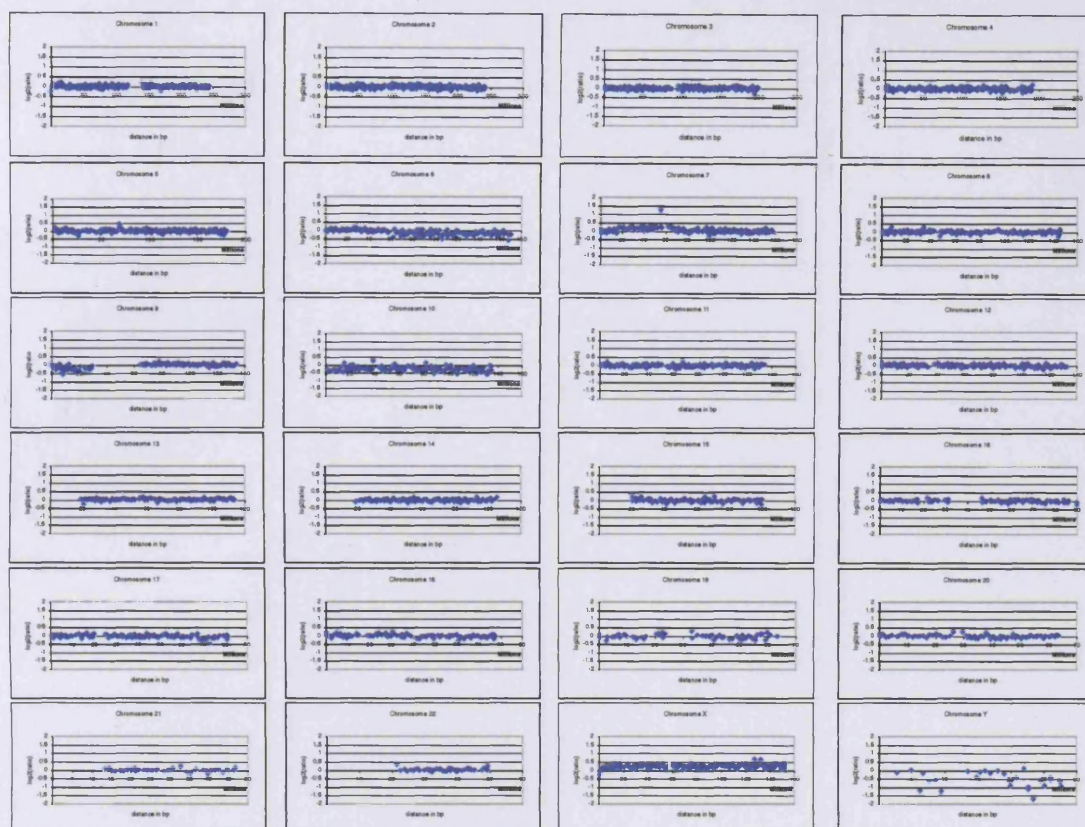
Appendix C5 Array CGH profile of Tumour T5



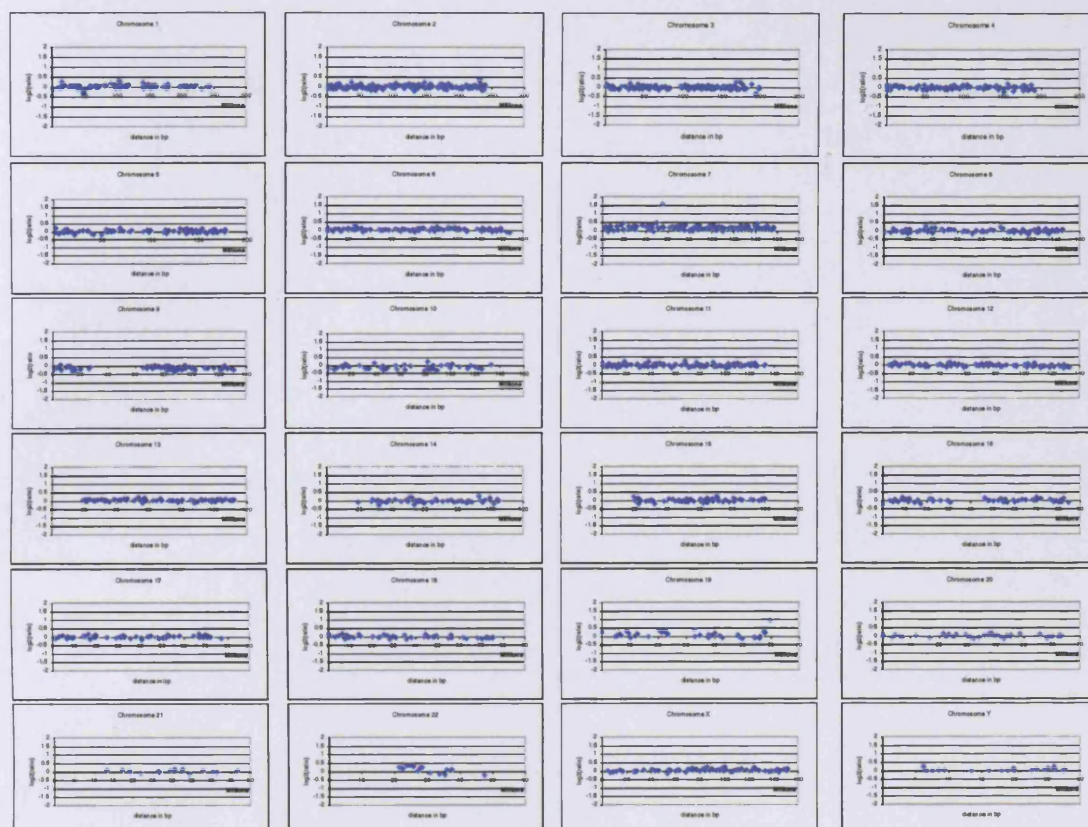
Appendix C6 Array CGH profile of Tumour T6



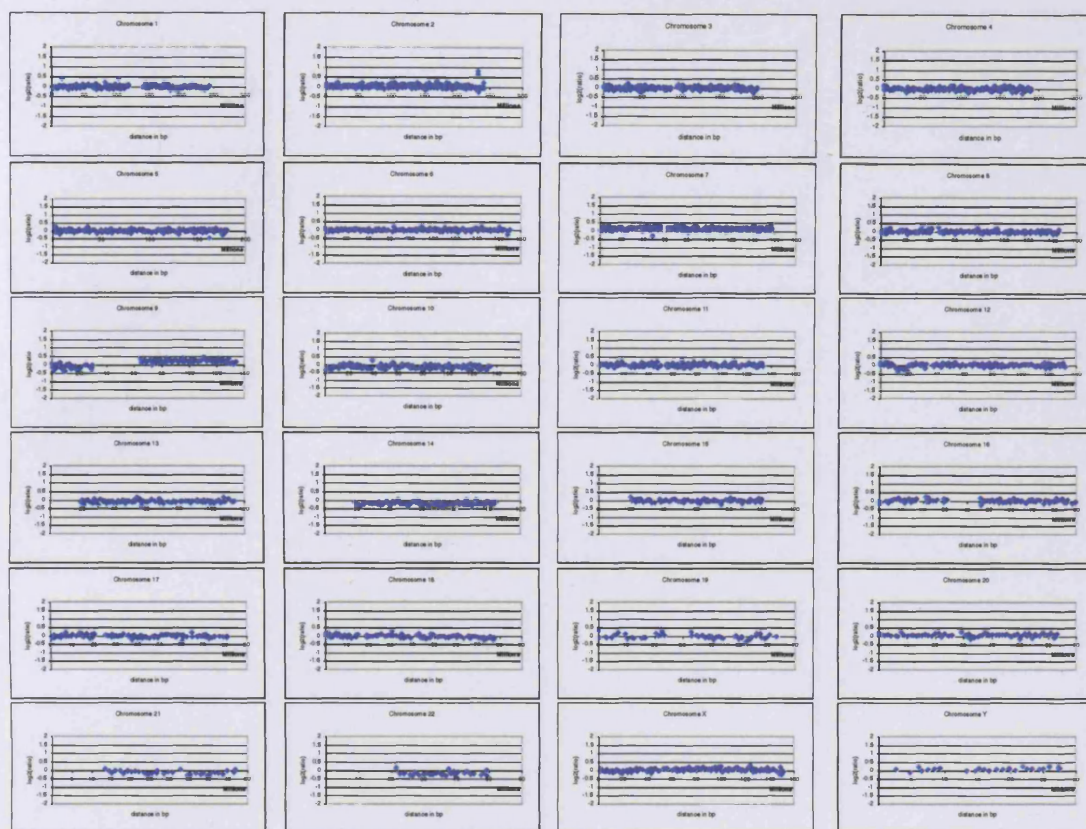
Appendix C7 Array CGH profile of Tumour T7



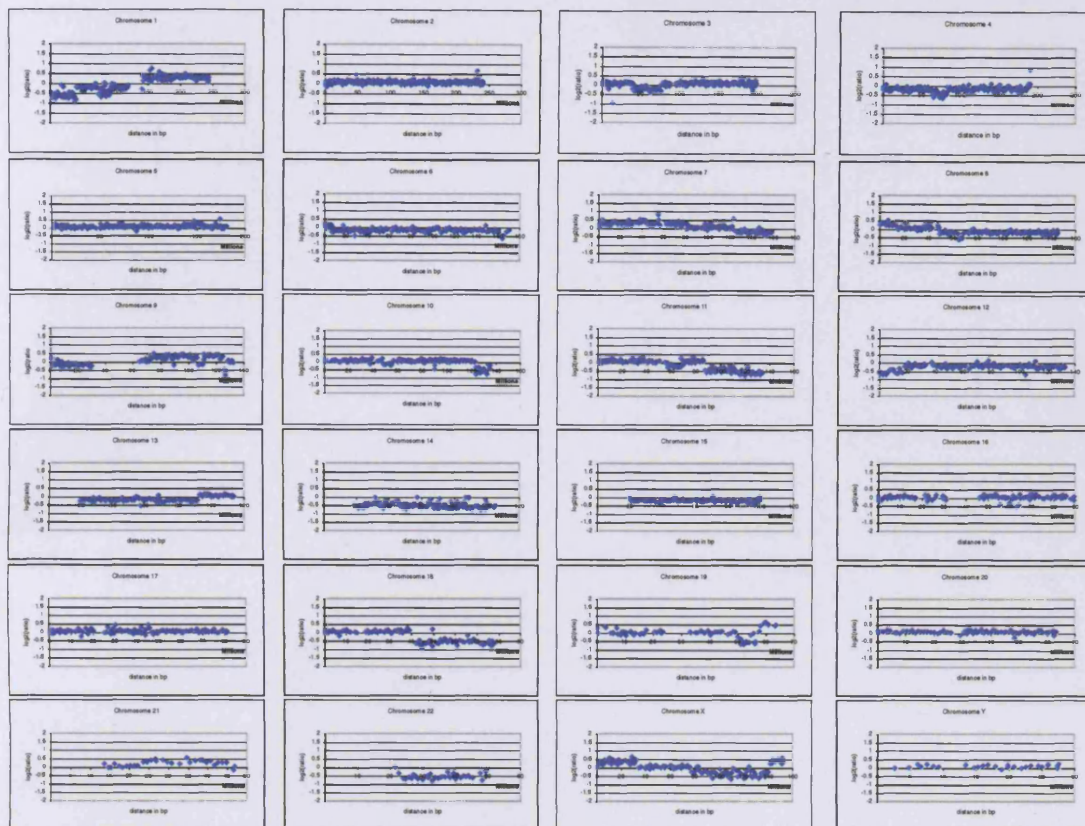
Appendix C8 Array CGH profile of Tumour T8



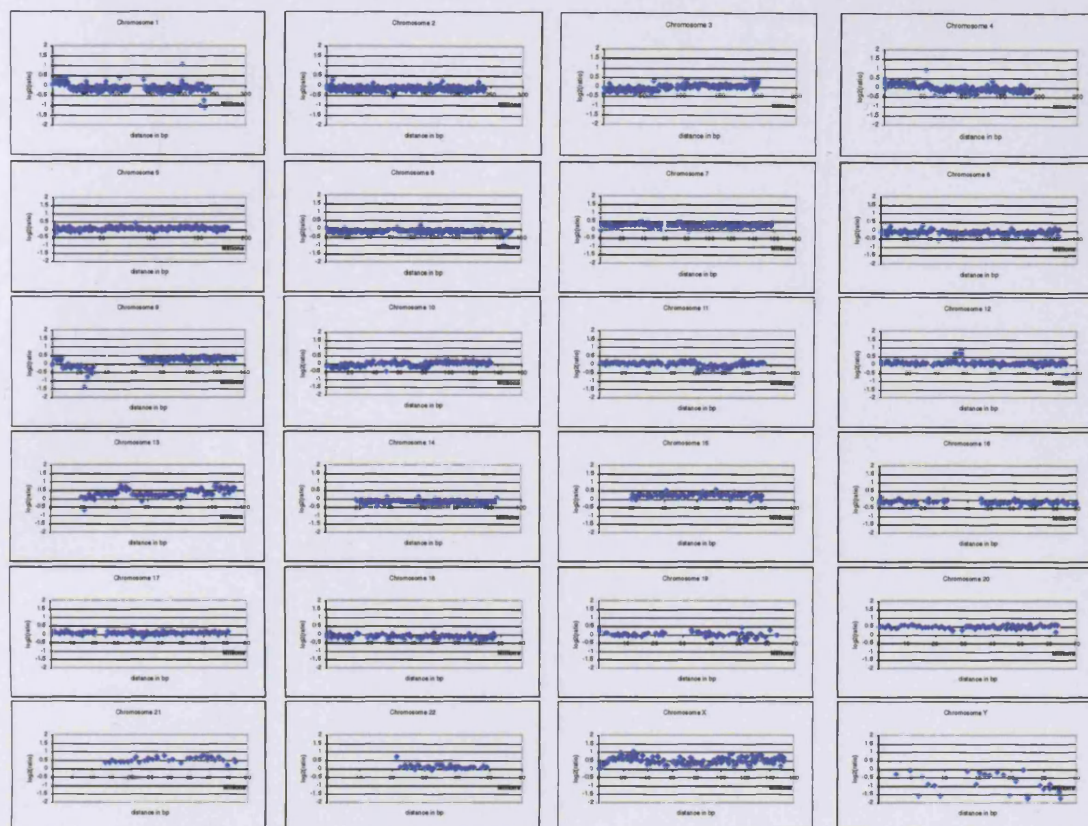
Appendix C9 Array CGH profile of Tumour T9



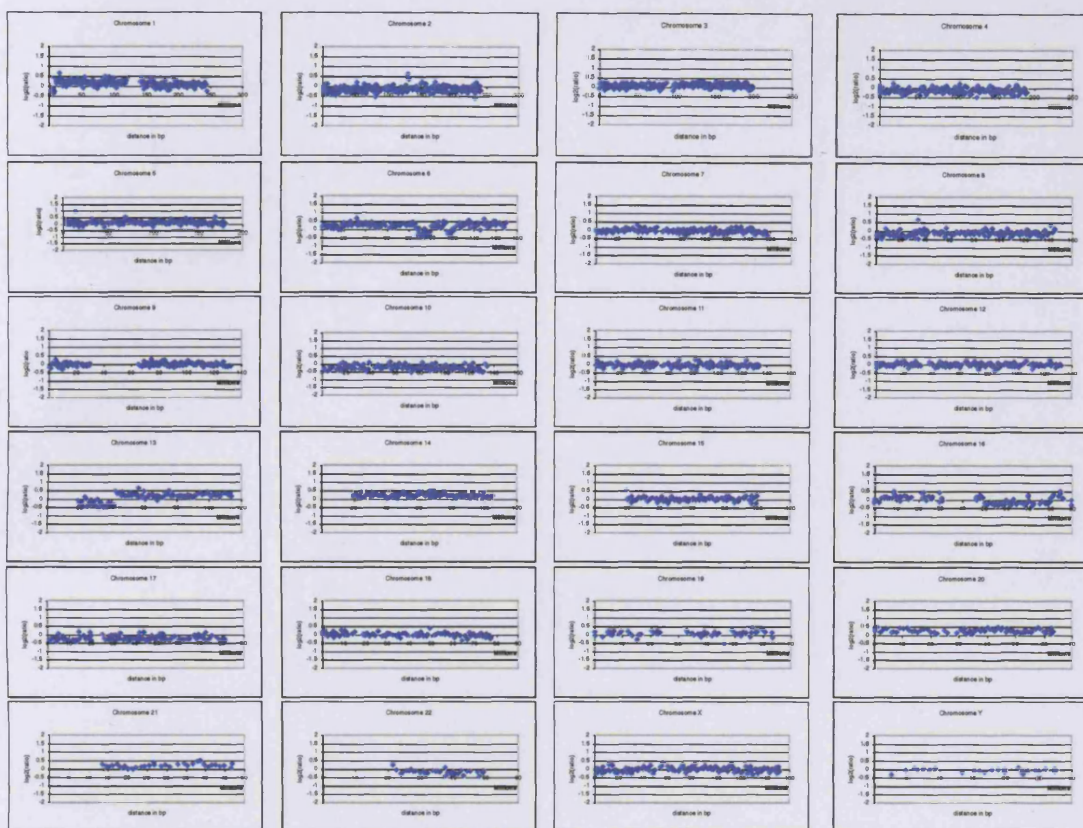
Appendix C10 Array CGH profile of Tumour T10



Appendix C11 Array CGH profile of cell line CRL1620



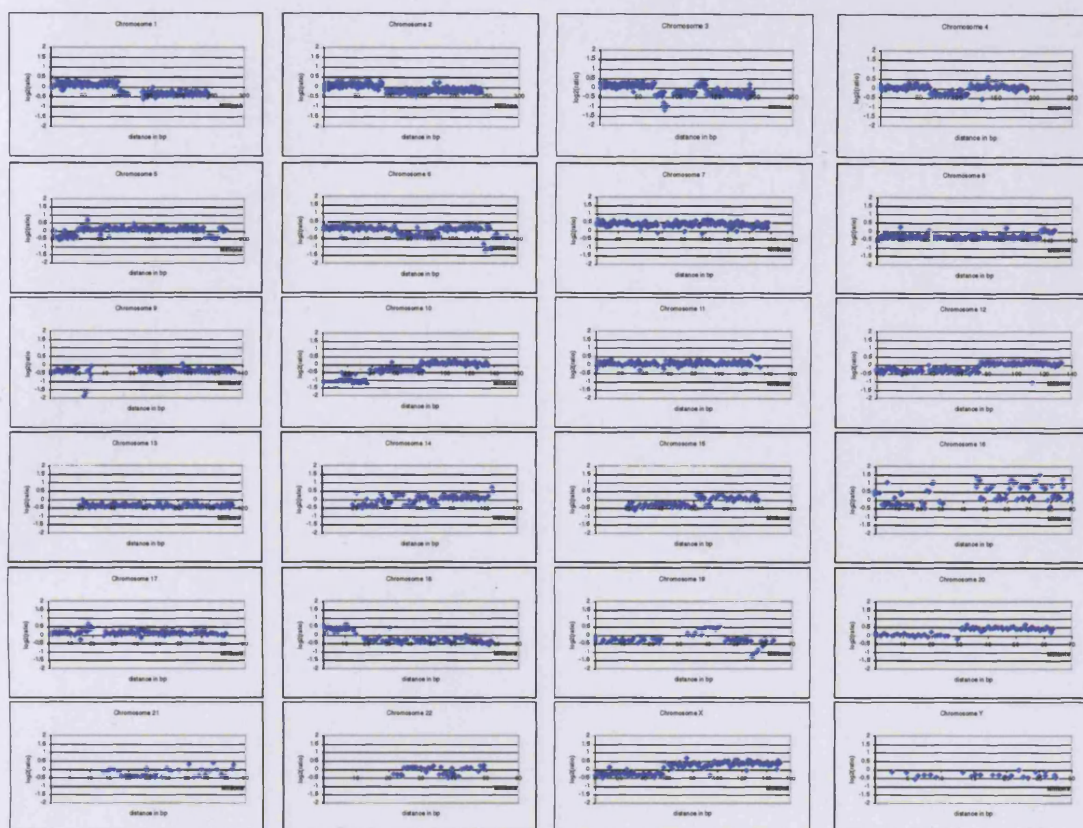
Appendix C12 Array CGH profile of cell line CRL2020



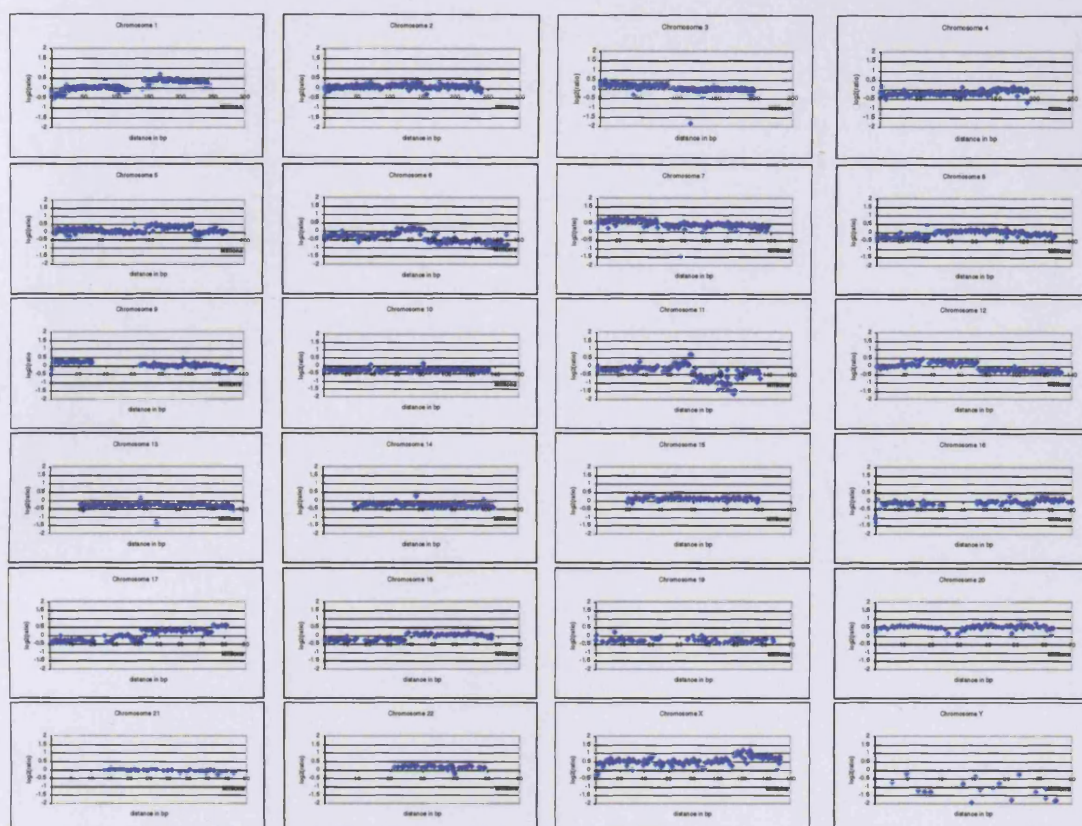
Appendix C13 Array CGH profiles of cell line CRL2365



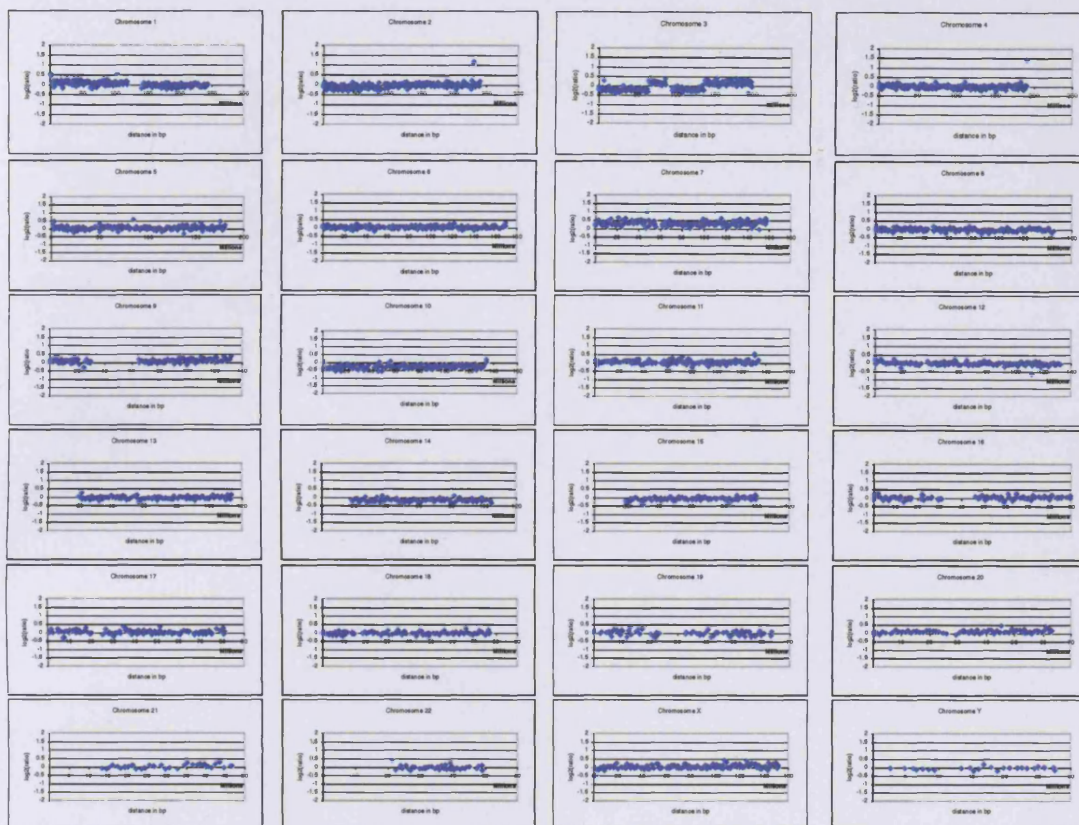
Appendix C14 Array CGH profile of cell line CRL2366



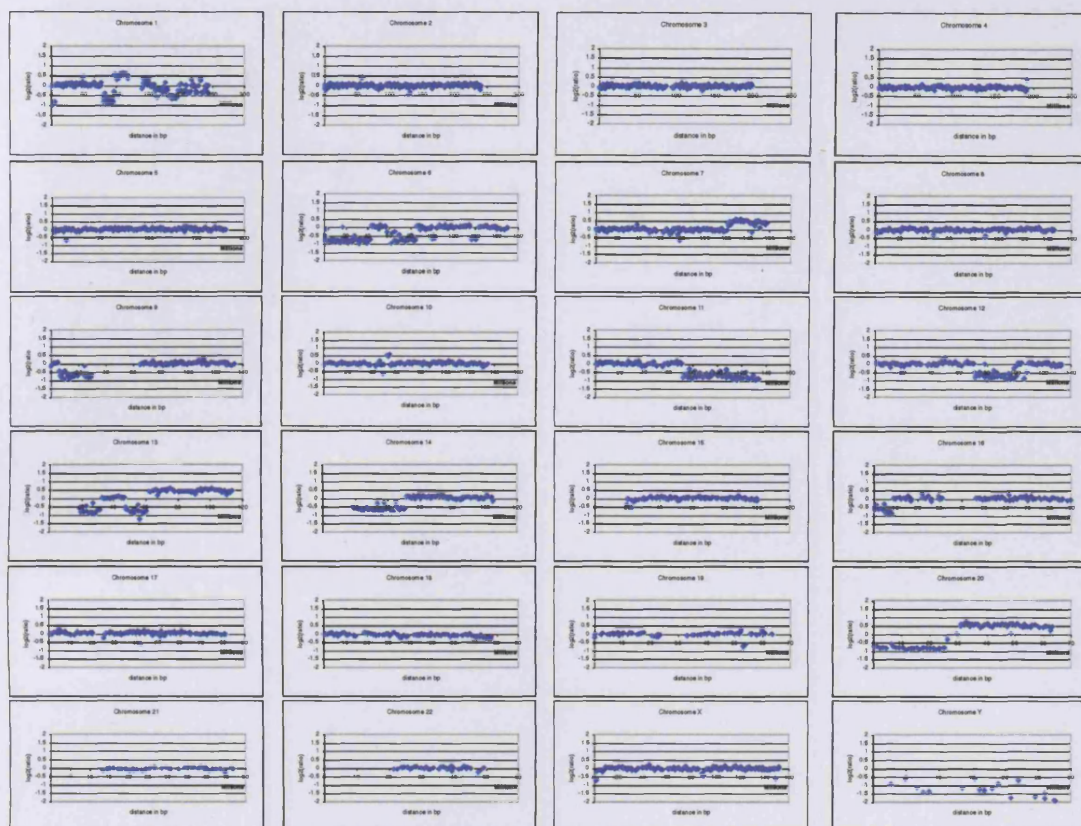
Appendix C15 Array CGH profile of cell line CRL2610



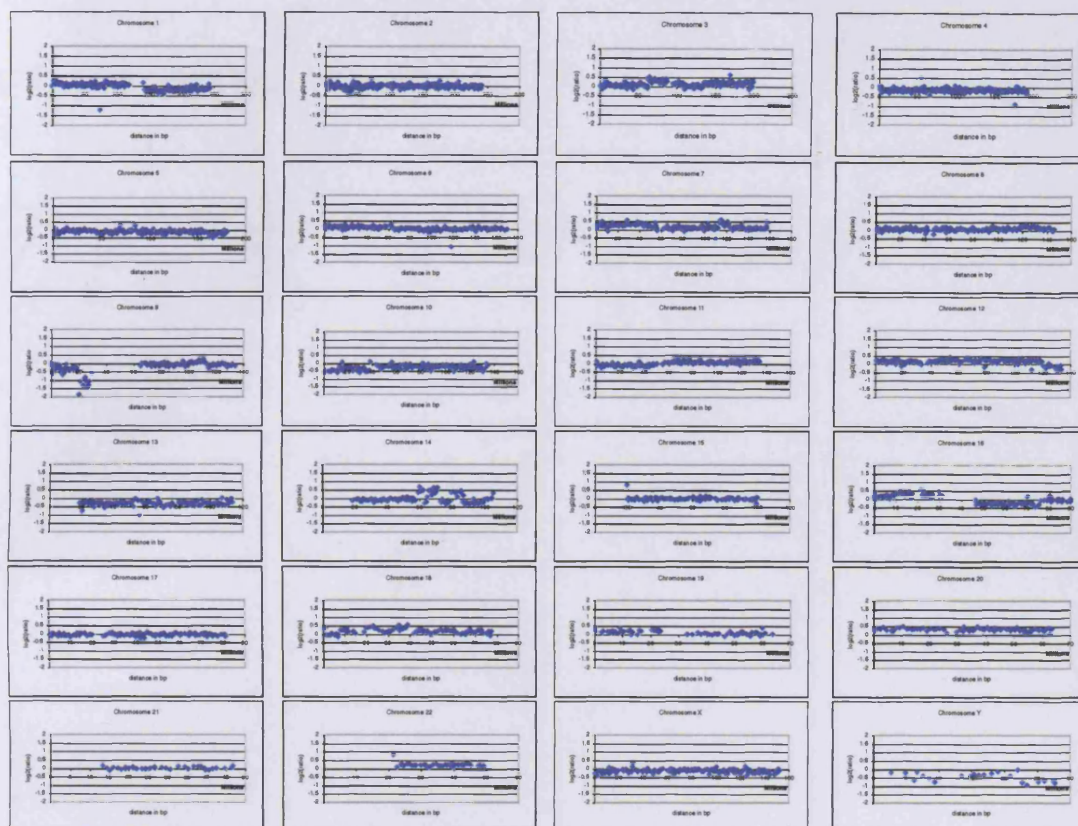
Appendix C16 Array CGH profile of cell line CRL2611



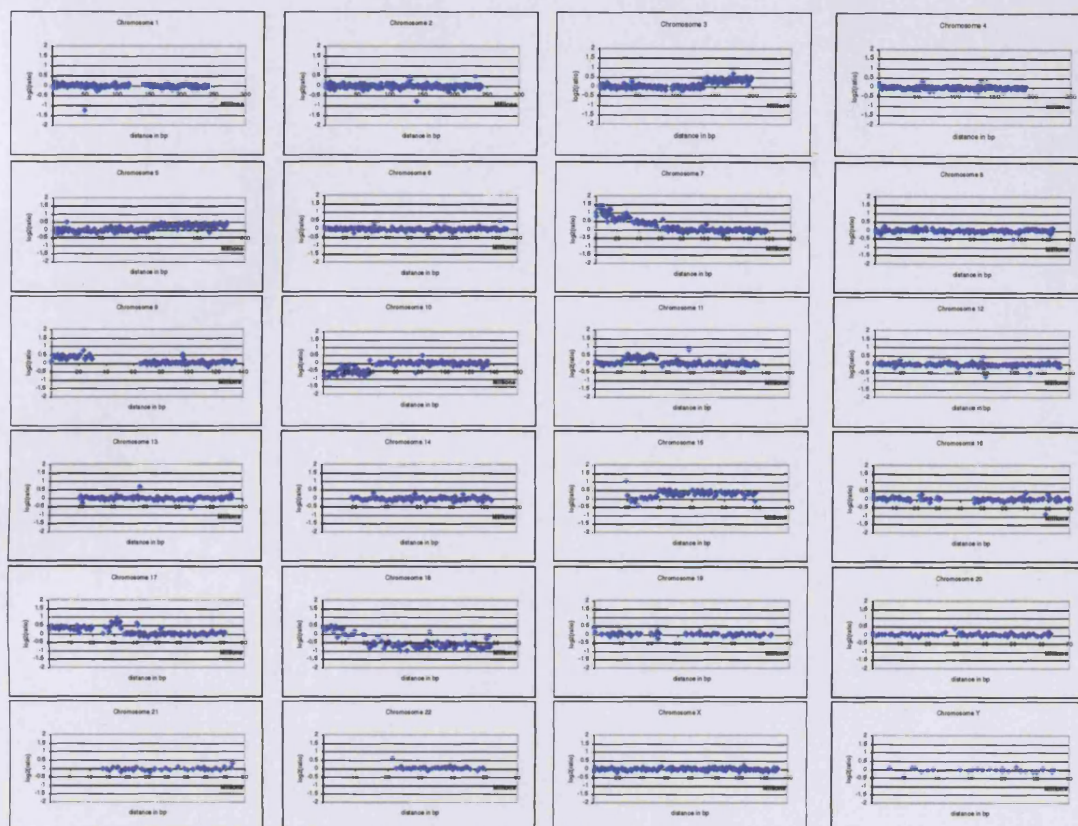
Appendix C17 Array CGH profile of cell line Htb138



Appendix C18 Array CGH profile of cell line U87



Appendix C19 Array CGH profile of cell line U118



Appendix C20 Array CGH profile of cell line U251